



Opara, Elaine Marie (2005) Carbon forming reactions over precious metal steam reforming catalyst. PhD thesis

<http://theses.gla.ac.uk/6919/>

Copyright and moral rights for this thesis are retained by the author

A copy can be downloaded for personal non-commercial research or study, without prior permission or charge

This thesis cannot be reproduced or quoted extensively from without first obtaining permission in writing from the Author

The content must not be changed in any way or sold commercially in any format or medium without the formal permission of the Author

When referring to this work, full bibliographic details including the author, title, awarding institution and date of the thesis must be given

# **Carbon Forming Reactions Over Precious Metal Steam Reforming Catalysts**

*A Thesis Presented to the University of Glasgow for the  
Degree of Doctor of Philosophy*

*by*

**Elaine Marie Opara**

*March 2005*

© *Elaine M Opara*  
*March 2005*



## **IMAGING SERVICES NORTH**

Boston Spa, Wetherby

West Yorkshire, LS23 7BQ

[www.bl.uk](http://www.bl.uk)

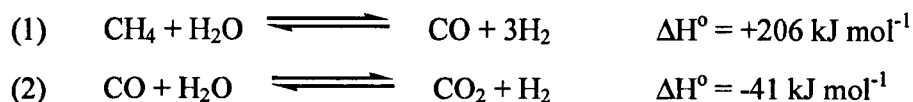
**SUB-HEADINGS ON EACH PAGE HAVE FAINT PRINT**

## **Declaration**

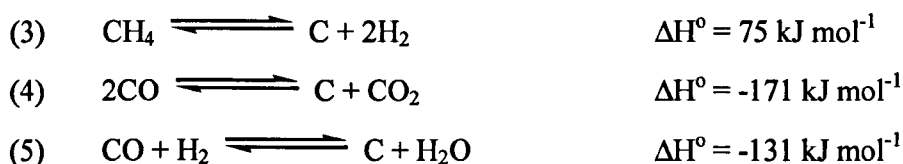
The work contained in this thesis, submitted for the degree of Doctor of Philosophy, is my own original work, except where due reference is made to other authors. No material within has been previously submitted for a degree at this or any other university.

Elaine Marie Opara

Steam reforming of CH<sub>4</sub> is an established industrial process for the formation of synthesis gas. It takes place in two reversible stages: CH<sub>4</sub> reforming reaction (1) followed by the water-gas shift (2).



Reaction (1) takes place at high temperature (approximately 1200K) and pressure (15-30bar) to maximise the efficiency and conversion while reaction (2) takes place at as low a temperature as possible. The biggest worry to the steam reforming industry is the formation of carbon which is produced favourably via three side-reactions:



The catalysts currently used for reaction (1) are based on Ni metal however, Ni is prone to formation of a type of carbon known as ‘whiskers’ (filamental carbon) which form when deposited carbon dissolves into the bulk metal. These structures result in a breakdown of the catalyst particles leading to reactor tube blockages and eventual costly damage. Certain measure can be taken to reduce carbon, namely, use of excess steam; partial poisoning of the catalyst with sulfur and alterations to the catalyst formulation such as alkali dopants and noble metals. In this project, the behaviour of eight supported noble metals (Rh, Pt, Ru and Ni supported on La-ZrO<sub>2</sub> and Al<sub>2</sub>O<sub>3</sub>) during reactions (3)-(5) at 20bar and 873K was investigated. It has been shown previously that noble metal catalysts can be more active than Ni during steam reforming and are more carbon resistant. More significantly, noble metal catalysts do not form whisker carbon.

High pressure reactions (3) and (4) combined with a series of low pressure pulses followed by mass spectrometry revealed the greater stability of the La-ZrO<sub>2</sub> supported catalysts due to strong metal support interactions (SMSI) and a faster rate of O-transfer. Ni was always the more reactive catalyst although it was not compared

at high pressure for risk of potential damage. Common mechanisms were proposed for all catalysts involving interaction of surface OH-groups with reactant species on all La-ZrO<sub>2</sub> and Al<sub>2</sub>O<sub>3</sub> catalysts. The reactivity of the Al<sub>2</sub>O<sub>3</sub> catalysts was related to percentage metal dispersion although this was not apparent for the La-ZrO<sub>2</sub> catalysts. Deactivation studies revealed the likely first and second order behaviour of reactions (4) and (3) respectively. These studies also showed how the rate of deactivation was greater over Pt than Rh. Theories on the type of carbon produced during reaction (3) were discussed.

Each noble metal catalyst produced a unique reaction profile during reaction (5) and the greater reactivity of the La-ZrO<sub>2</sub> catalysts was attributed to interfacial metal-support interactions (IMSI). The reaction profile was clearly affected by the nature of the metal and the support and so a mechanism was proposed with an explanation of each catalysts' behaviour in terms of type of metal and support.

An excess of steam can be used to prevent carbon formation and likewise, CO<sub>2</sub> can be used for the same purpose. An investigation of different CO/CO<sub>2</sub> ratios was made and it was apparent that ratios of approximately 1:1 were necessary for carbon prevention. A pre-treatment of each catalyst with CO/CO<sub>2</sub> changed the product selectivity during reaction (5).

There are many people that I owe a great deal of thanks to for the last three (and a bit) years of this PhD. Firstly, my supervisor, Prof. David Jackson, for his help, enthusiasm and encouragement when it was needed most. I would especially like to thank David Jackson for not once being too busy to discuss my work. All has been appreciated.

I would like to extend my gratitude to my industrial supervisors Dr. Martin Fowles and Dr. Phil Ingram of Johnson Matthey Catalysts for the project (of course) but also for lending their support by taking regular trips up to Glasgow and moreover, giving me the opportunity to spend time at JM in Billingham. Thanks also to Bill Sengelow and everyone from the catalyst test hall at JM especially Michelle Wilkinson and Anne-Marie Lausson.

There are many people in Glasgow that this thesis could not have been made without: To Ron Spence, for originally setting up the rig and always being on-hand in times of break-down (equipment!). To Andy Monaghan for some last-minute BETs and his constant eagerness to help in some way or another! To Arran Canning, Kenny Hindle, and Elaine Vass who were always available for an opinion or a presentation practice sesh or to simply help me talk the answers out of myself. To Sharon Burns Elaine Gelder, Gemma Parker, Sreekala Rugmini, and David Williams who all contributed.

Mum and Dad, thanks for being supportive, helpful and understanding! Dad, it's all done now! Thanks for protecting your investment. You can now retire!

Finally, a special thank you to Kenny Hindle and Kirsty Stewart.

<b>1</b>	<b>Introduction</b>	<b>1</b>
1.1	<b>The Environmental Challenge</b>	<b>1</b>
1.1.1	Petrochemicals Industry	3
1.1.2	H <sub>2</sub> Demand	5
1.2	<b>Reforming of Natural Gas</b>	<b>7</b>
1.2.1	Example Applications – NH <sub>3</sub> and CH <sub>3</sub> OH Synthesis	9
1.2.2	Steam Reforming Catalyst	11
1.2.3	Carbon Formation	14
1.2.3.1	Whisker Carbon	15
1.2.3.2	Modelling of Carbon Formation	17
1.2.3.3	Deactivation	19
1.2.3.4	Types of Carbon	20
1.2.3.5	Effect of Pressure	25
1.3	<b>Avoiding Carbon</b>	<b>26</b>
1.3.1	Sulfur Passivation	27
1.3.2	Alkali Dopants	27
1.3.3	Noble Metals	28
1.3.3.1	Activity	28
1.3.3.2	Carbon Formation	32
1.4	<b>Supports</b>	<b>35</b>
1.4.1	Supports for Reforming	36
1.4.2	Alumina	36
1.4.3	Zirconia	37
1.4.4	Typical Surface Areas	38
1.4.5	Support Effects	38
1.4.5.1	Physical Effects	39
1.4.5.2	Hydroxyl Spillover	40
1.4.5.3	Hydrogen Spillover	41
1.4.5.4	Electronic Effects	42
1.4.5.5	Oxygen Storage and Transfer	45
1.4.5.6	Complex Formation	48
1.5	<b>Project Aim</b>	<b>50</b>

<b>2</b>	<b><i>Experimental</i></b>	<b>52</b>
<b>2.1</b>	<b>Catalyst Preparation</b>	<b>52</b>
2.1.1	Properties of Supports	52
2.1.2	Catalyst Support Preparation	53
2.1.3	Support Impregnation	53
<b>2.2</b>	<b>Catalyst Characterisation</b>	<b>55</b>
2.2.1	Surface Area Analysis	55
2.2.1.1	Adsorption	55
2.2.1.2	BET	55
2.2.1.3	Chemisorption	56
<b>2.3</b>	<b>Reactions</b>	<b>56</b>
2.3.1	High Pressure Reactor	56
2.3.1.1	Gaseous Materials	59
2.3.1.2	Mass Flow Controllers (MFCs)	59
2.3.1.3	Mass Spectrometer	60
2.3.1.4	High-Pressure Reactions	62
2.3.2	Pulse Flow Reactor	63
2.3.2.1	Mass Spectrometer	65
2.3.2.2	Pulse Flow Reactions	66
2.3.2.3	Isotope Pulses	67
2.3.3	Tapered Element Oscillating Microbalance (TEOM)	68
2.3.3.1	TEOM Reactions	71
<b>3</b>	<b><i>Results</i></b>	<b>72</b>
<b>3.1</b>	<b>Catalyst Characterisation</b>	<b>72</b>
3.1.1	BET	72
3.1.2	H <sub>2</sub> Chemisorption	74
<b>3.2</b>	<b>Pulse Flow Reactions</b>	<b>75</b>
3.2.1	CO Pulses over La-ZrO <sub>2</sub> Support	75
3.2.1.1	Calculations From CO Pulses	76
3.2.2	CO Pulses over La-ZrO <sub>2</sub> Supported Catalysts	78
3.2.2.1	CO Pulses over Ni/La-ZrO <sub>2</sub>	82
3.2.3	CH <sub>4</sub> Pulses over La-ZrO <sub>2</sub> Support	83

3.2.4	CH <sub>4</sub> Pulses over La-ZrO <sub>2</sub> Supported Catalysts	84
3.2.4.1	Mass Spectrometer Splitting Patterns	86
3.2.4.2	Calculations from CH <sub>4</sub> Pulses	86
3.2.5	CO Pulses over Al <sub>2</sub> O <sub>3</sub> Support	91
3.2.6	CO Pulses over Al <sub>2</sub> O <sub>3</sub> Supported Catalysts	92
3.2.7	CH <sub>4</sub> Pulses over Al <sub>2</sub> O <sub>3</sub> Support	96
3.2.8	CH <sub>4</sub> Pulses over Al <sub>2</sub> O <sub>3</sub> Supported Catalysts	96
3.2.9	Isotope Pulses	101
3.2.9.1	Reference Pulse	101
3.2.9.2	Isotope Pulses over La-ZrO <sub>2</sub>	102
3.2.9.3	Isotope Pulses over La-ZrO <sub>2</sub> Supported Catalysts	103
3.2.9.4	Isotope Pulses Over Al <sub>2</sub> O <sub>3</sub> Support Material	109
3.2.9.5	Isotope Pulses Over Al <sub>2</sub> O <sub>3</sub> Supported Catalysts	111
<b>3.3</b>	<b>High Pressure Rig Reactions</b>	<b>118</b>
3.3.1	Boudouard Reaction over La-ZrO <sub>2</sub> Supported Catalysts	118
3.3.1.1	Mass of Carbon Produced	121
3.3.1.2	Deactivation	122
3.3.2	CO and H <sub>2</sub> over La-ZrO <sub>2</sub> Support	126
3.3.3	CO and H <sub>2</sub> over La-ZrO <sub>2</sub> Supported Catalysts	127
3.3.3.1	Percentage CO Conversion Over Rh and Pt	129
3.3.4	CO and CO <sub>2</sub> over La-ZrO <sub>2</sub> Supported Catalysts	132
3.3.4.1	Used Boudouard catalyst	132
3.3.4.2	CO:CO <sub>2</sub> , 10:1 Over La-ZrO <sub>2</sub> Catalysts	134
3.3.4.3	CO:CO <sub>2</sub> , 5:1 Over La-ZrO <sub>2</sub> Catalysts	139
3.3.4.4	CO:CO <sub>2</sub> , 1:1 Over La-ZrO <sub>2</sub> Catalysts	143
3.3.5	Boudouard Reaction over Al <sub>2</sub> O <sub>3</sub> Supported Catalysts	150
3.3.5.1	Mass of Carbon Produced	152
3.3.5.2	Deactivation	153
3.3.6	CO and H <sub>2</sub> over Al <sub>2</sub> O <sub>3</sub> Support	157
3.3.7	CO and H <sub>2</sub> over Al <sub>2</sub> O <sub>3</sub> Supported Catalysts	158
3.3.7.1	Percentage CO Conversion over Rh/Al <sub>2</sub> O <sub>3</sub>	160
3.3.7.2	Pt and Ru/Al <sub>2</sub> O <sub>3</sub>	161
3.3.8	CO and CO <sub>2</sub> over Al <sub>2</sub> O <sub>3</sub> Supported Catalysts	163

3.3.8.1	Used Boudouard Reaction Catalysts _____	163
3.3.8.2	CO:CO <sub>2</sub> (10:1) over Al <sub>2</sub> O <sub>3</sub> Supported Catalysts _____	165
3.3.8.3	CO:CO <sub>2</sub> (5:1) over Al <sub>2</sub> O <sub>3</sub> Supported Catalysts _____	169
3.3.8.4	CO:CO <sub>2</sub> (1:1) over Al <sub>2</sub> O <sub>3</sub> Supported Catalysts _____	173
<b>3.4</b>	<b>TEOM Reactions _____</b>	<b>179</b>
3.4.1	Apparent Mass Changes _____	179
3.4.1.1	Baseline Drift _____	179
3.4.1.2	Pressure Variations _____	179
3.4.1.3	Temperature Variations _____	180
3.4.1.4	Gas Composition _____	180
3.4.1.5	Changing Gas Flow Rate _____	180
3.4.1.6	Catalysis Due to Metal Cap _____	181
3.4.1.7	Noise _____	181
3.4.1.8	Present Study _____	181
3.4.2	CH <sub>4</sub> Cracking Reaction over La-ZrO <sub>2</sub> Support _____	181
3.4.3	CH <sub>4</sub> Cracking Reaction over Rh/La-ZrO <sub>2</sub> _____	182
3.4.3.1	Rh/La-ZrO <sub>2</sub> Catalyst Deactivation _____	185
3.4.4	CH <sub>4</sub> Cracking Reaction over Pt/La-ZrO <sub>2</sub> _____	186
3.4.4.1	Pt Catalyst Deactivation _____	189
3.4.5	CH <sub>4</sub> Cracking Reaction over Al <sub>2</sub> O <sub>3</sub> Support _____	190
3.4.6	CH <sub>4</sub> Cracking Reaction over Rh/Al <sub>2</sub> O <sub>3</sub> _____	190
3.4.6.1	Rh/Al <sub>2</sub> O <sub>3</sub> Catalyst Deactivation _____	192
3.4.7	CH <sub>4</sub> Cracking over Pt/Al <sub>2</sub> O <sub>3</sub> _____	192
3.4.7.1	Pt/Al <sub>2</sub> O <sub>3</sub> Catalyst Deactivation _____	194
3.4.8	Comparison of Results _____	195
<b>4</b>	<b>Discussion _____</b>	<b>196</b>
<b>4.1</b>	<b>Al<sub>2</sub>O<sub>3</sub> Catalysts _____</b>	<b>196</b>
4.1.1	CO Pulses _____	196
4.1.2	High Pressure CO _____	200
4.1.3	CH <sub>4</sub> Pulses _____	202
4.1.4	High Pressure CH <sub>4</sub> (TEOM) _____	205
<b>4.2</b>	<b>La-ZrO<sub>2</sub> Catalysts _____</b>	<b>207</b>

4.2.1	CO Pulses _____	207
4.2.2	Isotope Pulses Over La-ZrO <sub>2</sub> and Al <sub>2</sub> O <sub>3</sub> Catalysts _____	210
4.2.3	High Pressure CO _____	213
4.2.4	CH <sub>4</sub> Pulses _____	216
4.2.5	High Pressure CH <sub>4</sub> (TEOM) _____	223
4.3	High Pressure CO and H <sub>2</sub> over La-ZrO <sub>2</sub> and Al <sub>2</sub> O <sub>3</sub> Catalysts _____	226
4.4	CO and CO <sub>2</sub> over La-ZrO <sub>2</sub> and Al <sub>2</sub> O <sub>3</sub> Catalysts _____	230
5	Summary _____	235
5.1	Al <sub>2</sub> O <sub>3</sub> Catalysts _____	235
5.2	La-ZrO <sub>2</sub> Catalysts _____	236
5.3	Reaction with CO and H <sub>2</sub> _____	237
5.4	Reaction with CO and CO <sub>2</sub> _____	238
6	References _____	239

### Figures and Tables

**Table 1.1. Worldwide energy use in million tonnes of oil equivalent (MTOE), world population and per capita energy consumption in the 20<sup>th</sup> century (reproduced from ref. 2)**

**Table 1.2. Non-refinery US demand for H<sub>2</sub> (in billions of ft<sup>3</sup>)<sup>11</sup>**

**Table 1.3. Calculated product gas compositions (ref. 15)**

**Table 1.4. Compositions of commercial steam reforming catalysts (refs.<sup>15</sup>)**

**Table 1.5. Summary of types of carbon formed during steam reforming of hydrocarbons (reproduced from Ref. 15)**

**Table 1.6. Typical catalyst support surface areas**

**Table 2.1. Chemical analysis of Disperal Al<sub>2</sub>O<sub>3</sub> Support**

**Table 2.2. Chemical analysis of La-ZrO<sub>2</sub> Support**

**Table 2.3. Temperature programmes used during catalyst support synthesis**

**Table 2.4. Metal precursors**

**Table 2.5. Pore volumes of catalyst supports**

**Table 2.6. Temperature programme of kiln during catalyst calcinations.**

**Table 2.7. Gases used, supplier and purity**

**Table 2.8. Average Ion current of gases from mass spectrometer and relationship relative to CO**

**Table 2.9. Summary of reactions carried out on high pressure apparatus**

**Table 2.10. Species and their masses followed by mass spectrometry**

**Table 2.11. Pulse Flow Reactions**

**Table 2.12. Reactions carried out on the TEOM**

**Table 3.1 Determined BET surface area of each catalyst**

**Table 3.2 Catalyst pore volumes determined by BET analysis**

**Table 3.3 Catalyst pore diameters determined by BET analysis**

**Table 3.4 Percentage metal dispersion of each catalyst**

**Table 3.5. CO reference peak area with corresponding pressure and number of moles**

**Table 3.6. Area of CO<sub>2</sub> peak and calculated number of μmols**

**Table 3.7. Moles of CO<sub>2</sub> (CO<sub>2</sub> moles out) produced over La-ZrO<sub>2</sub> from each pulse. Calculated from peak areas**

**Table 3.8. Data obtained from five CO pulses over Rh/La-ZrO<sub>2</sub>**

**Table 3.9. Data obtained from five CO pulses over Pt/La-ZrO<sub>2</sub>**

**Table 3.10. Data obtained from five CO pulses over Ru/La-ZrO<sub>2</sub>**

**Table 3.11. Comparison: moles of CO<sub>2</sub> from support and moles of CO<sub>2</sub> from Ni catalyst**

**Table 3.12. Data obtained from five CO pulses over Ni/La-ZrO<sub>2</sub>**

**Table 3.13. Calculated CH<sub>4</sub> reference peak area and mole equivalent**

**Table 3.14. Equivalent H<sub>2</sub> reference area**

**Table 3.15. Pressure and moles of CH<sub>4</sub> flowing into reactor per pulse (CH<sub>4</sub> moles in)**

**Table 3.16. Area and moles of each CH<sub>4</sub> peak from mass spectrometer data (CH<sub>4</sub> moles out)**

**Table 3.17. % CH<sub>4</sub> conversion obtained for each pulse**

**Table 3.18. Areas and moles of H<sub>2</sub> produced during each pulse**

**Table 3.19. Data obtained from five CH<sub>4</sub> pulses over Pt/La-ZrO<sub>2</sub>**

**Table 3.20. Data obtained from five CH<sub>4</sub> pulses over Ru/La-ZrO<sub>2</sub>**

**Table 3.21. Data obtained from five CH<sub>4</sub> pulses over Ni/La-ZrO<sub>2</sub>**

**Table 3.22.  $H_2(\text{out})/CH_4$  (consumed) ratios obtained from each pulse of  $CH_4$  over the metal catalysts**

**Table 3.23. Data obtained from five CO pulses over  $Al_2O_3$  support**

**Table 3.24. Data obtained from five CO pulses over  $Rh/Al_2O_3$**

**Table 3.25. Data obtained from five CO pulses over  $Pt/Al_2O_3$**

**Table 3.26. Data obtained from five CO pulses over  $Ru/Al_2O_3$**

**Table 3.27. Data obtained from five CO pulses over  $Ni/Al_2O_3$**

**Table 3.28. Data obtained from five  $CH_4$  pulses over  $Rh/Al_2O_3$**

**Table 3.29. Data obtained from five  $CH_4$  pulses over  $Pt/Al_2O_3$**

**Table 3.30. Data obtained from five  $CH_4$  pulses over  $Ru/Al_2O_3$**

**Table 3.31. Data obtained from five  $CH_4$  pulses over  $Ni/Al_2O_3$**

**Table 3.32.  $H_2/CH_4$  ratios obtained from each pulse of  $CH_4$  over the metal  $Al_2O_3$  catalysts**

**Table 3.33.  $^{12}C$  mass balance from isotope pulses over  $Al_2O_3$  support**

**Table 3.34.  $^{13}C$  mass balance from isotope pulses over  $Al_2O_3$  support**

**Table 3.35.  $^{16}O$  mass balance from isotope pulses over  $Al_2O_3$  support**

**Table 3.36.  $^{12}C$  mass balance from isotope pulses over  $Rh/La-ZrO_2$  catalyst**

**Table 3.37.  $^{13}C$  mass balance from isotope pulses over  $Rh/La-ZrO_2$  catalyst**

**Table 3.38.  $^{16}O$  mass balance from isotope pulses over  $Rh/La-ZrO_2$  catalyst**

**Table 3.39.  $^{12}C$  mass balance from isotope pulses over  $Pt/La-ZrO_2$  catalyst**

**Table 3.40.  $^{13}C$  mass balance from isotope pulses over  $Pt/La-ZrO_2$  catalyst**

**Table 3.41.  $^{16}O$  mass balance from isotope pulses over  $Pt/La-ZrO_2$  catalyst**

**Table 3.42.  $^{12}C$  mass balance from isotope pulses over  $Ru/La-ZrO_2$  catalyst**

**Table 3.43.  $^{13}C$  mass balance from isotope pulses over  $Ru/La-ZrO_2$  catalyst**

**Table 3.44.  $^{16}O$  mass balance from isotope pulses over  $Ru/La-ZrO_2$  catalyst**

**Table 3.45.  $^{12}C$  mass balance from isotope pulses over  $Ni/La-ZrO_2$  catalyst**

**Table 3.46.  $^{13}C$  mass balance from isotope pulses over  $Ni/La-ZrO_2$  catalyst**

**Table 3.47.  $^{16}O$  mass balance from isotope pulses over  $Ni/La-ZrO_2$  catalyst**

**Table 3.48.  $^{12}C$  mass balance from isotope pulses over  $Al_2O_3$  support**

**Table 3.49.  $^{13}C$  mass balance from isotope pulses over  $Al_2O_3$  support**

**Table 3.50.  $^{16}O$  mass balance from isotope pulses over  $Al_2O_3$  support**

**Table 3.51.  $^{12}C$  mass balance from isotope pulses over  $Rh/Al_2O_3$  catalyst**

**Table 3.52.  $^{13}C$  mass balance from isotope pulses over  $Rh/Al_2O_3$  catalyst**

- Table 3.53.**  $^{16}\text{O}$  mass balance from isotope pulses over  $\text{Rh}/\text{Al}_2\text{O}_3$  catalyst
- Table 3.54.**  $^{12}\text{C}$  mass balance from isotope pulses over  $\text{Pt}/\text{Al}_2\text{O}_3$  catalyst
- Table 3.55.**  $^{13}\text{C}$  mass balance from isotope pulses over  $\text{Pt}/\text{Al}_2\text{O}_3$  catalyst
- Table 3.56.**  $^{16}\text{O}$  mass balance from isotope pulses over  $\text{Pt}/\text{Al}_2\text{O}_3$  catalyst
- Table 3.57.**  $^{12}\text{C}$  mass balance from isotope pulses over  $\text{Ru}/\text{Al}_2\text{O}_3$  catalyst
- Table 3.58.**  $^{13}\text{C}$  mass balance from isotope pulses over  $\text{Ru}/\text{Al}_2\text{O}_3$  catalyst
- Table 3.59.**  $^{16}\text{O}$  mass balance from isotope pulses over  $\text{Ru}/\text{Al}_2\text{O}_3$  catalyst
- Table 3.60.**  $^{12}\text{C}$  mass balance from isotope pulses over  $\text{Ni}/\text{Al}_2\text{O}_3$  catalyst
- Table 3.61.**  $^{13}\text{C}$  mass balance from isotope pulses over  $\text{Ni}/\text{Al}_2\text{O}_3$  catalyst
- Table 3.62.**  $^{16}\text{O}$  mass balance from isotope pulses over  $\text{Ni}/\text{Al}_2\text{O}_3$  catalyst
- Table 3.63.** Mass of carbon produced per gram of support from support and packing material after 30 minutes
- Table 3.64.** Moles of carbon produced per gram of catalyst after 30 minutes
- Table 3.65.** Mass spectrometer significant splitting patterns
- Table 3.66.** Moles/minute of each species at steady state over Rh
- Table 3.67.** %CO conversion and  $\text{CO}_2:\text{CH}_4$  product ratio over Rh
- Table 3.68.** Moles/minute of each species at steady state over Pt after one hour
- Table 3.69.** %CO conversion and  $\text{CO}_2:\text{CH}_4$  product ratio over Pt
- Table 3.71.** Moles/minute of each species at steady state over Rh after one hour
- Table 3.72.** %CO conversion and  $\text{CO}_2:\text{CH}_4$  product ratio over Rh
- Table 3.73.** Moles/minute of each species at steady state over Pt after one hour
- Table 3.74.** %CO conversion and  $\text{CO}_2:\text{CH}_4$  product ratio over Pt
- Table 3.75.** Moles of  $\text{CO}_2$  produced from support and packing after 30 minutes on stream
- Table 3.76.** Moles of  $\text{CO}_2$  and mass of carbon produced per gram of catalyst after 30 minutes
- Table 3.77.** Deactivation rate constants for Boudouard reaction
- Table 3.78.** Moles/minute of each species at steady state over  $\text{Rh}/\text{Al}_2\text{O}_3$  (section 1)
- Table 3.79.** %CO conversion and  $\text{CO}_2:\text{CH}_4$  product ratio over  $\text{Rh}/\text{Al}_2\text{O}_3$  (section 1)
- Table 3.80.** Moles/minute of each species at steady state over  $\text{Rh}/\text{Al}_2\text{O}_3$  (section 2)
- Table 3.81.** %CO conversion and  $\text{CO}_2:\text{CH}_4$  product ratio over  $\text{Rh}/\text{Al}_2\text{O}_3$  (stage 2)
- Table 3.82.** Moles/minute of each species at steady state over  $\text{Pt}/\text{Al}_2\text{O}_3$
- Table 3.83.** %CO conversion and  $\text{CO}_2:\text{CH}_4$  product ratio over  $\text{Pt}/\text{Al}_2\text{O}_3$

**Table 3.84. Moles/minute of each species at steady state over used Rh/Al<sub>2</sub>O<sub>3</sub>**

**Table 3.85. %CO conversion and CO<sub>2</sub>:CH<sub>4</sub> product ratio over Rh/Al<sub>2</sub>O<sub>3</sub>**

**Table 3.86. Moles/minute of each species at steady state over used Pt/Al<sub>2</sub>O<sub>3</sub>**

**Table 3.87. %CO conversion and CO<sub>2</sub>:CH<sub>4</sub> product ratio over Pt/Al<sub>2</sub>O<sub>3</sub>**

**Table 3.88. Mass of carbon deposited during CH<sub>4</sub> cracking over Rh/La-ZrO<sub>2</sub>**

**Table 3.89. Mass of carbon deposited during CH<sub>4</sub> cracking over Pt/La-ZrO<sub>2</sub>**

**Table 3.90. Mass of carbon deposited during CH<sub>4</sub> cracking over Rh/Al<sub>2</sub>O<sub>3</sub>**

**Table 3.91. Mass of carbon deposited during CH<sub>4</sub> cracking over Pt/Al<sub>2</sub>O<sub>3</sub>**

**Table 3.92. Mass of deposited carbon and deactivation rate constant, *k*  
support catalysts.**

**Table 4.2. Oxygen uptake at 723K (reproduced from ref.124)**

**Table 4.3. Deactivation rate constants of Boudouard reaction over La-ZrO<sub>2</sub>  
supported catalysts**

**Table 4.4. % CH<sub>4</sub> conversion from five pulses of CH<sub>4</sub> over La-ZrO<sub>2</sub>**

# 1 Introduction

## 1.1 The Environmental Challenge

Global warming is a common household term and its occurrence is gradually beginning to effect every living entity on our planet. By burning fossil fuels (coal, oil and natural gas), CO<sub>2</sub> gas is produced and released into the atmosphere. The predicted long-term effect of excessive CO<sub>2</sub> and other greenhouse gas emissions (CH<sub>4</sub>, nitrous oxides, CFCs) in the atmosphere is a global rise in temperature of 1-3.5°C by the end of this century. The consequences of what seems like a negligible difference are severe changes in our weather patterns specifically dramatic increases in rainfall, flooding and hurricanes. It is also acknowledged that many plant and animal species will become extinct<sup>1</sup>.

The burning of fossil fuels has seen a massive increase in the last century. This drastic increase in energy consumption from the year 1900 to 1997 is shown in table 1.1<sup>2</sup>. This is a direct consequence of rapid development in the industrial and transportation sectors also improvements in living standards and the ever-increasing world population<sup>2</sup>. Table 1.1 shows how there was twelve times as much global CO<sub>2</sub> emission in 1997 as there was in 1900. Fortunately, not all of the CO<sub>2</sub> produced remains in the atmosphere: Approximately half is absorbed by surface layers of the ocean and by trees and other green plants however, at the present rate at which we burn fossil fuels and destroy forests, we may expect the amount of CO<sub>2</sub> in the atmosphere to reach double the pre-industrial level in the second half of this century<sup>1</sup>.

**Table 1.1. Worldwide energy use in million tonnes of oil equivalent (MTOE), world population and per capita energy consumption in the 20<sup>th</sup> century (reproduced from ref. 2)**

Energy Source	1900		1997	
	MTOE	%	MTOE	%
Petroleum	18	2	2940	30
Natural gas	9	1	2173	23
Coal	501	55	2122	22
Nuclear	0	0	579	6
Renewable	383	42	1833	19
<b>TOTAL</b>	<b>911</b>	<b>100</b>	<b>9647</b>	<b>100</b>
Population (million)	1762		5847	
Per capita energy use (TOE)	0.52		1.65	
Global CO <sub>2</sub> emission (MMTC) <sup>a</sup>	534		6601	
Per capita CO <sub>2</sub> emission (MTC)	0.03		1.13	
Atmospheric CO <sub>2</sub> (ppmv) <sup>b</sup>	295		364	
Life expectancy (years) <sup>c</sup>	47		76	

<sup>a</sup> Global CO<sub>2</sub> emission from fossil fuel burning, cement manufacture and gas flaring; expressed in million metric tonnes of carbon (MMTC)

<sup>b</sup> Global atmospheric CO<sub>2</sub> concentrations expressed in parts per million by volume (ppmv)

<sup>c</sup> Life expectancy is based on the statistical record in the US<sup>3,4</sup>

The problems discussed above highlight the paramount importance of CO<sub>2</sub> emission reduction. The environmental challenge strives to make improvements in energy efficiency and the use of carbon-less (or carbon-free) energy<sup>2</sup>.

Gas emissions are not the only concern: Based on current annual consumption of energy, the known worldwide petroleum reserves will be consumed within 37 years however, on the same basis, the world natural gas reserves will last for 61 years at the current annual consumption level. Coal reserves are also more readily available than petroleum and have great potential as a future source of primary energy<sup>2</sup>. According to the Energy Information Administration (EIA), natural gas followed by coal is projected to be the fastest-growing component of primary world energy consumption up to 2020<sup>5</sup>.

Unfortunately, regardless of the extra years of fossil energy bought from natural gas and coal reserves, these supplies are non-renewable and will be exhausted before this century has ended. Thus, in order to protect our environment and preserve what little fuel we have left, we must explore more effective and efficient ways of comprehensive utilisation of all the fossil energy resources for sustainable development.

### 1.1.1 Petrochemicals Industry

Over the past two decades, environmental concerns have driven the petrochemical industry into a global research effort for the development of clean burning fuel for residential, industrial and transportation purposes as a replacement for the environmentally un-friendly and finite supply of fossil fuels. Therefore, the development of pathways to liquid hydrocarbon fuel is underway. These synthetic fuels are heteroatom (S and N) free and their combustion in vehicle engines leads to lower levels of contaminants in the exhaust gases<sup>6</sup>. Many of the processes for liquid fuel conversion have been summarised by Lange and Tijm<sup>7</sup>. The following are examples of different routes:

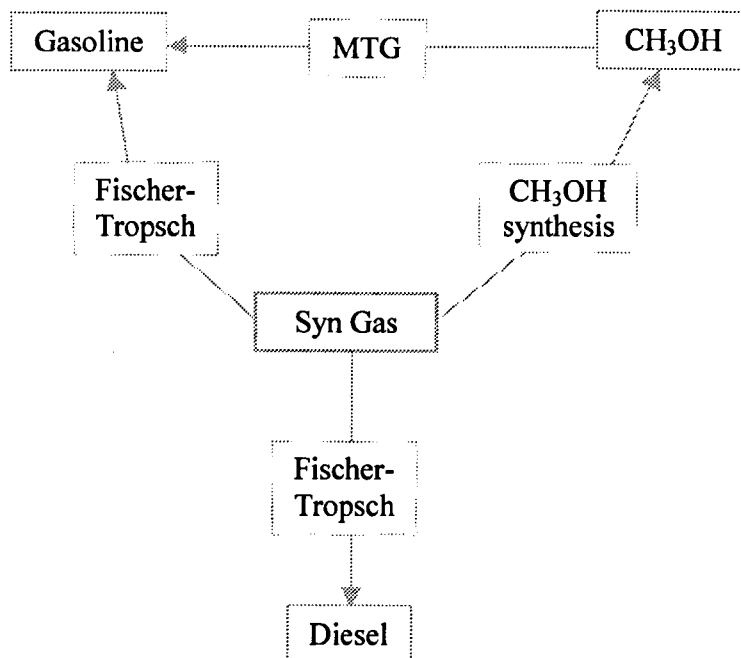
1. **Partial Oxidation to Methanol (POM):** Conversion of  $\text{CH}_4$  and  $\text{O}_2$  to  $\text{CH}_3\text{OH}$  at  $500^\circ\text{C}$  with 5 C% conversion then subsequent conversion to liquid hydrocarbons using the process applied for oligomerising the  $\text{C}_2$  pyrolysis product.
2. **Methane Pyrolysis (PYRO):** Pyrolysis takes place at  $1200^\circ\text{C}$  with 30 C % conversion and 55, 28 and 17 C% selectivities towards  $\text{C}_2$  hydrocarbons, liquid hydrocarbons and coke respectively. The feed was diluted with 30 mol%  $\text{H}_2$  to control the coke deposition. Two pyrolysis furnaces operating alternatively are required for periodic removal of coke. The  $\text{C}_2$  hydrocarbons were subsequently oligomerised to liquid fuels with 100 C% conversion.

The most successful routes to liquid fuels production are indirect  $\text{CH}_4$  conversions. Indirect conversions involve the initial production of synthesis gas (syn gas)<sup>\*</sup> as an intermediate to liquid fuel. The challenge associated with fuel from  $\text{CH}_4$  is the creation of C-C bonds from  $\text{CH}_4$ , a very thermodynamically stable molecule<sup>7</sup>. Considerable effort has gone into development of catalysts for the direct conversion of natural gas into the main intermediates of the petrochemical industry due to the high cost of synthesis gas production (60-70% of cost of overall process). The direct conversion of  $\text{CH}_4$  to higher hydrocarbons would be more economically attractive than indirect conversion however, it is not thermodynamically favourable and although research continues, attempts so far have been less successful and less economically attractive than indirect methods<sup>8, 9</sup>. Figure 1.1 shows indirect conversion routes to liquid fuels.

---

\* Composition of syn gas depends on its application eg. methanol synthesis ( $\text{CO}$ ,  $\text{CO}_2$ ,  $\text{H}_2$ ), Fischer-Tropsch synthesis ( $\text{CO}$  and  $\text{H}_2$ ), ammonia synthesis ( $\text{H}_2$ )

**Figure 1.1. Conversion of synthesis gas to fuel (ref.<sup>8</sup>)**



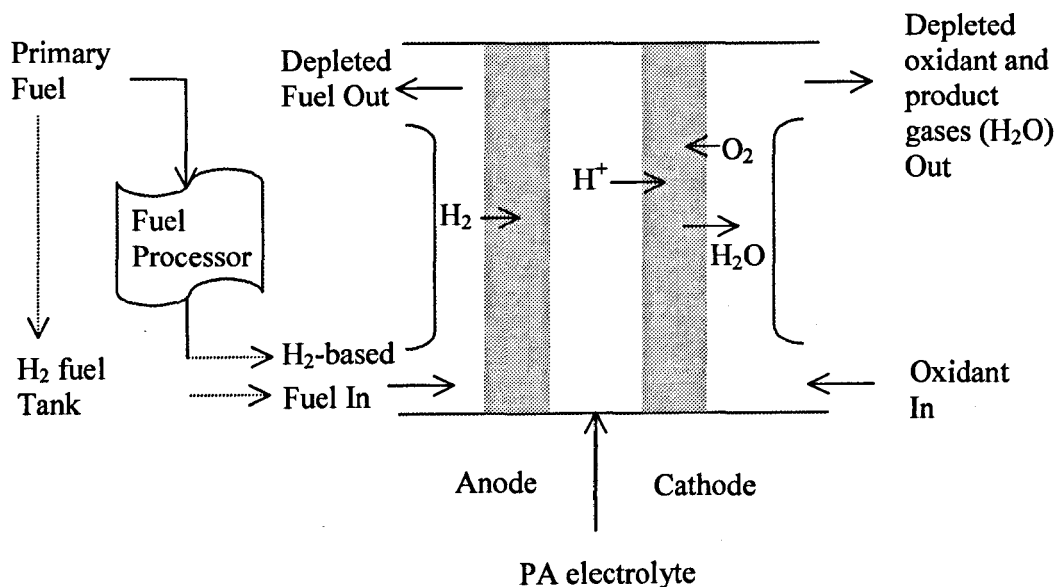
The environmental target for optimisation of such a process as shown in figure 1.1, is 100% yield with minimum use of energy<sup>10</sup>. A target, as such, seems unlikely however, measures in the right direction can be taken to improve the process: reduction of multi-step processes which consume excess energy (direct methods: research under-way); By-product identification and treatment or conversion into useful products (improve catalyst formulation giving greater selectivity to desired products).

### 1.1.2 H<sub>2</sub> Demand

Global concerns for the environment and the decreasing supply of fossil fuels has also stimulated the development of the fuel cell as an environmentally friendly and energy-conservative alternative power generator. A fuel cell is defined as an electrochemical device in which the chemical energy stored in a fuel is converted directly to electricity. Many types of fuel cell exist but all work on the same basic principle: An input fuel is catalytically reacted in the cell to create an electric current.

The input fuel passes over the anode where it splits into electrons and ions and oxygen passes over the cathode. The main product of the fuel cell is the DC current obtained from the flow of electrons from the anode to the cathode<sup>2</sup>. Different types of fuel cell exist, eg 'proton exchange membrane fuel cell' (PEMFC) and 'molten carbonate fuel cell' (MCFC). Figure 1.2 shows a simplified diagram of a 'phosphoric acid fuel cell' (PAFC).

**Figure 1.2. Simplified diagram of phosphoric acid fuel cell (ref.<sup>2</sup>)**



A fuel cell can be two to three times more energy efficient than an internal combustion (IC) engine in converting fuel to electricity; they have extremely low emissions of pollutants, including CO<sub>2</sub> and they have extremely low noise or acoustical pollution. The disadvantages are that they are more expensive than conventional power plants and that the necessary fuel (H<sub>2</sub>) is not readily available and must thus be produced on-board by reforming of hydrocarbons<sup>2</sup>. With consideration of the present research, fuel cells are definite promising candidates as truly energy efficient conversion devices.

Future implication of the fuel cell would, of course, further increase the demand for  $H_2$  alongside the present consumers.  $H_2$  is currently used in the chemical, foods and refining industries. Table 1.2 shows how the demand increased between 1994 and 2000<sup>11</sup>.

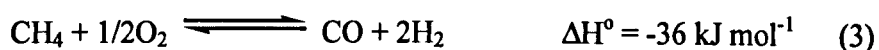
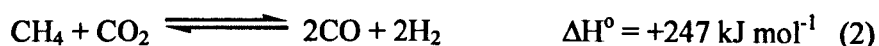
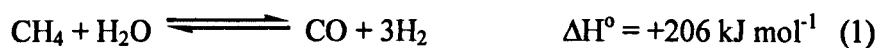
**Table 1.2. Non-refinery US demand for  $H_2$  (in billions of  $ft^3$ )<sup>11</sup>**

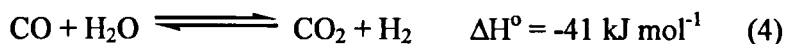
Market	1994	2000
Chemical Processing	82	128
Electronics	9	15
Food processing	4	5
Metal manufacturing	3	4
Other Markets	13	17
Total	111	169

The current route to syn-gas production will not be able to cope with the demands of  $H_2$  in the future hence reactor design and catalyst formulation must be reviewed in order to increase the efficiency of the process towards meeting the demands of tomorrow's world<sup>6</sup>.

## 1.2 Reforming of Natural Gas

There are three routes that are important in the conversion of natural gas to syn-gas. They are steam reforming, dry reforming and partial oxidation (equations 1-3 respectively). The aim of reforming is to extract the maximum quantity of  $H_2$  that is held in water and the hydrocarbon feedstock. Further manipulation of the products then takes place but this depends on the desired end product. Steam reforming of natural gas is the most widely used route to syn-gas<sup>6</sup>. It involves two processes:  $CH_4$  reforming reaction (1) and the water-gas shift reaction (4)<sup>12</sup>.





The reforming reaction is highly endothermic and is favoured by high temperatures and also low pressure. The water-gas shift on the other hand is favoured by low temperature but has no response to changes in pressure. To maximise the efficiency of the process, the reforming reaction (1) is carried out over a Ni catalyst at a high temperature of approximately 1200K and pressures of 15 – 30 bar while the shift reaction (4) utilises two catalysts bringing it to equilibrium at as low a temperature as possible<sup>6, 12</sup>.

CO<sub>2</sub> reforming is of industrial interest due to the lower H<sub>2</sub>/CO ratio in the product gas and its usage of the pollutant CO<sub>2</sub>. It was found that replacement of steam by CO<sub>2</sub> gave similar activation energies, indicating a very similar mechanism of the two cases<sup>13</sup> however, it is more endothermic than steam reforming so requires more heat<sup>14</sup>. Partial oxidation also has disadvantages: At the stoichiometric CH<sub>4</sub>:O<sub>2</sub> ratio used, carbon formation occurs. Increasing the O<sub>2</sub>:CH<sub>4</sub> ratio or increasing the operation temperature cannot reduce this undesirable reaction without increasing the potential risk of explosion<sup>14</sup>.

As has been discussed in section 1.1, steam reforming of CH<sub>4</sub> is a very important industrial process due the large number of consumers of the synthesis gas produced. For example, the CO and H<sub>2</sub> produced are used as feedstocks for NH<sub>3</sub>, CH<sub>3</sub>OH, oxo-alcohols and hydrocarbons (via Fischer-Tropsch). H<sub>2</sub> is required for refineries for processes such as hydrotreating and hydrocracking and also for fuel cells, hydrogenations and reducing gas<sup>12</sup>.

The H<sub>2</sub>O:C ratio of the reformer feedstock depends on the desired composition of product gas which depends on the product that the gas will eventually synthesise. Therefore, the reforming stage can be used as a means of gas preparation for the aforementioned purposes. Reactions (1) and (2) are reversible and therefore, at equilibrium there is a mixture of CH<sub>4</sub>, H<sub>2</sub>O, CO, H<sub>2</sub> and CO<sub>2</sub>. It is evident from the principle of Le Chatelier that during steam reforming at high temperatures, there will be more CO and less CH<sub>4</sub> and at high pressures the CH<sub>4</sub> content will further increase.

In most cases the product gas will be close to equilibrium and can be predicted by the use of thermodynamic calculations<sup>12</sup>. In practice, the pressure is determined by the overall layout of the process, leaving the steam:C ratio and the catalyst exit temperature as the major parameter in determination of the gas composition. Typical combinations of these parameters for common steam reforming applications are given in table 1.3<sup>15</sup>.

**Table 1.3. Calculated product gas compositions (ref. 15)**

Final Product	NH <sub>3</sub>	MeOH	Town Gas
Feedstock	CH <sub>4</sub>	CH <sub>4</sub>	naphtha
P <sub>exit</sub> / MPa	3.3	1.7	2.4
T <sub>exit</sub> / K	1073	1123	948
H <sub>2</sub> O:C <sub>n</sub> H <sub>m</sub>	3.7	3.0	2.4
H <sub>2</sub> O / vol %	44.3	32.2	45.6
H <sub>2</sub>	39.1	50.3	25.6
CO	5.0	9.5	3.3
CO <sub>2</sub>	6.0	5.4	10.1
CH <sub>4</sub>	5.5	2.6	15.4

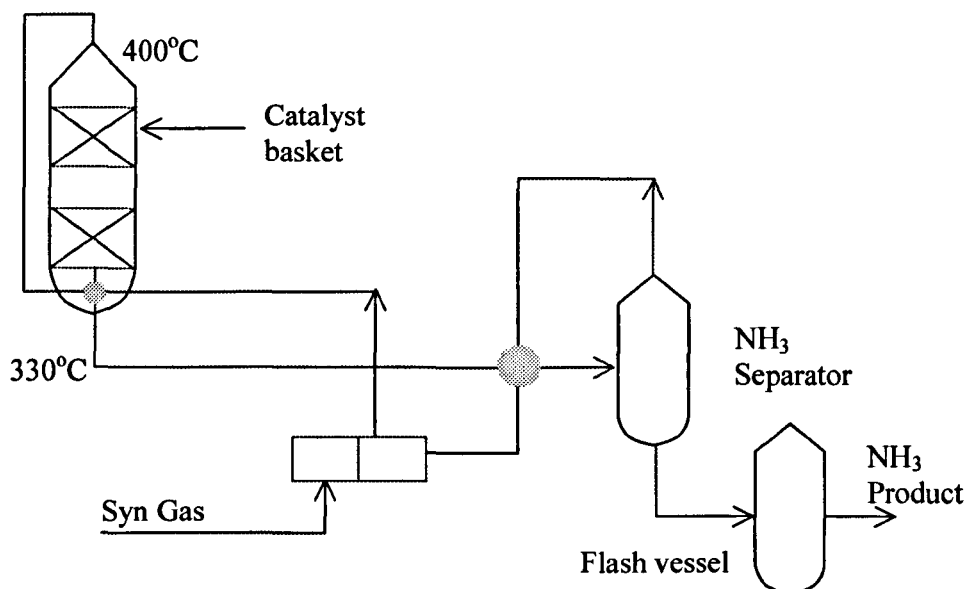
### 1.2.1 Example Applications – NH<sub>3</sub> and CH<sub>3</sub>OH Synthesis

An example of how steam reforming is utilised in industry can be described by using typical NH<sub>3</sub> and CH<sub>3</sub>OH plants as examples<sup>12, 15</sup>. A simplified diagram of the NH<sub>3</sub> synthesis plant is shown in figure 1.3.

The NH<sub>3</sub> synthesis plant uses the principle of circulating gases over the catalyst which was first appreciated by Haber in 1908. Figure 1.3 shows the synthesis loop for a typical 1000 tonnes day<sup>-1</sup> plant operating at 220 bar using a three-bed quench converter. Syn gas of the appropriate composition (table 1.3) from reforming of CH<sub>4</sub> passes through the catalyst beds and the NH<sub>3</sub> produced is condensed and recovered. Fresh make-up gas is added to the unconverted syn gas and recirculated through the catalyst. The temperature of the recirculated gas is raised up to 400°C in two stages

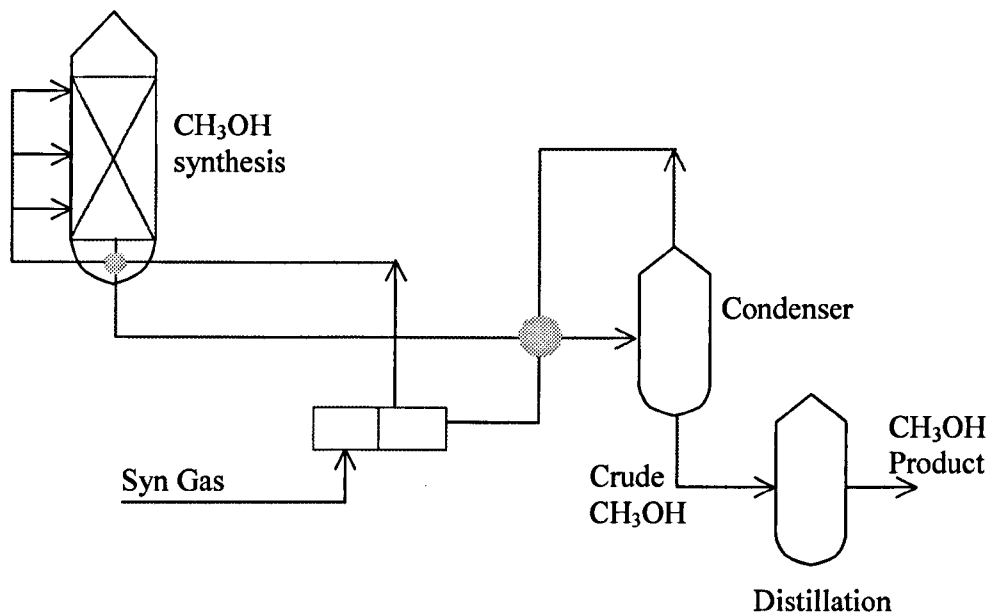
using heat exchangers and at the same time the temperature of the reactor effluent is decreased.

**Figure 1.3. Simplified diagram of natural gas based  $\text{NH}_3$  plant (ref.<sup>12</sup>)**



Another example of syn gas usage is the synthesis of  $\text{CH}_3\text{OH}$ . A simplified diagram of the process is given in figure 1.4. It is based on the recirculation loop described for  $\text{NH}_3$  synthesis. Syn gas of the appropriate composition (table 1.3) is continuously circulated through the loop in order to recycle unreacted gas. From the converter, the gases pass to the condenser which acts to remove crude  $\text{CH}_3\text{OH}$  liquor before the circulator carries the gas back to the converter. Fresh make-up gas is supplied continuously to maintain the pressure in the loop as synthesis proceeds.

**Figure 1.4. Simplified diagram of natural gas based  $\text{CH}_3\text{OH}$  plant (ref.<sup>12</sup>)**



In industry, a typical reformer consists of 40 to 400 tubes with a heated length between 6 and 12 metres that depends on the design of the furnace. The tubes are made of an alloy of Ni and Cr (Cr 25%, Ni 20%, Co 4%). The tubes are very expensive and account for a large part of the reformer costs. Reliability is important as long down time would prevent production, hence costing the company a huge amount of money<sup>15</sup>.

### 1.2.2 Steam Reforming Catalyst

There are several special requirements of a steam reforming catalyst<sup>12,15</sup>

- **Highly active:** The process requires a close approach to equilibrium at the reformer exit.
- **Low tube wall temperatures to ensure long-life:** A low activity catalyst will not fully convert the reactants hence will not absorb much heat from the furnace resulting in a short tube life

- **Constant pressure-drop:** To ensure there is equal gas-flow through each of the tubes.
- **Selectivity:** the catalyst should produce the desired products and should be resistant to reactions that form carbon.
- **Thermally and mechanically stable:** The catalyst needs to be stable under process conditions, including start-up and shut-down of the plant. Breakage of the catalyst will cause partial or full blockage of some tubes resulting in an increased pressure-drop. The gas flow into the tubes will then become uneven and result in hot-spots, hot-bands or totally hot-tubes. The eventual consequence of this is damaged tubes that must be replaced costing the industry money through down-time and replacement tubes. Particle size and shape of the catalyst is very important for control of the pressure-drop. A large particle size will minimise the pressure drop but size is limited by the need for effective packing of the tubes

Group VIII metals are all known to catalyse steam reforming of  $\text{CH}_4$  however, Ni has been well established in industry as the active component in steam reforming catalysts due to its sufficient activity, long term stability and reasonable cost. The reaction takes place on the Ni surface so a catalyst must be designed that maximises Ni surface area available to the reactants. The Ni catalysts are generally formed by impregnation of the support with a Ni salt which is calcined and subsequently reduces to the Ni metal by reduction with  $\text{H}_2$ . Impregnated catalysts are sufficiently strong to withstand reforming conditions. The temperature and pressure of the process limits the choice of support material hence, most are based on ceramic oxides or oxides stabilised with hydraulic cement. Typical supports are  $\alpha$ -alumina, magnesia, magnesium aluminium spinel and zirconia which will be discussed in more detail. Examples of the composition of commercial steam reforming catalysts are given in table 1.4. The choice of catalyst depends on the feedstock types and the operating conditions<sup>12</sup>.

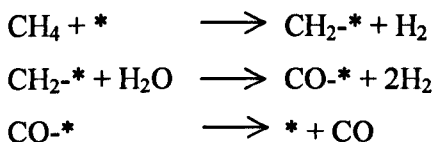
**Table 1.4. Compositions of commercial steam reforming catalysts (refs.<sup>15, 16</sup>)**

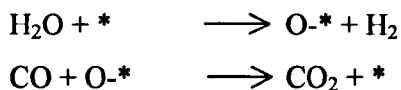
Producer	Catalyst	Feed	Components / wt%						
			NiO	Al <sub>2</sub> O <sub>3</sub>	MgO	MgAl <sub>2</sub> O <sub>4</sub>	CaO	SiO <sub>2</sub>	K <sub>2</sub> O
JM	CRG-F	naphtha	79	20-21					0.75
JM	46-3Q	naphtha	22	26	11		13	16	7
JM	57-4Q	CH <sub>4</sub>	12	78			10	0.1	
Topsoe	R-67-7H	CH <sub>4</sub>	15			85		0.1	

The size of the Ni catalyst is also an important consideration. Large size is essential in order to minimise pressure drop but should be less than 1/5 of the reformer tube diameter to ensure effective packing. The Ni particle tends to have ideal 6-fold symmetry which is stabilised by high temperatures and low catalyst dispersions<sup>15</sup>. Smith et al.<sup>17</sup> demonstrated that the Ni particle may not be a single crystal but may be composed of tetrahedra that are not completely space filling. Therefore, some lattice distortion is required and the resulting defects may play a role in the catalysis by Ni<sup>15</sup>.

The activity of a steam reforming catalyst is related to the amount of available Ni surface area which can be increased with increasing Ni content in the catalyst however the dispersion can also decrease with increasing mass of Ni, therefore, many commercial catalysts are optimised with loadings of around 15% by weight. As the size of the Ni catalyst particle increases, there are increased effects due to diffusion and heat transfer limitations resulting in a low effectiveness factor for steam reforming catalysts. Apparent activity increases as the catalyst particle is made smaller however size is limited due to pressure drop.

In a now classic study of 1964, Bodrov and co-workers<sup>18</sup> proposed a model for the reforming of CH<sub>4</sub> with steam over a Ni foil in order to eliminate any effects due to pore diffusion. CH<sub>4</sub> adsorption is assumed to be the rate-determining step (RDS):





From this they proposed a rate expression where the rate is proportional to the partial pressures of  $\text{H}_2\text{O}$ ,  $\text{CO}$  and  $\text{H}_2$ . Over a  $\text{Ni}/\text{Al}_2\text{O}_3$  catalyst, the rate was proportional to  $P_{\text{CH}_4}$  only. Studies carried out later did not support the existence of the  $\text{CH}_2\text{-*}$  species<sup>19, 20</sup> or the assumed RDS<sup>21</sup>. Other proposed models will be presented in later sections however; despite several studies, there is on-going debate over the detailed molecular-level pathways for conversion of  $\text{CH}_4$  to synthesis gas and their kinetic response to reactant concentrations.

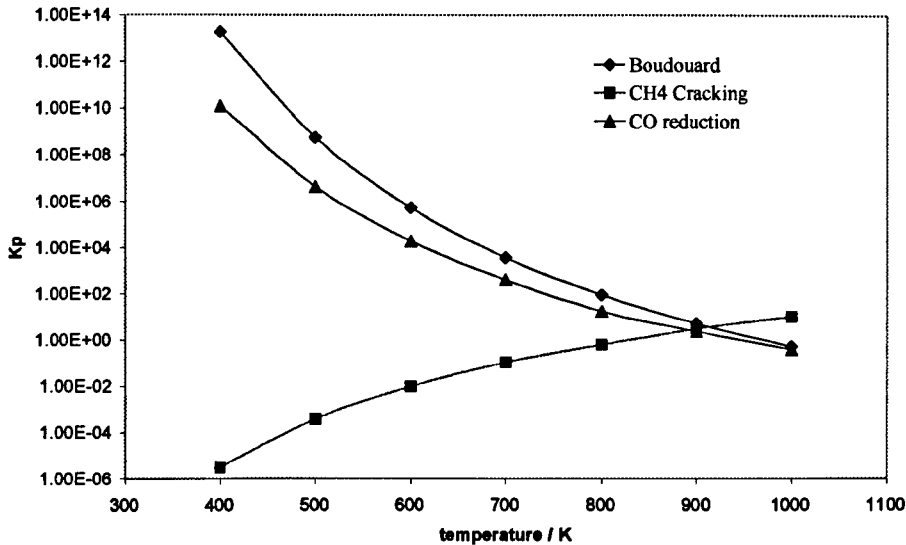
### 1.2.3 Carbon Formation

A major operational problem of the steam reforming industry is the ease at which carbon is formed over the Ni catalyst. In section 1.2, the two important reactions, (1) and (4), were introduced however three other processes, (5) to (7), are also in equilibrium under steam reforming conditions. They are known as methane cracking, Boudouard (CO disproportionation) and CO reduction respectively<sup>22</sup>.



Despite the similar thermodynamics of dry and steam reforming, the  $\text{CH}_4/\text{CO}_2$  mixture is more susceptible towards carbon formation due to the lower H/C ratio in the system<sup>22</sup>. A plot of how the equilibrium constant,  $K_p$ <sup>23</sup>, for each side-reaction varies with temperature is shown in figure 1.5. The graph shows that at temperatures greater than 900K, carbon will form more favourably from  $\text{CH}_4$  cracking, while, at temperatures less than 900K, more carbon would be expected from the Boudouard reaction.

**Figure 1.5.  $K$  vs. temperature in Kelvin for each carbon side reaction**



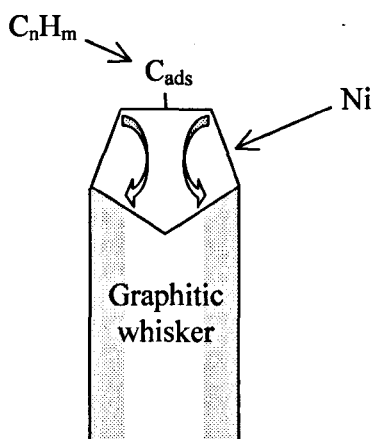
Claridge et al.<sup>24</sup> investigated the rate of carbon deposition from pure CO and pure CH<sub>4</sub> over a supported Ni catalyst at various temperatures. They found that both reactions were catalysed to an extent which depended on the process temperature. They found that after approximately 900K, carbon formation via the CH<sub>4</sub> cracking reaction was more feasible and prior to 900K, carbon was formed primarily from the Boudouard reaction. The results were in agreement with the calculated thermodynamics in figure 1.5.

### 1.2.3.1 Whisker Carbon

This is where the problem of reliability on a Ni catalyst emerges. It is particularly well established in the literature<sup>25, 26, 27, 28</sup> that Ni is prone to formation of a type of carbon under reforming conditions known as whisker carbon (also called filaments or fibres). Figure 1.6 illustrates the growth mechanism of a carbon whisker, the details of which are generally agreed throughout the literature<sup>25, 26</sup>. The hydrocarbon species (C<sub>n</sub>H<sub>m</sub>) decomposes on the active Ni surface to produce adsorbed carbon (C<sub>ads</sub>). Once the surface becomes saturated the carbon then migrates into the bulk Ni. Baker et al.<sup>29</sup> observed the growth directly and found that it had an equal rate to the estimated diffusion rate of carbon through a Ni particle. Baker et al.<sup>30</sup> later suggested that the

exothermic reaction on the Ni surface caused a temperature gradient across the Ni surface acting as a driving force for carbon diffusion. This reasoning was more recently debated by Chen et al.<sup>31</sup> who claimed there were different solubilities of carbon at the front and rear of the Ni particle which acted as a driving force. The Ni carbide is not stable under steam reforming conditions and nucleation of carbon takes place when the concentration of carbon dissolved in the Ni particle is greater than that at equilibrium. Nucleation takes place at the cold rear of particle where solubility is smaller<sup>30</sup>. The result is a long graphitic, hollow, tube-like structure with a Ni particle on the growing end. The nearly ideal shaped Ni crystal undergoes a reconstruction during whisker growth, leaving it pear-shaped which has been explained as due to the strong interaction (wetting) of Ni with graphite surfaces also observed by Baker et al.<sup>32</sup>.

**Figure 1.6. Whisker growth through diffusion of C through a Ni particle (Ref.<sup>15</sup>)**



Amidiris et al.<sup>33</sup> studied  $CH_4$  cracking over Ni/SiO<sub>2</sub> and observed that more carbon was accommodated on the catalyst than could be explained due to site-blocking or pore-mouth plugging models hence the excess carbon was explained as due to whisker formation.

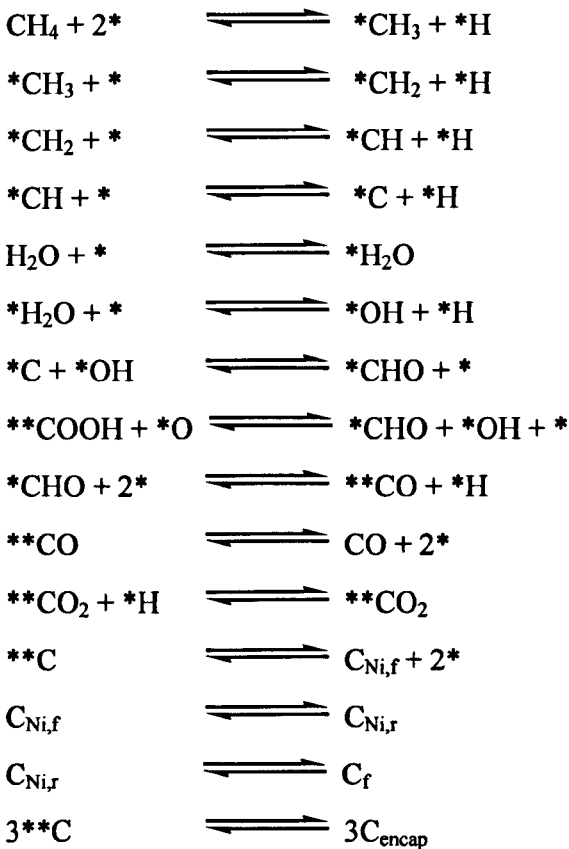
Ni catalysts are not prone to deactivation due to whisker carbon until the whiskers hit the pore walls. These spatial limitations are the only way the growth of carbon is

terminated. Whisker carbon presents the biggest worry to the steam reforming industry as it results in the breakdown of the catalyst which leads to an increased pressure drop within the tubes<sup>25</sup>. The problems associated with increasing pressure drop were discussed in section 1.2.1.

### 1.2.3.2 Modelling of Carbon Formation

Chen et al.<sup>31</sup> proposed a model as shown in scheme 1.1 for steam reforming of CH<sub>4</sub> over supported Ni catalysts accounting for elementary steps due to carbon formation. It is commonly agreed that activation of CH<sub>4</sub> on Ni involves dissociative adsorption followed by a series of dehydrogenation steps.

**Scheme 1.1. Microkinetic model for CH<sub>4</sub> reforming including carbon formation**



\* represents a site on the Ni crystallite,  $C_{Ni,f}$  is the concentration of carbon dissolved in the side of Ni in contact with  $CH_4$  and  $C_{Ni,r}$  is the concentration of carbon dissolved in the rear of the particle (filament side). All reaction is proposed to be taking place over the Ni crystallite but it will be seen later how this is not always the case. The properties of these carbons are different. They have different chemical potentials, which results in different solubility at the rear and front of the Ni particle, thus creating a driving force for the diffusion of carbon through Ni.  $C_{encap}$  is encapsulating carbon which will be discussed in a future section.

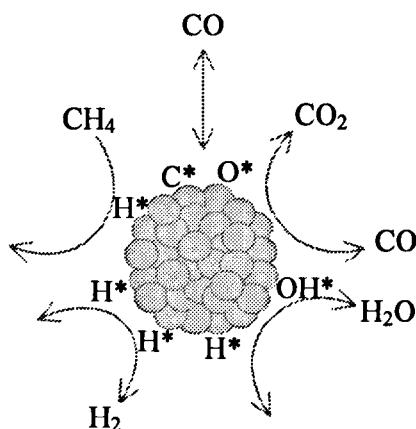
No RDS has been assumed in the model and activation energies for each elementary reaction have been calculated.

Kinetic measurements on reforming reactions are often corrupted by concentration and temperature gradients under the conditions of reforming according to Iglesia et al.<sup>34</sup>. Often, the kinetic contributions from reverse reactions that occur on the approach to equilibrium are overlooked while interpreting data. Since there are so many conflicting rate equations and reaction pathways proposed in the literature, Iglesia et al.<sup>34</sup> carried out a series of kinetic measurements during  $CO_2$  and  $H_2O$  reforming of  $CH_4$  over Ni/MgO catalysts. They interpreted their data by excluding all transport and thermodynamic artefacts and have produced a unified model of reforming,  $CH_4$  decomposition and water-gas shift corrected for approach to equilibrium and under relevant industrial conditions. They found, at a range of pressures and temperatures, that the rate of reforming and initial rate of  $CH_4$  decomposition increased linearly with increasing  $CH_4$  pressure but neither  $CO_2$  nor  $H_2O$  had any effect on reforming rate. It was also noted that the turnover rates were the same whether it was  $H_2O$  or  $CO_2$  reforming. They conclude from their results that the rate of  $CH_4/CO_2$ ,  $CH_4/H_2O$  and  $CH_4$  decomposition can be described by:

$$Rate = kP_{CH_4}$$

These results are consistent for three Ni catalysts over a range of conditions. They proposed the scheme shown in figure 1.7 for  $H_2O/CO_2$  reforming,  $CH_4$  decomposition and the water-gas-shift reaction.

**Figure 1.7. Proposed sequence of elementary steps for reforming, decomposition and water-gas-shift (reproduced from Ref. <sup>34</sup>)**



CH<sub>4</sub> decomposes to chemisorbed carbon (C\*) and hydrogen (H\*) via a series of dehydrogenation steps which become faster with each step then C\* is subsequently removed by co-reactant H<sub>2</sub>O/CO<sub>2</sub>. They found that the rate of carbon filament formation increased with increasing Ni crystallite diameter due to facile nucleation and lower thermodynamic carbon activity for larger filaments.

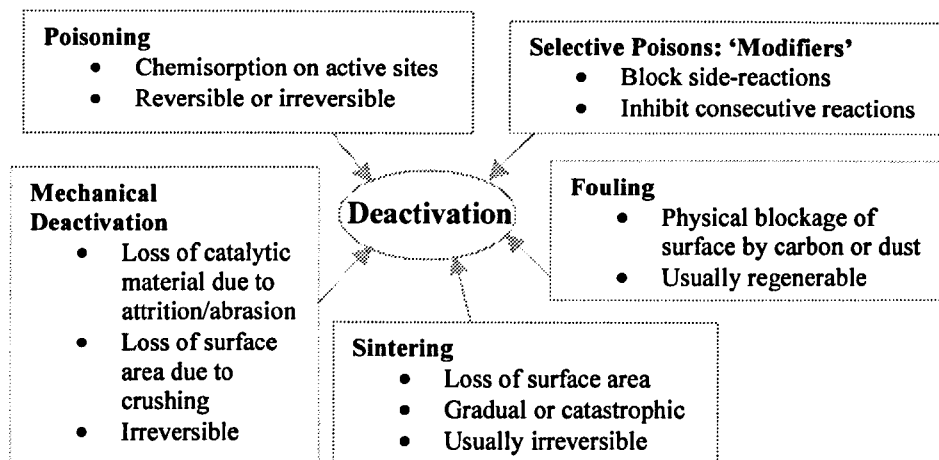
Iglesia et al.<sup>34</sup> carried out the reforming study under conditions of minimum carbon formation hence over 100 hours of reaction the Ni catalysts maintained their activity. In the case of CH<sub>4</sub> decomposition in the absence of H<sub>2</sub>O/CO<sub>2</sub>, the catalyst lost its activity with time on stream. Under these conditions the catalyst began to form whiskers but after a certain time the active Ni particles became encapsulated in carbon and as a result the catalyst deactivated.

### 1.2.3.3 Deactivation

Catalyst loss of activity with time on stream or “deactivation” is one of the major problems associated with heterogeneous catalysis. It is anticipated that a catalyst used for reforming will eventually deactivate. This process is chemical and physical in nature and occurs simultaneously with the main process. Deactivation is inevitable

in any process but it can be slowed or prevented and some of its consequences avoided<sup>35</sup>. Moulijn et al.<sup>36</sup> summarised the phenomena and their effects which inevitably lead to catalyst deactivation. The summary is shown in figure 1.8.

**Figure 1.8. Deactivation phenomena. Causes and effects. (ref. <sup>36</sup>)**



In the catalysed reforming of  $\text{CH}_4$ , the most significant form of deactivation is fouling of the catalyst surface with carbon (product of Boudouard) or coke (product of  $\text{CH}_4$  cracking). The carbon or coke then blocks active sites on the catalyst's surface and the result is a decrease in activity. Sintering can be significant in reforming due to the high temperature process conditions but deactivation is primarily due to fouling<sup>37</sup>.

Much of the recent literature concerning reforming of hydrocarbons is based around improvements in the catalyst formulation as a means of avoiding deactivation. The following sections, therefore, aim to examine other possible types of carbon, their origins and effects and also an overview in advances in catalyst formulations.

#### 1.2.3.4 Types of Carbon

Whisker carbon, particularly associated with Ni catalysts, has previously been introduced however, carbon can be formed via different routes that affect its

morphology. Six different types of carbon deposit have been reported throughout the literature<sup>15, 38, 39</sup>, they are;

**Type 1 ( $\beta$ -carbon):** Two types exist: low-density filamentous form and high-density scale carbon (polymerised amorphous carbon which exhibits domains similar to basal planes of graphite).

**Type 2 ( $\alpha$ -carbon):** 'reactive type': dispersed, isolated or diatomic surface atoms.

**Type 3 (Encapsulating polymer):** Slow polymerisation of  $C_nH_m$  radicals on Ni surface into encapsulating film.

**Type 4 (Permanently retained carbon):** crystalline elemental carbon.

**Type 5 (Bulk nickel carbide)**

**Type 6 (Pyrolytic carbon):** Thermal cracking of hydrocarbon to produce carbon precursors on catalyst surface.

Rostrup-Nielsen<sup>15</sup> summarised the main types of carbon that occur, the conditions for their occurrence and the affect they have on the reforming process. The summary is given in table 1.5.

**Table 1.5. Summary of types of carbon formed during steam reforming of hydrocarbons (reproduced from Ref. 15)**

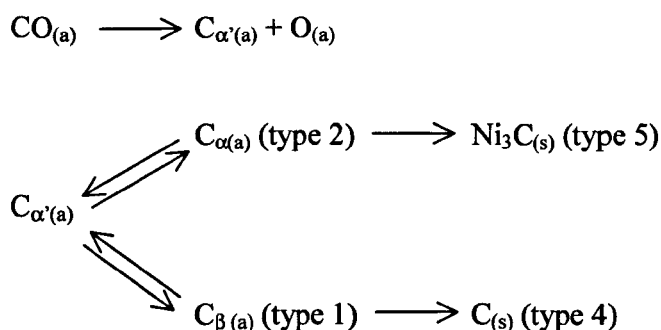
	<b>Whisker Carbon (type 1)</b>	<b>Encapsulating Polymers (type 3)</b>	<b>Pyrolytic Carbon (type 6)</b>
<b>Formation</b>	Diffusion of C through Ni particle, nucleation and crystallisation	Slow polymerisation of C <sub>n</sub> H <sub>m</sub> radicals on Ni surface into encapsulating film	Thermal cracking of hydrocarbon: deposition of C-precursors on catalyst
<b>Effects</b>	No deactivation of Ni surface: breakdown of catalyst and increasing pressure-drop	Progressive deactivation and increasing pressure-drop	Encapsulation of catalyst particle: deactivation and increasing pressure-drop
<b>Temperature Range / K</b>	> 720 K	< 770 K	> 870 K
<b>Critical Parameters</b>	High temp, low H <sub>2</sub> O:C <sub>n</sub> H <sub>m</sub>	Low temp, low H <sub>2</sub> O:C <sub>n</sub> H <sub>m</sub>	High temp, pressure, low H <sub>2</sub> O:C <sub>n</sub> H <sub>m</sub> , acidic catalyst

Jackson et al.<sup>39</sup> proposed a scheme for the formation of different surface species and types of carbon during steam reforming of hydrocarbons over a Ni/Al<sub>2</sub>O<sub>3</sub> catalyst as shown in scheme 1.2. Their proposed scheme is in good agreement with other literature<sup>38</sup>. They found that the type of carbon formed depended on the nature of the reactant hydrocarbon and the experimental conditions. Filamental (type 1) carbon was present on those catalysts where very little or no steam had been added but not to any significant amount when steam was present. The polymeric species (type 3) was the same irrespective of the presence of steam. Mass spectrometry and infrared spectroscopy revealed the structure as an extensively hydrogenated polymer with a chain length of 25-30 carbon atoms. With steam present, infrared spectroscopy also gave evidence of aldehyde groups of the type R-CHO and -CH=CH-CHO associated with the polymer chain. It was found that neither type (1) nor type (3) reacted with CO<sub>2</sub>, steam or H<sub>2</sub> but could be oxidised at high temperature through reaction with oxygen. Type (2), reactive carbon, however, did react with CO<sub>2</sub> and steam. It was suggested that this type probably exists on the surface as a carbon adatom.



Ni crystallite governed the type of surface carbon formed ( $\alpha$  or  $\beta$ ) but the rate of carbon deposition was insensitive to structure.

**Scheme 1.3. Interpretation of the interaction of CO on Ni/Al<sub>2</sub>O<sub>3</sub> catalyst, a = adspecies, s = bulk phase species. (ref. 38)**



Chen et al.<sup>40</sup> studied the formation and the characteristic properties of carbonaceous species on Ni<sub>x</sub>Mg<sub>1-x</sub>O catalysts during CO<sub>2</sub> reforming of CH<sub>4</sub>. They acknowledged that the principal reason for deactivation or destruction of the catalyst was due to carbon deposition from CH<sub>4</sub> cracking or the Boudouard reaction. From their work, they defined two types of carbon (types 1 and 2) and related the activity of the catalyst to the amount and reactivity of the 'reactive'  $\alpha$ -carbon (type 2) produced.  $\alpha$ -Carbon was defined as a combination consisting of a relatively small amount of CH<sub>x</sub> species and larger amounts of carbonate and formate species on the surface of the support. The amount of  $\beta$ -carbon increased with time especially on catalysts with high Ni -loading and on the Ni/MgO catalysts whereas  $\alpha$ -carbon did not change. Hence, these two forms of carbon played different roles, depending on the catalyst, during dry reforming of CH<sub>4</sub>.  $\beta$ -Carbon is accumulated during the reaction and is most likely to cause deactivation however; the  $\alpha$ -carbon increased the dry reforming activity of the catalyst suggesting it is a reaction intermediate.

In CO<sub>2</sub> reforming of CH<sub>4</sub>, Chen et al.<sup>40</sup> found that carbon deposition on the catalyst comes from two routes, one from CO<sub>2</sub> and the other from CH<sub>4</sub>.  $\alpha$ -Carbon was generated from CO<sub>2</sub> which reacts with H<sub>2</sub> to produce CH<sub>4</sub>. In agreement with

previous results<sup>39</sup>,  $\beta$ -carbon and  $\alpha$ -carbon were both produced from  $\text{CH}_4$  (As time on stream was increased, it was observed that  $\alpha$ -carbon aged into  $\beta$ -carbon). A similar observation was made by Bradford et al.<sup>41</sup> who proposed a reaction scheme:  $\text{CH}_4$  is initially adsorbed and activated on the Rh/MgO to form adsorbed hydrogen,  $\text{H}_{\text{ads}}$  and carbon  $(\text{CH}_x)_{\text{ads}}$ , species (where  $x = 1, 2$  and  $3$ ) before steam /  $\text{CO}_2$  mixed reforming took place.

Tomishige et al.<sup>42</sup> studied the same catalysts as Chen et al.<sup>40</sup>. It was found over Ni/MgO and  $\text{Ni}_{0.03}\text{Mg}_{0.97}\text{O}$  that on exposure to  $\text{CH}_4/\text{N}_2$  and  $\text{CO}/\text{N}_2$ , the amount of carbon only increased in the early stages of reaction then tended to be constant with time on stream. More whisker carbon was observed on the post  $\text{CH}_4$  reaction catalysts than post CO catalysts. The carbon also appeared thinner on post CO catalysts, suggesting that  $\text{CH}_4$  promoted Ni aggregation more than CO. Over NiO- $\text{Al}_2\text{O}_3$ , there was a smaller amount of whisker carbon produced and a smaller whisker diameter during  $\text{CO}/\text{N}_2$  flow. It was evident from the results that the presence of  $\text{CO}_2$  helped to perturb carbon formation.

### 1.2.3.5 Effect of Pressure

The effect that temperature has on the origin of the carbon formed has been discussed previously so for a true assessment of reforming catalysts the actual plant conditions must be considered. Armor and Martenak<sup>43</sup> studied the effect of elevated pressure on carbon formation during reforming of  $\text{CH}_4$  over a Ni/ $\text{Al}_2\text{O}_3$  steam reforming catalyst. It has been previously well established in industry that more carbon is produced at higher pressures and temperatures below  $900^\circ\text{C}$ , however, using a Tapered Element Oscillating Microbalance (TEOM), they were able to demonstrate the drastic difference between atmospheric and high pressure. It was found that after 10 minutes of reaction at atmospheric pressure,  $1 \times 10^{-3}$  g of carbon had been deposited. When the pressure was increased to 100psig, the amount of carbon deposited after 10 minutes was  $5 \times 10^{-3}$  hence five times the amount of atmospheric carbon was deposited at 100psig.

Several authors have carried out reforming studies at high pressure over Ni and the noble metals over a range of supports<sup>44, 45, 46</sup>. The same results have been reported in each case: both CH<sub>4</sub> and CO<sub>2</sub> conversion rates decreased while the rate of carbon deposition increased with increasing pressure. This leads to the question of whether the origin of carbon at atmospheric pressure is the same as that at high pressure.

Shamsi and Johnson<sup>47</sup> studied the effect on carbon formation of high and low pressure during dry reforming of CH<sub>4</sub>. They initially carried out thermodynamic calculations on the CH<sub>4</sub> cracking and Boudouard reactions that showed as pressure increased, the equilibrium amount of carbon from the CH<sub>4</sub> cracking reaction decreased while carbon from the Boudouard reaction increased. Dry reforming was carried out over a Pt/ZrO<sub>2</sub> catalyst at atmospheric and high pressure to determine the relative contributions of CH<sub>4</sub> and CO<sub>2</sub> as sources of carbon. In agreement with previous studies, it was found that the CH<sub>4</sub> and CO<sub>2</sub> conversions decrease with increasing pressure. At low pressure, it was observed that most of the carbon originated from CO<sub>2</sub> however at high pressure, CH<sub>4</sub> and CO<sub>2</sub> contributed equally. High levels of CO produced, were consistent with the Boudouard reaction being the more dominant at high pressure. The same study was conducted over Pt/Ce-ZrO<sub>2</sub>, Rh/Al<sub>2</sub>O<sub>3</sub> and Ni/La<sub>2</sub>O<sub>3</sub> and all were consistent. The carbon formation route at high pressure seems to be independent of the catalyst formulation, however, it will be discussed later how the catalyst composition can be modified to reduce the overall carbon formation.

### 1.3 Avoiding Carbon

The reforming industry is economically limited by the requirement for carbon free operation. Presently, the industry overcomes the problem by the use of an excess of steam which has two purposes: to drive the reforming reaction in favour of the products and to oxidise any deposited carbon. However using more steam than is necessary does not satisfy the environmental objectives towards a more energy efficient process moreover, superheated steam is expensive and results in a significant concentration of CO<sub>2</sub> in the product gas and the H<sub>2</sub>:CO ratio obtained is higher than

the optimum required for downstream syn gas to methanol, acetic acid and hydrocarbons. Instead, most of the recent research around reforming of hydrocarbons is concentrated on new catalytic formulations for carbon-free operation. The following subsections summarise advances in this area.

### 1.3.1 Sulfur Passivation

When CH<sub>4</sub> decomposes on active metal surface, it may decompose into carbon rather than react with steam or CO<sub>2</sub>. However the carbon-forming route can be blocked without blocking the CH<sub>4</sub> reforming route by chemisorbing sulfur onto the catalyst prior to reaction<sup>48</sup>. The effect can be explained by ensemble control: there is a certain size of Ni atom ensemble necessary for CH<sub>4</sub> dissociation into C and H<sub>2</sub> and another certain size necessary for conversion of adsorbed CH<sub>4</sub> with steam. When CH<sub>4</sub> dissociates on the Ni surface, it may be written as:



With increasing the size of the required ensemble, ie.  $m < n < p$ . In the absence of sulfur, CH<sub>4</sub> may well be completely dissociated, however at high surface coverage of sulfur the C-<sup>\*</sup>p is eliminated. The reason for the different ensemble sizes is explained in terms of surface physics: adsorbed carbon atoms result in a distortion of the local metal atom geometry<sup>49</sup> whereas, bonding of CH<sub>4</sub> may require only 3 or 4 free Ni atoms.

### 1.3.2 Alkali Dopants

The addition of an alkali-dopant to the reforming catalyst has been shown to enhance the adsorption of steam. The effect is not fully understood however, it is known that it is greater over a less-acidic support suggesting that alkalinity is important. A less acidic support has a weaker bond to the alkali-dopant resulting in easier transport (via the gas-phase) from the support to the metal.

Frusteri et al.<sup>50</sup> investigated bare and K-doped Ni/MgO during CO<sub>2</sub> reforming of CH<sub>4</sub>. The K-doped catalyst produced the least carbon and this was explained as due to electronic effects: Addition of K prevents excessive dissolution of carbon by increasing the interaction between Ni atoms and electron acceptor intermediates (O<sub>(ads)</sub>)

A more recent study by Frusteri et al.<sup>51</sup> on K-doped Ni/MgO for ethane steam reforming showed that K-addition had no effect on carbon formation but stabilised the Ni by depressing metal sintering. Again, the effect of K-doping was explained as due to a change in the electronic properties of the active phase.

Osaki et al.<sup>52</sup> reported enhanced adsorption of CO<sub>2</sub> in the dry reforming of CH<sub>4</sub> when K was added to Ni/Al<sub>2</sub>O<sub>3</sub>. They reported however that the rate of CO<sub>2</sub> dissociation to CO and O<sub>(ads)</sub> was not affected by K-addition. Therefore, increased concentration of O<sub>(ads)</sub> for carbon removal is not the route to carbon-free operation. The carbon-free properties of a K-doped Ni catalyst were ascribed to ensemble control. K plays a role in dividing the Ni surface into smaller ensembles which subsequently suppresses carbon formation.

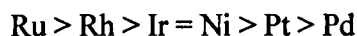
### 1.3.3 Noble Metals

It has been shown how Ni, Fe, Co and the noble metals can catalyse the reforming of natural gas to thermodynamic equilibrium<sup>15</sup> however Ni, until recently, has been the most practical. Carbon formation can be avoided by the use of noble metals as catalysts. It is well known that carbon diffusion through the noble metal does not take place hence whisker carbon formation is inhibited. It has also been shown that noble metal catalysts are more active towards steam reforming than Ni<sup>15, 53</sup>.

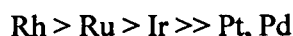
#### 1.3.3.1 Activity

During partial oxidation of CH<sub>4</sub>, Poirier et al.<sup>54</sup> found that a Ru catalyst with as little as 0.015 wt.% Ru/Al<sub>2</sub>O<sub>3</sub> gave a higher activity and selectivity than 5 wt.% Ni/SiO<sub>2</sub>. Many authors have proposed reactivity series for the noble metals for H<sub>2</sub>O/CO<sub>2</sub>

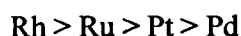
reforming and partial oxidation. The similarity for the orders of activity of the metals for H<sub>2</sub>O/CO<sub>2</sub> reforming and partial oxidation is apparent<sup>14</sup>. Rostrup-Nielsen and Bak-Hansen<sup>13</sup> compared the activity of noble metals and Ni catalysts for the dry reforming of CH<sub>4</sub>. The sequence of activity was:



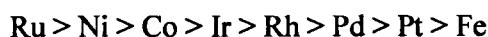
For dry reforming, Mark et al.<sup>55</sup> proposed the following similar scheme:



While, for partial oxidation of CH<sub>4</sub>, Qin et al.<sup>56</sup> proposed:



Linguras et al.<sup>57</sup> report, for low loaded catalysts during steam reforming, that Rh is far more active and selective for H<sub>2</sub> production than Ru, Pt and Pd which show a similar behaviour to each other (873-1500K). Nakagawa et al.<sup>58</sup> however, determined an order of activity of different metals at 650°C as:



In most cases Ru and Rh emerge as the most active of the noble metals.

Iglesia et al.<sup>59, 60, 61</sup> studied CO<sub>2</sub>/H<sub>2</sub>O reforming and CH<sub>4</sub> decomposition over a range of noble metals and Ni<sup>34</sup> with different metal dispersions. The exclusion of transport and thermodynamic artefacts, the rigorous correction to forward rates and the measurement of rates normalised by the relevant exposed surface metal atoms made these results a fair comparison of each metal. From calculations of CH<sub>4</sub> turnover rates, the results showed a unified order of activity of:



They claim discrepancies in the literature are, in part, due to differences in metal dispersions and to varying approaches to equilibrium. They found that turnover rates increased with increasing metal dispersion and with increasing CH<sub>4</sub> partial pressure. Partial pressures of CO<sub>2</sub>/H<sub>2</sub>O had no influence hence; as has been seen for Ni, CH<sub>4</sub> reforming reactions were described by a first order dependence on CH<sub>4</sub> and zero order dependence on CO<sub>2</sub>, H<sub>2</sub>O, CO and H<sub>2</sub>:

$$Rate = kP_{CH_4}$$

The reaction mechanism for reforming reactions over noble metals is identical to that proposed for Ni in figure 1.7 where C-H bond activation is the only kinetically relevant step.

Schuurman et al.<sup>62</sup> carried out temporal analysis of products (TAP) experiments to compare the effect of Ni versus Ru on the kinetics of dry reforming of CH<sub>4</sub>. Initially they studied Ni on SiO<sub>2</sub>, which they previously considered to be an inert support. H<sub>2</sub> was formed during a single pulse of CH<sub>4</sub> by the following step:



Two different routes were considered for the production of CO:

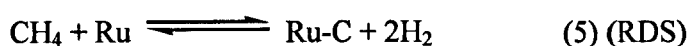


Step 3 was considered as the rate-determining step (RDS) for the reforming process over Ni/SiO<sub>2</sub>. Evidence was found that the RDS did not involve C-H bond cleavage or formation. H<sub>2</sub> from CH<sub>4</sub> cracking (step 1), is readily oxidised by the following route:



Hence, the combination of steps (2) and (4) form the water-gas shift equilibrium which is generally achieved under reforming conditions. They found that CH<sub>4</sub> activation was hindered on a highly oxidised Ni surface. Ironically, CH<sub>4</sub> conversion decreased further when no more surface oxygen was available to remove surface carbon via step 3. A geometric effect of surface poisoning by carbon deposits was accepted however they also proposed an electronic effect. Early single crystal studies show that H-metal and C-metal bonds are weakened on a carbided Ni surface due to the displacement of valency electrons of Ni to the strong Ni-C bonds of the carbide<sup>63</sup>.

Over Ru/SiO<sub>2</sub>, the same initial step was proposed, however the amount of H<sub>2</sub> produced was much larger than that produced from Ni/SiO<sub>2</sub> which suggested a much lower concentration of surface oxygen:



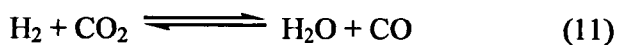
Step (5) was found to be the rate-determining step in the reaction over Ru. This point agrees well with the fact that Ru is known to maintain carbonaceous residue for longer periods than Ni<sup>62</sup>.

In contrast to the Ni catalyst, CO is produced over Ru in a single step which again suggested that no oxygen atoms were present on the Ru surface during reaction:



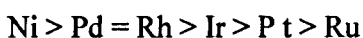
The latter discovery rules out a step equivalent to step (4) for Ru. Hence the difference in the kinetics of the two metals for CO<sub>2</sub> reforming of CH<sub>4</sub> was due to surface oxygen species.

The difference in the role of the support during the reforming reaction over Ni/Al<sub>2</sub>O<sub>3</sub> and Ru/Al<sub>2</sub>O<sub>3</sub> was again explained by surface oxygen coverage of the respective metals. High oxygen coverage of Ni would retard the spillover steps (7-9) and favour the reverse water – gas shift step (11):



### 1.3.3.2 Carbon Formation

Rostrup-Nielsen and Bak Hansen<sup>13</sup> examined CH<sub>4</sub> decomposition over different supported catalysts and found that Ni had the largest rate of carbon formation while Ru had the lowest. An HREM study on the post reaction catalysts revealed whisker carbon on Ni and Pd but not on the other catalysts. The type of carbon formed on Ru, Rh, Ir and Pt was identified. The structure was lamellar consisting of a few atomic layers of carbon that almost completely covered the catalyst surface (encapsulating carbon) and resulted in catalyst deactivation. The rate of carbon formation should be related to the different growth mechanisms ie dissolution and precipitation in Ni enhances rates and for Pd, formation of an interstitial solid solution of carbon in the metal<sup>64</sup> and its mobility enhances the rate of formation. The rate of carbon formation at 923K varied in the order:



Green et al.<sup>65</sup> showed that Ni, Ru, Rh, Pd, Pt and Ir supported on Al<sub>2</sub>O<sub>3</sub>, catalysed partial oxidation and dry reforming of CH<sub>4</sub>. Substantial carbon deposition was observed over Ni and Pd however, no macroscopic carbon deposition or catalyst deactivation was observed for the Ir and Rh catalysts.

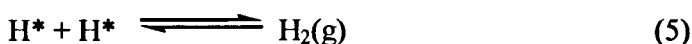
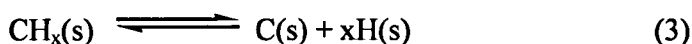
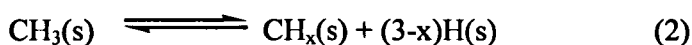
Claridge et al.<sup>66</sup> wrote a reactivity order for carbon deposition during partial oxidation of CH<sub>4</sub>. The order was:



Tsipouriari et al.<sup>67</sup> examined the types of carbon that occurred during exposure of Rh/Al<sub>2</sub>O<sub>3</sub> to CO<sub>2</sub>/He, CH<sub>4</sub>/He and CO<sub>2</sub>/CH<sub>4</sub>. During CH<sub>4</sub> decomposition (CH<sub>4</sub>/He), the initial rate was high but began to decrease as carbon was deposited on the catalyst surface. More than one monolayer of carbon was measured which suggests that it could not be atomically dispersed but rather in the form of graphite or whiskers.

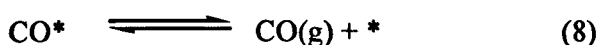
Some carbon may also have migrated from the metal to the support. Two types of carbon were identified and their structures were probed to identify them as graphitic or polymerised carbon. Both types aged into a third unreactive carbon.

They describe the decomposition by means of a reaction scheme, which is in agreement to previous schemes discussed for Ni (dissociative absorption of CH<sub>4</sub> followed by dehydrogenation steps)<sup>34</sup>:



Where \* represents an active Rh site.

When CO<sub>2</sub>/He was passed over Rh/Al<sub>2</sub>O<sub>3</sub>, much less carbon was formed. Again, two types were distinguished, both of which were more reactive than those from CH<sub>4</sub>. The main type of carbon formed is likely that of carbidic and/or small chains of carbon atoms. It is not as prone to aging as much as the species from CH<sub>4</sub>. The Rh surface is in a more reduced state during CH<sub>4</sub>/He than CO<sub>2</sub>/He exposure. In the latter case, the presence of adsorbed oxygen species may hinder the growth of adsorbed atomic carbon to whiskers or the graphite form. It may also prevent transport of carbon on the Al<sub>2</sub>O<sub>3</sub> surface. The only route for carbon deposition via CO<sub>2</sub> is outlined in the following scheme (also observed by McCarty et al.<sup>38</sup> over Ni based catalysts):



\* represents an active Rh site

During CH<sub>4</sub>/CO<sub>2</sub> exposure, three types of carbon were accumulated on the catalyst surface: a very active species (probably carbidic form) that was previously observed by Tsipouriari et al.<sup>68</sup> and a graphitic species, both of which aged into a more unreactive type.

Tsipouriari et al.<sup>69</sup> showed in earlier studies that most of the carbon formed during CO<sub>2</sub> reforming of CH<sub>4</sub> originated from the CO<sub>2</sub> molecular route. It has been shown that, over Ni based catalysts; the carbon produced is derived from both CO<sub>2</sub> and CH<sub>4</sub>. These results demonstrate the different chemistry and kinetics of carbon formation and removal over Rh and Ni catalysts.

Erdohelyi et al.<sup>70</sup> noted that during CH<sub>4</sub> cracking over a Rh/Al<sub>2</sub>O<sub>3</sub> catalyst at 473 – 573K, H<sub>2</sub>, carbonaceous residues and a small amount of C<sub>2</sub>H<sub>6</sub> were obtained. Tsipouriari et al.<sup>69</sup> did not see C<sub>2</sub>H<sub>6</sub> however this could be explained due to temperature: formation of CH<sub>3</sub> at 923K leads to rapid dehydrogenation to carbon, however at lower temperatures, two CH<sub>3</sub> species react to form C<sub>2</sub>H<sub>6</sub>. Erdohelyi et al.<sup>70</sup> also observed  $\alpha$  (type 2) and  $\beta$  (type 1) carbon and noted that the length and temperature of exposure influenced the distribution of carbon forms and their reactivity. At temperatures between 400 and 500°C, the highly reactive  $\alpha$ -carbon was missing and a large proportion of the less active,  $\beta$ -carbon was transformed into an even less reactive form (type 4).

Verykios<sup>71</sup> also studied CH<sub>4</sub> reforming over Rh/Al<sub>2</sub>O<sub>3</sub> and identified the same carbon species as that discussed for Tsipouriari et al.<sup>69</sup>. They also note that carbon produced was equivalent to a surface coverage of 0.2 at 923K of which, less than 0.02 was due to CH<sub>4</sub>.

Disagreements do however exist on the origin of the carbon. Theoretically, carbon could be produced from CH<sub>4</sub>, CO<sub>2</sub> or CO. Tsipouriari et al.<sup>68, 69</sup> and Verykios<sup>71</sup> claim carbon is formed from the dissociation of CO<sub>2</sub> while other authors who studied CO<sub>2</sub> reforming over precious metals claimed the origin was mainly CH<sub>4</sub><sup>72, 73</sup> and CO<sup>74</sup>. In terms of types of carbon formed, no report was made on any whisker carbon formation.

## 1.4 Supports

The active site of a catalytic material is on its surface and the most efficient catalysts have a large active area exposed to the reactant. One way of maximising the active surface area would be to have it present as a powder; however, heating would usually result in sintering of the particles (agglomeration of the catalyst into larger, lower surface area particles). The extent of sintering is dependent on the temperature and the time of exposure to heat. Most powders are known to sinter at temperatures of 373K so for processes such as steam reforming it is essential to attach the catalyst species to the surface of a thermostable material known as a catalyst support<sup>75</sup>.

The catalyst support acts to reduce sintering by keeping the active particles as far from each other as possible. A catalyst of low metal loading, for example, will be composed of very small metal crystallites, widely dispersed over the surface of the support. As the metal loading increases, the size of the active particles increases and they become closer together leading to an increased chance of sintering<sup>75</sup>.

Certain physical characteristics are important considerations when choosing a support for a particular process, namely: hardness, density, particle size and shape and pore volume, size and shape<sup>75</sup>.

Processes such as batch reactors, where the catalyst is stirred in liquid-phase reaction medium require a support material that is hard enough not to break up when disturbed by the propeller. The particles must also be small and light to allow suspension in the liquid. In a fixed bed process such as steam reforming, the catalyst is required to be larger pellets to minimise the pressure drop across the catalyst bed moreover, the particles must be strong enough to cope with the elevated pressure<sup>75</sup>.

In general it is desired to have maximum surface area however this is not always true. In some processes the reaction medium is a large molecule that needs large pores in order to diffuse through. A catalyst with large pores will have a smaller surface area than an equivalent catalyst with small pores<sup>75</sup>.

### 1.4.1 Supports for Reforming

In steam reforming, the choice of support is very restricted due to the high temperatures and high steam partial pressures however supports are essential for maintaining activity over prolonged periods. The specification of the support is, something strong enough to withstand the handling from manufacture, charging into the reformer and the start-up, reaction and shut down procedures: it must have a suitable shape to have sufficient surface area and pore volume to give acceptable activity while possessing low pressure-drop characteristics<sup>12</sup>.

High surface area  $\gamma$ -alumina and chromia suffer from substantial weakening and sintering at temperatures  $> 770\text{K}$  and high steam partial pressure. At high temperatures,  $\text{SiO}_2$  is volatile in the presence of steam and would be slowly removed from the catalyst and deposited in heat exchangers and reactors downstream of the catalyst. Use of alkali as a means of avoiding carbon formation would be slowly lost from the catalyst at high temperatures but may be avoided by use of acidic components ( $\text{SiO}_2$ ). Magnesia supports are stable at high temperature but are prone to hydration at low temperatures which can lead to breakdown of catalyst due to expansion of molecular volume<sup>15</sup>.

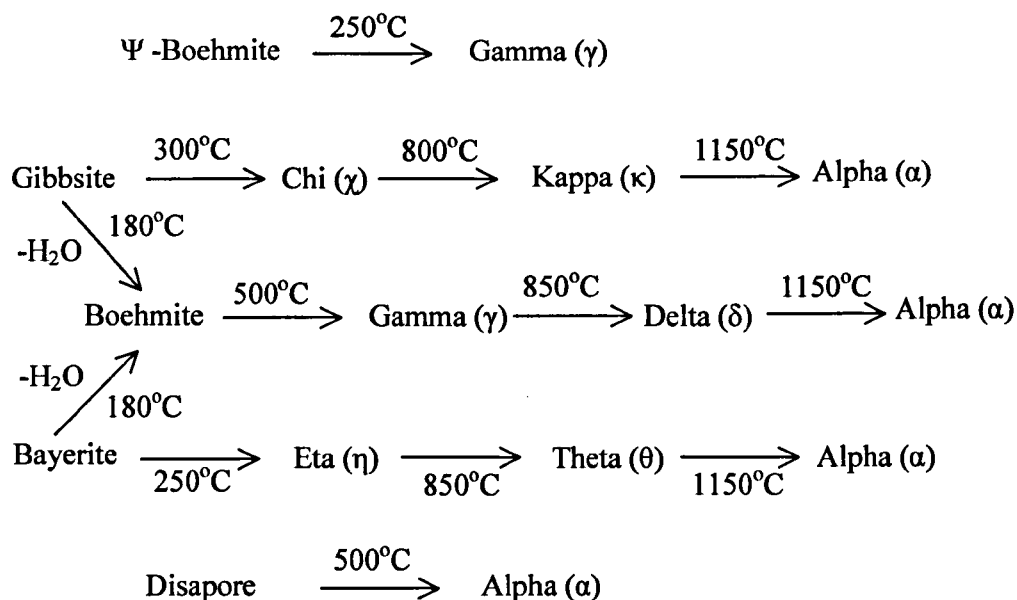
With consideration of the severe steam reforming conditions, most supports are based on oxides such as  $\alpha$ -alumina, magnesia, and zirconia that have been fired at temperatures well above  $1270\text{K}$ <sup>15</sup>.

### 1.4.2 Alumina

$\text{Al}_2\text{O}_3$  is widely used as a catalyst support material due to its ability to satisfy the surface characteristics needed for almost any process. Many types of  $\text{Al}_2\text{O}_3$  with different chemical composition and crystalline structure can be derived. Figure 1.9 shows the relationship between the different types of  $\text{Al}_2\text{O}_3$ <sup>75</sup>. There are the trihydroxides,  $\text{Al}(\text{OH})_3$ , of which Gibbsite and Bayerite are the most common. Loss of a water molecule leads to the oxyhydroxides,  $\text{AlO}(\text{OH})$ , boehmite, pseudo

boehmite ( $\Psi$ ) and disapore differing in crystalline arrangement. Complete dehydration leads to corundum or  $\alpha$ - $\text{Al}_2\text{O}_3$ .

**Figure 1.9. Relationship between the various "aluminas"**



### 1.4.3 Zirconia

$\text{ZrO}_2$  is attracting considerable interest as a support material for reforming of  $\text{CH}_4$ . As a carrier,  $\text{ZrO}_2$  gives a unique kind of interaction between the active phase and support<sup>76</sup>. It has moderate surface area, bi-functional properties of acid and base, reducing and oxidising ability and higher thermal stability<sup>77</sup>. Because of this range of properties,  $\text{ZrO}_2$  catalysts are used in reforming, hydrogenation, oxidation, polymerisation, isomerisation and environmental catalysis<sup>78</sup>.  $\text{ZrO}_2$  exhibits three well-established polymorphs: monoclinic, tetragonal and cubic phases<sup>79</sup>. The monoclinic phase is stable up to 1443 K at which temperature, it transforms into the tetragonal phase, which is stable up to 2643 K above which the cubic phase is stable<sup>78</sup>. Neither the tetragonal nor cubic phases can be retained on rapid cooling to room temperature but can be stabilised at room temperature by incorporation of different

metal cations (eg.  $\text{Mg}^{2+}$ ,  $\text{Ca}^{2+}$ ,  $\text{Sc}^{3+}$ ,  $\text{Y}^{3+}$ ,  $\text{La}^{3+}$  and  $\text{Ce}^{4+}$ ) to form solid solutions<sup>80</sup>. The amount of dopant required for stabilisation depends upon the dopant and upon the method of preparation. When the dopant cation has a lower valency than the zirconium ion (+4), oxygen vacancies are formed to preserve the lattice neutrality. The diffusion of oxygen ions is associated with the migration of lattice vacancies. Rare earth modification of  $\text{ZrO}_2$  is expected to produce useful materials for catalysts and catalytic supports. The system  $\text{ZrO}_2\text{-R}_2\text{O}_3$  (where R is a rare earth element) has been extensively examined at high temperatures in ceramic research but less as a catalyst<sup>81</sup>.

#### 1.4.4 Typical Surface Areas

Typical surface areas of common catalyst supports are given in table 1.6<sup>75</sup>.

**Table 1.6. Typical catalyst support surface areas**

Support	Surface Area ( $\text{m}^2/\text{g}$ )
$\gamma\text{-Al}_2\text{O}_3$	150-300
$\alpha\text{-Al}_2\text{O}_3$	0.1-5
$\text{SiO}_2$ Gel	200-800
$\text{SiO}_2$ (from alcohol suspension)	500-800
$\text{TiO}_2$	40-80
Graphite, natural	0.1-20

#### 1.4.5 Support Effects

The specification of a good catalyst support is that it should sustain the activity of the active metal but should not promote side reactions<sup>15</sup>. There is extensive literature available, which will be discussed in the following sub-sections, that attempts to elucidate the role of the support and assesses the affect of changing the support on the catalytic activity and selectivity during steam, dry reforming and partial oxidation of hydrocarbons. A support should not interfere with the steam reforming reaction and the authors referenced in the following sub-section have shown that it does not with

exception of the physical properties. In contrast, however, there is ample literature available on effects such as OH spillover, electronic effects, O<sub>2</sub> storage/transfer properties and carbon resistant complex formation all of which will be discussed in future sub-sections. It would appear that reported effects from the support material have a positive influence on the steam reforming process.

#### 1.4.5.1 Physical Effects

Mark et al.<sup>55</sup> studied dry reforming of CH<sub>4</sub> over Rh and Ir catalysts supported on  $\alpha/\gamma$ -Al<sub>2</sub>O<sub>3</sub>, TiO<sub>2</sub>, ZrO<sub>2</sub>, SiO<sub>2</sub>, ZrO<sub>2</sub>(5%)SiO<sub>2</sub>, Al<sub>2</sub>O<sub>3</sub>(5%)SiO<sub>2</sub> and TiO<sub>2</sub>(5%)SiO<sub>2</sub> and found that the rate of CH<sub>4</sub> conversion is independent of the nature of the support. CH<sub>4</sub> conversion rates increased with increasing metal surface area and no correlation of catalyst activity with any physical property of the support could be detected. The role of the support was limited to affecting the metal surface area during the catalyst preparation and stabilising it during the reforming reaction.

Erdohelyi et al.<sup>70</sup> studied reforming of CH<sub>4</sub> with CO<sub>2</sub> over Rh supported on Al<sub>2</sub>O<sub>3</sub>, TiO<sub>2</sub>, MgO and SiO<sub>2</sub>. They found the Al<sub>2</sub>O<sub>3</sub> catalyst to be the most active for CH<sub>4</sub> decomposition and attribute this to differences in the Rh crystallite size. The nature of the support was reported to be insignificant.

It was found by Perera et al.<sup>82</sup> that CH<sub>4</sub> conversion rates increased with increasing metal loading during dry reforming over Ru and Ir supported on Eu<sub>2</sub>O<sub>3</sub>. They compared their results to a previous study<sup>83</sup> with Ru and Ir supported on Al<sub>2</sub>O<sub>3</sub> and found that catalyst performance was similar. They conclude that the nature of the support is insignificant in the catalytic mechanism.

Iglesia et al.<sup>34, 59, 60, 61</sup> attempted to elucidate the role of the support during CO<sub>2</sub>/H<sub>2</sub>O reforming over Ni, Ru, Rh, Pt and Ir supported on a series of Al<sub>2</sub>O<sub>3</sub> and ZrO<sub>2</sub> supports. In agreement with the aforementioned results, they found that turnover rates were strongly influenced by the catalyst dispersion but essentially insensitive to the type of support.

All of the aforementioned literature agrees that catalytic activity depends only on the available surface area of the metal. The role of the support is to maximise the dispersion of the metal particles and to maintain it at high reforming temperatures. Any differences between supports are due only to their ability to disperse the metal.

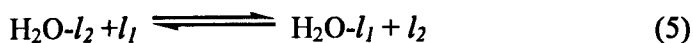
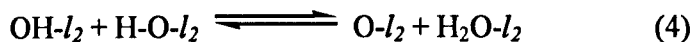
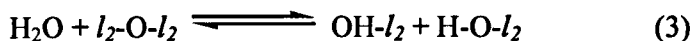
#### 1.4.5.2 Hydroxyl Spillover

It is well known that  $\gamma$ -Al<sub>2</sub>O<sub>3</sub> acts as a reservoir of hydroxyl groups due to its large concentration of acid and basic sites which favour the reverse spillover of H<sub>2</sub>O or OH groups onto the metal surface ( $\alpha$ -Al<sub>2</sub>O<sub>3</sub> is far more dehydrated). In turn, these metal hydroxyls will react fast with the carbided metal into H<sub>2</sub> and CO as proposed by Dalmon et al.<sup>84</sup> for dry reforming of CH<sub>4</sub> over Ni/Al<sub>2</sub>O<sub>3</sub>:



The OH groups are replenished by H<sub>2</sub>O that occurs during the process (most likely through reverse water-gas shift reaction).

Wang et al. proposed that H<sub>2</sub>O molecules adsorbed on the support during partial oxidation of CH<sub>4</sub> over a Rh/Al<sub>2</sub>O<sub>3</sub><sup>85</sup> and a Ru/Al<sub>2</sub>O<sub>3</sub><sup>86</sup> catalyst take place in the reaction mechanism. The mechanism on the support, similar to steps (1) and (2) is written as:



Where  $l_1$  and  $l_2$  represent respectively a Rh site and an Al<sub>2</sub>O<sub>3</sub> site.

Elementary step (5) shows how H<sub>2</sub>O spills over from the support to the Rh metal (reverse spillover) and this was proposed to take place between temperatures of 723

and 1023K. When H<sub>2</sub>O adsorbs onto the metal it dissociates into O<sub>(ad)</sub> and OH<sub>(ad)</sub> which then act to oxidise adsorbed CH<sub>x</sub> species before it dissociates into C and H<sub>2</sub>.

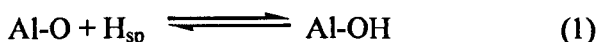
Schuurmaan et al.<sup>87</sup> also noted a major role of the support during dry reforming of CH<sub>4</sub> over Al<sub>2</sub>O<sub>3</sub> and SiO<sub>2</sub> supported metals. SiO<sub>2</sub> was inert as a support, whereas Al<sub>2</sub>O<sub>3</sub> supported catalysts had enhanced activity attributed to inverse spillover of H<sub>2</sub>O and OH groups. They also noted that Al<sub>2</sub>O<sub>3</sub> acted as a reservoir for reversible CO<sub>2</sub> and/or CO which has been previously reported<sup>88,89</sup>. They proposed the following equilibria, which are probably established with the acid/base groups on the Al<sub>2</sub>O<sub>3</sub>.



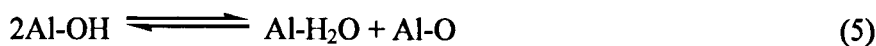
#### 1.4.5.3 Hydrogen Spillover

During CO<sub>2</sub> reforming of CH<sub>4</sub> over a Ni/γ-Al<sub>2</sub>O<sub>3</sub> catalyst, Cheng et al.<sup>90</sup> reported the occurrence of hydrogen spillover from metal to support which has proved to be a widely occurring phenomenon in the past<sup>91, 92</sup>. It is likely that the amount of spilt over hydrogen onto catalyst supports depends upon the supported metal, support acidity and thermal treatment of the catalyst. According to several authors<sup>93, 94, 95</sup>, spilt over hydrogen onto the Al<sub>2</sub>O<sub>3</sub> is in the form of Al-O<sub>(s)</sub>-H<sub>(sp)</sub> ((s)-support, (sp)-spilt over species) and plays a role in the catalysis of the reforming reaction. The proposed mechanism is as follows:

Reversible dissociation of CH<sub>4</sub> to yield CH<sub>x</sub> species and H on Ni<sup>0</sup> with a large portion of the H spilt onto the support:



H-promoted CO<sub>2</sub> dissociation occurred mainly on the support. The reaction on the support may be expressed as follows:



Where \* represents the oxygen vacancy and Eq. (2) is assisted by the spilt over hydrogen.

Finally, reaction of the  $\text{CH}_x$  species with  $\text{H}_2\text{O}$  to yield  $\text{CH}_x\text{O}$  and  $\text{H}_2$ ;  $\text{CH}_x\text{O}$  decomposition in the metal-support interfacial region to yield  $\text{H}_2$  and  $\text{CO}$ . The  $\text{H}_2\text{O}$  mainly comes from the support and migrates to the metal-support interfacial region as was discussed in the previous section.

#### 1.4.5.4 Electronic Effects

Results presented by Souza et al.<sup>96</sup> and Seshan et al.<sup>97, 98</sup> during  $\text{CO}_2$  reforming of  $\text{CH}_4$  over  $\text{Pt}/\text{Al}_2\text{O}_3$  and  $\text{Pt}/\text{ZrO}_2$  catalysts showed that the support had a decisive role on the activity and the stability of the catalyst. They found that the  $\text{Al}_2\text{O}_3$  supported catalyst deactivated due to fouling of the catalyst with carbon whereas the  $\text{ZrO}_2$  produced very little carbon and as a result maintained its stability for longer periods. Souza et al.<sup>96</sup> proposed three possible explanations for the difference in behaviour: the first was a difference in active metal dispersion, which has been previously claimed to be of paramount importance (section 1.4.4.1), The possibility of sintering was disregarded. The other two explanations were related to the surface acidity/basicity of the support and an interaction of Pt with  $\text{Zr}^{n+}$ . In a previous study, van Keulen et al.<sup>99</sup> proposed that the stability of the  $\text{ZrO}_2$  supported catalyst is attributed to the formation of a Pt-Zr surface alloy that helps to maintain a high Pt dispersion at high temperatures however, Stagg et al.<sup>100</sup> disagreed, providing EXAFS evidence that Pt is in an unmodified metallic state. Souza et al. therefore suggested that the high stability of  $\text{Pt}/\text{ZrO}_2$  and in a later study,  $\text{Pt}/\text{CeO}_2$ <sup>101</sup> is due to strong Pt- $\text{Zr}^{n+}/\text{Pt-Ce}^{n+}$  interactions and provide evidence for the existence of a  $\text{ZrO}_x$  species after reduction which may decorate the Pt surface and diminish  $\text{H}_2$  chemisorption

capacity. This effect is known as a 'strong metal support interaction' (SMSI) and has more often been observed on TiO<sub>2</sub> supported catalysts. Chemisorption results by Souza et al.<sup>96</sup> clearly showed that Pt-Zr<sup>n+</sup>/Pt-Ce<sup>n+</sup> interactions modified the CO adsorption capability on Pt in agreement with work carried out on Pt by Roberts et al.<sup>102</sup>. The effect was a decrease in the CO-Pt bond strength indicating that ZrO<sub>2</sub> inhibits CO disproportionation (Boudouard reaction).

It was also suggested by Souza et al.<sup>96</sup> that carbon suppression on ZrO<sub>2</sub> catalysts might be due to ensemble control. Theoretical calculations have shown that CO<sup>103</sup> and CH<sub>4</sub><sup>104</sup> decomposition require an ensemble of four or five metal atoms; therefore the presence of ZrO<sub>x</sub> species over the Pt surface decreases the number of large ensembles and subsequently inhibits CO/CH<sub>4</sub> dissociation.

It has been previously suggested that the stability of the ZrO<sub>2</sub> catalyst is due to its strong Lewis basicity<sup>105, 106</sup>. Increasing the Lewis basicity of the support increases the ability of the support to adsorb CO<sub>2</sub>, which in turn reduces carbon deposition via Boudouard reaction. The electron transfer from Pt to partially reduced ZrO<sub>2</sub> increases the basicity of the support. Narbeshuber et al.<sup>107</sup>, Masai et al.<sup>108</sup> and Bitter et al.<sup>109</sup> showed that the presence of Lewis acid sites facilitated the cleavage of C-H bonds of CH<sub>4</sub>, and hence, carbon formation however, Pt seemed to selectively block Lewis acid sites on ZrO<sub>2</sub> but not on Al<sub>2</sub>O<sub>3</sub>. Bitter et al.<sup>109</sup> related the ease of carbon formation on  $\gamma$ -Al<sub>2</sub>O<sub>3</sub> to ease of H<sub>2</sub> desorption: In the absence of Pt, coking on the support is limited by desorption of H<sub>2</sub> formed and when Pt is added H<sub>2</sub> desorption is enhanced via recombination on Pt. According to several authors<sup>110, 111, 112</sup> hydrocarbon activation on oxidic materials is strictly related to the nature, concentration and strength of the acid sites. The results of Souza et al.<sup>96</sup> showed a greater number of Lewis acid sites on Pt/ZrO<sub>2</sub> but less carbon formation therefore they claimed that there was not a straight relation between Lewis acidity of the support and carbon deposition.

Bitter et al.<sup>113, 114</sup> suggested that the ability to activate CO<sub>2</sub> (as carbonate) on the support material is essential for high activity and it has been shown that the heat of CO<sub>2</sub> adsorption varies with the support<sup>115</sup>. The heat of CO<sub>2</sub> adsorption varies in the

order  $\text{ZrO}_2 < \text{TiO}_2 = \gamma\text{-Al}_2\text{O}_3$  hence carbonates formed on  $\text{TiO}_2$  and  $\gamma\text{-Al}_2\text{O}_3$  are less stable resulting in fewer or less reactive forms. This, in turn, lowers the rate of carbon removal without influencing the rate of carbon formation (mainly determined by the pure metal).

Despite its ability to avoid deactivation through carbon fouling, Souza et al. found that  $\text{CH}_4$  turn over frequency (TOF) values were lower on  $\text{Pt/ZrO}_2$  than  $\text{Pt/Al}_2\text{O}_3$  and this was attributed to  $\text{CH}_4$  activation. C-H bond cleavage requires electron donation but since a Pt particle is electron deficient in a  $\text{Pt/ZrO}_2$  catalyst, its ability to cleave the C-H bond is decreased.

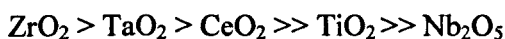
Wang et al.<sup>116</sup> compared the effect of reducible ( $\text{CeO}_2$ ,  $\text{Nb}_2\text{O}_5$ ,  $\text{Ta}_2\text{O}_5$ ,  $\text{TiO}_2$  and  $\text{ZrO}_2$ ) and irreducible ( $\gamma\text{-Al}_2\text{O}_3$ ,  $\text{La}_2\text{O}_3$ ,  $\text{MgO}$ ,  $\text{SiO}_2$  and  $\text{Y}_2\text{O}_3$ ) supports on  $\text{CO}_2$  reforming of  $\text{CH}_4$  over Rh catalysts. They reported how the activity of the catalysts was strongly dependent on the support. In general greater conversions and yields were obtained over the irreducible support catalysts as was previously observed for partial oxidation of  $\text{CH}_4$ <sup>117</sup>. It was observed that, prior to reduction of all catalysts, the surface areas of the reducible catalysts were less than the irreducible catalysts and this has been attributed to a covering of the Rh metal particles with partially reduced oxide species. Based on TPR results, Wang et al.<sup>116</sup> reported the reducibility of the reducible oxides in the order:



And the initial activity of the series decreases in the order:



Hence, with the exception of  $\text{ZrO}_2$ , the activity sequence is opposite to that of the reducibility. After 50 hours on stream the sequence of activity changed to:



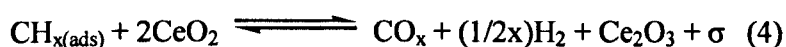
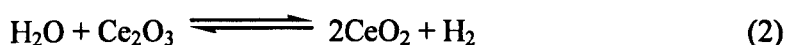
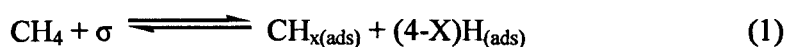
ZrO<sub>2</sub> and CeO<sub>2</sub> exhibited very long activation periods which were dependent on time on stream. This dependence is a typical feature of the reducible oxide supported Rh catalysts. It may have occurred due to an effect between the partially reduced oxide and metallic sites or because the reoxidation of the partially reduced species by the oxygen from CO<sub>2</sub> decreased the surface free energy over the particle and the new species migrated back to the surface of the substrate, thus exposing a larger number of sites. In summary, Nb<sub>2</sub>O<sub>5</sub> had a low activity, ZrO<sub>2</sub> and CeO<sub>2</sub> had a long activation period and deactivation occurred over Ta<sub>2</sub>O<sub>5</sub> and TiO<sub>2</sub>. Wang et al.<sup>116</sup> therefore claim that the reducible oxides are unsuitable as Rh supports for CO<sub>2</sub> reforming of CH<sub>4</sub>. For the irreducible oxides the sequence of activity was:



SiO<sub>2</sub> and Y<sub>2</sub>O<sub>3</sub> were shown to deactivate so MgO and  $\gamma$ -Al<sub>2</sub>O<sub>3</sub> emerged as the most suitable catalysts. Wang et al.<sup>116</sup> reported a strong interaction between rhodium oxide and La<sub>2</sub>O<sub>3</sub> or MgO to produce LaRhO<sub>3</sub> and MgRh<sub>2</sub>O<sub>4</sub>. With the exception of  $\gamma$ -Al<sub>2</sub>O<sub>3</sub>, all non-complex forming catalysts suffered decay in activity during reaction. No exact explanation is offered for the anomalous behaviour of  $\gamma$ -Al<sub>2</sub>O<sub>3</sub> but it is suggested that some non-compound forming interactions take place between Rh and  $\gamma$ -Al<sub>2</sub>O<sub>3</sub> that are sufficiently strong to ensure the stability of the catalyst.

#### 1.4.5.5 Oxygen Storage and Transfer

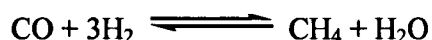
Wang et al.<sup>118</sup> found that Pd/CeO<sub>2</sub> had a greater rate of hydrocarbon steam reforming than Pd/Al<sub>2</sub>O<sub>3</sub>. They attributed their findings to the following dual-function mechanism of the catalyst whereby CeO<sub>2</sub> transferred oxygen to the supported metal and was in turn re-oxidised by H<sub>2</sub>O<sup>119</sup>.



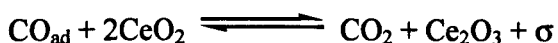
This ability of  $\text{CeO}_2$  to transfer oxygen to the metal is likely to maintain a surface that is relatively free of carbon. This phenomenon on  $\text{CeO}_2$  supported catalysts has been well documented in the literature for  $\text{H}_2\text{O}/\text{CO}_2$  reforming and partial oxidation<sup>120, 121, 122, 123</sup>

The previous section discussed and confirmed the stability of  $\text{Pt}/\text{ZrO}_2$  for  $\text{CO}_2$  reforming of  $\text{CH}_4$ . Mattos et al.<sup>124</sup> studied the affect of support material on Pt catalysts for partial oxidation and dry reforming of  $\text{CH}_4$ . The catalysts studied were  $\text{Pt}/\text{Al}_2\text{O}_3$ ,  $\text{Pt}/\text{ZrO}_2$  and  $\text{Pt}/\text{Ce-ZrO}_2$ . During partial oxidation, a strong deactivation was witnessed for  $\text{Pt}/\text{Al}_2\text{O}_3$  and  $\text{Pt}/\text{ZrO}_2$  but no deactivation within 24 hours was seen for  $\text{Pt}/\text{Ce-ZrO}_2$ . During  $\text{CO}_2$  reforming, both  $\text{ZrO}_2$  catalysts had much higher initial activity than the  $\text{Al}_2\text{O}_3$  catalyst. Over the 20 hours of reaction, the  $\text{Al}_2\text{O}_3$  catalyst rapidly deactivated due to coke formation; the  $\text{ZrO}_2$  catalyst only partially deactivated and the  $\text{Ce-ZrO}_2$  catalyst hardly deactivated at all. The observation was explained according to the  $\text{CO}_2$  reforming mechanism: the first stage of the reaction is the decomposition of  $\text{CH}_4$  on the metal surface. According to the  $\text{CH}_4$  cracking reaction, this forms C and  $\text{H}_2$ . At this point the  $\text{Al}_2\text{O}_3$  catalyst began to deactivate while for the others, a different mechanism was proposed: The carbon formed partially reduced the oxide support near the metal particles producing  $\text{CO}_x$  species and oxygen vacancies (in the absence of a reducible oxide, carbon will deposit on the metal). The second stage involved the dissociation of  $\text{CO}_2$  on the support producing CO and O to re-oxidise the support. The oxygen vacancies were then replenished enabling the support to carry out the redox mechanism for continual cleaning. The stability of a reforming catalyst is dependent on its ability to balance  $\text{CH}_4$  decomposition with oxygen transfer. It was shown in this work how the addition of Ce to  $\text{ZrO}_2$  resulted in a support ( $\text{Ce}_{0.75}\text{Zr}_{0.25}\text{O}_2$ ) with a greater number of oxygen vacancies in the proximity of the metal particles and a faster rate of oxygen transfer to the metal. A study by Noronha et al.<sup>125</sup> agreed that the increased stability of the  $\text{Ce-ZrO}_2$  supported catalyst was due to a higher density of O atoms on the support which favoured cleaning of the metal particle. They reported however, that an increase in total pressure or the  $\text{CH}_4:\text{CO}_2$  ratio resulted in deactivation of the  $\text{Ce-ZrO}_2$  catalyst since the rate of  $\text{CH}_4$  decomposition became greater than the rate of oxygen transfer.

Mizuno et al.<sup>126</sup> studied the affect of several supported Rh catalysts (CeO<sub>2</sub>, Al<sub>2</sub>O<sub>3</sub>, SiO<sub>2</sub>, ZrO<sub>2</sub>, MgO and TiO<sub>2</sub>) on the steam reforming of 2-propanol (IPA) at 673K. It was found that the catalytic properties of Rh were strongly dependent on the support and Rh/CeO<sub>2</sub> resulted in the highest IPA steam reforming activity. At higher temperatures, there was no difference observed in catalyst stability over the six-hour reaction period. The CeO<sub>2</sub>, Al<sub>2</sub>O<sub>3</sub> and SiO<sub>2</sub> catalysts produced relatively large amounts of CH<sub>4</sub> and this was shown from previous work<sup>127</sup> to be due to methanation of CO.



The selectivity of steam reforming of IPA over ZrO<sub>2</sub> and MgO catalysts was less than the Al<sub>2</sub>O<sub>3</sub> catalyst and instead both produced relatively large amounts of H<sub>2</sub> which was attributed to dehydrogenation of IPA. The acidity and basicity of the supports was considered for an explanation of the differences in reaction products but was found to have no influence. By comparison of the mean Rh particle size, surface areas and the products ratios of each catalyst, it was concluded that the product ratio is independent on the surface area and mean Rh particle size. It was therefore concluded that the difference in performance of each catalyst was a direct result of metal-support interactions. These interactions may be due to metal-support electronic interactions or to an effect of coverage of the metal particles by support sub-oxide species or to both. It was shown how ZrO<sub>2</sub>, MgO and TiO<sub>2</sub> had a selectivity for C<sub>3</sub> compounds which was attributed to partial transfer of electrons from the support to the metal resulting in a low ability for C-C cleavage. Rh/CeO<sub>2</sub> was the most stable (least deactivation) and produced the least amount of carbon during the steam reforming reaction. This has been explained due to the high reducibility of the support and its ability to mitigate coke. A mechanism has been proposed for the mitigation:



Where  $\sigma$  is an adsorption site on the metal or support. The use of CO in this mechanism means it is not available to form Boudouard carbon.

Rh/Al<sub>2</sub>O<sub>3</sub> however, deposited large amounts of coke during the reaction but was as stable as Rh/CeO<sub>2</sub>. This was accredited to its high dispersion.

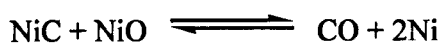
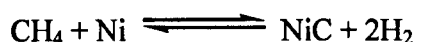
Roh et al.<sup>78</sup> studied the effect of doping ZrO<sub>2</sub> with Ce<sup>4+</sup>, La<sup>3+</sup> and Si<sup>4+</sup> on H<sub>2</sub>O reforming of CH<sub>4</sub>. It was found that doping increased the catalyst surface area but decreased the dispersion. The % CH<sub>4</sub> conversion values for Ni/Ce-ZrO<sub>2</sub>, Ni/La-ZrO<sub>2</sub> and Ni/Si-ZrO<sub>2</sub> were 97, 75 and 65% respectively however no comparison was made to non-doped ZrO<sub>2</sub>. Ce was therefore the best modifier of ZrO<sub>2</sub> and it was reported that this support played a role in providing active sites to adsorb H<sub>2</sub>O and in assisting coke removal. Zhuang et al.<sup>128</sup> had previously reported that CeOx enhanced the dissociation of H<sub>2</sub>O and accelerated the reaction of steam with adsorbed species on the Ni surface near the boundary area between metal and support thus decreasing carbon deposition.

#### 1.4.5.6 Complex Formation

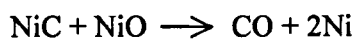
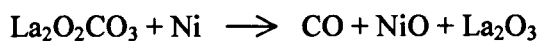
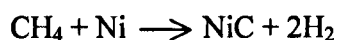
Verykios et al. prepared a novel Ni/La<sub>2</sub>O<sub>3</sub> catalyst<sup>129</sup> and compared its performance with other supported Ni catalysts (CaO and Al<sub>2</sub>O<sub>3</sub>) during CO<sub>2</sub> reforming of CH<sub>4</sub> and reported that the nature of the support had a significant effect<sup>130</sup>. They observed that Al<sub>2</sub>O<sub>3</sub> and CaO catalysts suffered from continuous deactivation while the La<sub>2</sub>O<sub>3</sub> catalyst was stable for the entire reaction. They also noted that the rate of reaction increased with time on stream over the La<sub>2</sub>O<sub>3</sub> supported catalyst. Chemisorption studies showed that the La<sub>2</sub>O<sub>3</sub> catalyst was not highly dispersed with large Ni particle size. In previous studies for methanol synthesis, Bell et al.<sup>131, 132, 133</sup> showed that a portion of La<sub>2</sub>O<sub>3</sub> support material covered the Pd metal (eg LaO<sub>x</sub>) and resulted in high activity and selectivity. Verykios et al. showed that this species interacted with metallic Ni to form a new type of complex at the interfacial area which suppressed H<sub>2</sub> and CO chemisorption. The complex was La<sub>2</sub>O<sub>2</sub>CO<sub>3</sub> and was formed through interaction of CO<sub>2</sub> and La<sub>2</sub>O<sub>3</sub> after 30 minutes of time on stream. Verykios et al. proposed that under CO<sub>2</sub> reforming conditions, CH<sub>4</sub> mainly cracked on the metallic

Ni surface to form  $H_2$  and surface carbon species ( $CH_x$ ), while  $CO_2$  preferentially adsorbs on the  $La_2O_3$  support to form  $La_2O_2CO_3$ . At high temperatures, the oxygen species of the complex may participate in reactions with the adsorbed carbon species on the neighbouring Ni sites to form CO thus offering active and stable performance. Over  $Ni/Al_2O_3$ , carbon deposition on the Ni crystallites resulted in deactivation of the catalyst. The slow initial rate of reaction has been attributed to slow establishment of the equilibrium concentration of the  $La_2O_2CO_3$  complex as well as other carbon species on the Ni crystallites.

$SiO_2$  is known to be an inert support during  $CO_2$  reforming of  $CH_4$ .  $Ni/SiO_2$  was called a “monofunctional” catalyst as both  $CH_4$  and  $CO_2$  activations occur directly from the metal surface. The following scheme summarises the elementary steps involved<sup>134</sup>:



In contrast, Verykios et al.<sup>135, 136</sup> proposed a mechanistic scheme for the “bi-functional”  $Ni/La_2CO_3$  catalyst, so called since  $CH_4$  is activated over Ni while  $La_2O_3$  activates the  $CO_2$ . The proposed scheme is as follows:



## 1.5 Project Aim

Carbon-forming reactions (5,6 and 7) are known to take place during steam reforming of CH<sub>4</sub>.



Ni is traditionally used as the steam reforming catalyst as it is sufficiently active and of reasonable cost. The most serious problem associated with Ni is its affinity for whisker carbon formation. It has been discussed in a previous section that whisker carbon causes the Ni catalyst to break down leading to a pressure drop and the eventual ruin of the reformer tubes. In order to avoid this, an excess of steam is applied to the system to remove any deposited carbon. Excess steam is not cost or energy effective causing environmental concern and therefore a more efficient catalyst system is required. It has been shown that much research is underway into new catalyst formulations for reforming. In particular catalysts can be passivated with sulfur, doped with alkali or rely on a variance of support effects as discussed in section 1. Another possibility is to replace the traditional Ni catalyst with noble metals as they have been shown to be more active for reforming and to have a greater resistance to carbon deposition. Most importantly, the carbon they form is not whisker-like.

The aim of the current project was to use each of the carbon-forming side-reactions to compare the behaviour of a series of supported noble metal catalysts, namely Rh, Pt and Ru. The conditions were to be as close to steam reforming as possible (high temperature, high pressure and continuous flow) although no steam was to be present.

The catalysts were to be made on two different supports, Al<sub>2</sub>O<sub>3</sub> and La-ZrO<sub>2</sub> and any aspects of the supports, which may affect the results, were to be considered. Two Ni catalysts were also to be prepared to act as a standard for comparison. Required

kinetic information included, reaction rates, reactant conversions and mechanistic schemes.

## 2 Experimental

### 2.1 Catalyst Preparation

The project required the preparation of a series of supported precious metal (Pt, Rh, and Ru) and Ni catalysts. Two catalysts were made from each metal, one supported on La stabilised ZrO<sub>2</sub> (La-ZrO<sub>2</sub>) and the other supported on dispersal Al<sub>2</sub>O<sub>3</sub>.

#### 2.1.1 Properties of Supports

Disperal Al<sub>2</sub>O<sub>3</sub> is an acid dispersible material with a Boehmite crystal structure. A chemical analysis from the manufacturer is given in table 2.1.

**Table 2.1. Chemical analysis of Disperal Al<sub>2</sub>O<sub>3</sub> Support**

Chemical Analysis	Typical data %
Al <sub>2</sub> O <sub>3</sub>	75
C	0.4
ScO <sub>2</sub>	0.022
Fe <sub>2</sub> O <sub>3</sub>	0.016
Na <sub>2</sub> O	0.002

The chemical analysis of the La-ZrO<sub>2</sub> support from the manufacturer is given in table 2.2. XRD phase analysis showed that the structure of the support was tetragonal ZrO<sub>2</sub> and La<sub>2</sub>Zr<sub>2</sub>O<sub>7</sub>.

**Table 2.2. Chemical analysis of La-ZrO<sub>2</sub> Support**

Chemical Analysis	Typical data %
ZrO <sub>2</sub>	80
La <sub>2</sub> O <sub>3</sub>	20
CeO <sub>2</sub>	0.1
Nd <sub>2</sub> O <sub>3</sub>	<0.1
SO <sub>3</sub>	<0.1

### 2.1.2 Catalyst Support Preparation

Both of the catalyst supports were purchased as fine powders but the required form was granular of diameter 1.003-1.400 mm. They were converted to granules before catalyst impregnation then heated to high temperature (1200K) to maintain their physical stability.

To convert the powders to granules: Several 50ml portions of water and a few drops of BDX surfactant were gradually mixed with 500g of Disperal Al<sub>2</sub>O<sub>3</sub> powder / (La-ZrO<sub>2</sub> powder) using a Kenwood electric food processor. After approximately 300ml of water, the powder was saturated. Dry powder was gradually added back to mixture until it became granular in appearance. Mixing was stopped and granules of the desired diameter were separated using a sieve. The remaining mixture continued stirring and when necessary more water was added. When a satisfactory yield of granules was obtained from the mixture, they were fired in the kiln at the temperatures shown in table 2.3.

*Table 2.3. Temperature programmes used during catalyst support synthesis*

Support	Stage	Final Temp/K	Ramp Time/hrs	Hold Time/hrs
Al <sub>2</sub> O <sub>3</sub>	1	1173	8	2
La-ZrO <sub>2</sub>	1	1373	10	1
	2	1473	3	5

### 2.1.3 Support Impregnation

The catalysts were prepared by impregnating the pre-dried support to incipient wetness with an aqueous solution containing the precursor salt. The wet catalyst was then oven dried before calcination. The metal precursors of the catalysts are listed in table 2.4.

**Table 2.4. Metal precursors**

Catalyst	Precursor
Ni	Ni(NO <sub>3</sub> ) <sub>2</sub>
Ru	Ru(NO)(NO <sub>3</sub> ) <sub>3</sub>
Pt	H <sub>2</sub> PtCl <sub>6</sub>
Rh	Rh(NO <sub>3</sub> ) <sub>2</sub>

To ensure uniform and maximum metal dispersion throughout the support, the precursor salt was dissolved in a volume of water equal to the support pore volume.

By measuring the volume of water necessary to fully saturate a 3g sample of each support, the support pore volumes were determined. The determined pore volumes are given in table 2.5

**Table 2.5. Pore volumes of catalyst supports**

Support	Pore Volume / (cm <sup>3</sup> /g <sup>-1</sup> )
Al <sub>2</sub> O <sub>3</sub>	1
La-ZrO <sub>2</sub>	0.4

From the values obtained in table 2.5, it was known that 100 ml of water would fully saturate 100g of Al<sub>2</sub>O<sub>3</sub> support and 40ml of water would fully saturate 100g of Zr-La support. Therefore, metal precursor (table 2.2) was dissolved in 100ml (for Al<sub>2</sub>O<sub>3</sub> catalysts)/ 40 ml (for Zr-La catalysts) of distilled water. 100g of support was weighed into a plastic container then the metal precursor solution was added quickly. The lid was tightly screwed on and the container was shaken vigorously for approximately 10 seconds. The contents of the container were then transferred to a ceramic bowl and dried in the oven for ½ hour. Each of the prepared catalysts had a metal loading of 0.2%.

The final stage of the catalyst preparation was calcination to produce a more thermally stable catalyst and to decompose the various catalyst precursors. This

involved heating the catalyst and holding at a given temperature for a period of time in a kiln as outlined in table 2.6.

*Table 2.6. Temperature programme of kiln during catalyst calcinations.*

Final Temp / K	Ramp Time / hrs	Hold Time / hrs
723	4.5	2

## 2.2 Catalyst Characterisation

### 2.2.1 Surface Area Analysis

#### 2.2.1.1 Adsorption

There are two different ways that a species can adsorb onto a surface, they are known as physisorption and chemisorption. Physisorption involves the non-site-selective and multi-layer condensation of molecules on a solid at relatively low temperatures (-200 to  $-25^{\circ}\text{C}$ ). The relatively strong, site-selective monolayer adsorption of chemically reactive gases occurs at higher temperatures (25 to  $400^{\circ}\text{C}$ ) and is known as chemisorption.

Chemisorption and physisorption are used to gain information on active metal surface area and total catalyst surface area respectively.

The total surface area of the catalyst was determined by Brunauer, Emmett, Teller (BET) analysis.

#### 2.2.1.2 BET

Total catalyst surface area was determined using a Micromeritics Gemini III 2375 Surface Area Analyser. Approximately 0.04 g of the catalyst sample was weighed into a glass tube and purged in a flow of  $\text{N}_2$  overnight at 383K before the measurement was carried out.

### 2.2.1.3 Chemisorption

During chemisorption, a chemical reaction takes place between the adsorbate molecule ( $\text{CO}$ ,  $\text{H}_2$  or  $\text{O}_2$ ) and the catalyst surface. It is only possible to have one monolayer of chemisorbed material. The purpose of the chemisorption technique was to determine the total active surface area and the dispersion of the catalyst. Theoretically, a small pulse of adsorbant is chemisorbed onto the active metal surface and hence, no peak detected on the GC. An identical pulse is then passed over and is also fully adsorbed by the catalyst. This procedure is continued until most of the active sites are used up. The final pulse is only partially adsorbed and the GC detects the remaining adsorbant. Pulses that follow are not adsorbed at all, hence fully detected by the GC. The number of moles of one monolayer can then be determined and if the metal:adsorbate molecule ratio is known then the active metal surface area and hence, the catalyst dispersion can be calculated.  $\text{H}_2$  chemisorption experiments were carried out by Johnson Matthey.

## 2.3 Reactions

Different aspects of the carbon forming side reactions were investigated using three different pieces of apparatus. The high-pressure microreactor and the pulse-flow apparatus were situated in Glasgow University. The tapered element oscillating Microbalance (TEOM) was at Johnson Matthey, Billingham.

### 2.3.1 High Pressure Reactor

A diagram of the apparatus is shown in figure 2.1. It consists of a  $\frac{1}{4}$ " inside-diameter glass-lined metal reactor tube positioned within an LPC elements heater. The reactor was charged with a fixed bed of packing material (fused alumina) on top of which sat the catalyst. The fused  $\text{Al}_2\text{O}_3$  had to be packed high enough to ensure the catalyst bed sat within the heater. A TC Ltd. N-type thermocouple was positioned inside the reactor tube in such a way that the tip sat inside the catalyst bed. The thermocouple and the heater were linked via a West 4400 temperature controller, which allowed temperature programs to be set and executed. The reactor tube was operational up to

900K. The total pressure in the apparatus was controlled with a Tescom variable pressure valve and the system was operational up to a maximum of 20 bar.

The flow rates of the gases entering the reactor were controlled using Brooks 5805S mass flow controllers that allowed gas flows between 5 and 250 cm<sup>3</sup>min<sup>-1</sup>. Three-way tap labelled '1' in figure 2.1 was in place to avoid mixing of oxidising (O<sub>2</sub>) and reducing (H<sub>2</sub>) gases. While the oxidising gas was flowing, tap 1 blocked the path from the reducing gas and vice versa.

The gases could be directed through the reactor tube in the direction indicated by the arrow in figure 2.1 or three-way taps 2 and 3 could be changed to isolate the reactor and direct the flow through the by-pass.

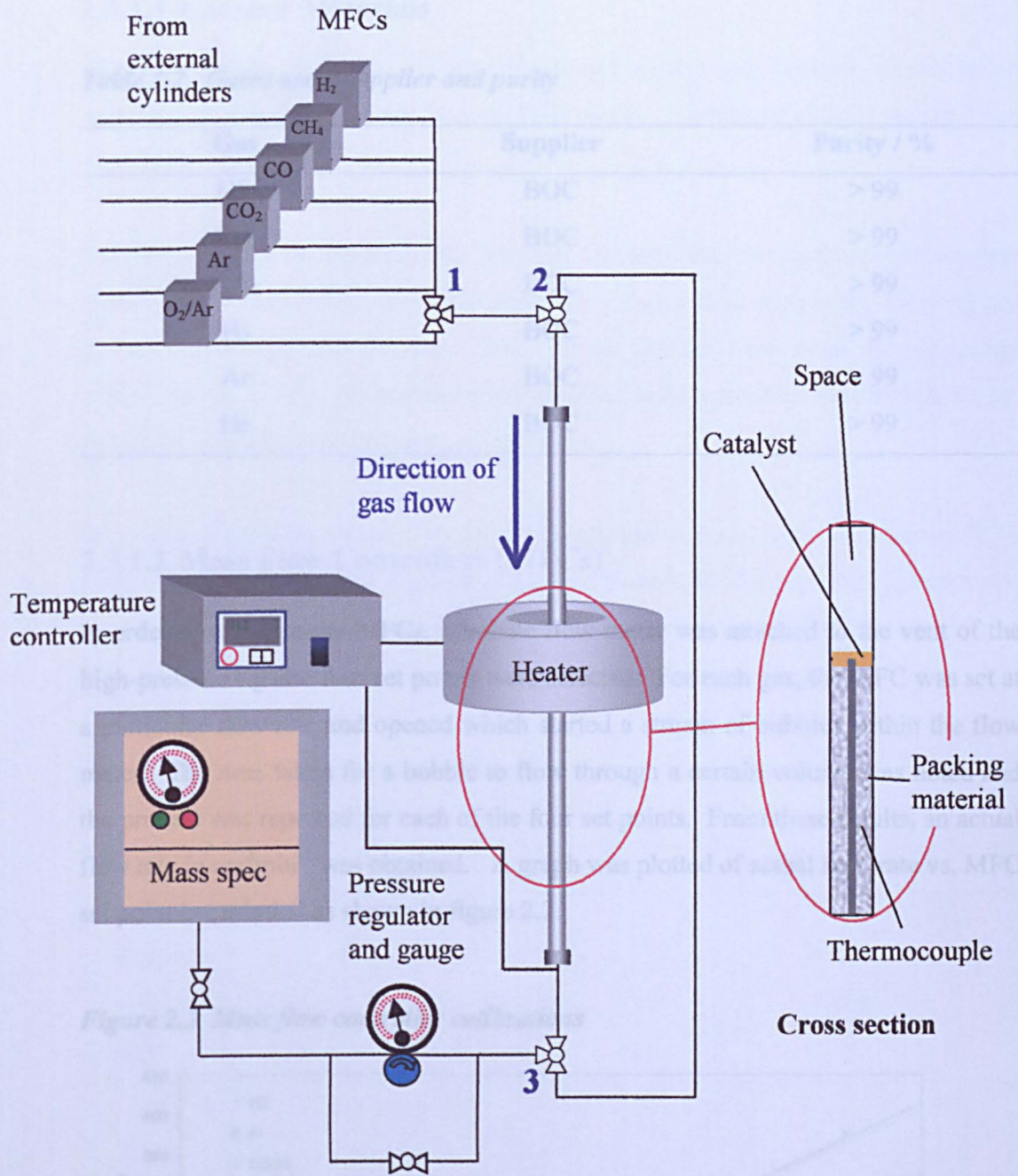


Figure 2.1. High-pressure apparatus

### 2.3.1.1 Gaseous Materials

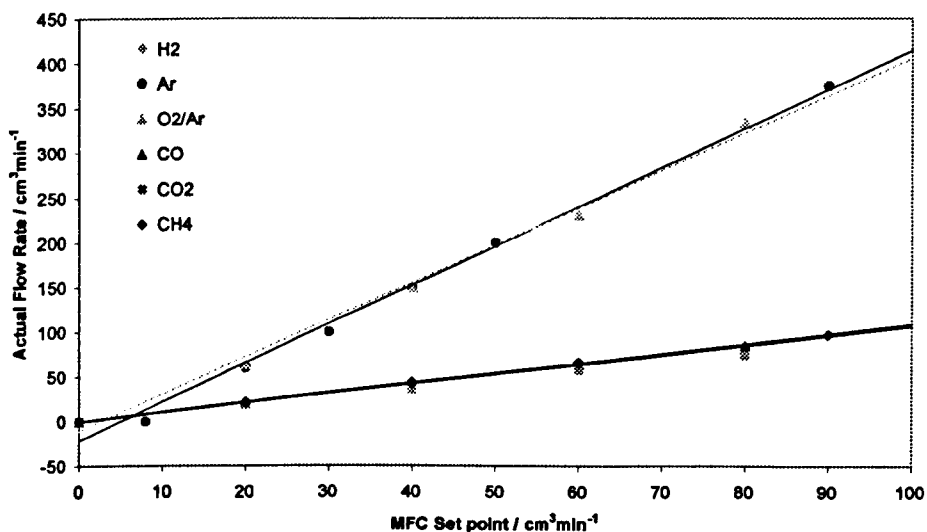
**Table 2.7. Gases used, supplier and purity**

Gas	Supplier	Purity / %
CO	BOC	> 99
CO <sub>2</sub>	BOC	> 99
CH <sub>4</sub>	BOC	> 99
H <sub>2</sub>	BOC	> 99
Ar	BOC	> 99
He	BOC	> 99

### 2.3.1.2 Mass Flow Controllers (MFCs)

In order to calibrate the MFCs, a bubble flow meter was attached to the vent of the high-pressure rig and four set points were selected. For each gas, the MFC was set at a particular flow rate and opened which started a stream of bubbles within the flow meter. The time taken for a bubble to flow through a certain volume was noted and the process was repeated for each of the four set points. From these results, an actual flow rate in  $\text{cm}^3\text{min}^{-1}$  was obtained. A graph was plotted of actual flow rate vs. MFC set point in  $\text{cm}^3\text{min}^{-1}$  as shown in figure 2.2.

**Figure 2.2. Mass flow controller calibrations**



### 2.3.1.3 Mass Spectrometer

The gases leaving the apparatus were monitored on-line and real-time via a Minitorr quadrupole mass spectrometer (MS) in MID mode. The computer software used was from ESS.

In MID mode, the ion current value for each gas component was not constant and was observed to change daily, therefore calibrating was not as simple as matching ion current to moles of gas. However, it was known that the ion currents did not change relative to one another. It was therefore essential to flow reaction gas through the bypass prior to each reaction to act as a reference.

In order to determine the relationships between ion currents, each of the gases (CO, CO<sub>2</sub>, CH<sub>4</sub> and H<sub>2</sub>) were flowed individually at 90cm<sup>3</sup>min<sup>-1</sup> through the apparatus and were recorded by the mass spectrometer. The average ion currents obtained along with their relationship relative to CO are given in table 2.8.

**Table 2.8. Average Ion current of gases from mass spectrometer and relationship relative to CO**

Gas	Average Ion Current	Relative to CO
CO	$2 \times 10^{-7}$	1
CO <sub>2</sub>	$2 \times 10^{-7}$	1
H <sub>2</sub>	$8 \times 10^{-8}$	0.4
CH <sub>4</sub>	$2 \times 10^{-7}$	1

Figure 2.3 shows the result of changing the ratio of the gas composition at constant flow rate (90cm<sup>3</sup>min<sup>-1</sup>) and pressure (20 bar) in order to determine the relationship between actual flow rate and ion current. CO and Ar were passed into the mass spectrometer at a range of compositions while the total flow rate was constant (ie 40 cm<sup>3</sup>min<sup>-1</sup> CO/50 cm<sup>3</sup>min<sup>-1</sup> Ar; 10 cm<sup>3</sup>min<sup>-1</sup> CO/ 80 cm<sup>3</sup>min<sup>-1</sup> Ar). This was repeated for each of the gases. It was found for CO, CO<sub>2</sub>, CH<sub>4</sub> and H<sub>2</sub> that the relationship was linear. This is shown in figure 2.3 for CO and CO<sub>2</sub> only for clarity.

Figure 2.3. CO ion current vs. flow rate ( $\text{cm}^3 \text{min}^{-1}$ )

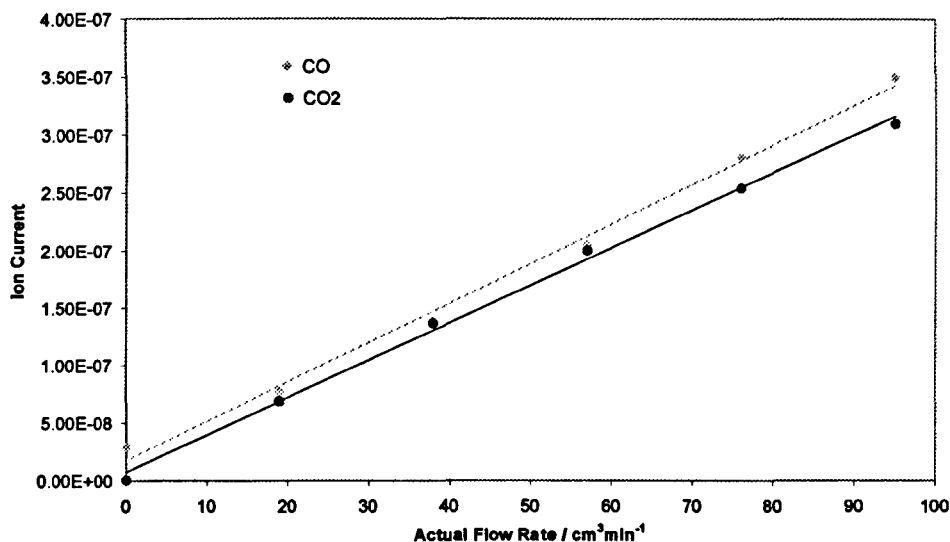


Figure 2.3 shows that there was a linear relationship between ion current and flow rate of gas and table 2.8 shows the relationship between ion current of each of the gases. The ion current of the reactant gas (of known flow rate) was recorded preceding each reaction and was converted from  $\text{cm}^3 \text{min}^{-1}$  to  $\text{moles min}^{-1}$  and related to the product gases. The flow rate in  $\text{cm}^3 \text{min}^{-1}$  was converted to  $\text{moles min}^{-1}$  by the procedure in the following sub-section.

#### *Relationship Between Flow Rate and Moles of Gas*

Conversion of  $\text{cm}^3 \text{min}^{-1}$  to  $\text{moles min}^{-1}$  was done using the following relationships:

(1) 1 mole of gas occupies 22.4 litres (standard temperature and pressure)

$$(2) P_1 V_1 = P_2 V_2$$

Where  $P$  is pressure and  $V$  is volume.

Since the calibrations were done at 20 bar pressure and standard temperature, the above relationships were used to convert a reaction flow rate of  $90\text{cm}^3\text{min}^{-1}$  into  $0.08\text{ moles min}^{-1}$ .

#### 2.3.1.4 High-Pressure Reactions

The reactions carried out on the high pressure apparatus are outlined in table 2.9<sup>†</sup>.

**Table 2.9. Summary of reactions carried out on high pressure apparatus**

Reactant Catalyst	CO		CO:CO <sub>2</sub>	CO:CO <sub>2</sub>	CO:CO <sub>2</sub>
	CO	CO:H <sub>2</sub> (1:1)	(10:1)	(5:1)	(1:1)
La-ZrO <sub>2</sub>	✓	✓			
Rh/La-ZrO <sub>2</sub>	✓	✓	✓	✓	✓
Pt/La-ZrO <sub>2</sub>	✓	✓	✓	✓	✓
Ru/La-ZrO <sub>2</sub>	✓	✓	✓	✓	✓
Al <sub>2</sub> O <sub>3</sub>	✓	✓			
Rh/Al <sub>2</sub> O <sub>3</sub>	✓	✓	✓	✓	✓
Pt/Al <sub>2</sub> O <sub>3</sub>	✓	✓	✓	✓	✓
Ru/Al <sub>2</sub> O <sub>3</sub>	✓	✓	✓	✓	✓

All reactions carried out on the high-pressure rig followed the same initial procedure. The reactor was filled with 10g of fused Al<sub>2</sub>O<sub>3</sub> boiling chips followed by 0.5g of catalyst. The catalyst was then heated from room temperature to a reaction temperature of 873K over 2 hours in a flow of  $50\text{ cm}^3\text{min}^{-1}$  of H<sub>2</sub> and  $50\text{ cm}^3\text{min}^{-1}$  of Ar at 20 bar pressure. The remaining H<sub>2</sub> was then flushed out of the reactor with Ar at reaction temperature and pressure for 1 hour. Taps 2 and 3 in figure 2.1 were adjusted to isolate the reactor and direct the gas flow through the by-pass leaving a pressure of Ar inside the reactor. The reaction gas was passed through the by-pass

<sup>†</sup> CO only was passed over Ni/La-ZrO<sub>2</sub> however; ample carbon was formed instantly which resulted in a blockage of the reactor tube. In order to safe guard the apparatus, the use of Ni was discontinued.

and recorded by mass spectrometry in order to act as a reference to be used for calibrating. When the ion current was constant on the mass spectrometer, taps 2 and 3 were switched back to isolate the by-pass and allow the gas to pass through the catalyst in the reactor.

After this stage, the procedure differed for each reaction and this is outlined in the following sub-sections.

#### *CO Only*

The gases were left flowing through the reactor until no further reaction was apparent from the mass spectrometer. CH<sub>4</sub> was also studied as a single gas however, the H<sub>2</sub> produced gave a very weak and noisy signal on the mass spectrometer. It will be shown elsewhere how the TEOM was used instead to study CH<sub>4</sub> single gas reactions.

#### *CO and H<sub>2</sub> (1:1) Only*

The reaction gases flowed until a steady state was reached or until no further reaction was observed

#### *CO and CO<sub>2</sub> Only*

The reaction gases flowed over the catalyst for one hour then the reactor was flushed with Ar until reaction gases were no longer detected on the mass spectrometer. In order to assess the activity of the used catalysts from this stage, they were subjected to a CO:H<sub>2</sub> 1:1 gas mixture which flowed over the catalyst until a steady state was reached or no further reaction occurred.

### **2.3.2 Pulse Flow Reactor**

This glass apparatus consisted of three main parts separated by vacuum taps: gas manifold, sample loop and continuous flow section. A diagram is given in figure 2.4. The gas manifold could be evacuated to a minimum pressure of  $1 \times 10^{-1}$  torr using a vacuum pump. The pressure was monitored with an Edwards Barocel pressure sensor. After evacuation, the manifold was isolated from the vacuum pump and filled with a pressure of reactant gas from a storage bulb.

The sample loop is labelled in figure 2.4. It was the connection between the gas manifold and the continuous flow section. Within the sample loop, a fixed volume of gas (pre-determined volume was 8.62 cm<sup>3</sup>) of known pressure from the manifold (pulse sample) could be stored (between taps 3 and 4) and carrier gas coming in to the apparatus could flow through this section to deliver the pulse to the catalyst. It could then be isolated from the continuous flow section by initially opening tap 5 to allow the carrier gas to continue flowing and closing taps 3 and 4. Finally, opening taps 1 and 2 evacuated the sample section.

The continuous flow section consisted of a removable quartz glass u-bend reactor, which contained a sinter necessary to load the catalyst onto. A K-type thermocouple was connected to a temperature controller and was placed in a quartz glass pocket inside the reactor, on top of the catalyst bed. The reactor could be isolated allowing the gases to by-pass it. The continuous flow section also had a gas trap positioned in the line after the reactor which allowed product gases to be trapped out by freezing. A gauge was also attached to monitor the pressure in this section.

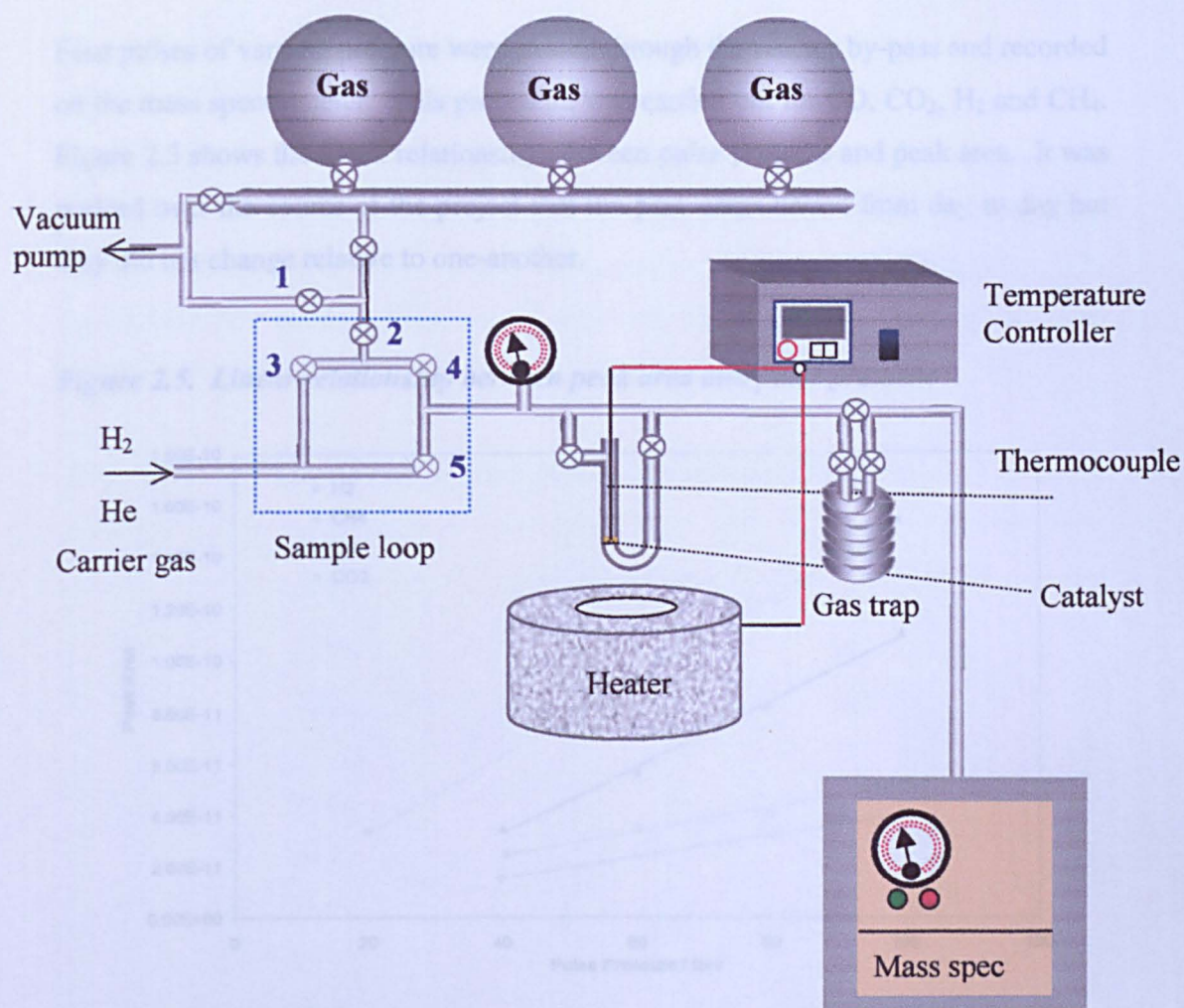


**Figure 2.4. Pulse flow apparatus**

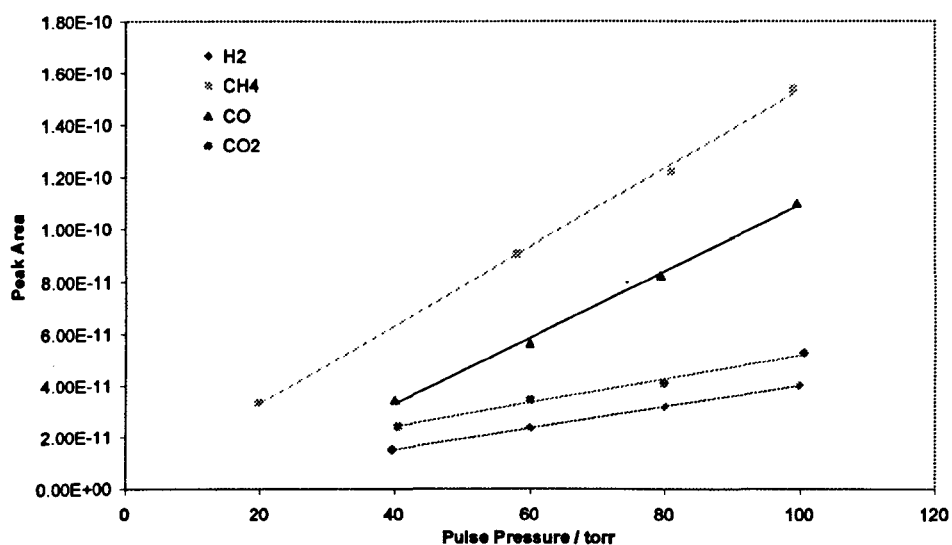
### 2.3.2.1 Mass Spectrometer

A Genesys quadrupole mass spectrometer with ESS software was used to analyse the gases emerging from the pulse flow reactor. Since discrete pulses of gas were used as opposed to continuous flow of gas, calibration was done by relating the area of pulses of varying pressure to the number of moles of gas. Calibrations were carried out on each gas beforehand to ensure that peak areas were directly proportional to the pulse

pressure (relating the number of moles to pulse pressure and hence peak areas will be discussed in the results section).

Four pulses of varying pressure were passed through the reactor by-pass and recorded on the mass spectrometer. This procedure was carried out for CO, CO<sub>2</sub>, H<sub>2</sub> and CH<sub>4</sub>. Figure 2.5 shows the linear relationship between pulse pressure and peak area. It was noticed over the course of the project that the peak areas varied from day to day but they did not change relative to one-another.

**Figure 2.5. Linear relationship between peak area and pulse pressure**



### 2.3.2.2 Pulse Flow Reactions

The gas manifold was filled with approximately 50 μmol of reaction gas. Meanwhile, the catalyst was reduced in a flow of 10 cm<sup>3</sup> min<sup>-1</sup> H<sub>2</sub> at atmospheric pressure for one hour as it was heated up to 873 K. It was then purged with 25 cm<sup>3</sup> min<sup>-1</sup> of He at this temperature for a further hour. The temperature, pressure and He flow rate were maintained for the duration of the reaction.

The first pulse of reaction gas flowed through the by-pass and was used as a reference for reasons discussed in the previous section. Five pulses of approximately 50 μmol

were subsequently passed through the catalyst using He gas as a carrier. All pulses were recorded on the mass spectrometer.

### 2.3.2.3 Isotope Pulses

A 5:1 ratio of  $^{13}\text{CO}:\text{C}^{18}\text{O}_2$  ( $28\mu\text{mol}$ ) was pulsed over each of the catalysts and followed using mass spectrometry in order to identify exchange reactions taking place between reactants and also between the reactants and the catalyst support. The species and their corresponding masses that were followed on the mass spectrometer are given in table 2.10:

*Table 2.10. Species and their masses followed by mass spectrometry*

Species	Mass
$^{13}\text{CO}$	29
$\text{C}^{18}\text{O}$	30
$\text{CO}$	28
$^{13}\text{C}^{18}\text{O}$	31
$\text{C}^{18}\text{O}_2$	48
$\text{CO}_2$	44
$^{13}\text{CO}_2$	45
$^{13}\text{C}^{18}\text{O}_2$	49
$\text{C}^{18}\text{OO}$	46
$^{13}\text{C}^{18}\text{OO}$	47

The gas manifold was filled with  $28\mu\text{mol}$  of reaction gas in a 5:1 ratio then left for around 20 minutes to equilibrate. The catalyst was reduced in a flow of  $10\text{ cm}^3\text{min}^{-1}$   $\text{H}_2$  at atmospheric pressure for one hour as it was heated up to 873 K. It was then purged with  $25\text{ cm}^3\text{min}^{-1}$  of He at this temperature for a further hour. The temperature, pressure and He flow were maintained for the duration of the reaction.

The first pulse of reaction gas was passed through the by-pass to act as a reference. The gas trap that was situated in the glass-line after the reactor (figure 2.2) was submerged in liquid  $\text{N}_2$  in order to freeze all  $^x\text{C}^y\text{O}_2$  components out of the gas flow

while allowing  $^{13}\text{C}^{18}\text{O}$  components to pass through. After one pulse was detected by the mass spectrometer, the liquid  $\text{N}_2$  was removed and the trap was heated with a heat gun in order to volatilise all contents. The  $^{13}\text{C}^{18}\text{O}_2$  contents of the trap were also recorded by the mass spectrometer. Five pulses were subsequently passed through the reactor following the same procedure.

All reactions carried out on the glass-line apparatus are given in table 2.11.

**Table 2.11. Pulse Flow Reactions**

Catalyst	Reactant	CO	CH <sub>4</sub>	<sup>13</sup> CO:C <sup>18</sup> O <sub>2</sub> (5:1)
	La-ZrO <sub>2</sub>	✓	✓	✓
	Rh/La-ZrO <sub>2</sub>	✓	✓	✓
	Pt/La-ZrO <sub>2</sub>	✓	✓	✓
	Ru/La-ZrO <sub>2</sub>	✓	✓	✓
	Ni/La-ZrO <sub>2</sub>	✓	✓	✓
	Al <sub>2</sub> O <sub>3</sub>	✓	✓	✓
	Rh/Al <sub>2</sub> O <sub>3</sub>	✓	✓	✓
	Pt/Al <sub>2</sub> O <sub>3</sub>	✓	✓	✓
	Ru/Al <sub>2</sub> O <sub>3</sub>	✓	✓	✓
	Ni/Al <sub>2</sub> O <sub>3</sub>	✓	✓	✓

### 2.3.3 Tapered Element Oscillating Microbalance (TEOM)

A Rupprecht and Patashnick TEOM series 1500 pulse mass analyser was used as a direct method of determining the mass of carbon formed on the catalyst during reaction. A diagram is available in figure 2.6. The TEOM 'head' consisted of the high-temperature-glass tapered element (TE) where the catalyst sat and the protective metal sheath around the TE. The head was sealed inside a heater connected to a temperature controller. A thermocouple was placed on the protective sheath wall and the temperature of the wall only was controlled as no thermocouple was placed inside

the catalyst bed. The maximum temperature of the wall was 923 K and the maximum pressure setting of the unit was 20 bar. A loudspeaker facing the bowl of the TE applied energy to it forcing it to vibrate in a similar fashion to a tuning fork. Two optics (transmitter and receiver) positioned at either side of the bowl recorded the frequency of the vibration and this was related to mass change by the following equation:

$$\Delta M = k_o \left( \frac{1}{f_1^2} - \frac{1}{f_0^2} \right)$$

Where  $\Delta M$  is change in mass of the catalyst sample;  $K_o$  is the spring constant of the TE;  $f_0$  is the natural oscillating frequency at time,  $t = 0$  and  $f_1$  is the natural oscillating frequency at time  $t = 1$ .

The TEOM software recorded  $f_1$  and hence,  $\Delta M$  every cycle. The level of noise was also noted.

CO, CO<sub>2</sub>, CH<sub>4</sub>, H<sub>2</sub> and N<sub>2</sub> were available to the TEOM as continuous flow gases. The gases flowed from individual mass flow controllers<sup>‡</sup> (MFC) to the TE inlet, through the catalyst bed then out of the TE exit to eventually vent or they could pass through the by-pass and vent. The reaction gases had to pass through a four-way valve on their way to the TE, which was in place as a safety precaution. In one mode the N<sub>2</sub> purge gas flowed to the vent and the reaction gases to the TE and in the other mode, the reaction gases were vented as the purge gas flowed to the TE.

---

<sup>‡</sup> MFC ranges: CO (5-25 Lh<sup>-1</sup>), CO<sub>2</sub> (5-25Lh<sup>-1</sup>), H<sub>2</sub> (1-3Lh<sup>-1</sup>), CH<sub>4</sub> (5-25Lh<sup>-1</sup>), and N<sub>2</sub> (5-25Lh<sup>-1</sup>)

## 2.2.3.4. TEOM Headlines

Approximately 30 mg of catalyst was heated to 873 K by a flow of  $10 \text{ Lh}^{-1} \text{ N}_2$  gas at 20 cm diameter before reduction in  $1 \text{ Lh}^{-1}$  of  $\text{H}_2$  for one hour. The remaining  $\text{H}_2$  was then purged with a  $10 \text{ Lh}^{-1}$  flow of  $\text{N}_2$  for 15 minutes. The sample was then subjected to a flow of  $10 \text{ Lh}^{-1} \text{ CO}_2$  for 20 minutes to remove any carbon deposited by  $\text{CH}_4$ . Following this, the catalyst was purged with  $\text{N}_2$  before  $\text{CH}_4$  was reintroduced for a further hour. The reactions carried out in this study are summarized in table 2.12<sup>3</sup>. During the  $\text{CH}_4$  reaction, the catalyst was heated to 873 K by a flow of  $10 \text{ Lh}^{-1} \text{ N}_2$  gas at 20 cm diameter before reduction in  $1 \text{ Lh}^{-1}$  of  $\text{H}_2$  for one hour. The remaining  $\text{H}_2$  was then purged with a  $10 \text{ Lh}^{-1}$  flow of  $\text{N}_2$  for 15 minutes. The sample was then subjected to a flow of  $10 \text{ Lh}^{-1} \text{ CO}_2$  for 20 minutes to remove any carbon deposited by  $\text{CH}_4$ . Following this, the catalyst was purged with  $\text{N}_2$  before  $\text{CH}_4$  was reintroduced for a further hour. The reactions carried out in this study are summarized in table 2.12<sup>3</sup>.

Table 2.12. Reactions carried out in the TEOM

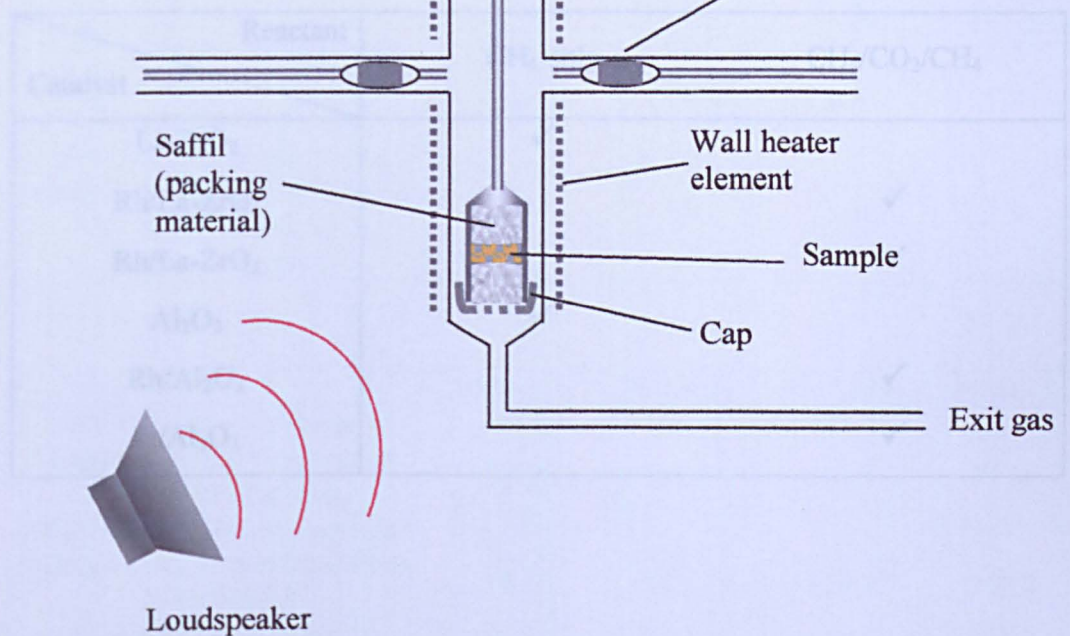


**Figure 2.6. Simplified diagram of TEOM head, heaters and optics**

<sup>3</sup> This table was taken from the TEOM manual. However, the large amount of carbonaceous material deposited on the TEOM during the use of  $\text{CO}_2$  was regarded as a problem for the TEOM and the TEOM was not used for the study.

### 2.3.3.1 TEOM Reactions

Approximately 30 mg of catalyst was heated to 873 K in a flow of 10 Lh<sup>-1</sup> N<sub>2</sub> gas at 20 bar pressure before reduction in 3 Lh<sup>-1</sup> of H<sub>2</sub> for one hour. The remaining H<sub>2</sub> was then purged with a 10 Lh<sup>-1</sup> flow of N<sub>2</sub>. CH<sub>4</sub> was subsequently passed over the catalyst for an hour before purging with N<sub>2</sub>. The sample was then subjected to a flow of 10 Lh<sup>-1</sup> CO<sub>2</sub> for 30 minutes in an attempt to remove any carbon deposited by CH<sub>4</sub>. Following this, the catalyst was purged with N<sub>2</sub> before CH<sub>4</sub> was reintroduced for a further hour. The reactions carried out in this way are summarised in table 2.12<sup>§</sup>. Due to time constraints the Ru catalysts were not studied.

**Table 2.12. Reactions carried out on the TEOM**

Catalyst \ Reactant	CH <sub>4</sub> only	CH <sub>4</sub> /CO <sub>2</sub> /CH <sub>4</sub>
La-ZrO <sub>2</sub>	✓	
Rh/La-ZrO <sub>2</sub>		✓
Rh/La-ZrO <sub>2</sub>		✓
Al <sub>2</sub> O <sub>3</sub>	✓	
Rh/Al <sub>2</sub> O <sub>3</sub>		✓
Pt/Al <sub>2</sub> O <sub>3</sub>		✓

<sup>§</sup>CO only over Rh/La-ZrO<sub>2</sub> was studied in the TEOM however, the large amount of carbon formed resulted in damage to the TE hence the use of CO was negated and for similar reasons the Ni catalysts were never studied.

### 3 Results

#### 3.1 Catalyst Characterisation

##### 3.1.1 BET

The data obtained from the BET analysis is tabulated below. It can be seen how the Al<sub>2</sub>O<sub>3</sub> supported catalysts have a significantly greater surface area, pore volume and pore diameter than their La-ZrO<sub>2</sub> equivalents.

*Table 3.1 Determined BET surface area of each catalyst*

	Rh/La-ZrO <sub>2</sub>	Pt/La-ZrO <sub>2</sub>	Ru/La-ZrO <sub>2</sub>	Ni/La-ZrO <sub>2</sub>
BET surface area/(sq.m/g)	4.8	4.1	3.5	2.8
Single point surface area at P/Po 0.1995/(sq.m/g)	3.6	3.9	3.2	2.8
BJH cumulative adsorption surface area of pores between 17 & 3000 Å diameter/(sq.m/g)	4.0	3.6	3.6	1.5

	Rh/Al <sub>2</sub> O <sub>3</sub>	Pt/Al <sub>2</sub> O <sub>3</sub>	Ru/Al <sub>2</sub> O <sub>3</sub>	Ni/Al <sub>2</sub> O <sub>3</sub>
BET surface area/(sq.m/g)	101.3	106.9	104.0	78.7
Single point surface area at P/Po 0.1995/(sq.m/g)	97.5	102.1	101.5	77.36
BJH cumulative adsorption surface area of pores between 17 & 3000 Å diameter/(sq.m/g)	98.1	101.3	129.1	100.2

**Table 3.2 Catalyst pore volumes determined by BET analysis**

	Rh/La- ZrO <sub>2</sub>	Pt/La- ZrO <sub>2</sub>	Ru/La- ZrO <sub>2</sub>	Ni/La- ZrO <sub>2</sub>
Single point total pore vol. of pores < 3345.8406 Å diameter at p/Po 0.9943/(cc/g)	0.008	0.007	0.006	0.009
BJH cumulative adsorption pore vol. of pores between 17 and 500 Å diameter/(cc/g)	0.005	0.005	0.004	0.005

	Rh/Al <sub>2</sub> O <sub>3</sub>	Pt/Al <sub>2</sub> O <sub>3</sub>	Ru/Al <sub>2</sub> O <sub>3</sub>	Ni/Al <sub>2</sub> O <sub>3</sub>
Single point total pore vol. of pores < 3345.8406 Å diameter at p/Po 0.9943/(cc/g)	0.430	0.431	0.419	0.298
BJH cumulative adsorption pore vol. of pores between 17 and 500 Å diameter/(cc/g)	0.406	0.401	0.419	0.298

**Table 3.3 Catalyst pore diameters determined by BET analysis**

	Rh/La- ZrO <sub>2</sub>	Pt/La- ZrO <sub>2</sub>	Ru/La- ZrO <sub>2</sub>	Ni/La- ZrO <sub>2</sub>
Average pore diameter (4V/Å by BET)/ Å	64.5	72.4	97.1	125.9
BJH Adsorption average pore diameter(4V/A <sup>0</sup> )/ Å	51.1	51.2	74.3	146.6

	Rh/Al <sub>2</sub> O <sub>3</sub>	Pt/Al <sub>2</sub> O <sub>3</sub>	Ru/Al <sub>2</sub> O <sub>3</sub>	Ni/Al <sub>2</sub> O <sub>3</sub>
Average pore diameter (4V/Å by BET)/ Å	169.67	162.20	161.1	151.5
BJH Adsorption average pore diameter(4V/A <sup>0</sup> )/ Å	165.37	159.55	129.9	119.1

### 3.1.2 H<sub>2</sub> Chemisorption

The percentage metal dispersion of each catalyst has been calculated and given in table 3.4

*Table 3.4 Percentage metal dispersion of each catalyst*

Catalyst	Percentage Dispersion
Rh/La-ZrO <sub>2</sub>	9.34
Pt/La-ZrO <sub>2</sub>	8.71
Ru/La-ZrO <sub>2</sub>	4.51
Rh/Al <sub>2</sub> O <sub>3</sub>	3.66
Pt/Al <sub>2</sub> O <sub>3</sub>	17.77
Ru/Al <sub>2</sub> O <sub>3</sub>	1.54

## 3.2 Pulse Flow Reactions

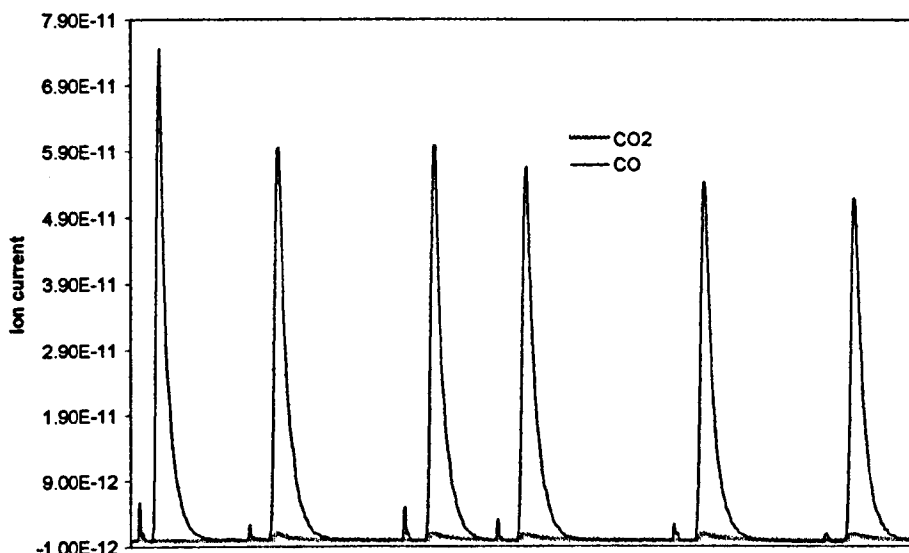
Five discrete pulses of CO then CH<sub>4</sub> were passed over each of the catalysts (including Ni) at 873K and atmospheric pressure. Following these studies, a 5:1 mixture of isotopic <sup>13</sup>CO and C<sup>18</sup>O<sub>2</sub> were used to study each catalyst.

### 3.2.1 CO Pulses over La-ZrO<sub>2</sub> Support

Five CO pulses of approximately 46 μmol were initially passed over La-ZrO<sub>2</sub> support material at 873K to determine the extent of catalysis occurring on it. The mass spectrometer data obtained is given in figure 3.1. The figure shows six peaks: the first is a reference peak and was obtained by flowing a single pulse of CO through the reactor by-pass then into the mass spectrometer. The following five were obtained by flowing CO pulses over the support before entering the mass spectrometer. Each of the five reaction peaks obtained from the mass spectrometer contain a signal due to CO and a relatively small signal due to CO<sub>2</sub> as expected from the Boudouard reaction:



Since CO<sub>2</sub> was formed, it was also assumed that carbon was deposited on the catalyst during each pulse according to the stoichiometry of the Boudouard reaction.

**Figure 3.1. Five pulses of CO over La-ZrO<sub>2</sub> support**

As expected, no CO<sub>2</sub> was produced during the reference pulse. The relatively small peaks of CO<sub>2</sub> present in the five reaction pulses show that the support material (a) has a low level of activity under the reaction conditions and (b) is active. The smaller peaks that occur prior to the main peaks result from gas switching.

### 3.2.1.1 Calculations From CO Pulses

The La-ZrO<sub>2</sub> support material was used as an example to show how the number of moles of CO<sub>2</sub> produced per pulse was calculated.

The pressure of the CO reference pulse was known and from this information, the number of moles of CO could be calculated. This was done by application of the following equation.

$$n = \frac{PV}{RT}$$

where:

P = pulse pressure (113.2 torr)

V = volume of sample loop (8.62 cm<sup>3</sup>)

R = molar gas constant ( $62388 \text{ cm}^3 \text{ torr mol}^{-1} \text{ K}^{-1}$ )

T = temperature of reaction (room temperature – although the reaction was carried out and 873 K, the gas in the sample loop was at room temperature)

The area under the CO reference pulse was calculated and this represents a known number of moles as shown in table 3.5.

**Table 3.5. CO reference peak area with corresponding pressure and number of moles**

Pulse	Area*	Pressure / torr	$\mu\text{Mol}$
Reference	$3.64 \times 10^{-9}$	113.2	52.5

The relationship between peak area of CO and CO<sub>2</sub> was pre-determined as discussed in section 2.3.2.1; therefore, the equivalent peak area for CO<sub>2</sub> at 113.2 torr was calculated and is given in table 3.6:

**Table 3.6. Area of CO<sub>2</sub> peak and calculated number of  $\mu\text{mols}$**

Pulse	Pressure / torr	$\mu\text{Mol}$	Peak Area
CO <sub>2</sub>	113.2	52.5	$2.07 \times 10^{-9}$

For each pulse, the area under the CO<sub>2</sub> signal was calculated and this was converted to moles (CO<sub>2</sub> moles out) using the data in table 3.6 and the pre-determined relationship from section 2.3.2.1. The results are given in table 3.7.

\* Area was calculated as opposed to peak heights as, unlike the reference pulse, gas flowing through the reactor had to pass through the catalyst and the sinter. This resulted in mixing across the catalyst bed which subsequently broadened the peak.

**Table 3.7. Moles of CO<sub>2</sub> (CO<sub>2</sub> moles out) produced over La-ZrO<sub>2</sub> from each pulse. Calculated from peak areas**

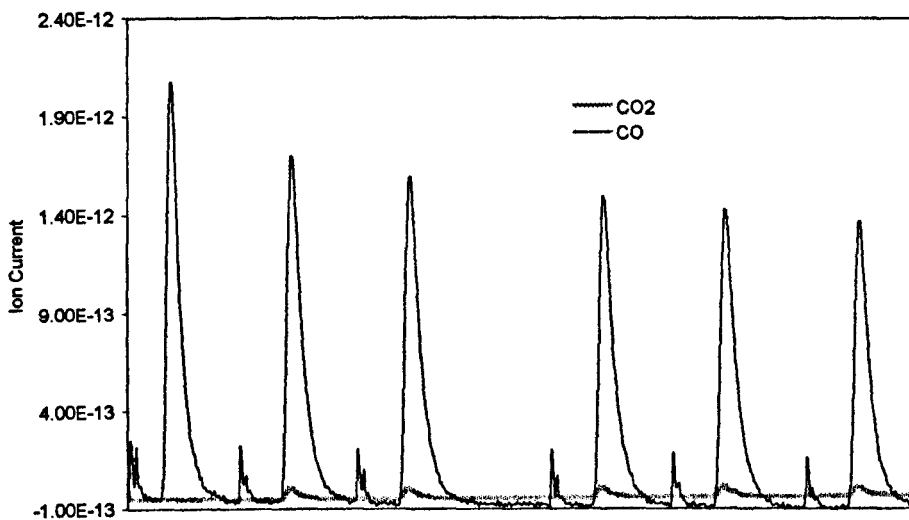
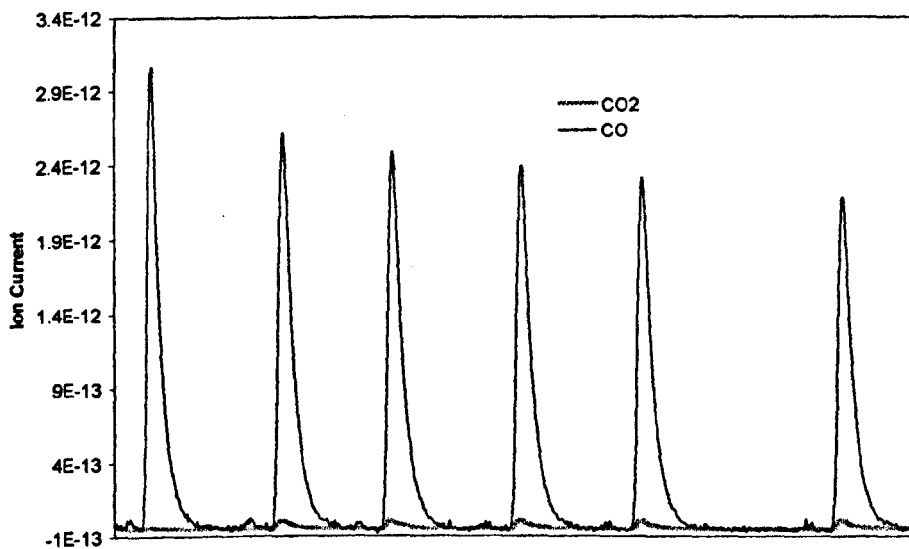
Pulse	Area/x10 <sup>-11</sup>	CO <sub>2</sub> μmol out
1	9.08	2
2	9.36	2
3	8.56	2
4	8.60	3
5	8.64	2

Percentage conversion is usually calculated using the following equation, however there was very little difference between the number of CO moles in and the number of CO moles out making this calculation difficult.

$$\frac{CH_{4in} - CH_{4out}}{CH_{4in}} \times 100$$

### 3.2.2 CO Pulses over La-ZrO<sub>2</sub> Supported Catalysts

Five CO pulses were passed over Rh, Pt, Ru and Ni catalysts at 873K. In advance a reference peak was passed through the reactor by-pass. The mass spectra obtained are given in figures 3.2 to 3.5 respectively. As expected, no CO<sub>2</sub> was obtained from the reference pulse but relatively small peaks of CO<sub>2</sub> can be seen from the pulses that have been passed over the catalyst.

**Figure 3.2. Five pulses of CO over Rh/La-ZrO<sub>2</sub>****Figure 3.3. Five pulses of CO over Pt / La-ZrO<sub>2</sub>**

**Figure 3.4.** Five pulses of CO over Ru/La-ZrO<sub>2</sub>

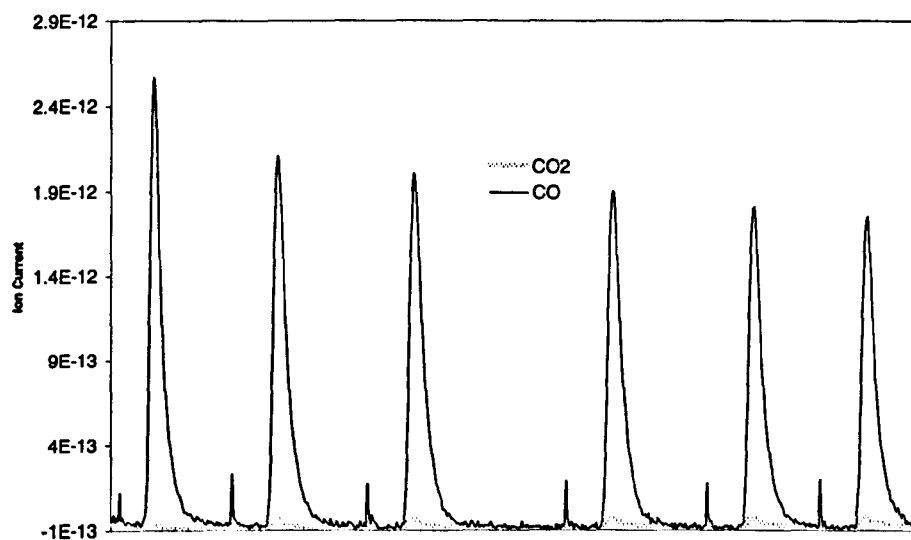
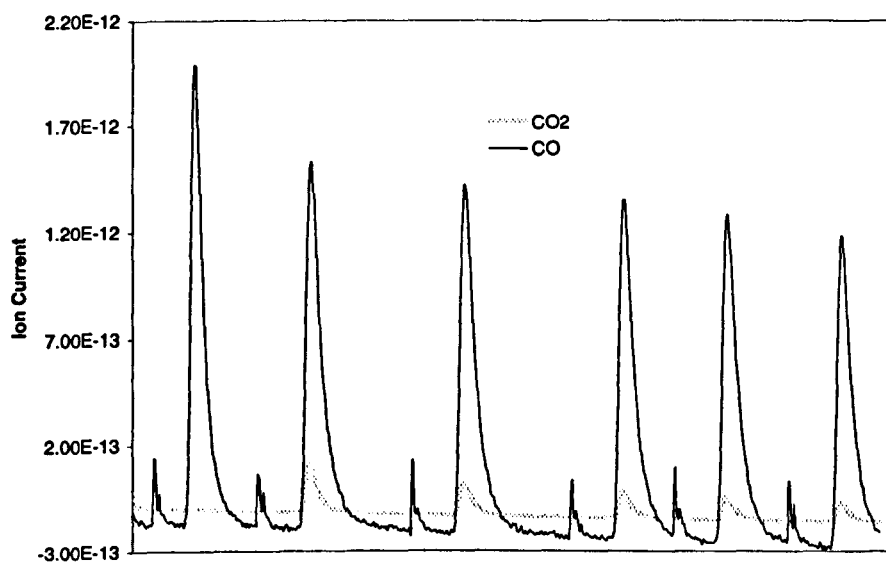


**Figure 3.5.** Five pulses of CO over Ni/La-ZrO<sub>2</sub>



The results from each series of pulses were treated the same way as the peaks obtained from the La-ZrO<sub>2</sub> support material, as described in section 3.3.1.1. The results for Rh, Pt and Ru are given in tables 3.8 to 3.10 respectively.

**Table 3.8. Data obtained from five CO pulses over Rh/La-ZrO<sub>2</sub>**

Pulse	CO $\mu\text{mol}$ in	CO <sub>2</sub> $\mu\text{mol}$ out
1	52	3
2	49	3
3	47	3
4	46	3
5	44	3

**Table 3.9. Data obtained from five CO pulses over Pt/La-ZrO<sub>2</sub>**

Pulse	CO $\mu\text{mol}$ in	CO <sub>2</sub> $\mu\text{mol}$ out
1	52	2
2	50	2
3	49	2
4	47	2
5	45	2

**Table 3.10. Data obtained from five CO pulses over Ru/La-ZrO<sub>2</sub>**

Pulse	CO $\mu\text{mol}$ in	CO <sub>2</sub> $\mu\text{mol}$ out
1	52	2
2	51	2
3	49	2
4	47	2
5	46	2

Each table shows how the number of moles of CO<sub>2</sub> produced is very similar over each catalyst. When compared to the number of moles of CO<sub>2</sub> produced over the support (table 3.7) it can be seen that the values are the same. Therefore under the conditions of the low pressure Boudouard reaction, only the support appeared to be active.

### 3.2.2.1 CO Pulses over Ni/La-ZrO<sub>2</sub>

Table 3.11 shows that the amount of CO<sub>2</sub> produced over Ni/La-ZrO<sub>2</sub>, during each pulse, was greater than that produced over the support. Therefore the Ni metal was apparently active under the conditions of reaction.

*Table 3.11. Comparison: moles of CO<sub>2</sub> from support and moles of CO<sub>2</sub> from Ni catalyst*

Pulse	CO <sub>2</sub> μmol out from La-ZrO <sub>2</sub>	CO <sub>2</sub> μmol out from Ni/La-ZrO <sub>2</sub>
1	2	9
2	2	6
3	2	6
4	3	4
5	2	3

For each pulse, the percentage CO conversion has been calculated and the results are shown in table 3.12.

It was expected, from the stoichiometry of the Boudouard reaction, that every mole of CO that reacted would produce 0.5 mole of CO<sub>2</sub>. The number of CO moles consumed divided by the number of CO<sub>2</sub> moles produced should equal 2. Table 3.12 shows that the results tend towards 2 with increasing pulse number.

*Table 3.12. Data obtained from five CO pulses over Ni/La-ZrO<sub>2</sub>*

Pulse	CO μmol in	CO μmol out	CO μmol consumed	CO % conversion	CO <sub>2</sub> μmol out	CO (consumed)/CO <sub>2</sub>
1	48	42	6	12	9	0.65
2	48	38	9	20	6	1.65
3	46	37	9	20	6	1.66
4	44	37	8	18	4	1.85
5	43	36	7	17	3	2.29

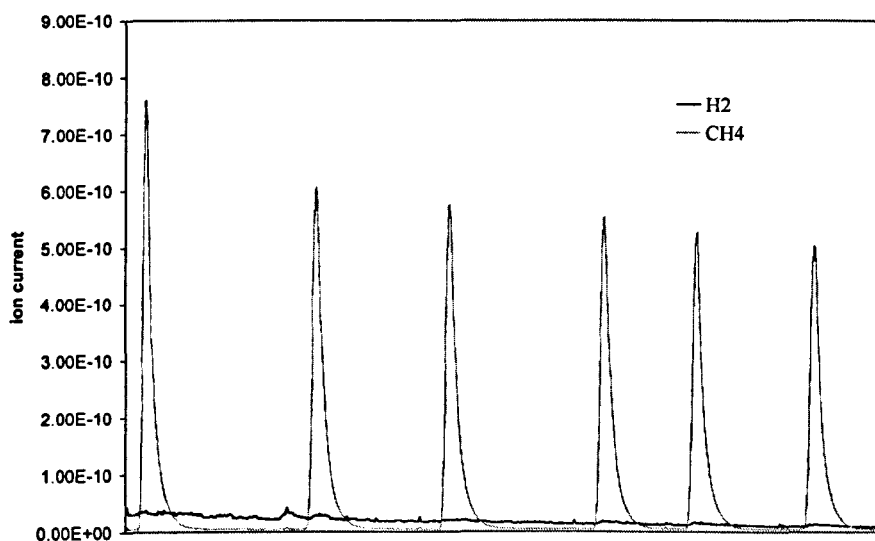
### 3.2.3 CH<sub>4</sub> Pulses over La-ZrO<sub>2</sub> Support

Five pulses of CH<sub>4</sub> were passed over the La-ZrO<sub>2</sub> support material at 873K. According to the CH<sub>4</sub> cracking reaction, each mole of CH<sub>4</sub> consumed should produce 2 moles of H<sub>2</sub>.



The mass spectra obtained from the pulses over the support are shown in figure 3.6. The first pulse was passed through the reactor by-pass before entering the mass spectrometer and the following five pulses flowed through the catalyst bed before entering the mass spectrometer. It can be seen from the five reaction peaks that no H<sub>2</sub> was produced; hence no catalysis occurred on the support material.

*Figure 3.6. Five pulses of CH<sub>4</sub> over La-ZrO<sub>2</sub> support*

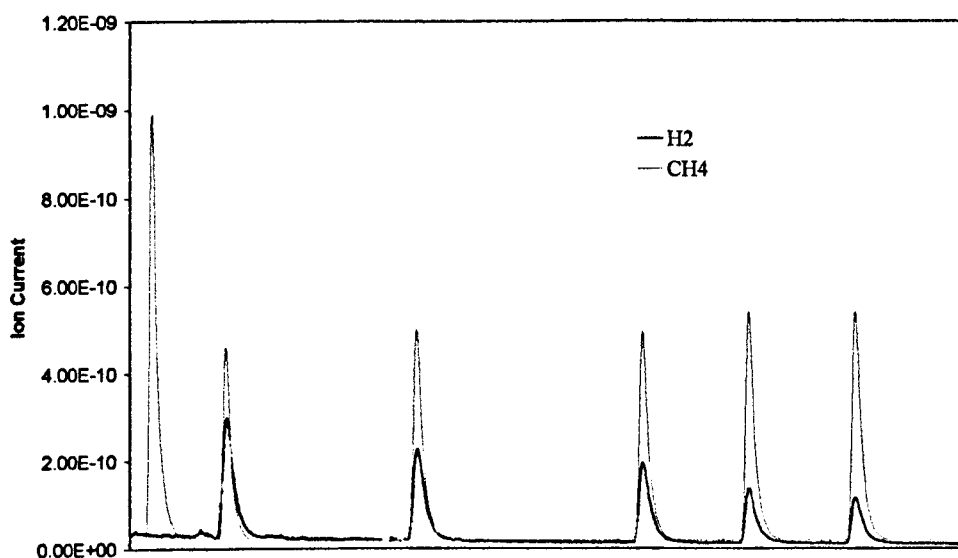


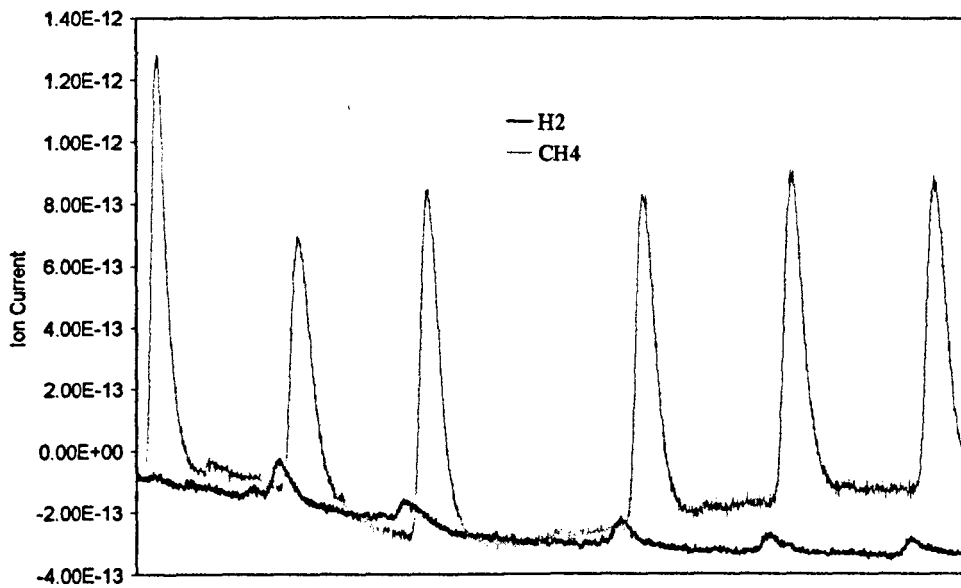
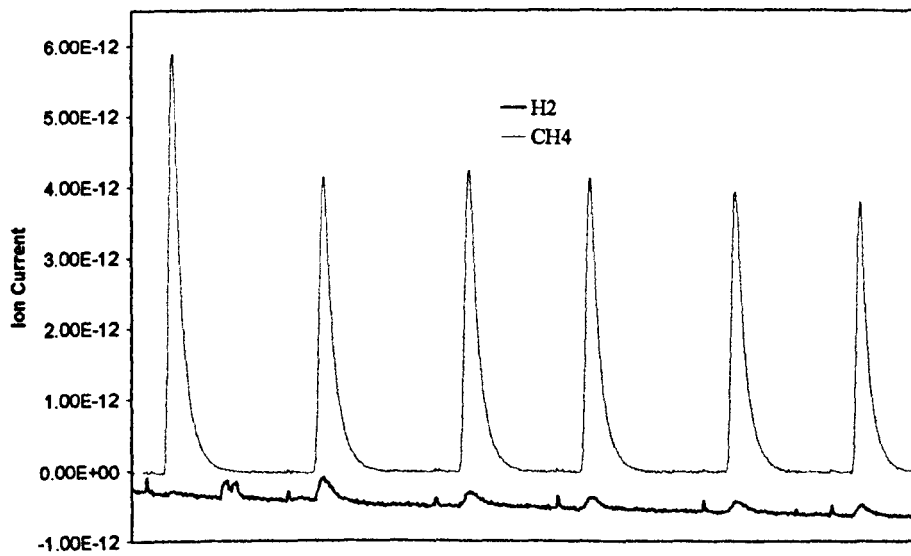
### 3.2.4 CH<sub>4</sub> Pulses over La-ZrO<sub>2</sub> Supported Catalysts

Figures 3.7 to 3.10 show the mass spectra obtained from five CH<sub>4</sub> pulses over Rh, Pt, Ru and Ni respectively. The first peak shown in each is the reference peak that was passed through the reactor by-pass prior to the five reaction pulses.

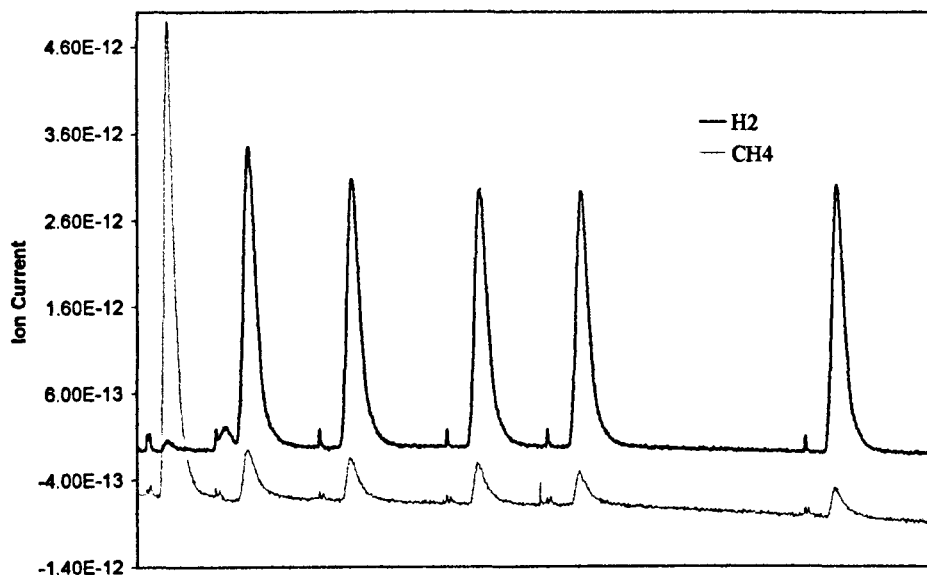
It can be seen from the figures that the loss of CH<sub>4</sub> and the production of H<sub>2</sub> is greater than their equivalents from section 1.3; therefore, a mass balance calculated from the loss of CH<sub>4</sub> and the production of H<sub>2</sub> was carried out.

*Figure 3.7. Five pulses of CH<sub>4</sub> over Rh/La-ZrO<sub>2</sub>*



**Figure 3.8.** Five pulses of  $\text{CH}_4$  over  $\text{Pt/La-ZrO}_2$ **Figure 3.9.** Five pulses of  $\text{CH}_4$  over  $\text{Ru/La-ZrO}_2$ 

**Figure 3.10.** Five pulses of  $\text{CH}_4$  over  $\text{Ni/La-ZrO}_2$



### 3.2.4.1 Mass Spectrometer Splitting Patterns

For the  $\text{CH}_4$  pulse reaction, splitting patterns must be accounted for before accurate analysis of the results can take place. It was discovered, through experiment, that  $\text{CH}_4$  produces a signal due to mass 2 (mass of  $\text{H}_2$ ), which is 1% of the size of the  $\text{CH}_4$  signal. This value was subtracted from the  $\text{H}_2$  signal where necessary.

### 3.2.4.2 Calculations from $\text{CH}_4$ Pulses

The percentage  $\text{CH}_4$  conversion was calculated for each of the five pulses over every catalyst. The calculation carried out is explained using  $\text{Rh/La-ZrO}_2$  as an example:

The area under the  $\text{CH}_4$  reference pulse from figure 3.7 was calculated and converted to moles from the pulse pressure. The data obtained is shown in table 3.13

**Table 3.13. Calculated CH<sub>4</sub> reference peak area and mole equivalent**

Pulse	Area	Pressure/torr	μmol
CH <sub>4</sub> Reference	5.20 x10 <sup>-8</sup>	116.5	54

The equivalent H<sub>2</sub> area was calculated and given in table 3.14

**Table 3.14. Equivalent H<sub>2</sub> reference area**

Pulse	Pressure/torr	μmol	H <sub>2</sub> Area
H <sub>2</sub>	116.5	54	4.23x10 <sup>-8</sup>

The number of moles of CH<sub>4</sub> per pulse going into the reactor (CH<sub>4moles in</sub>) was then calculated using the above information and section 2.3.2.1 the results are shown in table 3.15.

**Table 3.15. Pressure and moles of CH<sub>4</sub> flowing into reactor per pulse (CH<sub>4moles in</sub>)**

Pulse	Pressure/torr	CH <sub>4 in</sub> /μmol
1	112.6	52
2	109.1	51
3	105.6	49
4	102.0	47
5	98.7	46

The areas of each of the CH<sub>4</sub> peaks (CH<sub>4moles out</sub>) were then converted to and the results are shown in table 3.16.

**Table 3.16. Area and moles of each CH<sub>4</sub> peak from mass spectrometer data (CH<sub>4</sub> moles out)**

Pulse	Area/x10 <sup>-8</sup>	μmol
1	2.7	28
2	3.1	32
3	3.0	32
4	3.5	36
5	3.6	37

The percentage CH<sub>4</sub> conversion was then calculated using the relationship:

$$\frac{CH_{4in} - CH_{4out}}{CH_{4in}} \times 100$$

The data obtained is given in table 3.17.

**Table 3.17. % CH<sub>4</sub> conversion obtained for each pulse**

Pulse	% CH <sub>4</sub> Conversion
1	47
2	37
3	36
4	24
5	19

The area under each of the H<sub>2</sub> reaction peaks was then calculated and converted to moles (H<sub>2</sub> moles out) using (3). CH<sub>4</sub> produces a signal due to mass 2 in the mass

spectrometer therefore, this number had to be subtracted from the actual H<sub>2</sub> signal as described in section 1.3.4.1. The resulting data is given in table 3.18.

**Table 3.18. Areas and moles of H<sub>2</sub> produced during each pulse**

Pulse	Area/x10 <sup>-8</sup>	μmol
1	2.38	30
2	1.74	22
3	1.54	19
4	1.06	13
5	9.44	12

The number of CH<sub>4</sub> moles consumed (CH<sub>4</sub>moles<sub>in</sub> - CH<sub>4</sub>moles<sub>out</sub>) was compared to H<sub>2</sub>moles<sub>out</sub>, and it was noticed that they were related by the following relationship:

$$\text{CH}_4\text{moles consumed} : \text{H}_2\text{moles out} \quad 1:1.2$$

Therefore, the ratio was not 1:2 as expected.

An identical calculation process was carried out on the data obtained from the other catalysts and the results are shown in tables 3.19 to 3.21.

**Table 3.19. Data obtained from five CH<sub>4</sub> pulses over Pt/La-ZrO<sub>2</sub>**

Pulse	CH <sub>4</sub> μmol in	CH <sub>4</sub> μmol out	CH <sub>4</sub> μmol consumed	% conversion	H <sub>2</sub> μmol out
1	47	36	11	23	5
2	52	48	4	8	3
3	50	48	2	5	3
4	49	46	3	6	2
5	47	43	4	9	3

**Table 3.20. Data obtained from five CH<sub>4</sub> pulses over Ru/La-ZrO<sub>2</sub>**

Pulse	CH <sub>4</sub> μmol in	CH <sub>4</sub> μmol out	CH <sub>4</sub> μmol consumed	% conversion	H <sub>2</sub> μmol out
1	53	42	11	21	3
2	52	41	11	21	2
3	50	38	12	23	2
4	49	36	12	25	2
5	47	31	15	33	2

**Table 3.21. Data obtained from five CH<sub>4</sub> pulses over Ni/La-ZrO<sub>2</sub>**

Pulse	CH <sub>4</sub> μmol in	CH <sub>4</sub> μmol out	CH <sub>4</sub> μmol consumed	% conversion	H <sub>2</sub> μmol out
1	48	7	41	85	143
2	47	5	42	89	128
3	45	5	40	89	140
4	43	4	39	91	140
5	42	3	39	92	129

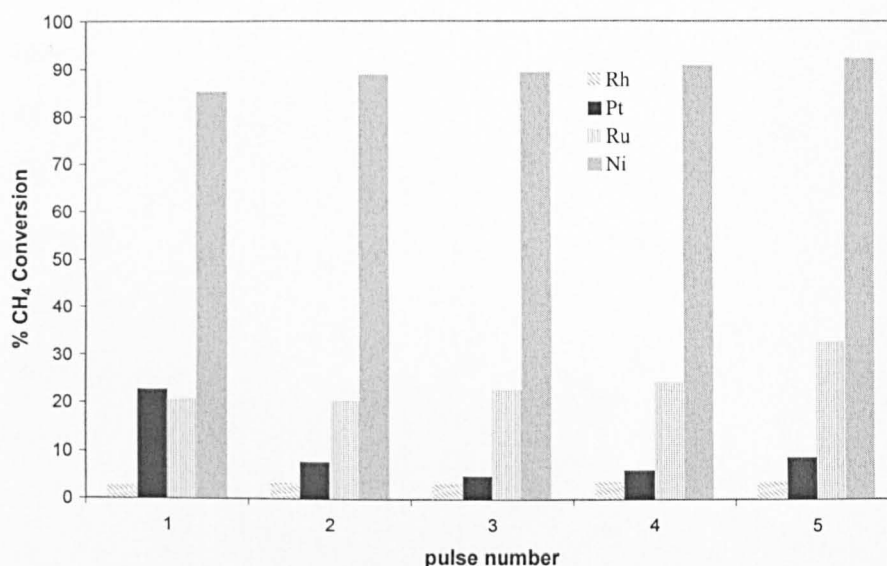
From the stoichiometry of the CH<sub>4</sub> cracking reaction, it was expected that 1 mole of CH<sub>4</sub> would produce 2 moles of H<sub>2</sub> ie it was expected that the H<sub>2(out)</sub>:CH<sub>4(consumed)</sub> ratio would equal 2. When the number of moles of H<sub>2</sub> produced was compared to the number of moles of CH<sub>4</sub> consumed it was discovered that CH<sub>4</sub>:H<sub>2</sub> ratio of 1:2 was invalid. The CH<sub>4</sub>:H<sub>2</sub> ratios obtained for each pulse are given in table 3.22. It can be seen that Rh and Pt are approximately equal to 1. Ru is much less than 1 while Ni is closest to 3.5

**Table 3.22. H<sub>2(out)</sub>/CH<sub>4</sub> (consumed) ratios obtained from each pulse of CH<sub>4</sub> over the metal catalysts**

Pulse \ Catalyst	Rh	Pt	Ru	Ni
1	1.2	0.5	0.3	3.5
2	1.2	0.8	0.2	3.1
3	1.1	1.1	0.1	3.5
4	1.2	0.8	0.2	3.6
5	1.4	0.6	0.1	3.4

The percentage conversions of  $\text{CH}_4$  for five pulses over the La-ZrO<sub>2</sub> supported precious metal catalysts has been summarised in figure 3.11.

**Figure 3.11.** %  $\text{CH}_4$  conversion over Ni, Rh, Pt and Ru for five  $\text{CH}_4$  pulses

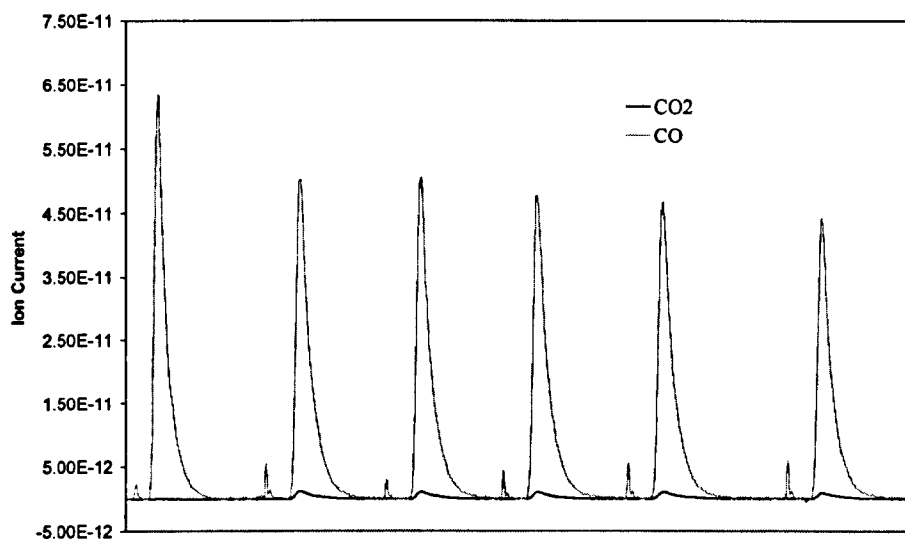


### 3.2.5 CO Pulses over Al<sub>2</sub>O<sub>3</sub> Support

Five pulses of CO were passed over the Al<sub>2</sub>O<sub>3</sub> support. Again, an initial pulse was passed through the by-pass and this acted as a reference. The following five pulses passed through the catalyst bed.

Figure 3.12 shows the mass spectrometer data obtained from passing pulses over the Al<sub>2</sub>O<sub>3</sub> support material. No peak due to CO<sub>2</sub> was seen during the reference pulse but in the five pulses that passed over the catalyst, there is a relatively small signal due to CO<sub>2</sub>. The Al<sub>2</sub>O<sub>3</sub> support was therefore active.

Using the method outlined for the La-ZrO<sub>2</sub> catalysts, the moles of CO<sub>2</sub> obtained in the reaction were calculated. This data is shown in table 3.23.

**Figure 3.12. Five pulses of CO over Al<sub>2</sub>O<sub>3</sub> support material****Table 3.23. Data obtained from five CO pulses over Al<sub>2</sub>O<sub>3</sub> support**

Pulse	CO μmol in	CO <sub>2</sub> μmol out
1	51	3
2	49	3
3	47	2
4	46	2
5	44	2

### 3.2.6 CO Pulses over Al<sub>2</sub>O<sub>3</sub> Supported Catalysts

The mass spectrometer data obtained from passing pulses over Rh, Pt, Ru and Ni are shown in figures 3.13 to 3.16. The numerical data obtained from the mass spectra are tabulated in tables 3.24 to 3.27.

The percentage CO conversion due to the support material is less than that due to the metal catalyst; hence not all catalysis is due to the support material.

**Figure 3.13.** Five pulses of CO over Rh/Al<sub>2</sub>O<sub>3</sub>

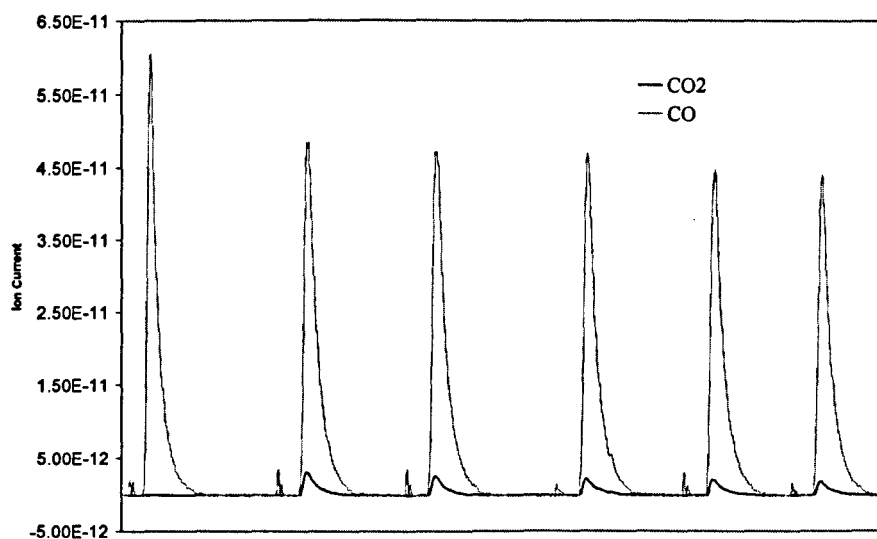


**Figure 3.14.** Five pulses of CO over Pt/Al<sub>2</sub>O<sub>3</sub>

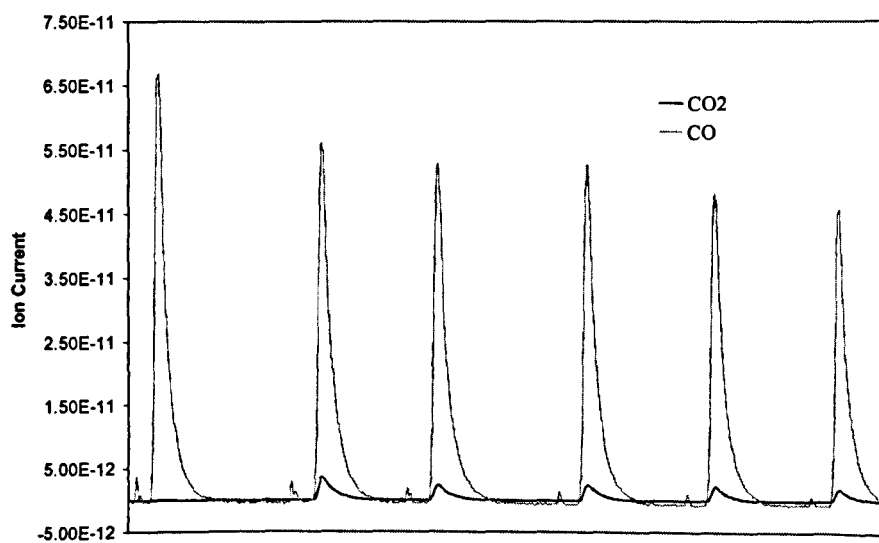


**Figure 3.15.** Five pulses of CO over Ru/Al<sub>2</sub>O<sub>3</sub>

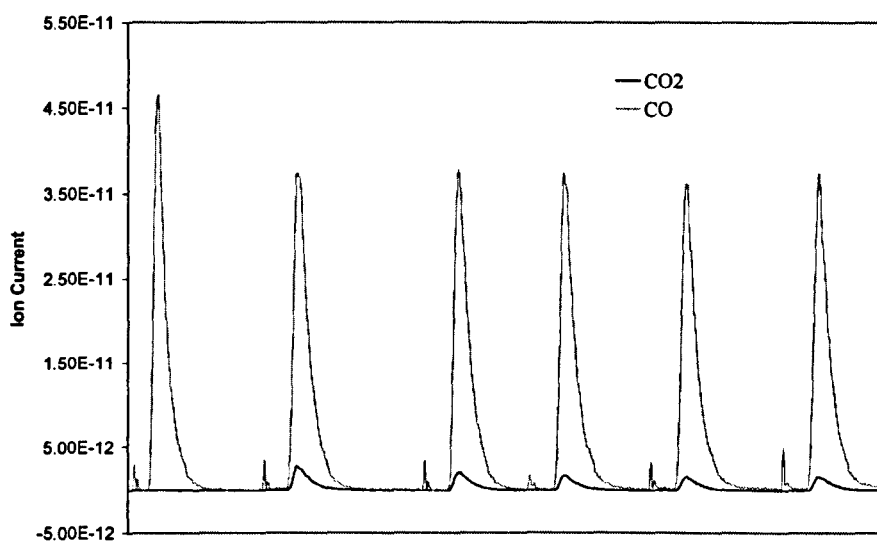


**Figure 3.16.** Five pulses of CO over Ni/Al<sub>2</sub>O<sub>3</sub>

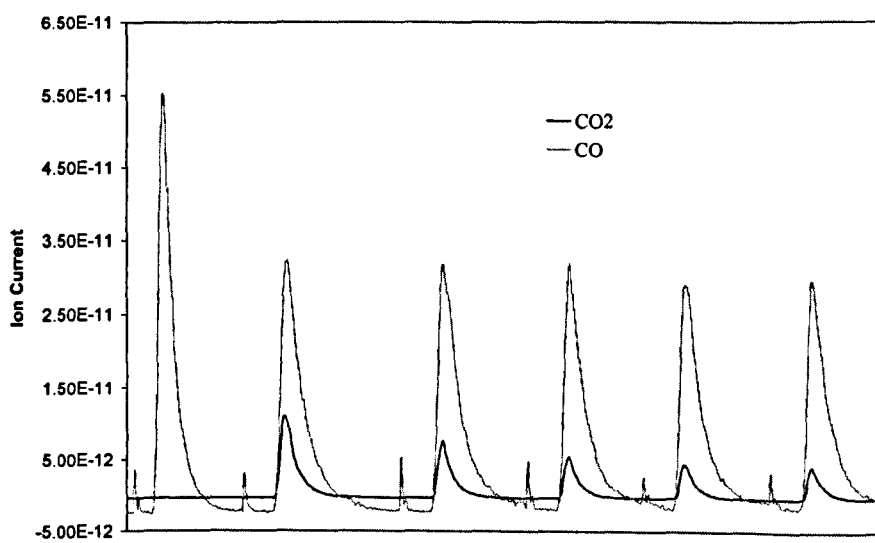


*Table 3.24. Data obtained from five CO pulses over Rh/Al<sub>2</sub>O<sub>3</sub>*

Pulse	CO μmol in	CO μmol out	CO μmol consumed	CO % conversion	CO <sub>2</sub> μmol out	CO consumed /CO <sub>2</sub> out
1	50	45	4	9	5	0.87
2	48	44	4	9	4	1.04
3	46	44	2	5	4	0.61
4	45	42	3	7	4	0.81
5	43	41	2	4	3	0.56

*Table 3.25. Data obtained from five CO pulses over Pt/Al<sub>2</sub>O<sub>3</sub>*

Pulse	CO μmol in	CO μmol out	CO μmol consumed	CO % conversion	CO <sub>2</sub> μmol out	CO consumed /CO <sub>2</sub> out
1	51	46	5	10	6	0.84
2	49	46	4	7	4	0.83
3	47	41	7	14	5	1.39
4	46	39	7	16	4	1.88
5	44	37	7	16	3	2.04

*Table 3.26. Data obtained from five CO pulses over Ru/Al<sub>2</sub>O<sub>3</sub>*

Pulse	CO μmol in	CO μmol out	CO μmol consumed	CO % conversion	CO <sub>2</sub> μmol out	CO consumed /CO <sub>2</sub> out
1	52	47	5	9	8	0.61
2	50	47	4	8	7	0.61
3	49	46	2	5	6	0.39
4	47	47	0	0	5	0
5	46	46	0	0	5	0

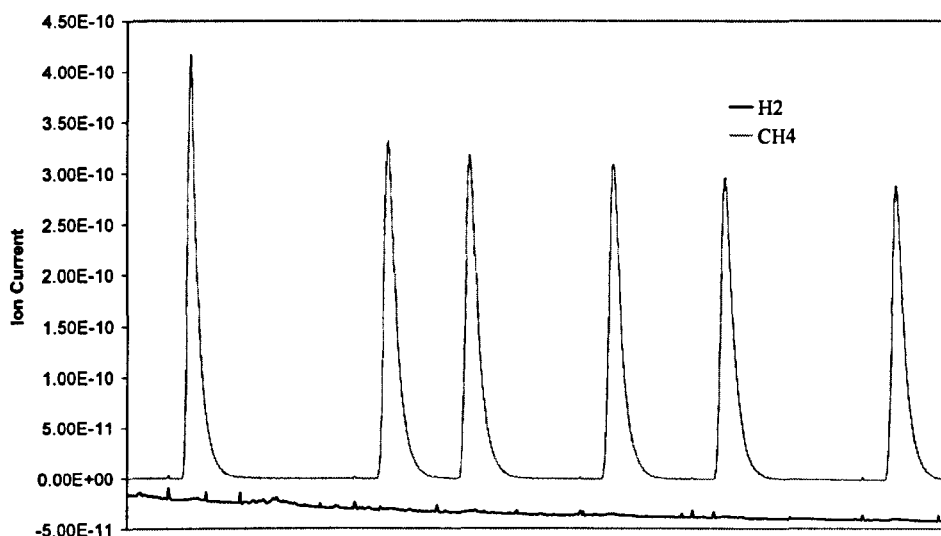
*Table 3.27. Data obtained from five CO pulses over Ni/Al<sub>2</sub>O<sub>3</sub>*

Pulse	CO μmol in	CO μmol out	CO μmol consumed	CO % conversion	CO <sub>2</sub> μmol out	CO consumed /CO <sub>2</sub> out
1	51	32	19	38	19	1.02
2	50	36	14	28	11	1.20
3	48	36	12	25	8	1.40
4	46	36	10	22	7	1.41
5	45	36	9	21	7	1.32

### 3.2.7 CH<sub>4</sub> Pulses over Al<sub>2</sub>O<sub>3</sub> Support

Five pulses of CH<sub>4</sub> were passed over the Al<sub>2</sub>O<sub>3</sub> support following the reference peak. The spectra obtained are shown in figure 3.17. It was expected from the CH<sub>4</sub> cracking reaction that H<sub>2</sub> would be formed. Since there was no trace of H<sub>2</sub> from the reaction peaks it was concluded that the support material was inactive.

*Figure 3.17. Five pulses of CH<sub>4</sub> over Al<sub>2</sub>O<sub>3</sub> support*



### 3.2.8 CH<sub>4</sub> Pulses over Al<sub>2</sub>O<sub>3</sub> Supported Catalysts

Figures 3.18 to 3.21 show the mass spectra obtained from the five reaction pulses over Rh, Pt, Ru and Ni catalysts respectively. Prior to the set of five pulses, a reference pulse was passed through the by-pass, which is also shown in each figure. It can be seen that no H<sub>2</sub> was produced during the reference pulse as expected.

Tables 3.28 to 3.31 display the percentage CH<sub>4</sub> conversions obtained per pulse. This data was calculated by the method described in section 2.

**Figure 3.18.** Five pulses of  $\text{CH}_4$  over  $\text{Rh}/\text{Al}_2\text{O}_3$

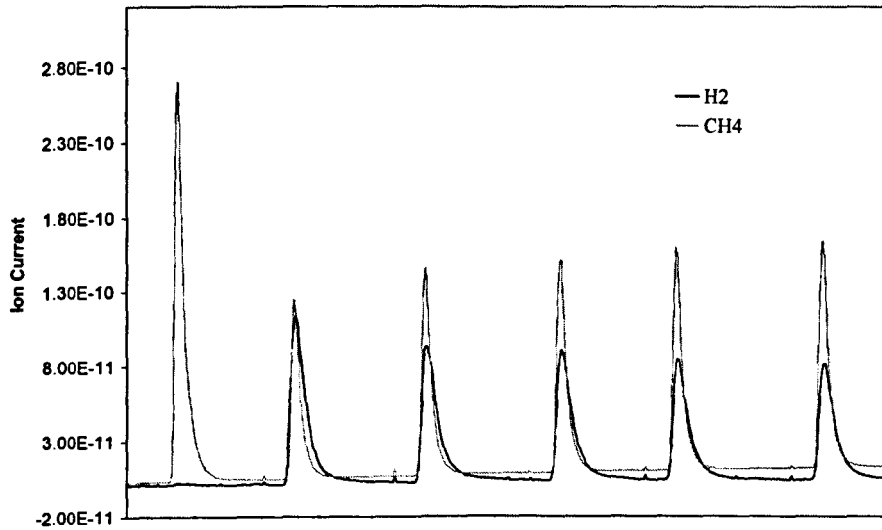


**Figure 3.19.** Five pulses of  $\text{CH}_4$  over  $\text{Pt}/\text{Al}_2\text{O}_3$

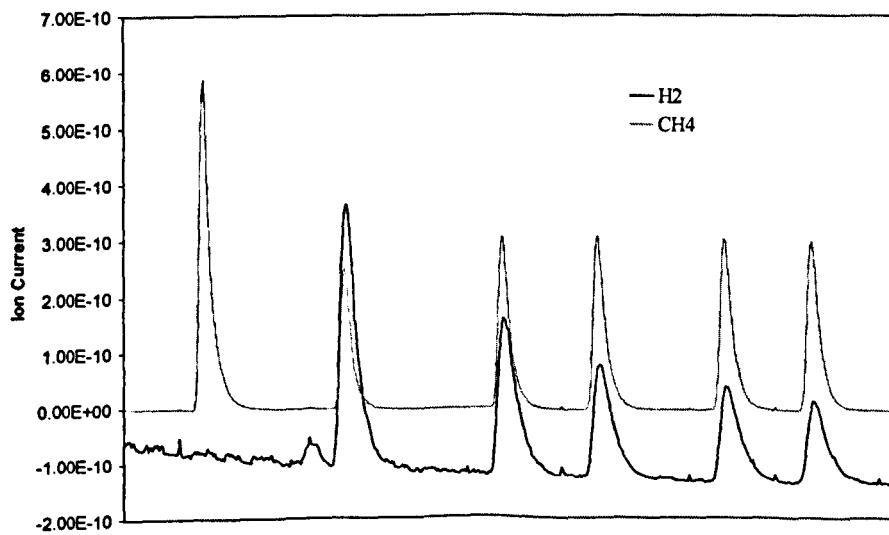


**Figure 3.20.** Five pulses of  $\text{CH}_4$  over  $\text{Ru}/\text{Al}_2\text{O}_3$

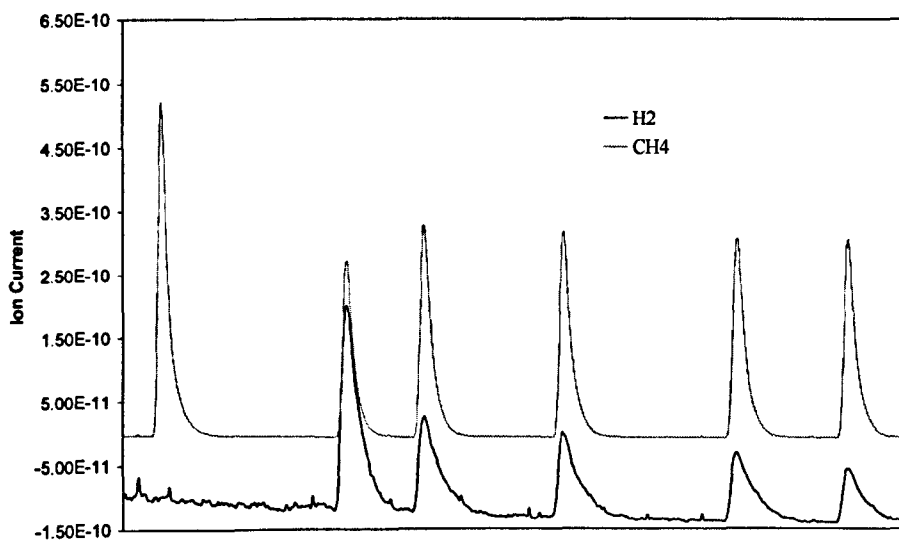


**Figure 3.21.** Five pulses of  $\text{CH}_4$  over  $\text{Ni}/\text{Al}_2\text{O}_3$

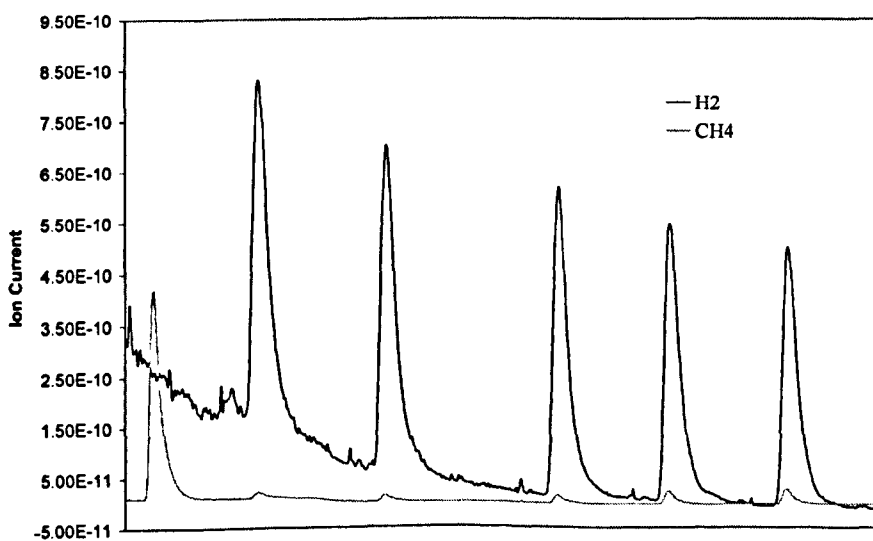


*Table 3.28. Data obtained from five CH<sub>4</sub> pulses over Rh/Al<sub>2</sub>O<sub>3</sub>*

Pulse	CH <sub>4</sub> μmol in	CH <sub>4</sub> μmol out	CH <sub>4</sub> μmol consumed	% CH <sub>4</sub> conversion	H <sub>2</sub> μmol out
1	48	23	25	52	43
2	46	26	20	43	34
3	45	25	20	45	30
4	43	26	17	40	28
5	42	29	13	32	28

*Table 3.29. Data obtained from five CH<sub>4</sub> pulses over Pt/Al<sub>2</sub>O<sub>3</sub>*

Pulse	CH <sub>4</sub> μmol in	CH <sub>4</sub> μmol out	CH <sub>4</sub> μmol consumed	% CH <sub>4</sub> conversion	H <sub>2</sub> μmol out
1	52	24	29	55	81
2	50	29	22	43	53
3	49	33	16	33	37
4	47	34	14	29	35
5	46	33	12	27	28

*Table 3.30. Data obtained from five CH<sub>4</sub> pulses over Ru/Al<sub>2</sub>O<sub>3</sub>*

Pulse	CH <sub>4</sub> μmol in	CH <sub>4</sub> μmol out	CH <sub>4</sub> μmol consumed	% CH <sub>4</sub> conversion	H <sub>2</sub> μmol out
1	49	30	20	40	60
2	48	36	12	26	35
3	46	35	11	24	26
4	45	34	11	24	25
5	43	34	10	22	19

*Table 3.31. Data obtained from five CH<sub>4</sub> pulses over Ni/Al<sub>2</sub>O<sub>3</sub>*

Pulse	CH <sub>4</sub> μmol in	CH <sub>4</sub> μmol out	CH <sub>4</sub> μmol consumed	% CH <sub>4</sub> conversion	H <sub>2</sub> μmol out
1	51	0.6	50	99	159
2	49	0.6	49	99	136
3	48	0.5	47	99	135
4	46	0.5	46	99	119
5	44	0.4	44	99	110

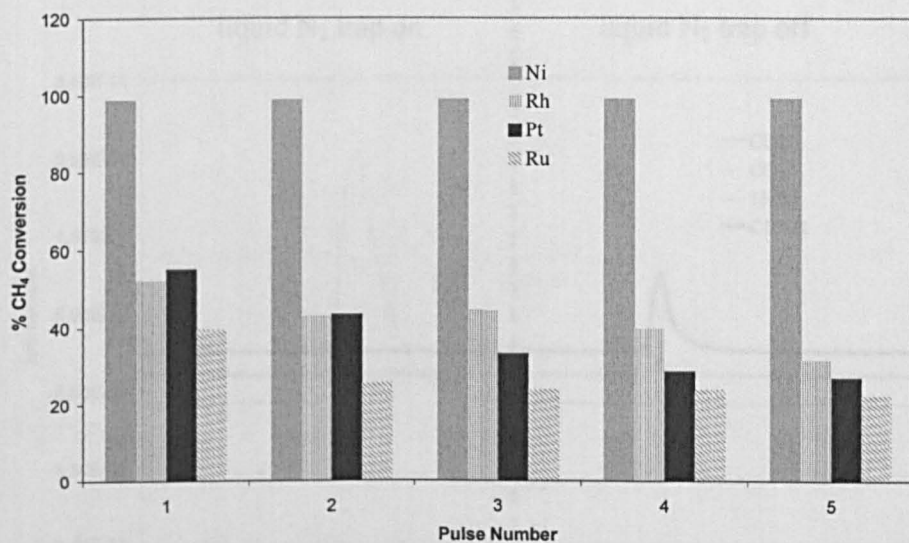
From the stoichiometry of the  $\text{CH}_4$  Cracking reaction, it was expected that 1 mole of  $\text{CH}_4$  would produce 2 moles of  $\text{H}_2$  ( $\text{H}_2/\text{CH}_4 = 2$ ), however table 3.32 shows the actual  $\text{CH}_4:\text{H}_2$  ratios obtained for each catalyst.

**Table 3.32.**  $\text{H}_2/\text{CH}_4$  ratios obtained from each pulse of  $\text{CH}_4$  over the metal  $\text{Al}_2\text{O}_3$  catalysts

Pulse	Catalyst			
	Rh	Pt	Ru	Ni
1	1.7	2.8	3.1	3.1
2	1.7	2.4	2.9	2.8
3	1.5	2.3	2.3	2.9
4	1.6	2.6	2.3	2.6
5	2.1	2.3	2.0	2.5

Figure 3.22 compares the percentage  $\text{CH}_4$  Conversion for each pulse over the metal catalysts. Rh and Pt have very similar values and both begin to decrease with pulse number. Ru starts with a lower value and decreases between the first two pulses and stays constant thereafter. The percentage  $\text{CH}_4$  conversion over Ni is almost 100% and it does not decrease with pulse number.

**Figure 3.22.** Percentage  $\text{CH}_4$  Conversion from five  $\text{CH}_4$  pulses over Rh, Pt, Ru and Ni



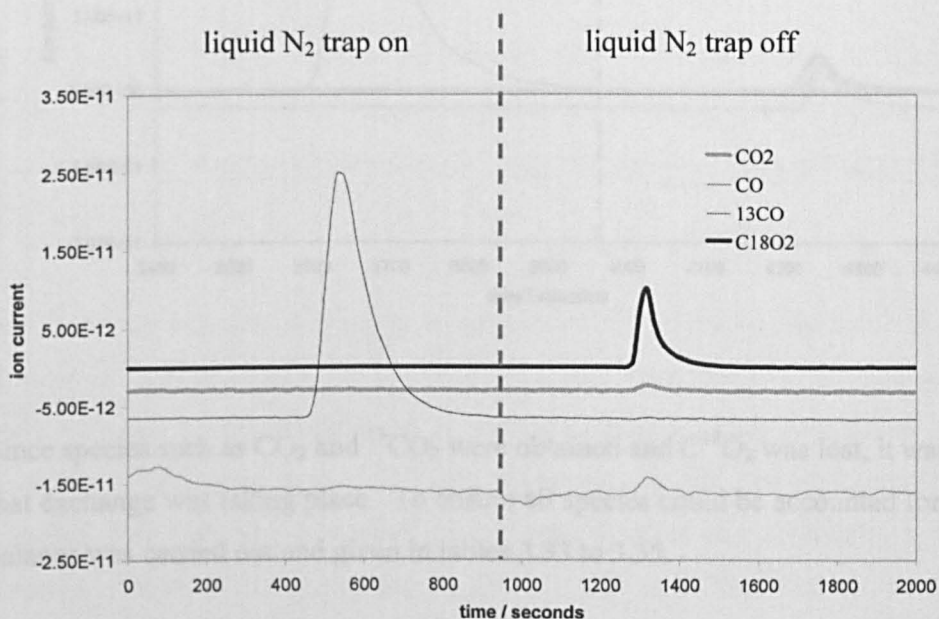
### 3.2.9 Isotope Pulses

#### 3.2.9.1 Reference Pulse

A mixed isotope reference pulse (5:1  $^{13}\text{CO}:\text{C}^{18}\text{O}_2$ ) was passed through the reactor bypass prior to four pulses over the support at 873 K. Figure 3.23 is an example of the spectra obtained from the reference pulse which, for clarity, is shown separately from the spectra of the other pulses. The left hand spectra were obtained when the gas trap was submerged in liquid  $\text{N}_2$ .  $\text{C}^x\text{O}_2$  froze when it entered the trap while  $^y\text{CO}$  remained in the gaseous phase and passed into the mass spectrometer. Note that the only signal is due to  $^{13}\text{CO}$  and that there is no CO impurity.

Once the peak obtained from  $^{13}\text{CO}$  was complete, the liquid  $\text{N}_2$  was removed from the gas trap to allow  $\text{C}^{18}\text{O}_2$  to return to gaseous phase and flow into the mass spectrometer. The largest peak, represented by a thick black line, was due to  $\text{C}^{18}\text{O}_2$ , however there was a relatively small impurity due to  $\text{CO}_2$ . A small peak of CO was visible, due to fragmentation of  $\text{CO}_2$ .

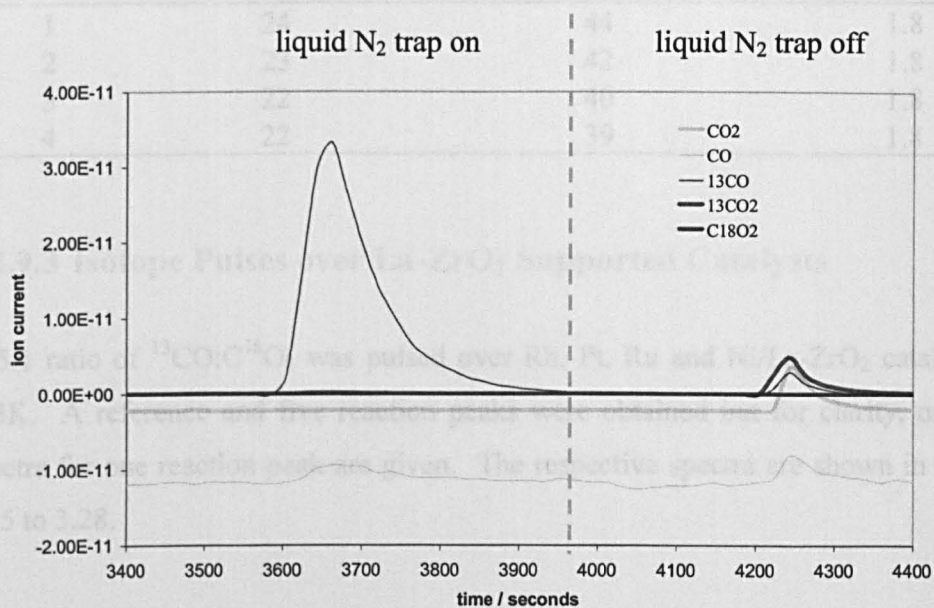
Figure 3.23 Typical reference spectra of isotopes species:  $^{13}\text{CO}:\text{C}^{18}\text{O}_2$  (5:1)



### 3.2.9.2 Isotope Pulses over La-ZrO<sub>2</sub>

Following the by-pass pulse, the reactor containing the catalyst was opened and a pulse (pulse 1) of identical ratio to the reference pulse was passed through. The spectra obtained from pulse 1 are shown in figure 3.24. For clarity, only the result from pulse 1 will be shown. Initially, the trap was submerged in liquid N<sub>2</sub> as the pulse passed through in order to freeze all <sup>x</sup>C<sup>y</sup>O<sub>2</sub> species. The left-hand side of figure 3.24 shows the <sup>a</sup>C<sup>b</sup>O species that were obtained. It can be seen that <sup>13</sup>CO and a relatively small amount of CO emerged. When the liquid N<sub>2</sub> was removed from the trap, the right hand spectra were obtained. With comparison to the reference spectra (figure 3.23), it can be seen that C<sup>18</sup>O<sub>2</sub> was lost while CO<sub>2</sub> and <sup>13</sup>CO<sub>2</sub> were produced. The signals due to <sup>13</sup>CO and CO are splitting patterns.

**Figure 3.24. Spectra obtained from 'pulse 1' over La-ZrO<sub>2</sub> support from isotopes species: <sup>13</sup>CO:C<sup>18</sup>O<sub>2</sub> (5:1)**



Since species such as CO<sub>2</sub> and <sup>13</sup>CO<sub>2</sub> were obtained and C<sup>18</sup>O<sub>2</sub> was lost, it was known that exchange was taking place. To ensure all species could be accounted for, a mass balance was carried out and given in tables 3.33 to 3.35.

**Table 3.33.**  $^{12}\text{C}$  mass balance from isotope pulses over  $\text{Al}_2\text{O}_3$  support

Pulse	$\mu\text{mol IN}$	$\mu\text{mol OUT}$	OUT/IN
1	4.5	5.1	1.1
2	4.3	4.9	1.1
3	4.2	4.4	1.1
4	4.0	4.2	1.0

**Table 3.34.**  $^{13}\text{C}$  mass balance from isotope pulses over  $\text{Al}_2\text{O}_3$  support

Pulse	$\mu\text{mol IN}$	$\mu\text{mol OUT}$	OUT/IN
1	24	29	1.2
2	23	28	1.2
3	22	27	1.2
4	22	26	1.2

**Table 3.35.**  $^{16}\text{O}$  mass balance from isotope pulses over  $\text{Al}_2\text{O}_3$  support

Pulse	$\mu\text{mol IN}$	$\mu\text{mol OUT}$	OUT/IN
1	24	44	1.8
2	23	42	1.8
3	22	40	1.8
4	22	39	1.8

### 3.2.9.3 Isotope Pulses over La-ZrO<sub>2</sub> Supported Catalysts

A 5:1 ratio of  $^{13}\text{CO}:\text{C}^{18}\text{O}_2$  was pulsed over Rh, Pt, Ru and Ni/La-ZrO<sub>2</sub> catalysts at 873K. A reference and five reaction peaks were obtained but for clarity, only the spectra for one reaction peak are given. The respective spectra are shown in figures 3.25 to 3.28.

The left hand side (liquid N<sub>2</sub> trap is on) in each figure shows that most of the  $^x\text{C}^y\text{O}$  species is  $^{13}\text{CO}$  and that there is a relatively small peak due to CO. Note also that a peak of mass 2, corresponding to H<sub>2</sub> was also detected after each pulse over each catalyst. H<sub>2</sub> is shown in red for Pt and Ru however in the case of Rh and Ni the H<sub>2</sub> baseline was very low compared to the other species and for clarity it has been omitted. No H<sub>2</sub> was detected for La-ZrO<sub>2</sub>. The right hand side shows the  $^a\text{C}^b\text{O}_2$  species and it can be seen that no  $\text{C}^{18}\text{O}_2$  was detected however, CO<sub>2</sub> and  $^{13}\text{CO}_2$  were.

The peaks due to  $^{13}\text{CO}$  and  $\text{CO}$  are fragmentations of the  $^a\text{C}^b\text{O}_2$  species. The tables following each set of spectra show the results of the mass balance.

**Figure 3.25** Mass spectra of species obtained after isotope pulses over Rh/La-ZrO<sub>2</sub> (pulse 1)

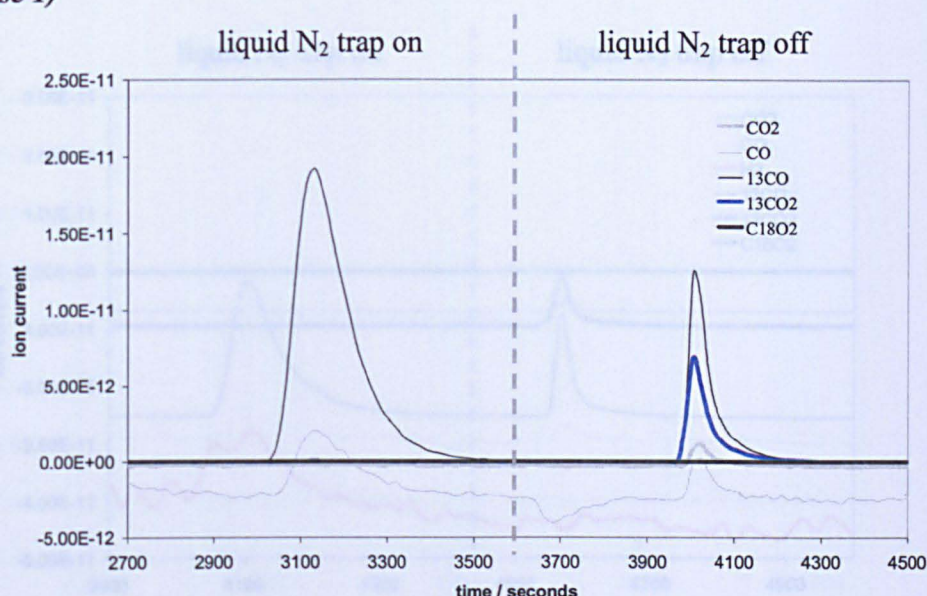


**Table 3.36.** <sup>12</sup>C mass balance from isotope pulses over Rh/La-ZrO<sub>2</sub> catalyst

Pulse	μmol IN	μmol OUT	OUT/IN
1	4.6	5.5	1.2
2	4.5	6.5	1.5
3	4.3	6.2	1.4
4	4.2	5.9	1.4
5	4.1	5.4	1.3

**Table 3.37.** <sup>13</sup>C mass balance from isotope pulses over Rh/La-ZrO<sub>2</sub> catalyst

Pulse	μmol IN	μmol OUT	OUT/IN
1	22	28	1.3
2	22	27	1.2
3	21	26	1.2
4	20	27	1.3
5	20	25	1.3

**Table 3.38.** <sup>16</sup>O mass balance from isotope pulses over Rh/La-ZrO<sub>2</sub> catalyst

Pulse	μmol IN	μmol OUT	OUT/IN
1	2.2	3.7	1.7
2	2.2	3.7	1.7
3	2.1	3.6	1.7
4	2.0	3.7	1.8
5	2.0	3.4	1.8

**Figure 3.26** Mass spectra of species obtained after isotope pulses over Pt/La-ZrO<sub>2</sub> (pulse 1)

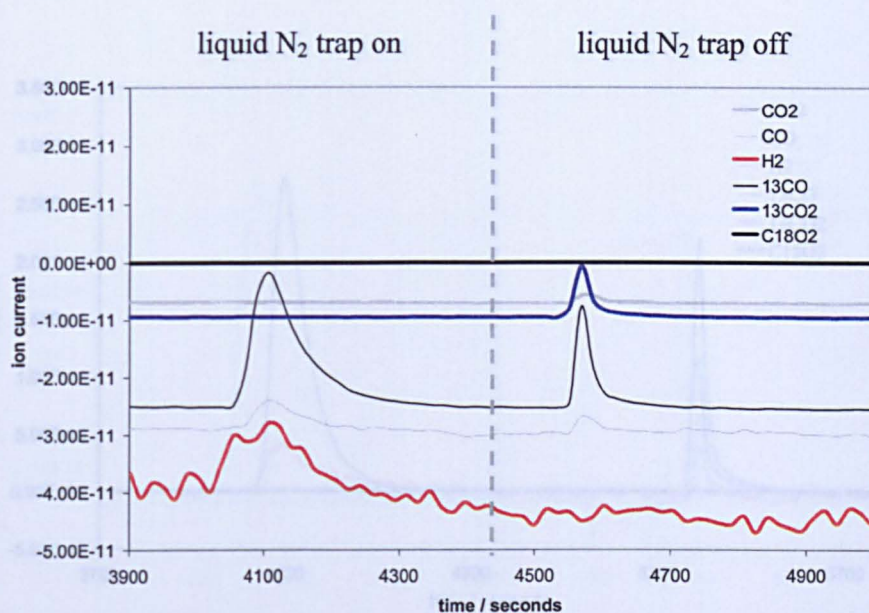


**Table 3.39.** <sup>12</sup>C mass balance from isotope pulses over Pt/La-ZrO<sub>2</sub> catalyst

Pulse	μmol IN	μmol OUT	OUT/IN
1	4.5	5.0	1.1
2	4.3	6.3	1.4
3	4.2	5.1	1.2
4	4.1	4.6	1.1
5	3.9	4.1	1.0

**Table 3.40.** <sup>13</sup>C mass balance from isotope pulses over Pt/La-ZrO<sub>2</sub> catalyst

Pulse	μmol IN	μmol OUT	OUT/IN
1	23	28	1.2
2	22	28	1.3
3	21	24	1.1
4	21	25	1.2
5	20	24	1.2

**Table 3.41.** <sup>16</sup>O mass balance from isotope pulses over Pt/La-ZrO<sub>2</sub> catalyst

Pulse	moles IN x10 <sup>-5</sup>	moles OUT x10 <sup>-5</sup>	OUT/IN
1	25	43	1.7
2	24	42	1.7
3	23	40	1.7
4	22	40	1.8
5	22	37	1.7

**Figure 3.27.** Mass spectra of species obtained after isotope pulses over Ru/La-ZrO<sub>2</sub> (pulse 1)

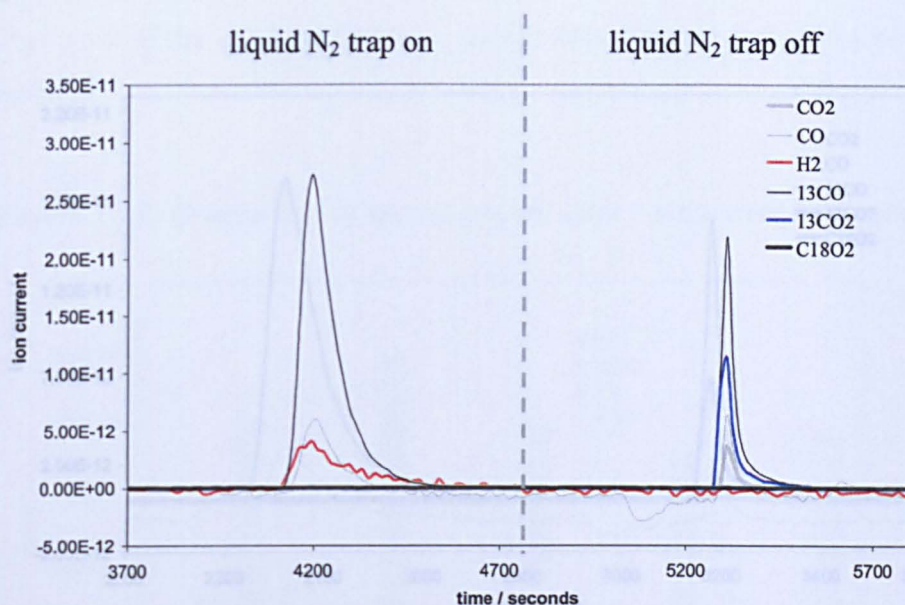


**Table 3.42.** <sup>12</sup>C mass balance from isotope pulses over Ru/La-ZrO<sub>2</sub> catalyst

Pulse	μmol IN	μmol OUT	OUT/IN
1	0.38	0.51	1.3
2	0.37	0.51	1.4
3	0.36	0.52	1.4
4	0.35	0.47	1.3
5	0.34	0.41	1.2

**Table 3.43.** <sup>13</sup>C mass balance from isotope pulses over Ru/La-ZrO<sub>2</sub> catalyst

Pulse	μmol IN	μmol OUT	OUT/IN
1	23	28	1.2
2	22	28	1.3
3	21	24	1.1
4	21	25	1.2
5	20	24	1.2

**Table 3.44.** <sup>16</sup>O mass balance from isotope pulses over Ru/La-ZrO<sub>2</sub> catalyst

Pulse	μmol IN	μmol OUT	OUT/IN
1	23	36	1.6
2	22	37	1.7
3	21	33	1.5
4	21	33	1.6
5	20	32	1.6

**Figure 3.28** Mass spectra of species obtained after isotope pulses over Ni/La-ZrO<sub>2</sub> (pulse 1)

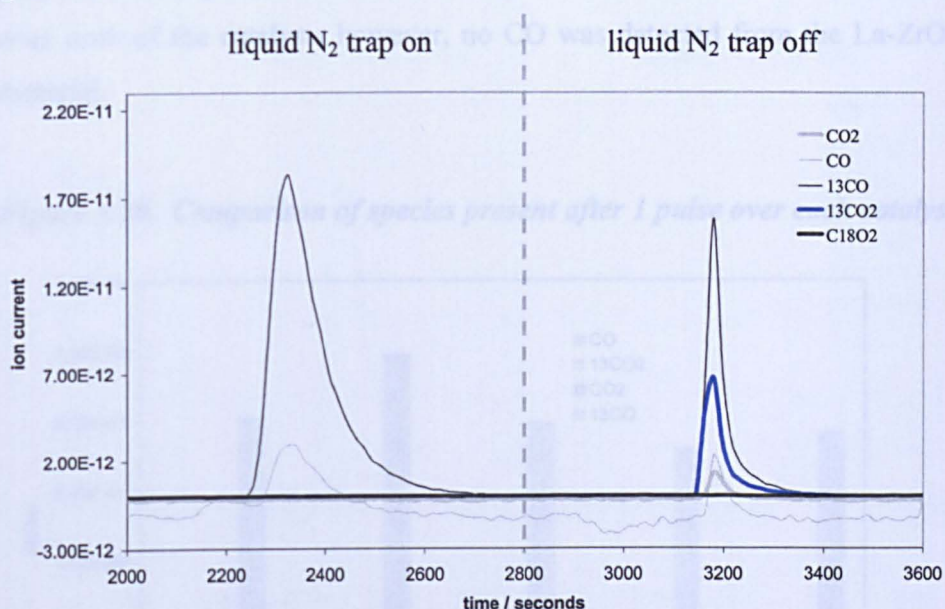


**Table 3.45.** <sup>12</sup>C mass balance from isotope pulses over Ni/La-ZrO<sub>2</sub> catalyst

Pulse	μmol IN	μmol OUT	OUT/IN
1	6.0	4.1	0.7
2	5.8	6.2	1.1
3	5.6	5.9	1.1
4	5.4	5.7	1.0
5	5.3	5.7	1.1

**Table 3.46.** <sup>13</sup>C mass balance from isotope pulses over Ni/La-ZrO<sub>2</sub> catalyst

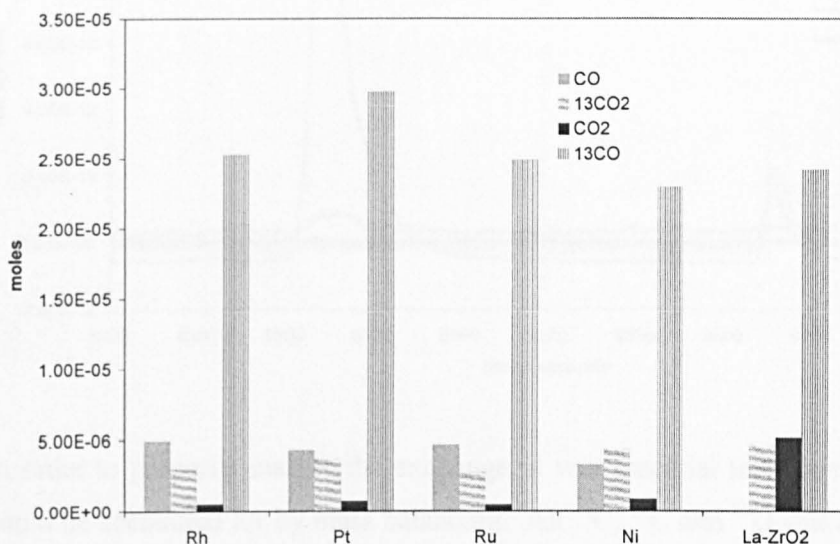
Pulse	μmol IN	moles OUT	OUT/IN
1	22	27	1.2
2	21	27	1.2
3	21	27	1.3
4	20	27	1.3
5	20	26	1.3

**Table 3.47.** <sup>16</sup>O mass balance from isotope pulses over Ni/La-ZrO<sub>2</sub> catalyst

Pulse	μmol IN	μmol OUT	OUT/IN
1	22	37	1.6
2	21	38	1.8
3	21	38	1.8
4	20	38	1.9
5	20	37	1.9

For an easy comparison of the species present after 1 pulse over each substrate, a bar graph has been plotted and shown in figure 3.29. The extent of reaction is similar over each of the catalysts however, no CO was detected from the La-ZrO<sub>2</sub> support material.

*Figure 3.29. Comparison of species present after 1 pulse over each catalyst*

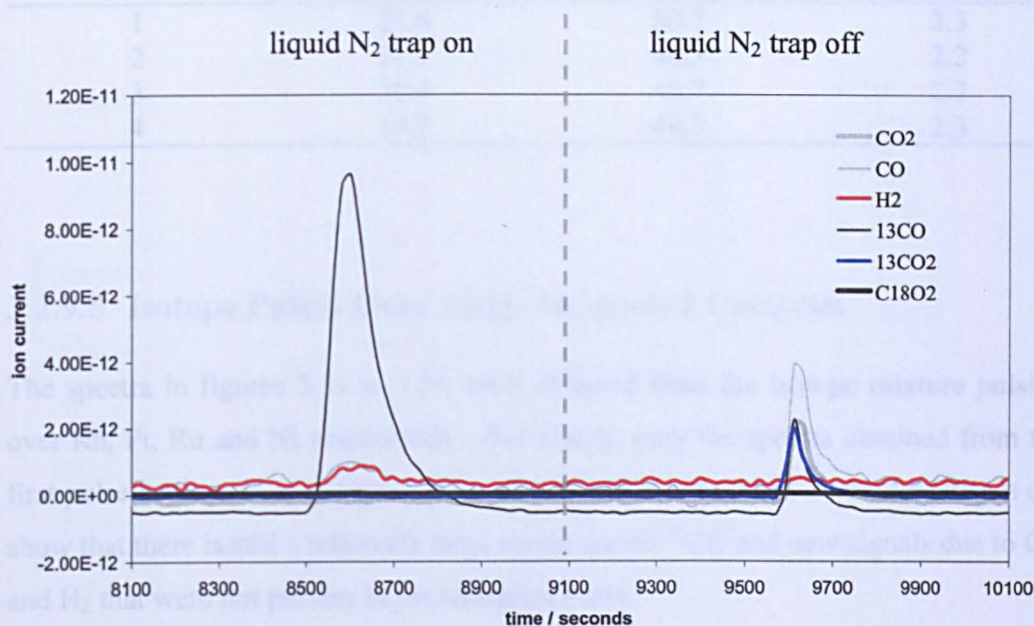


#### 3.2.9.4 Isotope Pulses Over Al<sub>2</sub>O<sub>3</sub> Support Material

The 5:1 ratio of <sup>13</sup>CO:C<sup>18</sup>O<sub>2</sub> was pulsed over Al<sub>2</sub>O<sub>3</sub> at 873K. A reference and five reaction peaks were obtained but for clarity, only the spectra of one reaction peak are given. The spectra are shown in figure 3.30.

The left hand side (liquid N<sub>2</sub> trap is on) shows that most of the <sup>x</sup>C<sup>y</sup>O species is <sup>13</sup>CO and that there is a relatively small peak due to CO. The right hand side shows the <sup>a</sup>C<sup>b</sup>O<sub>2</sub> species and it can be seen that no C<sup>18</sup>O<sub>2</sub> was detected however, CO<sub>2</sub> and <sup>13</sup>CO<sub>2</sub> were. The peaks due to <sup>13</sup>CO and CO are fragmentations of the <sup>a</sup>C<sup>b</sup>O<sub>2</sub> species. Tables 3.48 to 3.50 which follow each set of spectra show the results of the mass balance.

**Figure 3.30.** Mass spectra of species obtained after isotopes pulsed over  $Al_2O_3$  support material



In order to properly analyse the exchange, it was essential to ensure that all species could be accounted for by mass balancing. All  $^{12}C$ ,  $^{13}C$  and  $^{16}O$  was accounted for as shown in table 3.48 to 3.50.  $^{18}O$  was not mass balanced as no  $^{18}O$ -containing species were present in the reactor effluent that entered the mass spectrometer after each pulse.

**Table 3.48.**  $^{12}C$  mass balance from isotope pulses over  $Al_2O_3$  support

Pulse	$\mu\text{mol IN}$	$\mu\text{mol OUT}$	OUT/IN
1	5.4	6.8	1.3
2	5.3	6.5	1.2
3	5.1	6.5	1.3
4	4.9	6.2	1.3

**Table 3.49.**  $^{13}C$  mass balance from isotope pulses over  $Al_2O_3$  support

Pulse	$\mu\text{mol IN}$	$\mu\text{mol OUT}$	OUT/IN
1	21.6	30.2	1.4
2	21.1	27.9	1.3
3	20.4	27.4	1.3
4	19.7	27.4	1.4

*Table 3.50. <sup>16</sup>O mass balance from isotope pulses over Al<sub>2</sub>O<sub>3</sub> support*

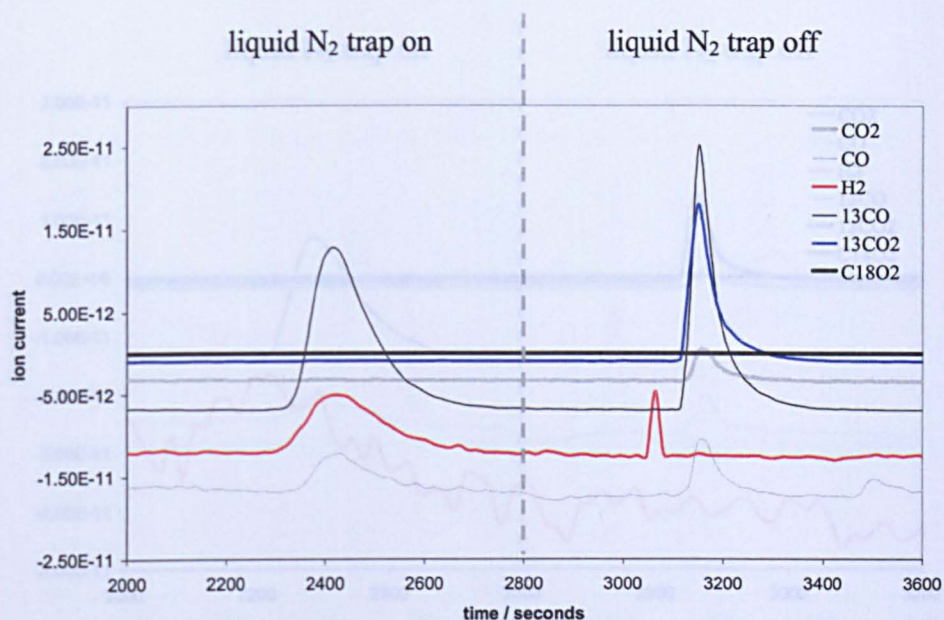
Pulse	μmol IN	μmol OUT	OUT/IN
1	21.6	50.7	2.3
2	21.1	46.3	2.2
3	20.4	45.7	2.2
4	19.7	44.5	2.3

### 3.2.9.5 Isotope Pulses Over Al<sub>2</sub>O<sub>3</sub> Supported Catalysts

The spectra in figures 3.31 to 3.34 were obtained from the isotope mixture pulsing over Rh, Pt, Ru and Ni respectively. For clarity, only the spectra obtained from the first pulse is given in each figure. The left hand side of each set of spectra (trap is on) show that there is still a relatively large signal due to <sup>13</sup>CO and new signals due to CO and H<sub>2</sub> that were not present in the reference pulse.

When the N<sub>2</sub> trap was removed, all <sup>x</sup>C<sup>y</sup>O<sub>2</sub> species that were condensed were now volatilised and flowed into the mass spectrometer. There was no longer any signal due to C<sup>18</sup>O<sub>2</sub>. <sup>13</sup>CO<sub>2</sub> is the most prominent peak which has a fragmentation peak of mass 29 (same as <sup>13</sup>CO). CO<sub>2</sub> is also visible and has a fragmentation peak of mass 28 (same as CO)

As was done for the isotope reaction over the Al<sub>2</sub>O<sub>3</sub> support material, all <sup>12</sup>C, <sup>13</sup>C and <sup>16</sup>O species were accounted for by mass balancing. The results are given in the tables following the mass spectra.

Figure 3.31. Mass spectra of species obtained after isotopes pulsed over Rh/Al<sub>2</sub>O<sub>3</sub>Table 3.51. <sup>12</sup>C mass balance from isotope pulses over Rh/Al<sub>2</sub>O<sub>3</sub> catalyst

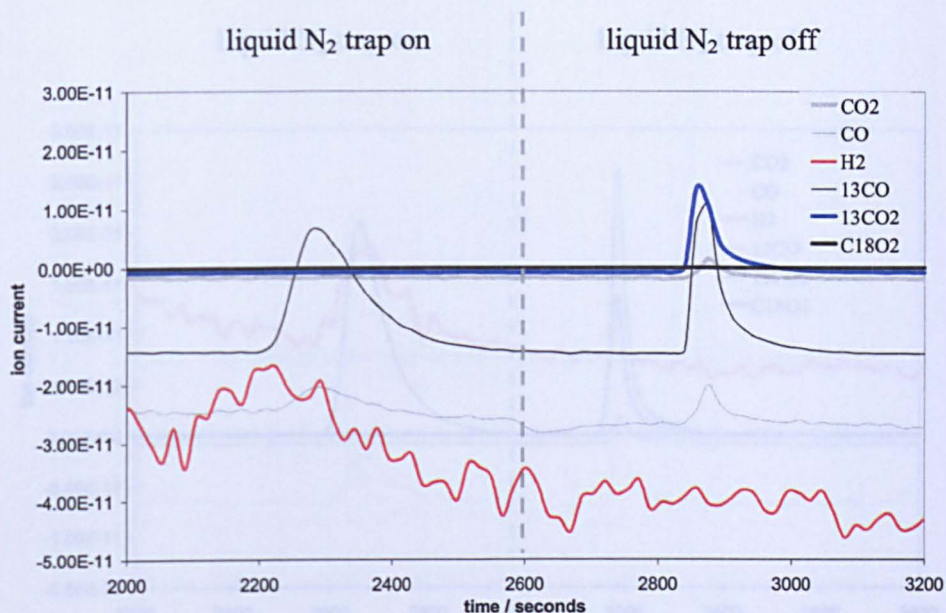
Pulse	μmol IN	μmol OUT	OUT/IN
1	4.3	5.0	1.3
2	4.1	5.1	1.4
3	3.3	4.0	1.1
4	3.2	4.1	1.3
5	3.3	4.1	1.3

Table 3.52. <sup>13</sup>C mass balance from isotope pulses over Rh/Al<sub>2</sub>O<sub>3</sub> catalyst

Pulse	μmol IN	μmol OUT	OUT/IN
1	22.0	23.4	1.0
2	22.1	21.2	0.9
3	21.1	18.1	0.9
4	20.4	17.0	0.8
5	20.1	16.1	0.8

Table 3.53. <sup>16</sup>O mass balance from isotope pulses over Rh/Al<sub>2</sub>O<sub>3</sub> catalyst

Pulse	μmol IN	μmol OUT	OUT/IN
1	22.1	37.3	1.7
2	22.1	33.4	1.5
3	21.3	29.2	1.4
4	20.3	27.0	1.3
5	20.2	26.0	1.3

Figure 3.32 Mass spectra of species obtained after isotopes pulsed over Pt/Al<sub>2</sub>O<sub>3</sub>Table 3.54. <sup>12</sup>C mass balance from isotope pulses over Pt/Al<sub>2</sub>O<sub>3</sub> catalyst

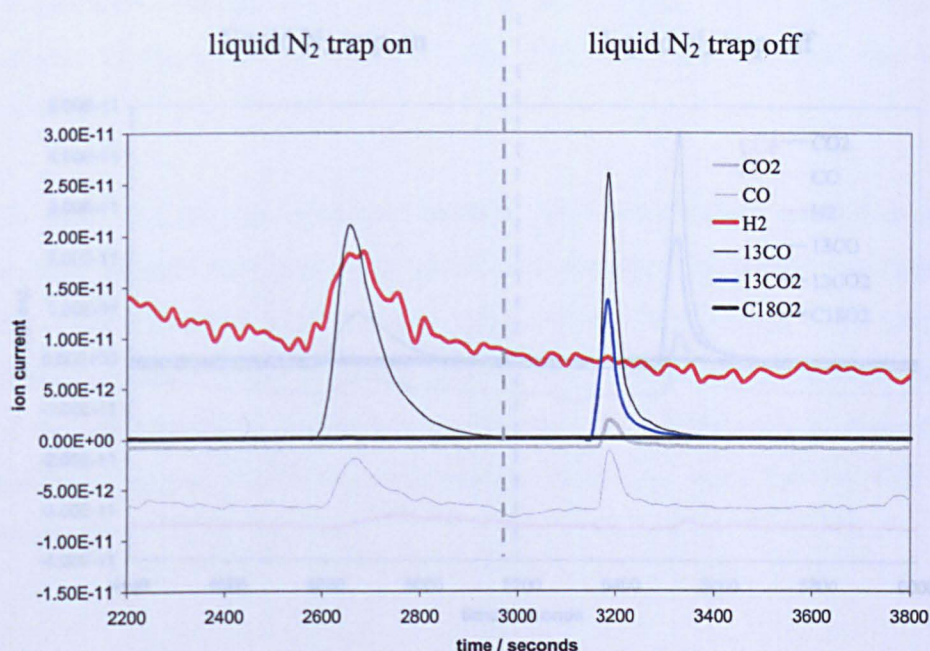
Pulse	μmol IN	μmol OUT	OUT/IN
1	4.4	5.3	1.2
2	4.2	5.4	1.3
3	4.1	5.8	1.4
4	4.0	4.4	1.1
5	3.8	3.3	0.9

Table 3.55. <sup>13</sup>C mass balance from isotope pulses over Pt/Al<sub>2</sub>O<sub>3</sub> catalyst

Pulse	μmol IN	μmol OUT	OUT/IN
1	23.1	27.4	1.2
2	22.3	27.3	1.2
3	21.4	27.2	1.3
4	21.0	22.3	1.1
5	20.3	20.2	1.0

Table 3.56. <sup>16</sup>O mass balance from isotope pulses over Pt/Al<sub>2</sub>O<sub>3</sub> catalyst

Pulse	μmol IN	μmol OUT	OUT/IN
1	23.2	39.3	1.7
2	22.0	38.2	1.8
3	21.3	40.2	1.9
4	21.2	33.1	1.6
5	20.3	29.0	1.5

Figure 3.33 Mass spectra of species obtained after isotopes pulsed over Ru/Al<sub>2</sub>O<sub>3</sub>Table 3.57. <sup>12</sup>C mass balance from isotope pulses over Ru/Al<sub>2</sub>O<sub>3</sub> catalyst

Pulse	μmol IN	μmol OUT	OUT/IN
1	4.5	4.5	1.0
2	4.3	5.2	1.2
3	4.2	5.1	1.2
4	4.0	5.2	1.3
5	3.9	4.6	1.2

Table 3.58. <sup>13</sup>C mass balance from isotope pulses over Ru/Al<sub>2</sub>O<sub>3</sub> catalyst

Pulse	μmol IN	μmol OUT	OUT/IN
1	23.1	26.7	1.2
2	22.4	27.1	1.2
3	21.6	27.2	1.3
4	20.9	25.7	1.2
5	20.3	24.1	1.2

Table 3.59. <sup>16</sup>O mass balance from isotope pulses over Ru/Al<sub>2</sub>O<sub>3</sub> catalyst

Pulse	μmol IN	μmol OUT	OUT/IN
1	23.1	38.0	1.6
2	22.4	38.4	1.7
3	21.6	39.1	1.8
4	20.9	37.3	1.8
5	20.3	35.1	1.7

Figure 3.34 Mass spectra of species obtained after isotopes pulsed over Ni/Al<sub>2</sub>O<sub>3</sub>

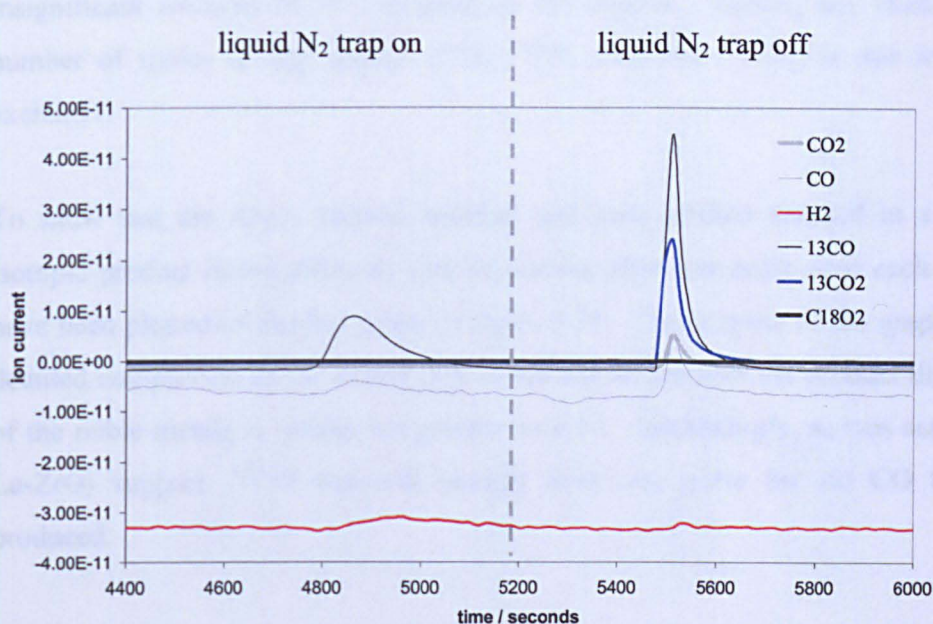


Table 3.60. <sup>12</sup>C mass balance from isotope pulses over Ni/Al<sub>2</sub>O<sub>3</sub> catalyst

Pulse	μmol IN	μmol OUT	OUT/IN
1	4.3	5.6	1.3
2	4.1	4.8	1.2
3	4.0	4.6	1.1
4	3.9	4.3	1.1
5	3.8	2.5	0.7

Table 3.61. <sup>13</sup>C mass balance from isotope pulses over Ni/Al<sub>2</sub>O<sub>3</sub> catalyst

Pulse	μmol IN	μmol OUT	OUT/IN
1	22.1	26.3	1.2
2	21.3	26.1	1.2
3	21.0	25.2	1.2
4	20.4	23.3	1.2
5	20.0	22.2	1.1

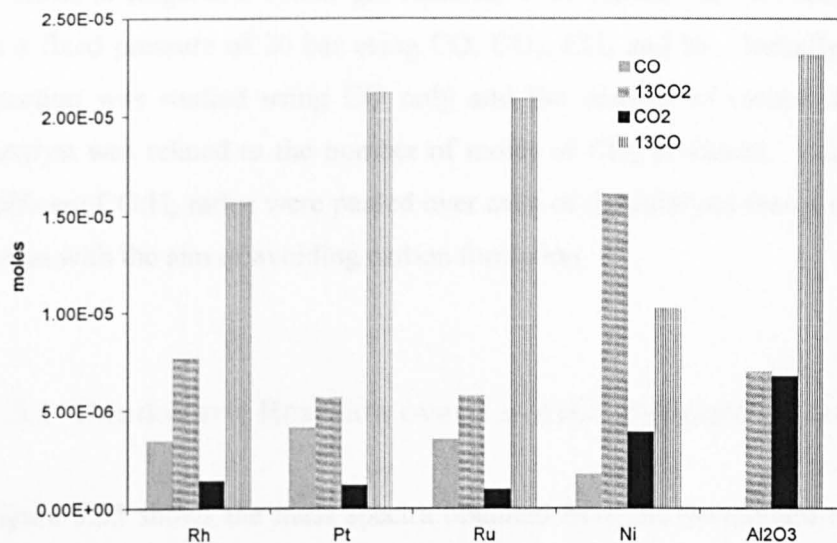
Table 3.62. <sup>16</sup>O mass balance from isotope pulses over Ni/Al<sub>2</sub>O<sub>3</sub> catalyst

Pulse	μmol IN	μmol OUT	OUT/IN
1	22.3	52.1	2.3
2	21.4	49.2	2.3
3	21.2	46.1	2.2
4	20.3	43.0	2.2
5	20.0	41.3	2.1

Since all  $^{13}\text{C}$  species were accounted for in the gas phase, this meant that there were insignificant amounts of  $^{13}\text{C}$  deposited on the catalyst. Hence, any change in the number of moles of any species ( $\text{CO}$ ,  $^{13}\text{CO}$ ,  $\text{CO}_2$  and  $^{13}\text{CO}_2$ ) is due to isotopic exchange.

To show that the  $\text{Al}_2\text{O}_3$  support material and each catalyst resulted in a different isotopic product distribution, all species present after one pulse over each substrate have been plotted on the bar graph in figure 3.35. The purpose of the graph is not a detailed comparison of the extent of reaction but shows how the product distribution of the noble metals is similar but greater over Ni. Interestingly, as was seen for the La- $\text{ZrO}_2$  support,  $^{13}\text{CO}$  was still present after one pulse but no CO had been produced.

**Figure 3.35.** Number of moles of each species present over each catalyst after 1 pulse



As described previously, the reactant gas flowed through the by-pass initially before it was collected over the catalyst support only. In figure 3.34 this has been associated. Before the reactant and product gases can be seen emerging from the reactor, the Ar gas that was used to cool the reactor emerges. Ar gas was followed on the mass spectrometer for a short time for clarity. The point at which Ar emerged from the reactor was recognised by a dip in the CO signal just after the by-pass. While Ar is being used in the reactor, CO re-emerges from the reactor and simultaneously, a relatively weak CO<sub>2</sub> signal is detected. As the Ar signal increases, this signal slowly decreases towards the baseline.

The mass spectra obtained from the diaphragm pressure over Rh, Pt and Ru catalysts respectively are given in figures 3.36 to 3.38. Each mass spectrum followed the same general trend: CO<sub>2</sub> was produced immediately and reached a maximum before decreasing towards the baseline. The amount of CO<sub>2</sub> peaks differed, as did the time taken for complete decay. In figures 3.35 to 3.38, the mass spectrometer units have been converted to a gas flow rate in units of moles cm<sup>-2</sup> s<sup>-1</sup>, the calculation given in section 2. The flow rate of CO<sub>2</sub> is shown on the left hand axis and CO on the right hand axis.

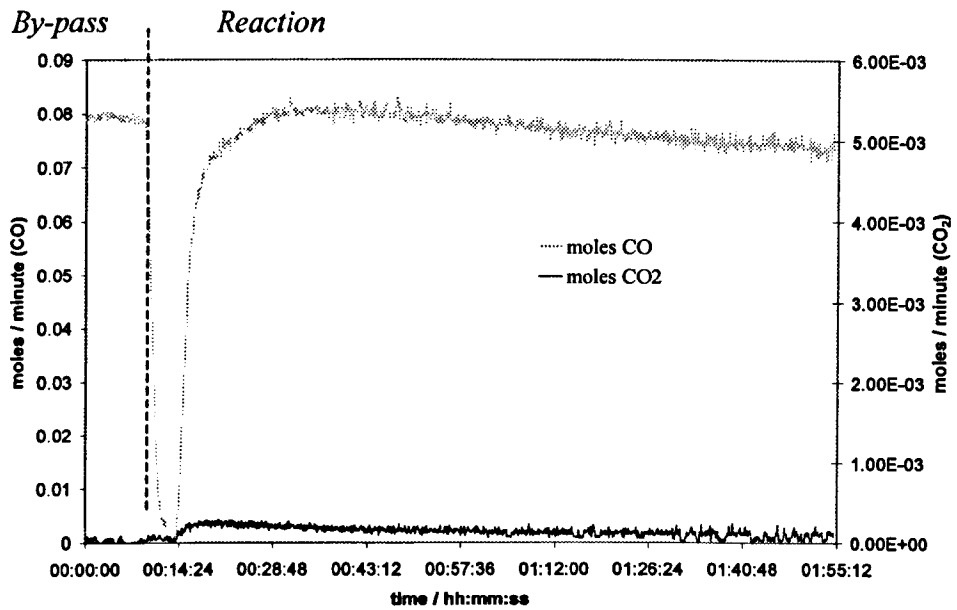
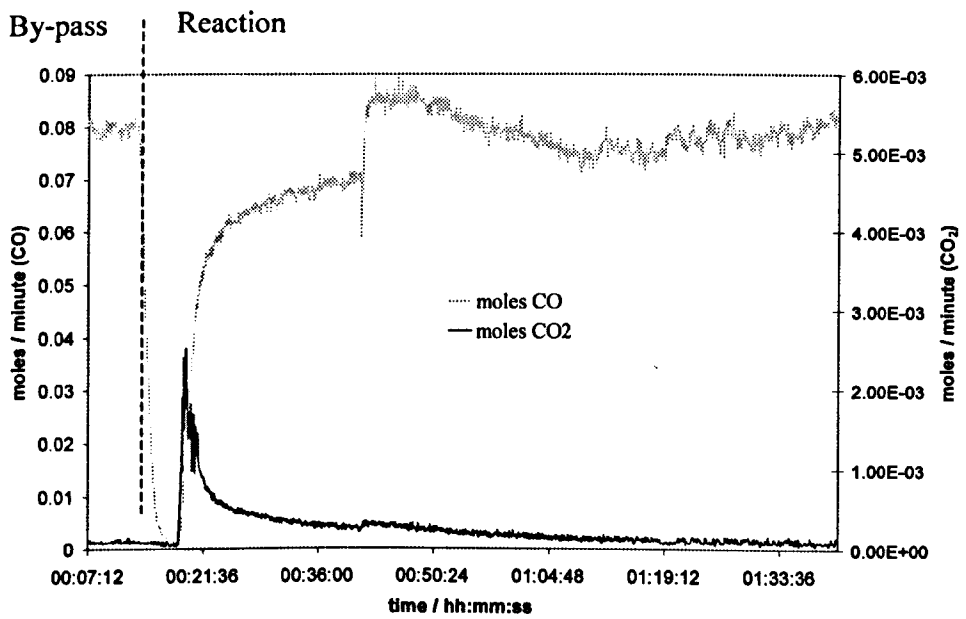
### 3.3 High Pressure Rig Reactions

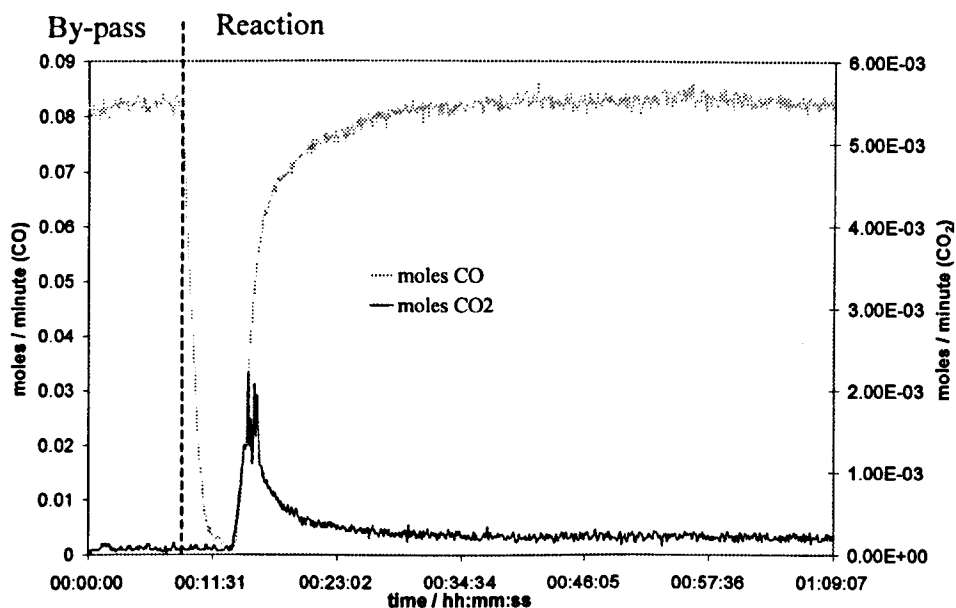
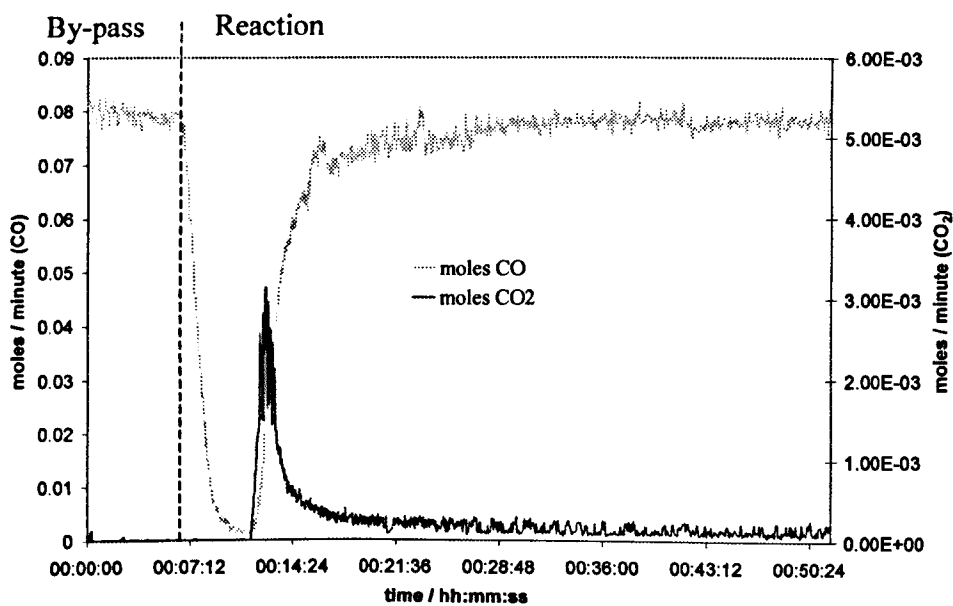
A series of single and double gas reactions were carried out over each of the catalysts at a fixed pressure of 20 bar using CO, CO<sub>2</sub>, CH<sub>4</sub> and H<sub>2</sub>. Initially, the Boudouard reaction was studied using CO only and the amount of carbon deposited on the catalyst was related to the number of moles of CO<sub>2</sub> produced. Following this, two different CO:H<sub>2</sub> ratios were passed over each of the catalysts then a range of CO:CO<sub>2</sub> ratios with the aim of avoiding carbon formation.

#### 3.3.1 Boudouard Reaction over La-ZrO<sub>2</sub> Supported Catalysts

Figure 3.35 shows the mass spectra obtained from the Boudouard reaction over the La-ZrO<sub>2</sub> catalyst support only. As described in section 2, the reactant gas flowed through the by-pass initially before it was redirected through the reactor. In figure 3.35 this has been annotated. Before the reactant and product gases can be seen emerging from the reactor, the Ar gas that was initially in the reactor emerges. Ar gas was followed on the mass spectrometer but is not shown in the graph for clarity. The point at which Ar emerged from the reactor can be recognised by a dip in the CO spectra just after the by-pass. While Ar is flushing out of the reactor, CO re-emerges from the reactor and simultaneously, a relatively small CO<sub>2</sub> signal is detected. As time on stream increases, this signal slowly decreases towards the baseline.

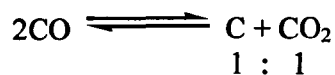
The mass spectra obtained from the Boudouard reaction over Rh, Pt and Ru catalysts respectively are given in figures 3.36 to 3.38. Each reaction profile followed the same general trend: CO<sub>2</sub> was produced immediately and reached a maximum before decreasing towards the baseline. The areas of the CO<sub>2</sub> peaks differed, as did the time taken for complete decay. In figures 3.35 to 3.38, the mass spectrometer units have been converted to a gas flow rate in units of moles min<sup>-1</sup> using the calculation given in section 2. The flow rate of CO is shown on the left hand axis and CO<sub>2</sub> on the right hand axis.

**Figure 3.35. CO only over La-ZrO<sub>2</sub> support****Figure 3.36. CO only over Rh/La-ZrO<sub>2</sub>**

**Figure 3.37. CO only over Pt/La-ZrO<sub>2</sub>****Figure 3.38. CO only over Ru/La-ZrO<sub>2</sub>**

### 3.3.1.1 Mass of Carbon Produced

By integrating the area underneath the CO<sub>2</sub> peak, the number of moles of CO<sub>2</sub> was obtained. This, in turn, was related to the number of moles of carbon produced according to the Boudouard stoichiometry:



The areas underneath the CO<sub>2</sub> peaks were calculated once the reaction gases had been passing through the reactor for 30 minutes (the point at which the CO<sub>2</sub> signal started to increase was zero minutes). Since each reaction had a slightly different CO<sub>2</sub> profile, 30 minutes was chosen as a standard comparison time. The moles of carbon deposited (and hence, the mass) on the support and packing material (figure 3.35) were calculated and are given in table 3.63.

**Table 3.63. Mass of carbon produced per gram of support from support and packing material after 30 minutes**

	Mass of C g/g of support
La-ZrO <sub>2</sub> / fused Al <sub>2</sub> O <sub>3</sub> packing	0.12

Table 3.64 shows the number of moles of CO<sub>2</sub> produced over each catalyst after 30 minutes. The last column relates the number of moles of carbon formed to the mass of catalyst used (mass of catalyst used was 0.5g).

**Table 3.64. Moles of carbon produced per gram of catalyst after 30 minutes**

Catalyst	Moles of CO <sub>2</sub>	Mass of Cg/g of catalyst
Rh	0.02	0.24
Pt	0.02	0.24
Ru	0.02	0.24

### 3.3.1.2 Deactivation

In each of the Boudouard reactions in figures 3.36 to 3.38, CO<sub>2</sub> was produced but quickly decreased suggesting that the catalysts had deactivated. The rate of loss of CO<sub>2</sub> between one and eight minutes of the reaction was calculated taking the point of maximum CO<sub>2</sub> as zero. A deactivation model was obtained from the literature and fitted to the data from the Boudouard reaction. The model was a first order deactivation relation of the form:<sup>137, 138</sup>

$$R = R_0 \exp(-kt)$$

It was used by taking the natural log of both sides converting it into straight line format:

$$\ln R_t = \ln R_0 - kt$$

$R_t$  is the rate at time  $t$ ,  $R_0$  is the initial rate and  $k$  is the deactivation rate constant. A plot of  $\ln R_t$  against  $t$  should give a straight line of slope  $-k$ . Figures 3.39 to 3.41 show the graphs of  $\ln R_t$  versus  $t$  in minutes for Rh, Pt and Ru respectively.

**Figure 3.39. Plot of  $\ln R_t$  vs. time for Rh deactivation during Boudouard reaction**

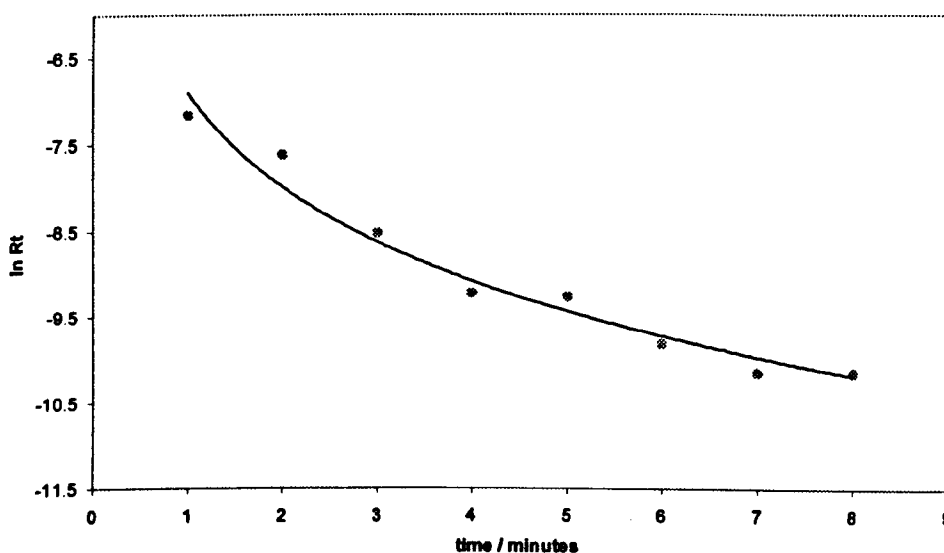


**Figure 3.40.** Plot of  $\ln R_t$  vs. time for Pt deactivation during Boudouard reaction

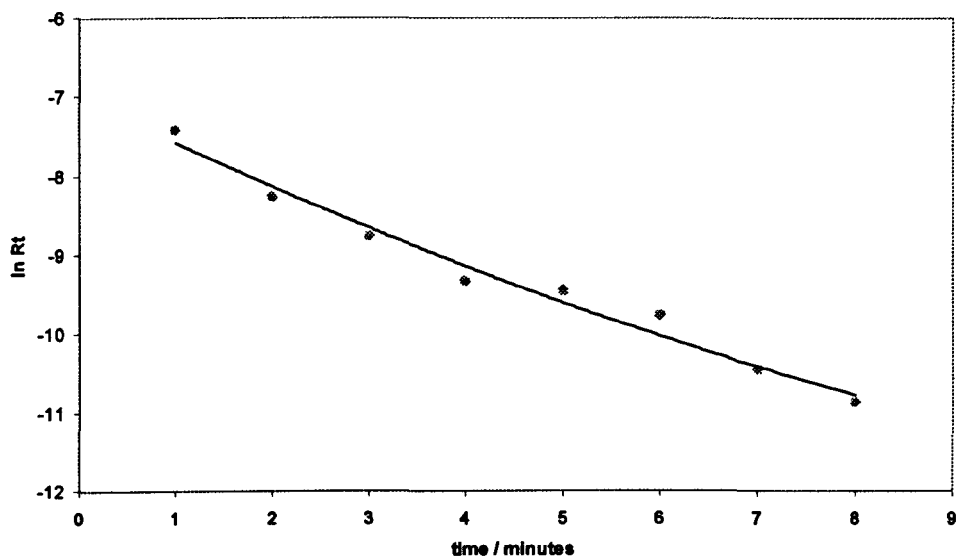
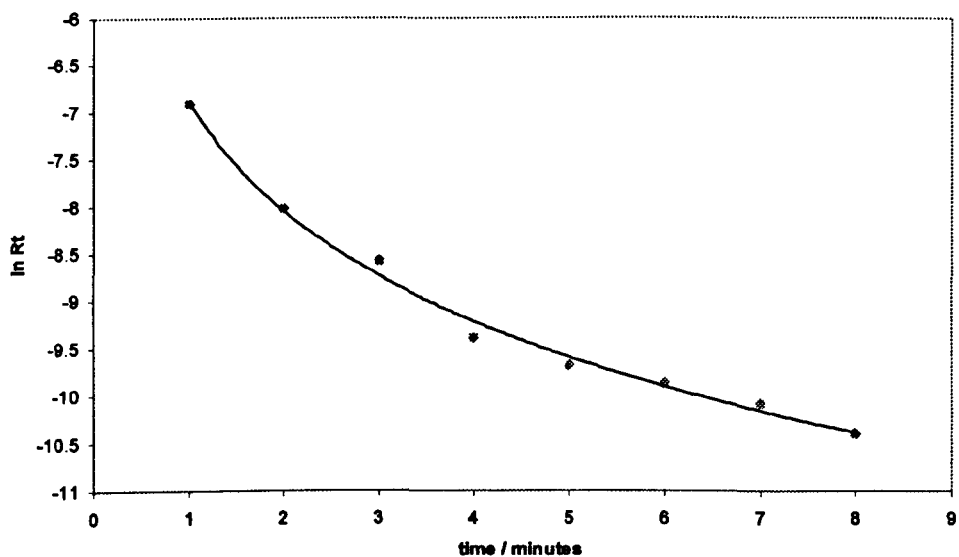


**Figure 3.41.** Plot of  $\ln R_t$  vs. time for Ru deactivation during Boudouard reaction



As can be seen for each of the first order deactivation plots, a straight line was obtained over Pt only. The possibility of a second order reaction was therefore investigated, since two CO moles were involved in the reaction. A deactivation

model for a second order process was derived<sup>139</sup> then integrated and rearranged<sup>140</sup> to give:

$$\frac{1}{R_t} = \frac{1}{R_i} + \alpha t$$

where  $R_t$  is the rate at time  $t$ ,  $R_i$  is the initial rate and  $\alpha$  is a deactivation parameter. A plot of  $1/R_t$  vs.  $t$  should give a straight line of gradient  $\alpha$ .

The deactivation parameter can be related to the rate constant,  $k$ , from the following expressions where  $C$  is the accumulated coke concentration on the catalyst<sup>140</sup>:

$$R_t = kR_i$$

$$k = \exp(-\alpha C)$$

Therefore, as the rate increases,  $\alpha$ , will decrease. The plots are given in figures 3.42 to 3.44.

**Figure 3.42.** Plot of  $1/R_t$  vs. time for Rh/La-ZrO<sub>2</sub> deactivation during Boudouard reaction

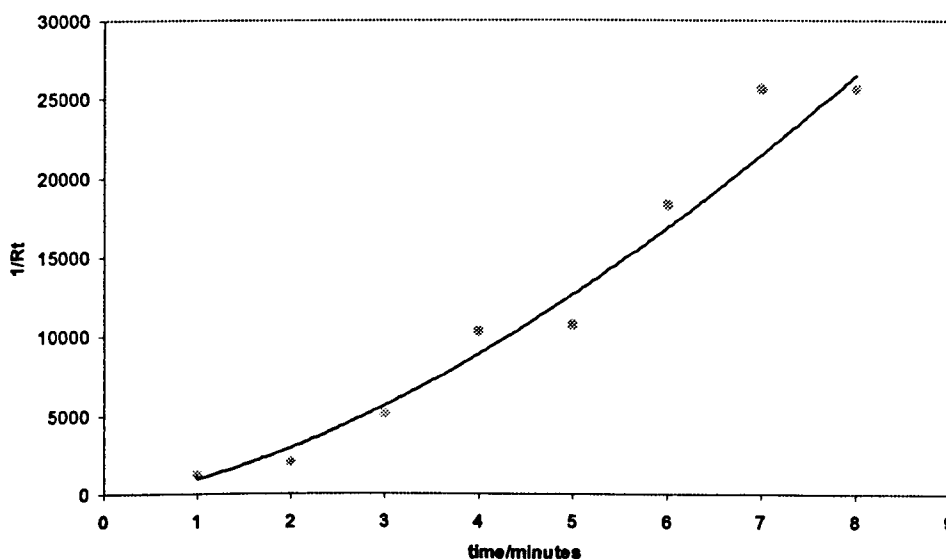


**Figure 3.43.** Plot of  $1/R_t$  vs. time for Pt/La-ZrO<sub>2</sub> deactivation during Boudouard reaction

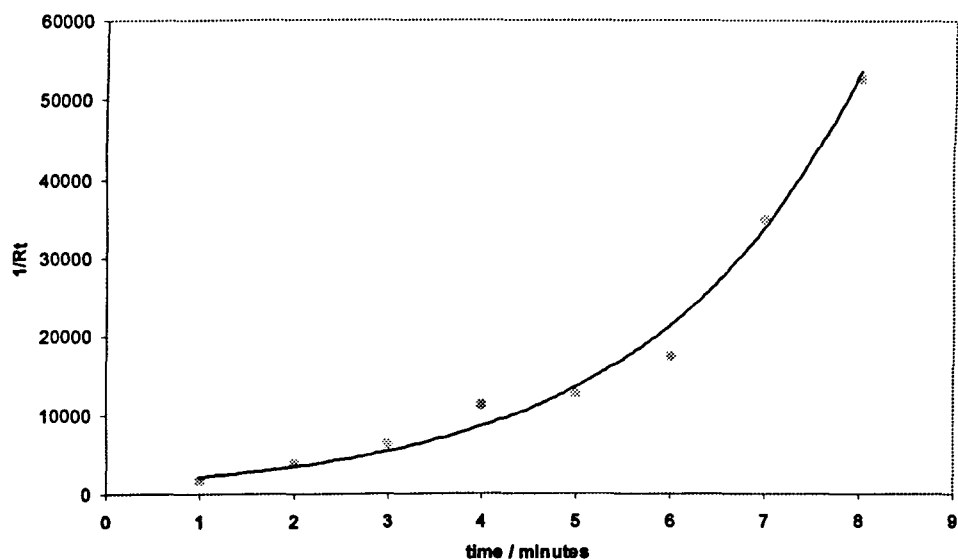
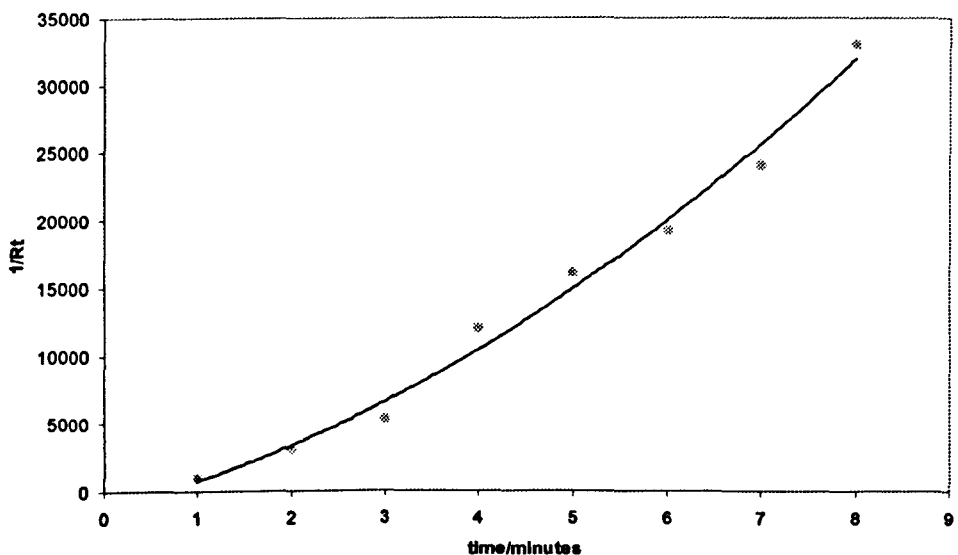


**Figure 3.44.** Plot of  $1/R_t$  vs. time for Ru/La-ZrO<sub>2</sub> deactivation during Boudouard reaction



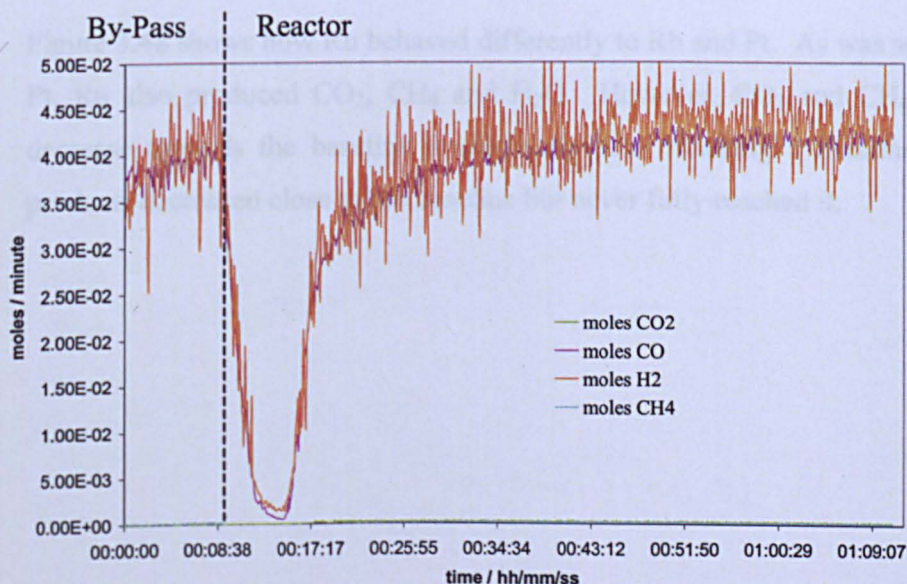
It can be seen from the plots of  $1/R_t$  vs.  $t$ , that Pt undoubtedly produced a curved line. The lines obtained from Rh and Ru were generally straight but there was an initial

inflection present in both and therefore a conclusion of the reaction order was difficult to make.

### 3.3.2 CO and H<sub>2</sub> over La-ZrO<sub>2</sub> Support

Figure 3.45 shows the mass spectra obtained from CO and H<sub>2</sub> at a 1:1 ratio over the La-ZrO<sub>2</sub> catalyst support only. Note that the mass spectrometer ion current has been converted to moles per minute using the method in section 2. The masses of several potential products of CO and H<sub>2</sub> were followed on the mass spectrometer including CO<sub>2</sub>, H<sub>2</sub>O, CH<sub>3</sub>OH, CH<sub>3</sub>CHO, C<sub>2</sub>H<sub>5</sub>OH, CH<sub>4</sub>, HCO<sub>2</sub>CH<sub>3</sub> (methyl formate), CH<sub>3</sub>CO<sub>2</sub>CH<sub>3</sub> (methyl acetate) and CH<sub>3</sub>CO<sub>2</sub>C<sub>2</sub>H<sub>5</sub> (ethyl acetate). Initially, the CO and H<sub>2</sub> reactant gases flowed through the reactor by-pass, as annotated on the figure. This by-pass flow was used as a reference. The by-pass was then closed as the reactor was simultaneously opened to re-direct the gas flow through the catalyst. The switching of the gases from by-pass to reactor can be recognised by a dip in the mass spectra. This is due to Ar gas which was present in the reactor prior to CO and H<sub>2</sub>. For clarity only the spectra of CO, H<sub>2</sub>, CO<sub>2</sub> and CH<sub>4</sub> are shown on the figure. It was observed that there was no conversion of either CO or H<sub>2</sub> since both returned to their by-pass values and that no significant product was detected.

**Figure 3.45. CO and H<sub>2</sub> over La-ZrO<sub>2</sub> support**



### 3.3.3 CO and H<sub>2</sub> over La-ZrO<sub>2</sub> Supported Catalysts

Figures 3.46 to 3.48 show the respective spectra obtained from the CO:H<sub>2</sub> 1:1 reaction over Rh, Pt and Ru supported on La-ZrO<sub>2</sub>. CO and H<sub>2</sub> were initially passed through the reactor by-pass before flowing through the reactor. The masses followed on the mass spectrometer were outlined in section 3.2.2 however, for clarity, only those detected are shown on the spectra. Ar gas initially emerged from the reactor as can be recognised by a dip in the CO and H<sub>2</sub> mass spectra. The flow of the reactant gases through the by-pass and the reactor has been labelled.

Each of the catalysts produced unique reaction profiles. In figure 3.46, Rh immediately produced CO<sub>2</sub> in greatest quantity and also CH<sub>4</sub> to a lesser extent. Both products emerged simultaneously to the reactants and all gases reached steady state showing no signs of decrease during the timeframe of the reaction. It should be noted at this stage that H<sub>2</sub>O production was also expected but not detected on the mass spectrometer. It was, however, found in the reactor post-reaction but unfortunately, it could not be quantified.

The Pt catalyst also produced CO<sub>2</sub>, CH<sub>4</sub> and H<sub>2</sub>O but in relatively smaller quantities compared to Rh as can be seen in figure 3.47. It can also be seen that product production gradually decreased throughout the reaction but never reached the baseline within the 2 hour and 10 minute timeframe studied.

Figure 3.48 shows how Ru behaved differently to Rh and Pt. As was seen for Rh and Pt, Ru also produced CO<sub>2</sub>, CH<sub>4</sub> and H<sub>2</sub>O. However, CO<sub>2</sub> and CH<sub>4</sub> were seen to decrease towards the baseline immediately after reaching a maximum. The two products decreased close to the baseline but never fully reached it.

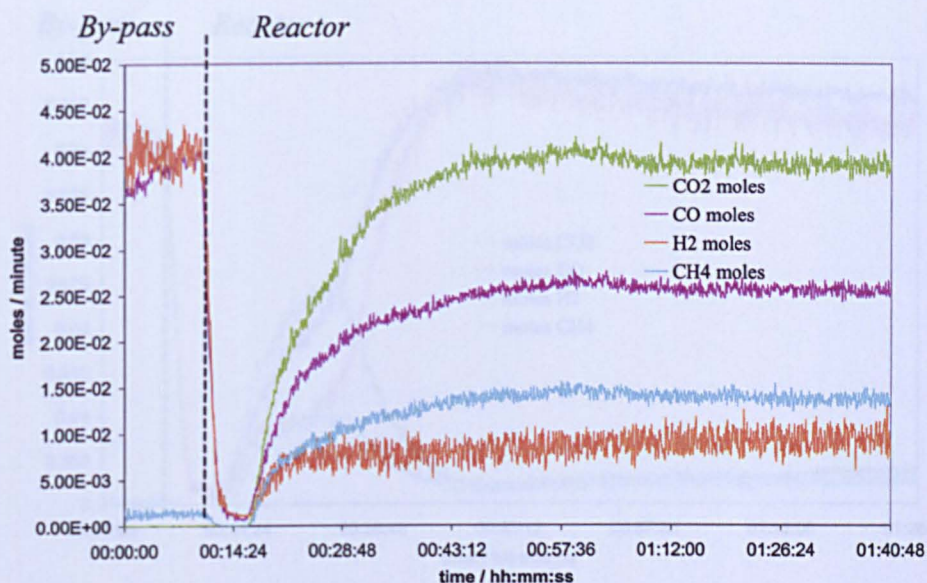
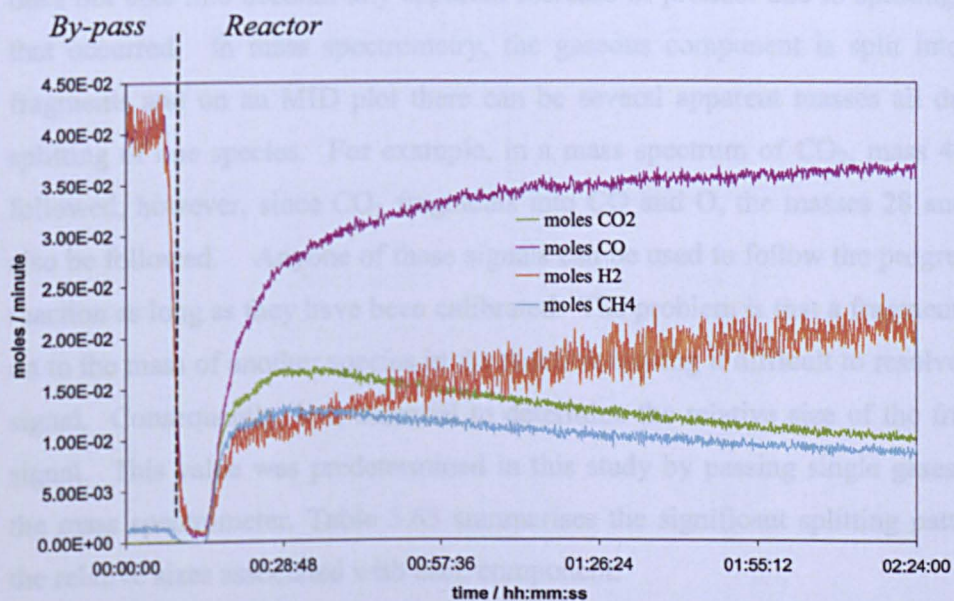
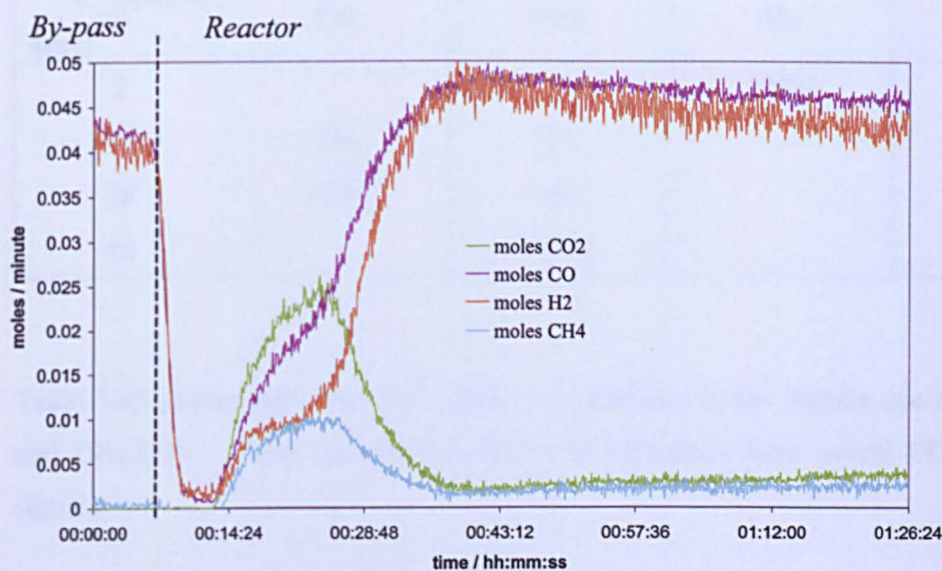
Figure 3.46. CO and H<sub>2</sub> over Rh/La-ZrO<sub>2</sub>Figure 3.47. CO and H<sub>2</sub> over Pt/La-ZrO<sub>2</sub>

Figure 3.48. CO and H<sub>2</sub> over Ru/La-ZrO<sub>2</sub>

### 3.3.3.1 Percentage CO Conversion Over Rh and Pt

It appeared, at first glance of figure 3.46, that the combined number of moles of CO, CH<sub>4</sub> and CO<sub>2</sub> is far greater than the number of moles of CO going in. There are two reasons for this. Firstly, the mass spectrometer data presented in figures 3.46 to 3.48 does not take into account any apparent increase of product due to splitting patterns that occurred. In mass spectrometry, the gaseous component is split into several fragments and on an MID plot there can be several apparent masses all due to the splitting of one species. For example, in a mass spectrum of CO<sub>2</sub>, mass 44 can be followed, however, since CO<sub>2</sub> fragments into CO and O, the masses 28 and 16 can also be followed. Anyone of these signals can be used to follow the progress of the reaction as long as they have been calibrated. The problem is that a fragment can add on to the mass of another species in the reaction making it difficult to resolve the true signal. Consequently, it is essential to determine the relative size of the fragment's signal. This value was predetermined in this study by passing single gases through the mass spectrometer. Table 3.65 summarises the significant splitting patterns and the relative sizes associated with each component.

**Table 3.65. Mass spectrometer significant splitting patterns**

<b>Species</b> <i>Mass</i>	<b>CO</b>	<b>CO<sub>2</sub></b>	<b>H<sub>2</sub></b>	<b>CH<sub>4</sub></b>
2			100%	
16	3%	8%		100%
28	100%	14%		
44		100%		

Table 3.65 shows that when CO<sub>2</sub> splits, it contributes to the signals due to CO (28) and CH<sub>4</sub> (16). These contributions must be subtracted from actual CO and CH<sub>4</sub> signals.

Secondly, the conversion of the reactants was large and on converting from CO and H<sub>2</sub> to CO, H<sub>2</sub>, CO<sub>2</sub>, H<sub>2</sub>O and CH<sub>4</sub>, there was a change in total volume. The moles of CO going into the reactor were known (by-pass value) and since there was no deactivation, it can be assumed that no carbon was deposited on the catalyst surface. Therefore, the combined number of moles of CO, CO<sub>2</sub> and CH<sub>4</sub> at the exit equal the number of CO moles at the inlet and the two values can be made relative to one another. Table 3.66 shows the number of moles of each carbon species extracted directly from the mass spectra, the value after subtraction of the splitting pattern and the relative percentage of each species.

**Table 3.66. Moles/minute of each species at steady state over Rh**

<b>Species</b>	<b>Moles/min</b> <b>(from figure 3.6)</b>	<b>Moles/min</b> <b>(- splitting pattern)</b>	<b>Relative</b> <b>%</b>
CO	$2.56 \times 10^{-2}$	$2.01 \times 10^{-2}$	29
CO <sub>2</sub>	$3.96 \times 10^{-2}$	$3.96 \times 10^{-2}$	57
CH <sub>4</sub>	$1.33 \times 10^{-2}$	$9.53 \times 10^{-3}$	14

The CO<sub>2</sub>:CH<sub>4</sub> product ratio was calculated as was the percentage CO conversion using the following calculation. Both results are given in table 3.67:

$$\frac{\text{moles}_{in} - \text{moles}_{out}}{\text{moles}_{in}} \times 100$$

**Table 3.67. %CO conversion and CO<sub>2</sub>:CH<sub>4</sub> product ratio over Rh**

Catalyst	% CO Conversion	CO <sub>2</sub> :CH <sub>4</sub> product ratio
Rh	71	4.1

A similar treatment was carried out on the results obtained over the Pt catalyst. It was known that carbon was formed over Pt since deactivation was apparent. However, in comparison to the speed of deactivation due to carbon observed during the Boudouard reaction (figures 3.36 to 3.38), it was concluded that the amount of carbon produced over Pt due to CO and H<sub>2</sub> was very small. The results are given in table 3.68. Since the signals of the species do decrease gradually throughout the duration of the reaction, all measurements in the table were made at the chosen time of one hour on stream.

**Table 3.68. Moles/minute of each species at steady state over Pt after one hour**

Species	Moles/min (from figure 3.6)	Moles/min (- splitting pattern)	Relative %
CO	3.33x10 <sup>-2</sup>	3.14x10 <sup>-2</sup>	58
CO <sub>2</sub>	1.38x10 <sup>-2</sup>	1.38x10 <sup>-2</sup>	25
CH <sub>4</sub>	1.15x10 <sup>-2</sup>	9.32x10 <sup>-3</sup>	17

The percentage CO conversion and the CO<sub>2</sub>:CH<sub>4</sub> product ratio after one hour were also calculated and given in table 3.69.

**Table 3.69. %CO conversion and CO<sub>2</sub>:CH<sub>4</sub> product ratio over Pt**

Catalyst	% CO Conversion	CO <sub>2</sub> :CH <sub>4</sub> product ratio
Pt	42	1.5

### 3.3.4 CO and CO<sub>2</sub> over La-ZrO<sub>2</sub> Supported Catalysts

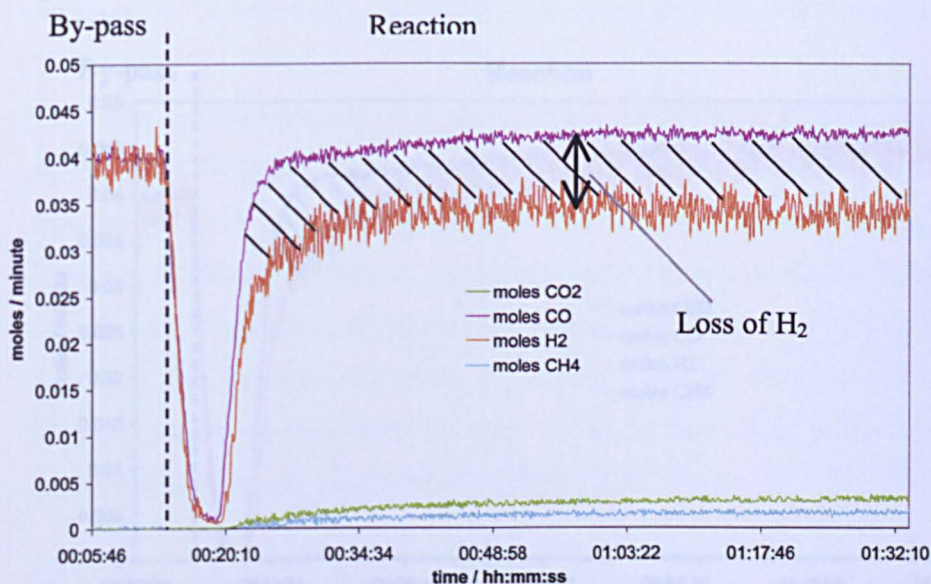
Different ratios of CO and CO<sub>2</sub> (10:1, 5:1 and 1:1) were passed over each of the catalysts for approximately one hour. In order to assess the activity of the used catalysts, a 1:1 ratio of CO and H<sub>2</sub> was then passed over.

#### 3.3.4.1 Used Boudouard catalyst

Initially, the activities of the used Boudouard catalysts (used catalysts from section 1.2) were tested by passing CO:H<sub>2</sub> 1:1 over. In section 1.2 it was shown how each of the catalysts deactivated as CO was passed over.

The resulting spectra obtained from the Rh catalyst are given in figure 3.49. Initially, the CO and H<sub>2</sub> reaction gases were passed through the by-pass to act as a reference. It can be seen that, compared to the CO:H<sub>2</sub> 1:1 reaction over the fresh catalyst sample (figure 3.46), there was relatively less activity. However, some CO<sub>2</sub> and CH<sub>4</sub> products were formed and there was a uniform loss of H<sub>2</sub> throughout the reaction as indicated on figure 3.49 by the shaded region.

**Figure 3.49. CO and H<sub>2</sub> (1:1) over spent Rh/La-ZrO<sub>2</sub> Boudouard reaction catalyst**



The used Pt and Ru catalysts showed similar behaviour. Both produced negligible amounts of product after exposure to CO:H<sub>2</sub> 1:1 as can be observed from figures 3.50 and 3.51 respectively. Unlike Rh, a loss of H<sub>2</sub> was observed in the initial stages of the reaction only. The shaded region in both figures indicates this.

**Figure 3.50. CO and H<sub>2</sub> (1:1) over spent Pt/La-ZrO<sub>2</sub> Boudouard reaction catalyst**

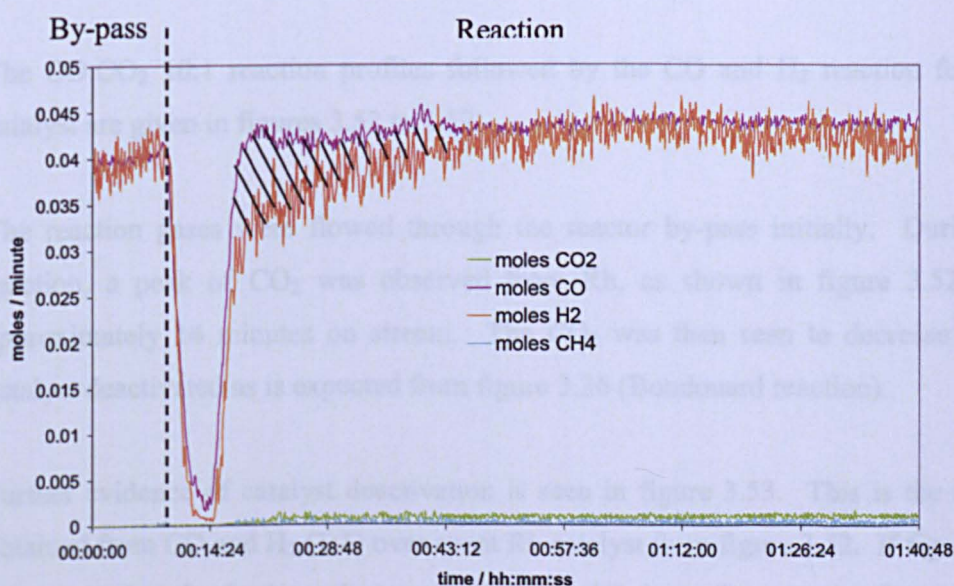
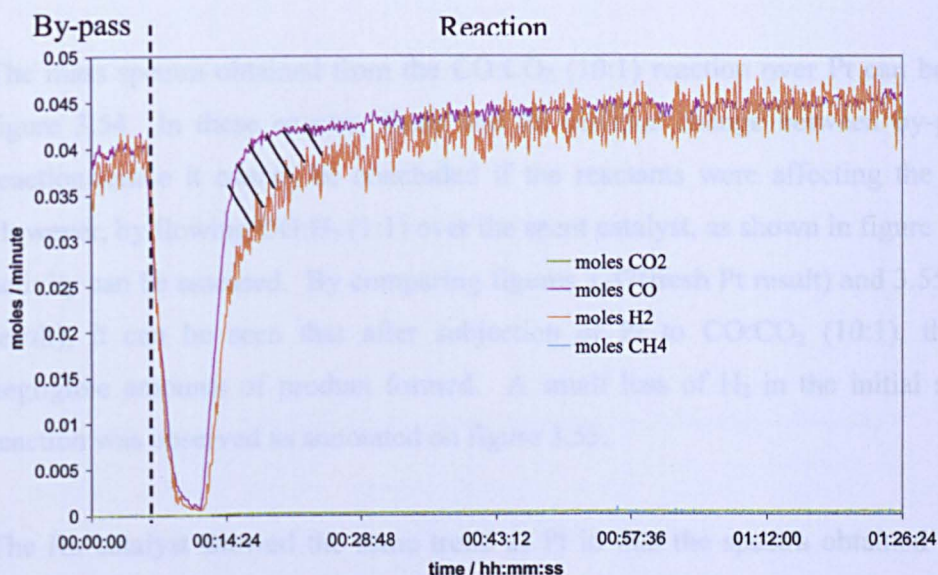


**Figure 3.51. CO and H<sub>2</sub> (1:1) over spent Ru/La-ZrO<sub>2</sub> Boudouard reaction catalyst**



### 3.3.4.2 CO:CO<sub>2</sub>, 10:1 Over La-ZrO<sub>2</sub> Catalysts

In the previous section, each of the La-ZrO<sub>2</sub> catalysts were tested for activity after they were subjected to CO only. In this section, a 10:1 ratio of CO:CO<sub>2</sub> was passed over each of the La-ZrO<sub>2</sub> catalysts at 873K. Subsequent passing of a 1:1 ratio of CO and H<sub>2</sub> over the used catalyst at 873K assessed the activity of each used catalyst.

The CO:CO<sub>2</sub> 10:1 reaction profiles followed by the CO and H<sub>2</sub> reaction for each catalyst are given in figures 3.52 to 3.57

The reaction gases were flowed through the reactor by-pass initially. During the reaction, a peak of CO<sub>2</sub> was observed from Rh, as shown in figure 3.52, after approximately 14 minutes on stream. The CO<sub>2</sub> was then seen to decrease as the catalyst deactivated as is expected from figure 3.36 (Boudouard reaction).

Further evidence of catalyst deactivation is seen in figure 3.53. This is the spectra obtained from CO and H<sub>2</sub> (1:1) over spent Rh catalyst from figure 3.52. If figure 3.53 is compared to the fresh catalyst result (figure 3.46), it can be seen that the catalyst's

activity has been affected. Products  $\text{CO}_2$  and  $\text{H}_2$  were observed but did not reach steady state as quickly as the fresh catalyst (fig. 3.46). There was also a loss of  $\text{H}_2$  which occurred near the end of the reaction as the products were increasing.

The mass spectra obtained from the  $\text{CO}:\text{CO}_2$  (10:1) reaction over Pt can be seen in figure 3.54. In these spectra, there was no obvious change between by-pass and reaction hence it cannot be concluded if the reactants were affecting the catalyst. However, by flowing  $\text{CO}:\text{H}_2$  (1:1) over the spent catalyst, as shown in figure 3.55, the activity can be assessed. By comparing figures 3.47 (fresh Pt result) and 3.55 (used Pt result), it can be seen that after subjection of Pt to  $\text{CO}:\text{CO}_2$  (10:1), there was negligible amounts of product formed. A small loss of  $\text{H}_2$  in the initial stages of reaction was observed as annotated on figure 3.55.

The Ru catalyst showed the same trend as Pt in that the spectra obtained from the  $\text{CO}:\text{CO}_2$  reaction (figure 3.56) did not show any obvious reaction taking place. However, the reaction profile obtained from  $\text{CO}:\text{H}_2$  (1:1) over the used catalyst (figure 3.57) did not show the same characteristics as were observed in figure 3.48 (fresh Ru) suggesting that the catalyst had been affected by the  $\text{CO}:\text{CO}_2$  (10:1).  $\text{CO}_2$  and  $\text{CH}_4$  products were produced however and tended towards a steady state.

Figure 3.52. CO and CO<sub>2</sub> (10:1) over Rh/La-ZrO<sub>2</sub>

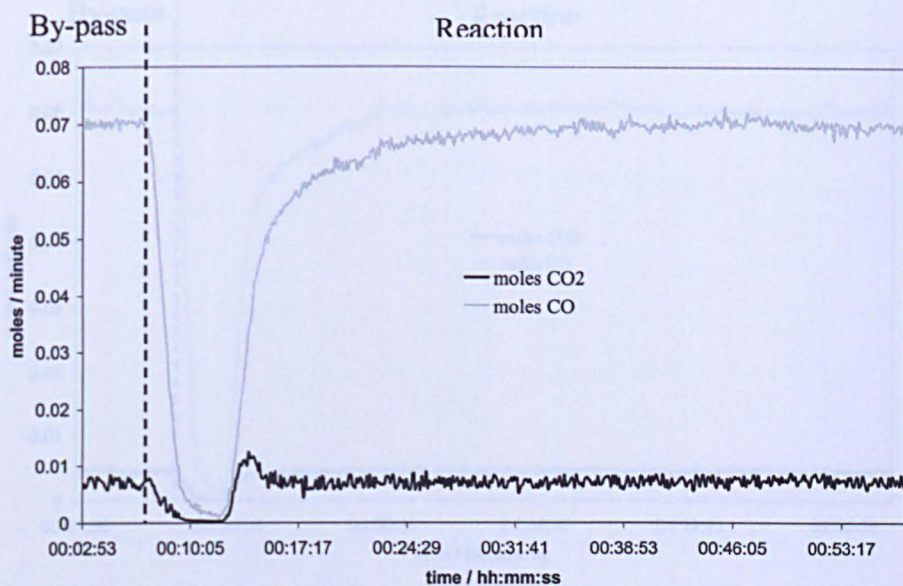
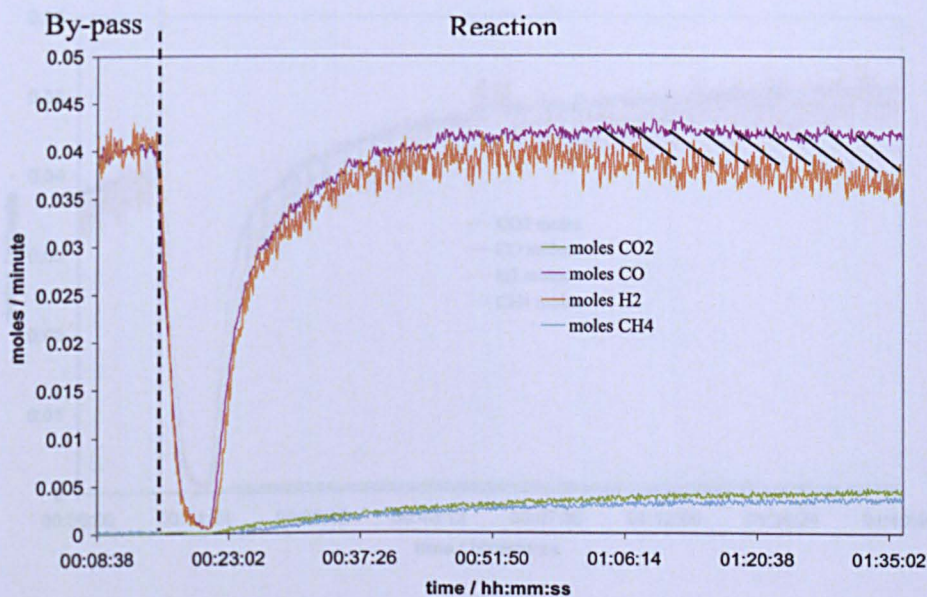
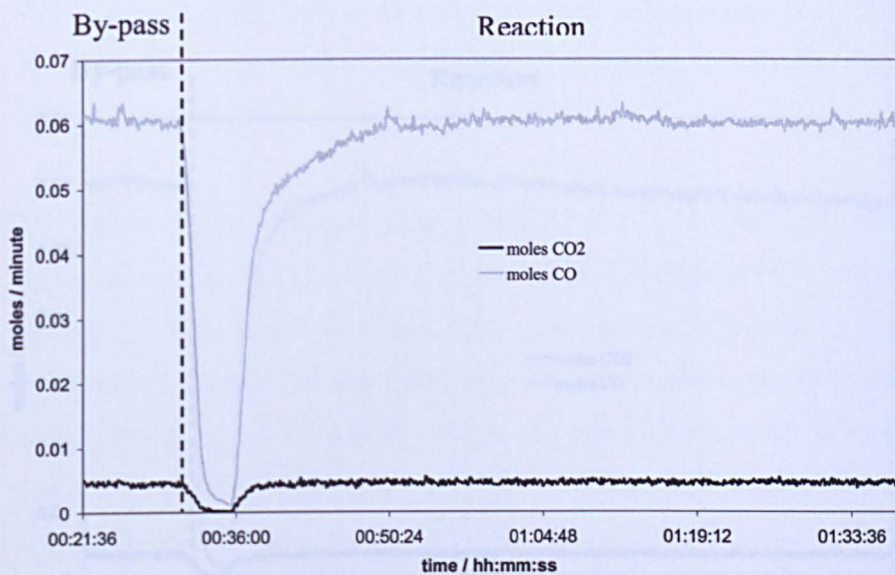
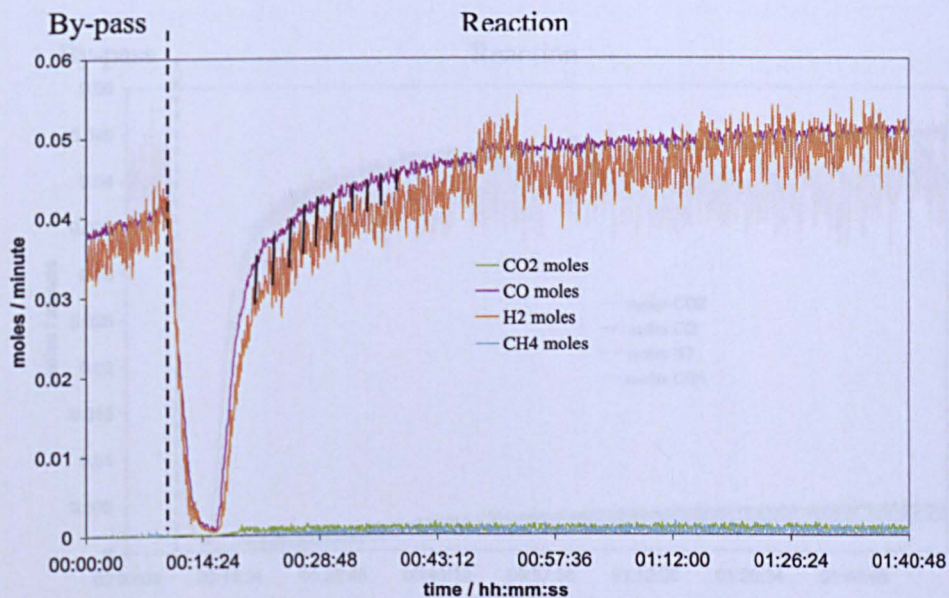
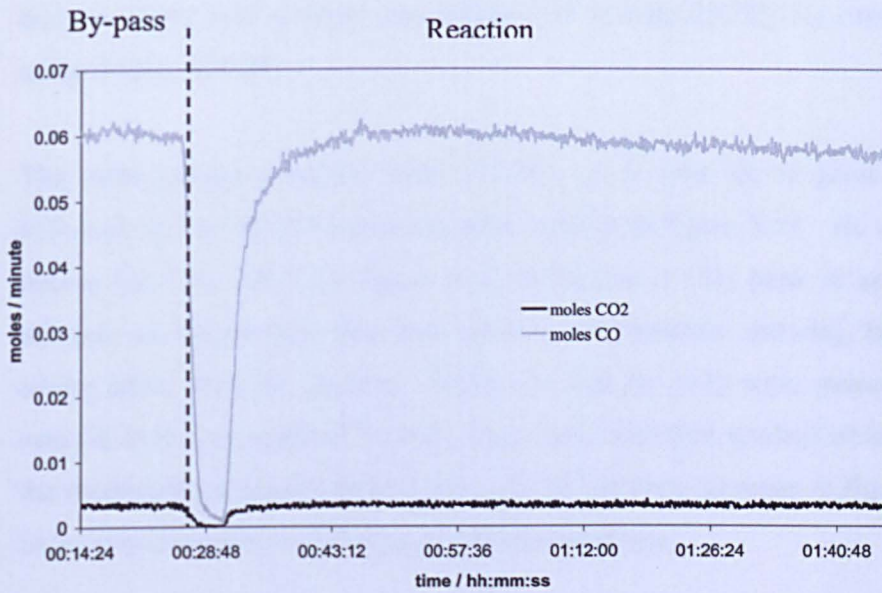
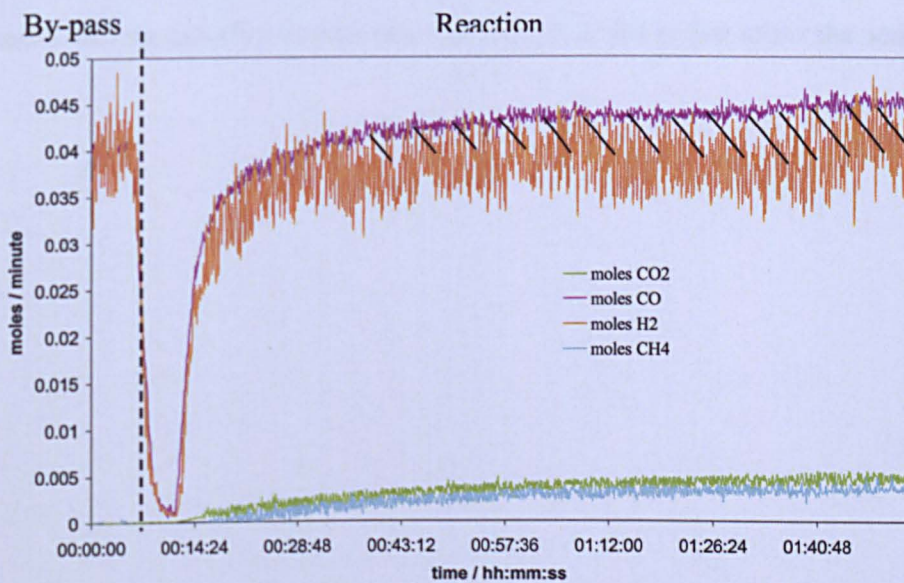


Figure 3.53. CO and H<sub>2</sub> (1:1) over spent Rh/La-ZrO<sub>2</sub> CO and CO<sub>2</sub> (10:1)

Figure 3.53. CO and H<sub>2</sub> (1:1) over spent Rh/La-ZrO<sub>2</sub> CO and CO<sub>2</sub> (10:1)



**Figure 3.54. CO and CO<sub>2</sub> (10:1) over Pt/La-ZrO<sub>2</sub>****Figure 3.55. CO and H<sub>2</sub> (1:1) over spent Pt/La-ZrO<sub>2</sub> CO and CO<sub>2</sub> (10:1)**

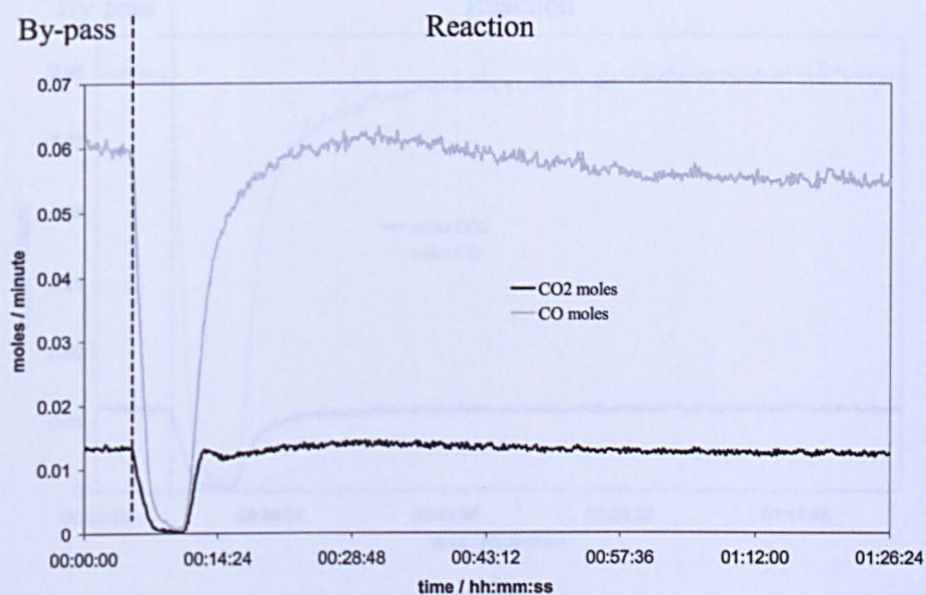
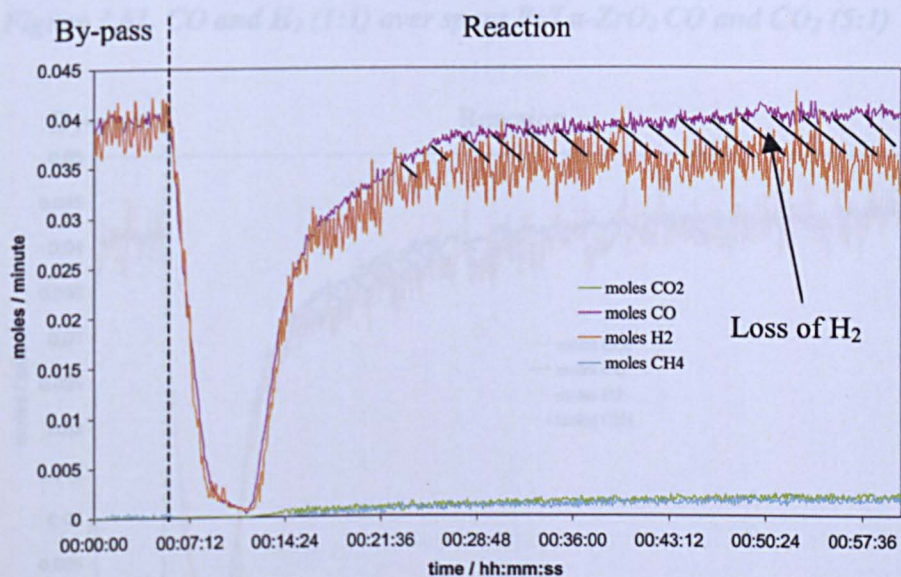
**Figure 3.56. CO and CO<sub>2</sub> (10:1) over Ru/La-ZrO<sub>2</sub>****Figure 3.57. CO and H<sub>2</sub> (1:1) over spent Ru/La-ZrO<sub>2</sub> CO and CO<sub>2</sub> (10:1)**

### 3.3.4.3 CO:CO<sub>2</sub>, 5:1 Over La-ZrO<sub>2</sub> Catalysts

A 5:1 ratio of CO:CO<sub>2</sub> was flowed over each of the catalysts at 873K and then the activity of the used catalyst was assessed by flowing CO:H<sub>2</sub> 1:1 over, maintaining a temperature of 873K.

The mass spectra obtained from CO:CO<sub>2</sub> (5:1) over Rh is given in figure 3.58 followed by CO:H<sub>2</sub> (1:1) over the used catalyst in figure 3.59. As was seen for Rh during CO:CO<sub>2</sub> (10:1) in figure 3.52, there was a CO<sub>2</sub> peak at approximately 13 minutes on stream that decreases down to the baseline showing that reaction was taking place over the catalyst. When CO and H<sub>2</sub> (1:1) were passed over the used catalyst to test for residual activity, there was very little product produced relative to the fresh catalyst result (figure 3.46). As the products increase in figure 3.59, H<sub>2</sub> can be seen to decrease as indicated by the shaded region.

The results from the Pt and Ru catalysts in figures 3.60 to 3.61 and 3.62 to 3.63 respectively showed similar behaviour to that seen for the CO:CO<sub>2</sub> (10:1) case. Neither showed any obvious reaction while CO:CO<sub>2</sub> ratio was being passed over however, the change in the mass spectra from the fresh catalyst sample (figures 3.47 and 3.48 respectively) showed that CO:CO<sub>2</sub> (5:1) did in fact affect the activity.

**Figure 3.58. CO and CO<sub>2</sub> (5:1) over Rh/La-ZrO<sub>2</sub>****Figure 3.59. CO and H<sub>2</sub> (1:1) over spent Rh/La-ZrO<sub>2</sub> CO and CO<sub>2</sub> (5:1)**

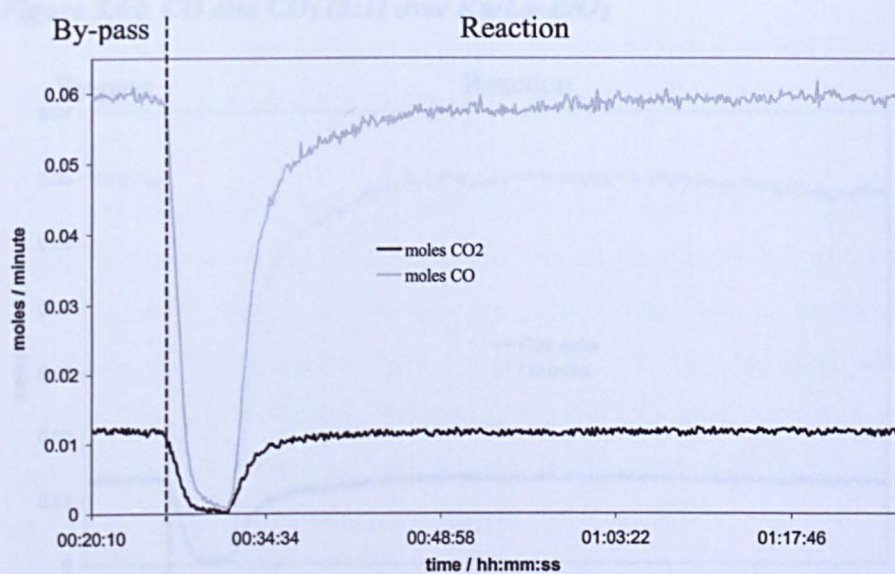
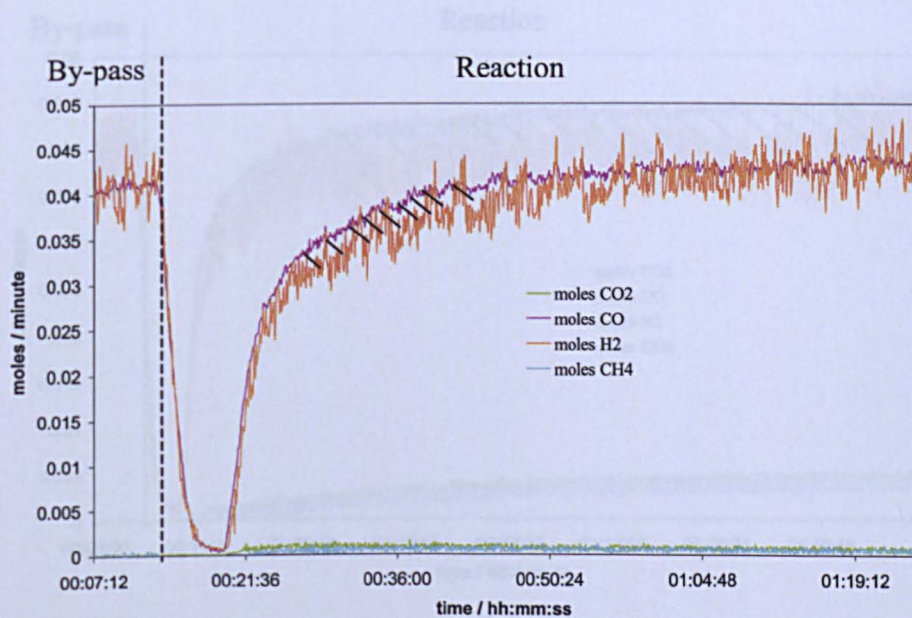
**Figure 3.60. CO and CO<sub>2</sub> (5:1) over Pt/La-ZrO<sub>2</sub>****Figure 3.61. CO and H<sub>2</sub> (1:1) over spent Pt/La-ZrO<sub>2</sub> CO and CO<sub>2</sub> (5:1)**

Figure 3.62. CO and CO<sub>2</sub> (5:1) over Ru/La-ZrO<sub>2</sub>

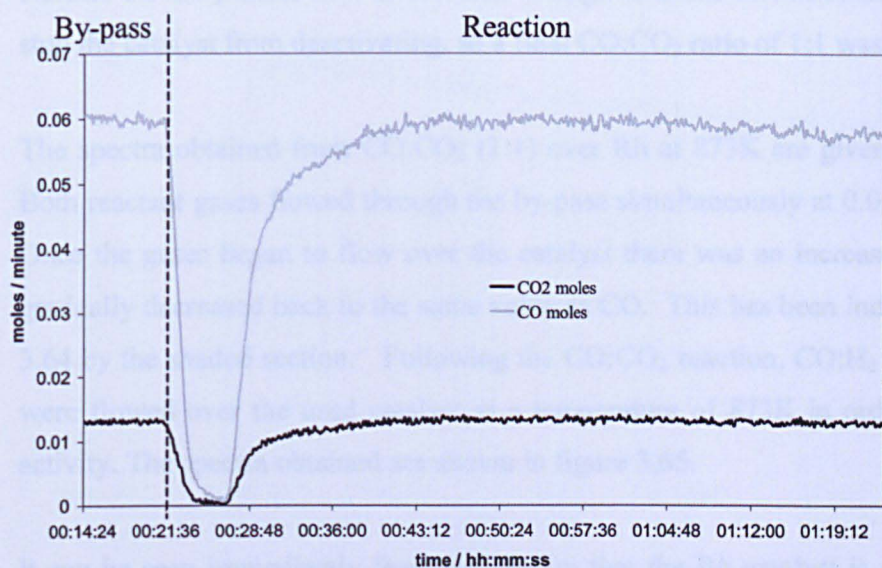
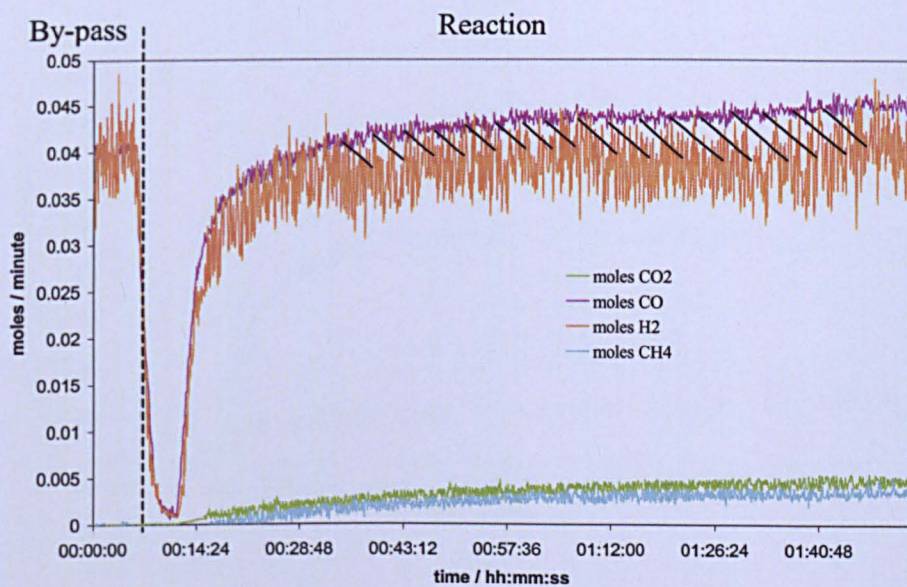


Figure 3.63. CO and H<sub>2</sub> (1:1) over spent Ru/La-ZrO<sub>2</sub> CO and CO<sub>2</sub> (5:1)

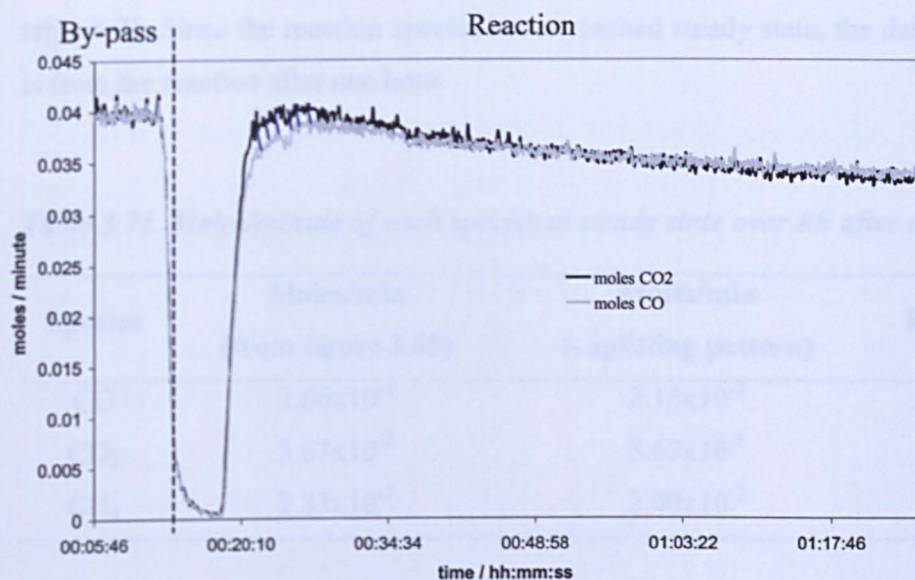
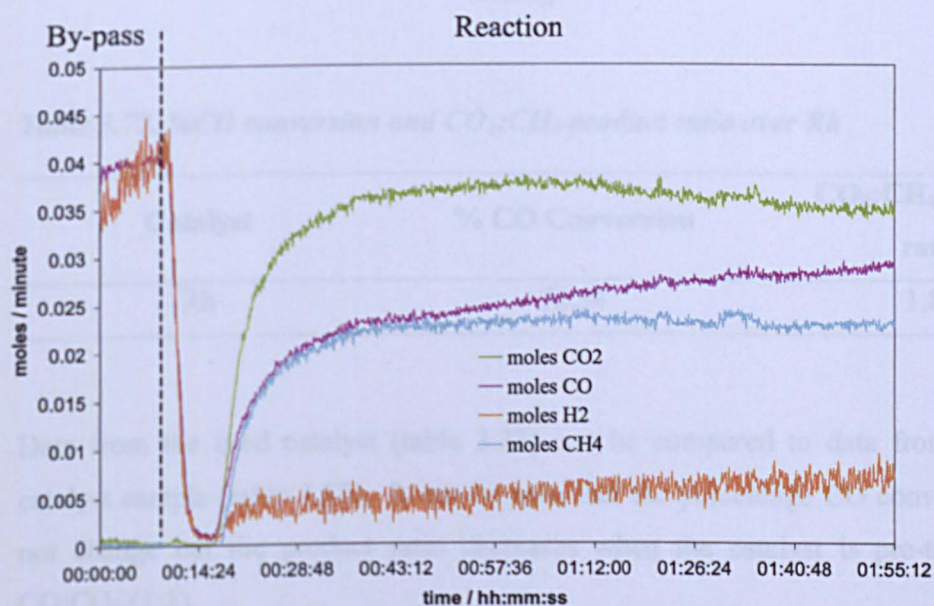


#### 3.3.4.4 CO:CO<sub>2</sub>, 1:1 Over La-ZrO<sub>2</sub> Catalysts

Neither CO:CO<sub>2</sub> ratios 10:1 or 5:1 were enough to avoid carbon formation and hence stop the catalyst from deactivating, so a final CO:CO<sub>2</sub> ratio of 1:1 was studied.

The spectra obtained from CO:CO<sub>2</sub> (1:1) over Rh at 873K are given in figure 3.64. Both reactant gases flowed through the by-pass simultaneously at 0.04 moles/minute. Once the gases began to flow over the catalyst there was an increase in CO<sub>2</sub> which gradually decreased back to the same value as CO. This has been indicated on figure 3.64 by the shaded section. Following the CO:CO<sub>2</sub> reaction, CO:H<sub>2</sub> at a ratio of 1:1 were flowed over the used catalyst at a temperature of 873K in order to assess the activity. The spectra obtained are shown in figure 3.65.

It can be seen immediately from the spectra that the Rh catalyst is still active after subjection to CO:CO<sub>2</sub> (1:1). CO<sub>2</sub> is also produced in a greater quantity than CH<sub>4</sub>. The spectra in figure 3.65 can be compared to the spectra obtained from CO:H<sub>2</sub> (1:1) over the fresh catalyst sample (figure 3.46). The most obvious difference is that in figure 3.65, the products do not reach a steady state within the time frame of the reaction. It was also noticed that the CO<sub>2</sub>:CH<sub>4</sub> product ratio differed between the two reactions.

Figure 3.64. CO and CO<sub>2</sub> (1:1) over Rh/La-ZrO<sub>2</sub>Figure 3.65. CO and H<sub>2</sub> (1:1) over spent Rh/La-ZrO<sub>2</sub> CO and CO<sub>2</sub> (1:1)

The moles per minute after one hour on stream were calculated. Again, splitting patterns and the volume effect had to be taken into account. The results are given in table 3.71. Since the reaction species never reached steady state, the data in the table is from the reaction after one hour.

**Table 3.71. Moles/minute of each species at steady state over Rh after one hour**

Species	Moles/min (from figure 3.65)	Moles/min (- splitting pattern)	Relative %
CO	$2.66 \times 10^{-2}$	$2.15 \times 10^{-2}$	27.45
CO <sub>2</sub>	$3.67 \times 10^{-2}$	$3.67 \times 10^{-2}$	46.96
CH <sub>4</sub>	$2.33 \times 10^{-2}$	$2.00 \times 10^{-2}$	25.59

The percentage CO conversion was then calculated using equation x and is given in table 3.72 with the CO<sub>2</sub>:CH<sub>4</sub> product ratio.

$$\frac{\text{moles}_{in} - \text{moles}_{out}}{\text{moles}_{in}} \times 100$$

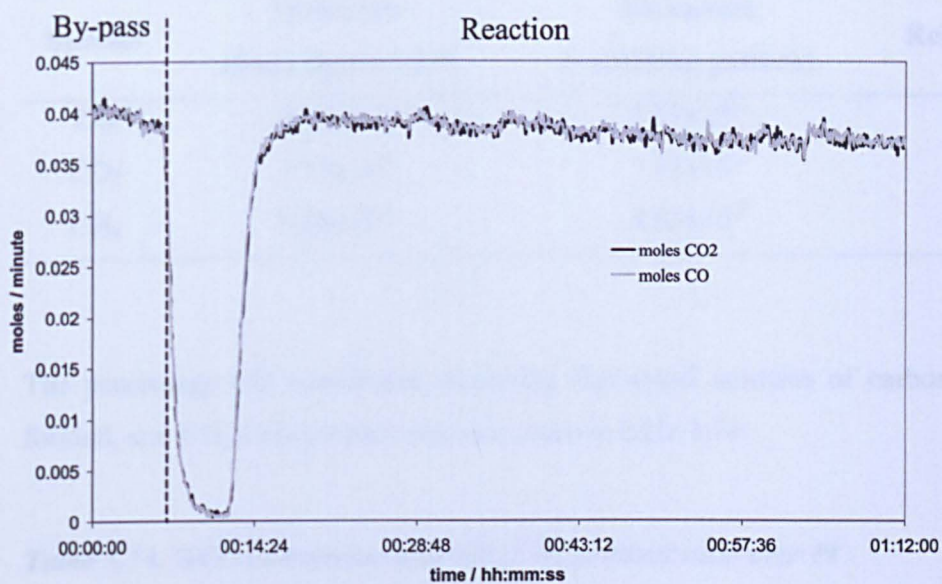
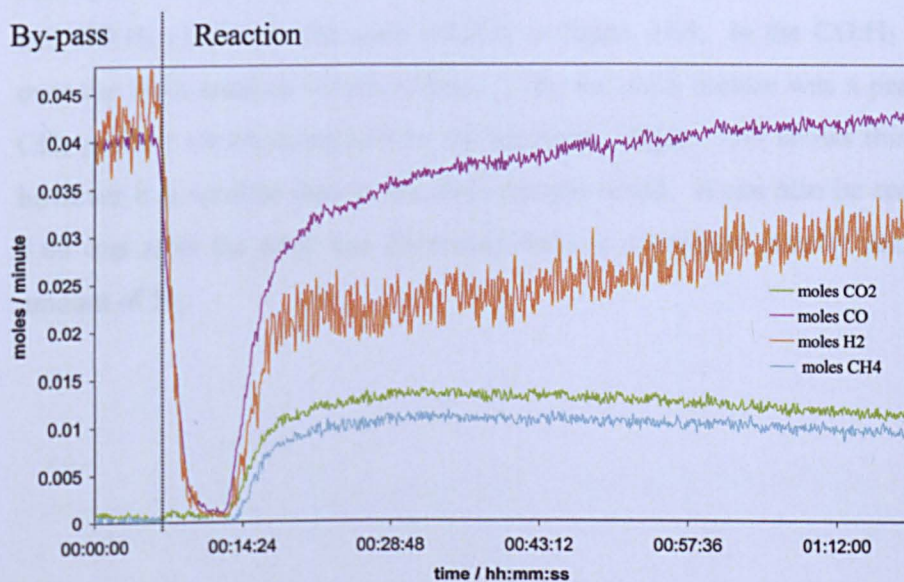
**Table 3.72. %CO conversion and CO<sub>2</sub>:CH<sub>4</sub> product ratio over Rh**

Catalyst	% CO Conversion	CO <sub>2</sub> :CH <sub>4</sub> product ratio
Rh	72.54	1.84

Data from the used catalyst (table 3.72) can be compared to data from the fresh catalyst sample (table 3.67). It can be seen that the percentage CO conversion does not change but the product ratio decreases when the catalyst is pre-treated with CO:CO<sub>2</sub> (1:1).

Figure 3.66 shows the spectra obtained from CO:CO<sub>2</sub> (1:1) over Pt at 873K. It was unknown if there was any reaction taking place since the CO and CO<sub>2</sub> spectra mirrored one another exactly.

The spectra obtained when CO and H<sub>2</sub> (1:1) were passed over the used Pt catalyst are shown in figure 3.67. It can be seen that this used CO:CO<sub>2</sub> (1:1) catalyst is far more active than the equivalent used CO:CO<sub>2</sub> (10:1) and (5:1) catalysts. CO<sub>2</sub> and CH<sub>4</sub> are produced and both tend towards the baseline over the course of the reaction. The moles per minute of each reaction species after one hour were calculated and the results are given in table 3.73.

**Figure 3.66. CO and CO<sub>2</sub> (1:1) over Pt/La-ZrO<sub>2</sub>****Figure 3.67. CO and H<sub>2</sub> (1:1) over used Pt/La-ZrO<sub>2</sub> CO and CO<sub>2</sub> (1:1)**

**Table 3.73. Moles/minute of each species at steady state over Pt after one hour**

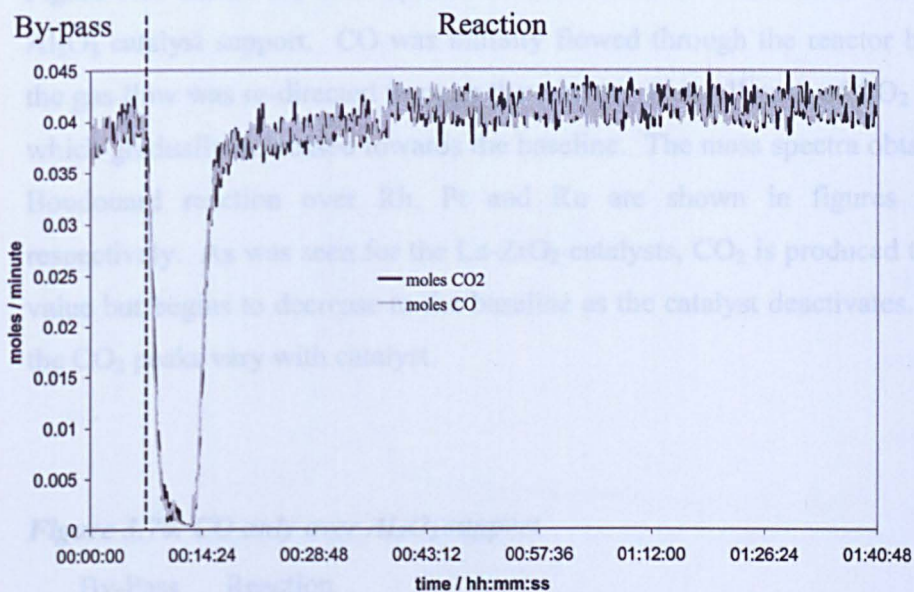
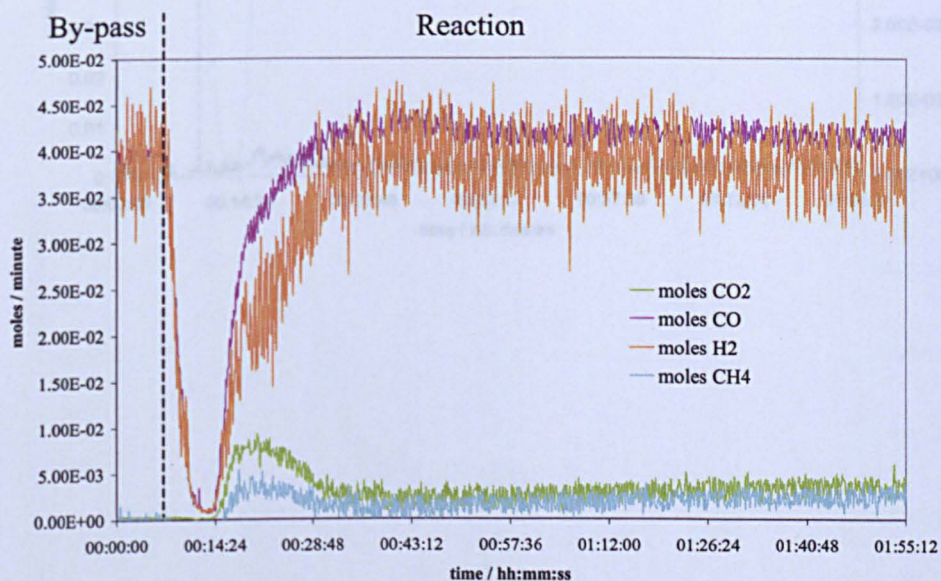
Species	Moles/min (from figure 3.25)	Moles/min (- splitting pattern)	Relative %
CO	$4.23 \times 10^{-2}$	$4.07 \times 10^{-2}$	66.67
CO <sub>2</sub>	$1.15 \times 10^{-2}$	$1.15 \times 10^{-2}$	18.85
CH <sub>4</sub>	$9.86 \times 10^{-3}$	$8.83 \times 10^{-3}$	14.46

The percentage CO conversion, assuming that small amounts of carbon are being formed, and CO<sub>2</sub>:CH<sub>4</sub> product ratio are given in table 3.74.

**Table 3.74. %CO conversion and CO<sub>2</sub>:CH<sub>4</sub> product ratio over Pt**

Catalyst	% CO Conversion	CO <sub>2</sub> :CH <sub>4</sub> product ratio
Rh	33.31	1.30

Finally the reaction spectra of CO:CO<sub>2</sub> (1:1) reaction over Ru are given in figure 3.68 and CO:H<sub>2</sub> (1:1) over the used catalyst in figure 3.69. In the CO:H<sub>2</sub> (1:1) reaction over the fresh catalyst sample (figure 3.48), the main feature was a peak of CO<sub>2</sub> and CH<sub>4</sub> product which decreased to the baseline. Figure 3.69 shows this main feature however it is smaller than in the fresh sample result. It can also be seen from figure 3.69 that after the peak has decreased there is a residual activity and a loss in the amount of H<sub>2</sub>.

**Figure 3.68. CO and CO<sub>2</sub> (1:1) over Ru/La-ZrO<sub>2</sub>****Figure 3.69. CO and H<sub>2</sub> (1:1) over used Ru/La-ZrO<sub>2</sub> CO and CO<sub>2</sub> (1:1)**

### 3.3.5 Boudouard Reaction over $\text{Al}_2\text{O}_3$ Supported Catalysts

Figure 3.70 shows the mass spectra obtained from the reaction of CO only over the  $\text{Al}_2\text{O}_3$  catalyst support. CO was initially flowed through the reactor by-pass before the gas flow was re-directed through the reactor. A small peak of  $\text{CO}_2$  was produced which gradually decreased towards the baseline. The mass spectra obtained from the Boudouard reaction over Rh, Pt and Ru are shown in figures 3.71 to 3.73 respectively. As was seen for the La- $\text{ZrO}_2$  catalysts,  $\text{CO}_2$  is produced to a maximum value but begins to decrease to the baseline as the catalyst deactivates. The areas of the  $\text{CO}_2$  peaks vary with catalyst.

**Figure 3.70. CO only over  $\text{Al}_2\text{O}_3$  support**

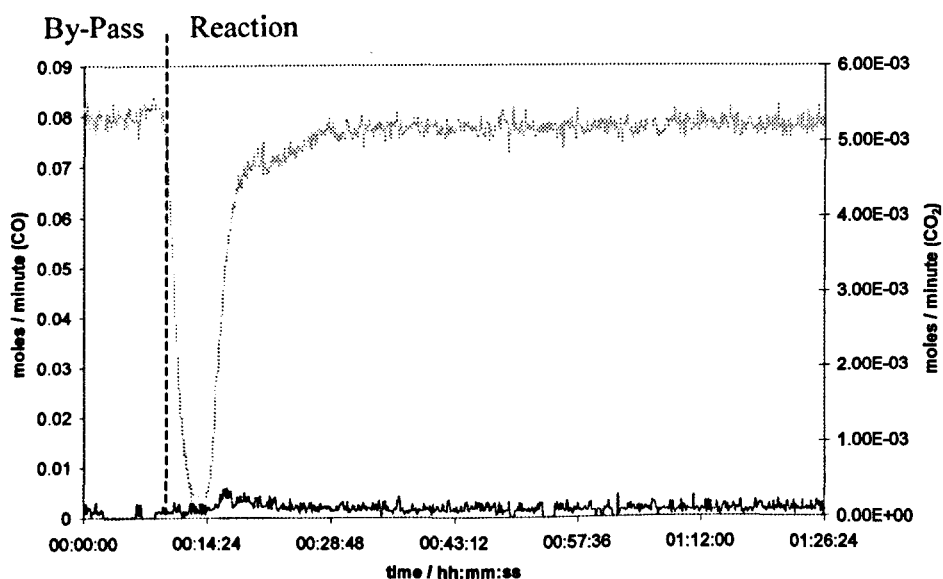
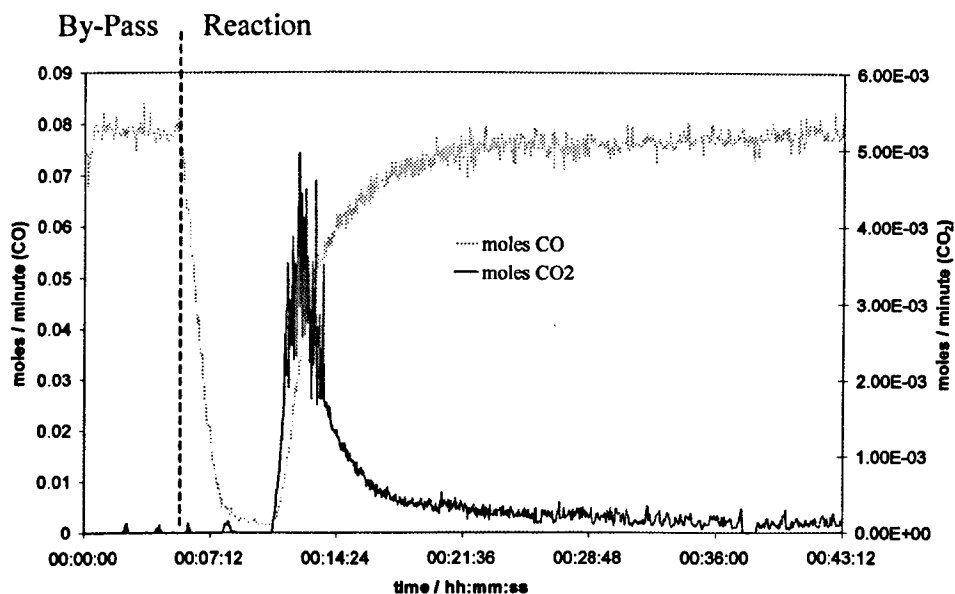
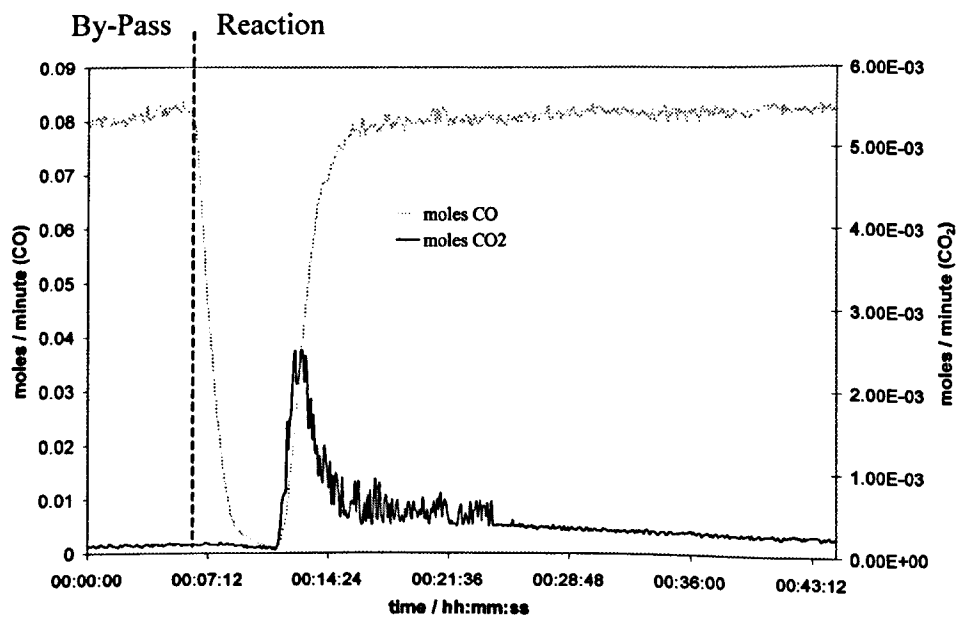
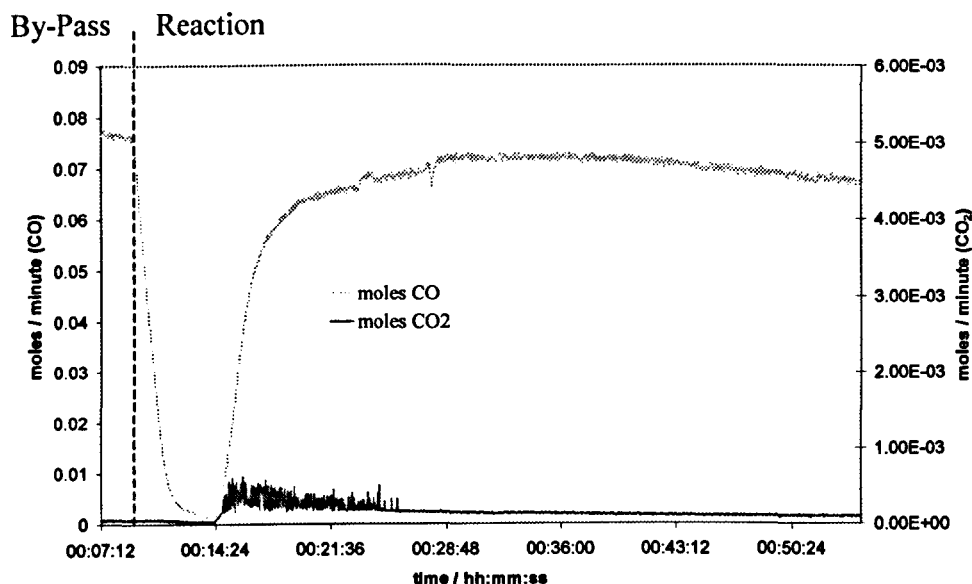


Figure 3.71. CO only over Rh/Al<sub>2</sub>O<sub>3</sub>Figure 3.72. CO only over Pt/Al<sub>2</sub>O<sub>3</sub>

**Figure 3.73. CO only over Ru/Al<sub>2</sub>O<sub>3</sub>**

### 3.3.5.1 Mass of Carbon Produced

By integration of the CO<sub>2</sub> peak, the number of moles of CO<sub>2</sub> produced in the reaction was deduced. By relating this to the stoichiometry of the Boudouard reaction, as described in section 3.3.1.1, the number of moles of carbon produced was determined. Table 3.75 shows the calculated mass of carbon produced over the support and packing material after 30 minutes on stream.

**Table 3.75. Moles of CO<sub>2</sub> produced from support and packing after 30 minutes on stream**

	Mass of Carbon g/g of support
Al <sub>2</sub> O <sub>3</sub> / fused Al <sub>2</sub> O <sub>3</sub> packing	0.04

Table 3.76 shows the number of moles of CO<sub>2</sub> produced for each catalyst after 30 minutes. The last column relates the number of moles of carbon formed to the mass of catalyst used (mass of catalyst used was 0.5g).

**Table 3.76. Moles of CO<sub>2</sub> and mass of carbon produced per gram of catalyst after 30 minutes**

Catalyst	Moles of CO <sub>2</sub>	Mass of C g/g of catalyst
Rh	$2.6 \times 10^{-2}$	0.32
Pt	$2.4 \times 10^{-2}$	0.29
Ru	$0.7 \times 10^{-2}$	0.08

### 3.3.5.2 Deactivation

The CO<sub>2</sub> peaks obtained from reaction over the Al<sub>2</sub>O<sub>3</sub> catalysts were treated with the same deactivation equations as the La-ZrO<sub>2</sub> catalysts. Figures 3.74-3.76 show the lines obtained from the first order equation for Rh, Pt and Ru respectively.

**Figure 3.74. Plot of  $\ln Rt$  vs. time for Rh deactivation during Boudouard reaction**

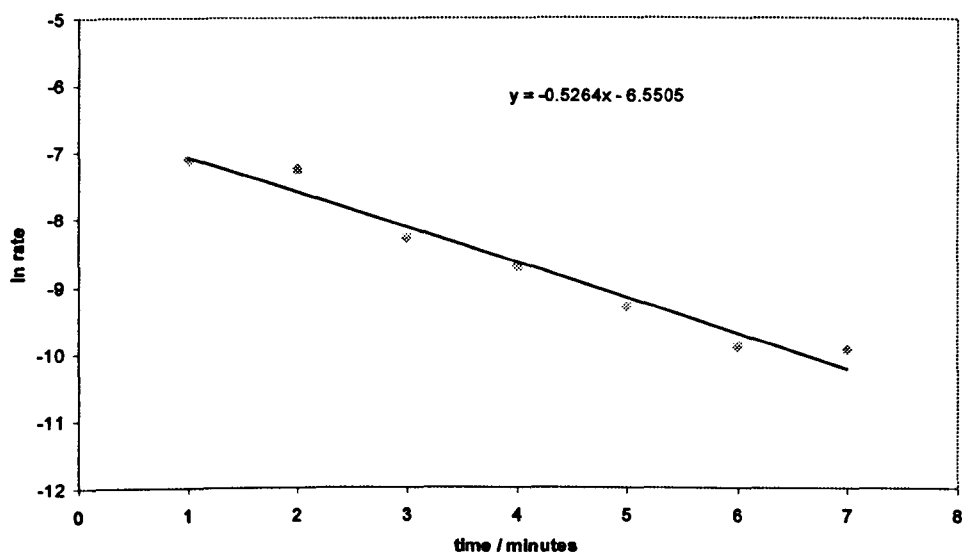


**Figure 3.75.** Plot of  $\ln Rt$  vs. time for Pt/ $\text{Al}_2\text{O}_3$  deactivation during Boudouard reaction

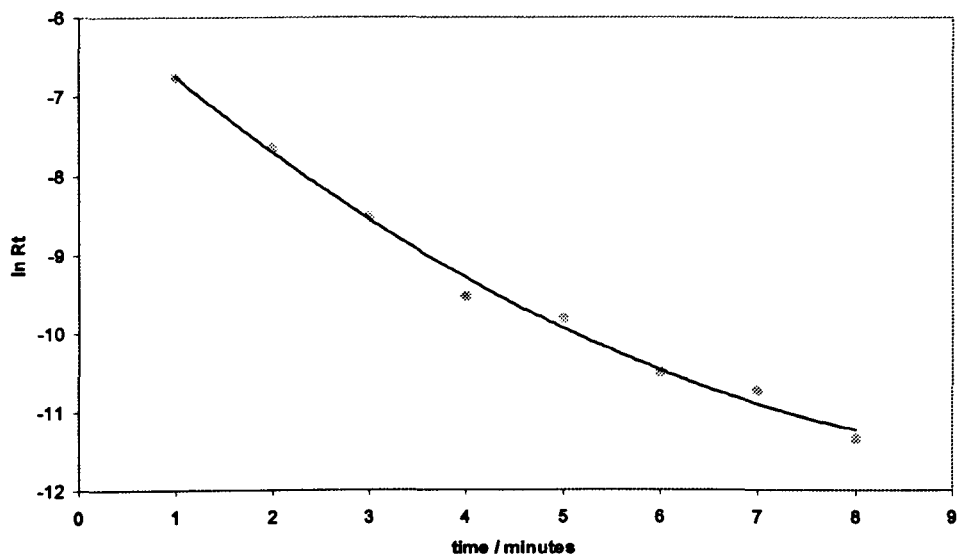
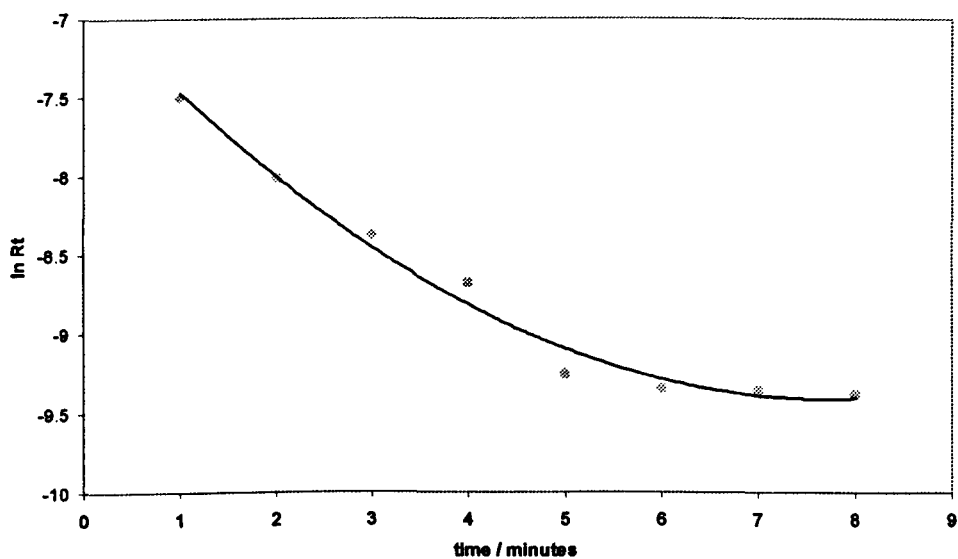


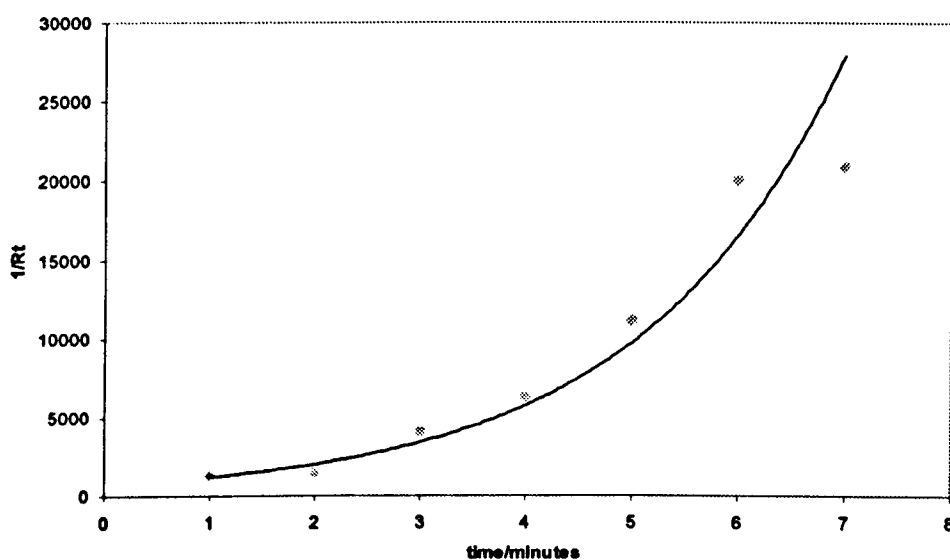
**Figure 3.76.** Plot of  $\ln Rt$  vs. time for Ru deactivation during Boudouard reaction



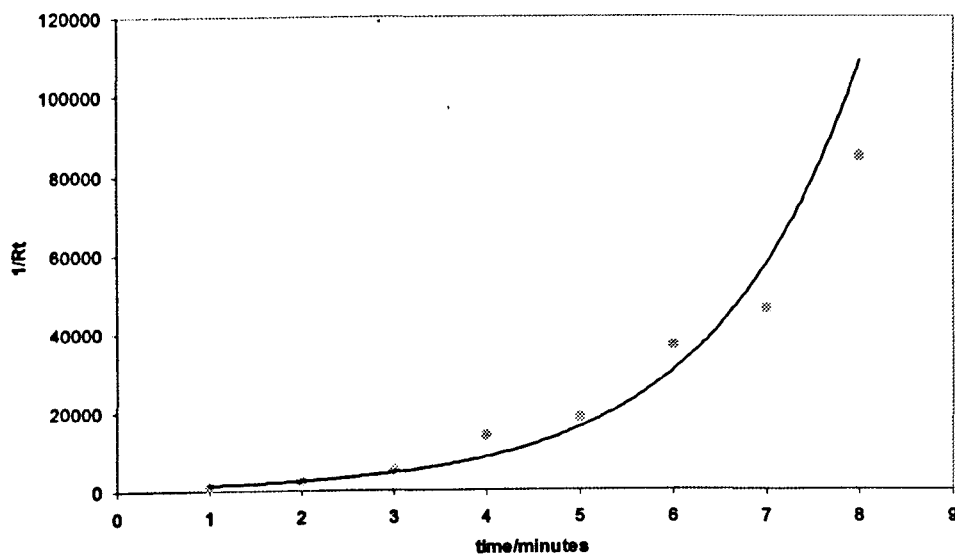
The line from Rh appeared to be straight while that from Pt had a slight curve. For Ru, the line was straight for the first five minutes of reaction and thereafter, it was straight. This was because the rate of decrease of  $\text{CO}_2$  was constant after five

minutes. Therefore, the gradient of this stage is horizontal and hence has a value of 0. Figures 3.77 to 3.79 show the plots obtained from the second order deactivation over Rh, Pt and Ru respectively (for Ru, the plot stops after five minutes). Each reaction produced a very definite curve rather than straight lines to show that the deactivations were not second order. According to the plots, it looked more likely that the deactivations were first order although, it was clear that further work will be required to fully prove that this is the case. Table 3.77 shows the first order deactivation rate constants.

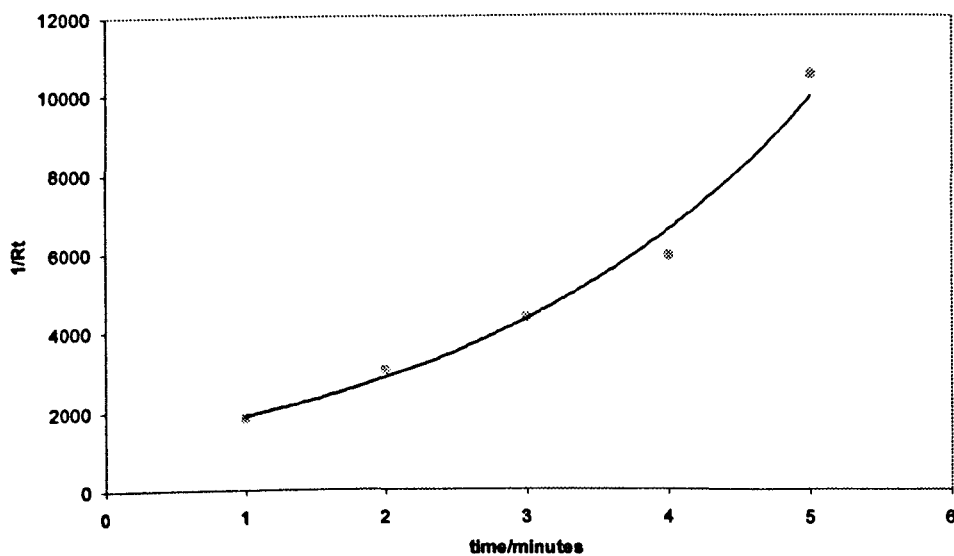
**Figure 3.77.** Plot of  $1/Rt$  vs. time for Rh/ $Al_2O_3$  deactivation during Boudouard reaction



**Figure 3.78.** Plot of  $1/Rt$  vs. time for  $Pt/Al_2O_3$  deactivation during Boudouard reaction



**Figure 3.79.** Plot of  $1/Rt$  vs. time for  $Ru/Al_2O_3$  deactivation during Boudouard reaction

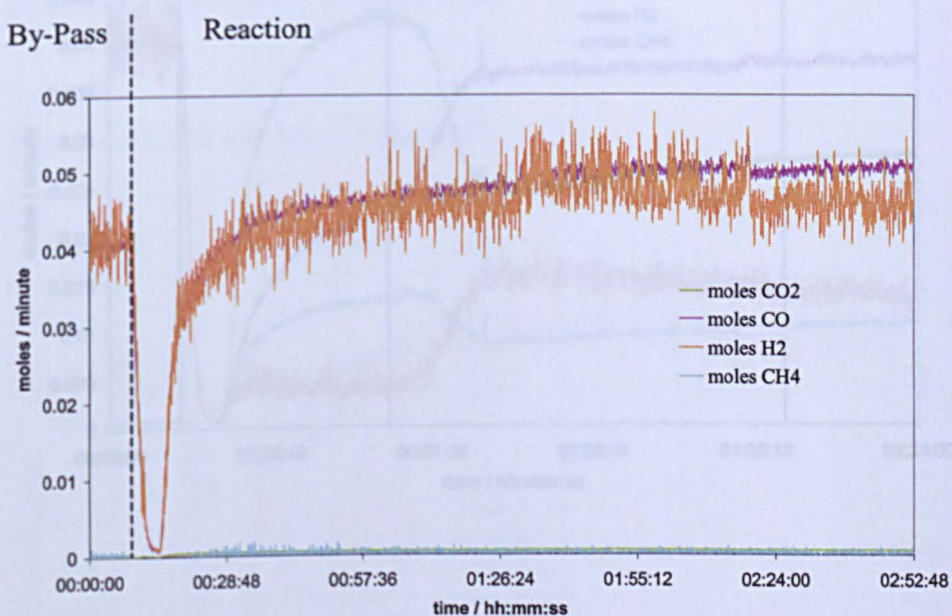


**Table 3.77. Deactivation rate constants for Boudouard reaction**

Catalyst	Deactivation Rate Constant, $\text{k}/\text{min}^{-1}$
Rh/ $\text{Al}_2\text{O}_3$	0.55
Pt/ $\text{Al}_2\text{O}_3$	0.64
Ru/ $\text{Al}_2\text{O}_3$	0.42

### 3.3.6 CO and H<sub>2</sub> over Al<sub>2</sub>O<sub>3</sub> Support

A 1:1 ratio of CO and H<sub>2</sub> was initially flowed over the Al<sub>2</sub>O<sub>3</sub> support and the fused Al<sub>2</sub>O<sub>3</sub> packing material. The mass spectra from this reaction are given in figure 3.80. The reactant gases initially flowed through the reactor by-pass. When they were passed over the support, there was a negligible amount of product produced. Therefore, any effect due to the support and packing material is negligible.

**Figure 3.80. CO and H<sub>2</sub> (1:1) over Al<sub>2</sub>O<sub>3</sub> support**

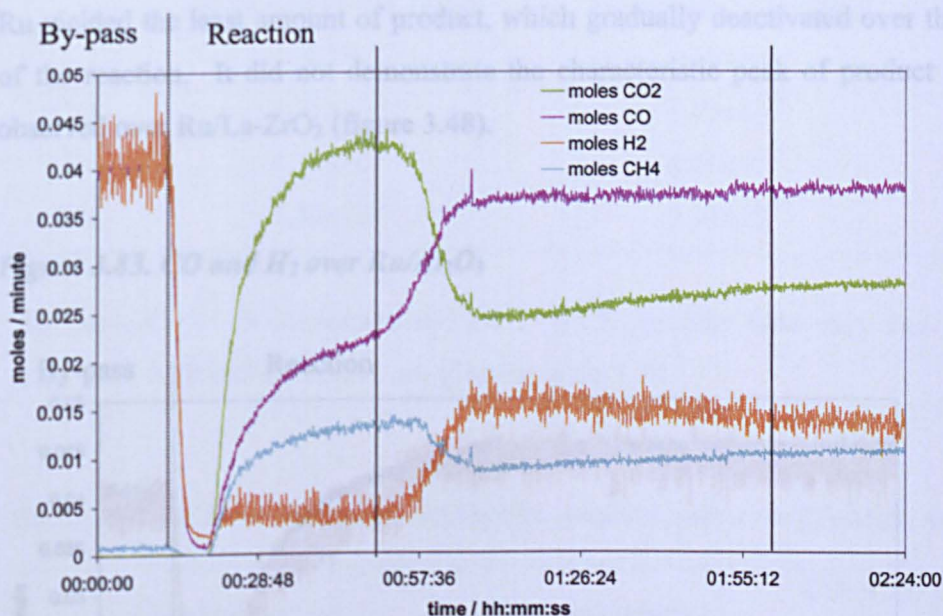
### 3.3.7 CO and H<sub>2</sub> over Al<sub>2</sub>O<sub>3</sub> Supported Catalysts

Figure 3.81. CO and H<sub>2</sub> over Pt/Al<sub>2</sub>O<sub>3</sub>

CO and H<sub>2</sub> (1:1) over each of the catalysts in the order Rh, Pt, Ru was then examined and the resulting spectra are shown in figures 3.81 to 3.83 respectively. Each reaction profile had similar aspects to that observed over the La-ZrO<sub>2</sub> supported catalysts in section 3.3.2, in that each catalyst produced the same three products: CO<sub>2</sub>, CH<sub>4</sub> and H<sub>2</sub>O.

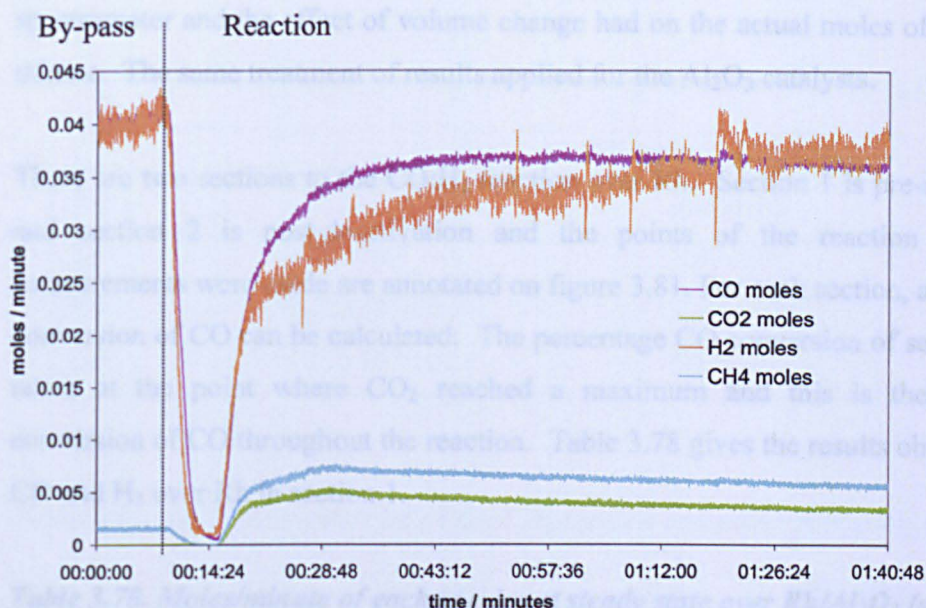
Rh showed the greatest activity and predominantly produced CO<sub>2</sub> over CH<sub>4</sub>. However, after approximately 40 minutes on stream, the two products, CO<sub>2</sub> and CH<sub>4</sub> began to decrease and simultaneously, the two reactants CO and H<sub>2</sub> began to increase. This suggests that the catalyst partially deactivated after a certain point in the reaction.

Figure 3.81. CO and H<sub>2</sub> over Rh/Al<sub>2</sub>O<sub>3</sub>



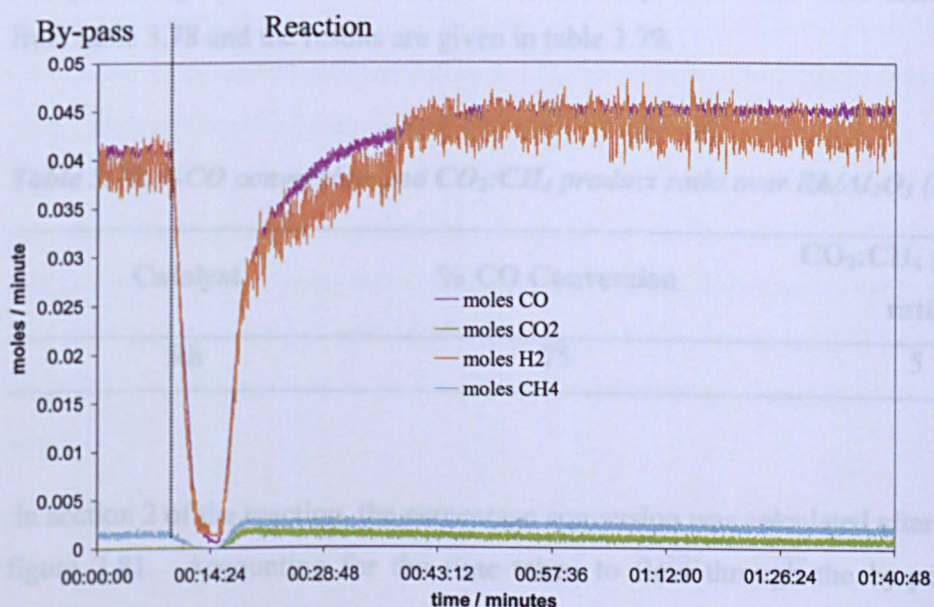
Pt produced the products at a lower yield than Rh and then slowly decreased suggesting slow deactivation of the catalyst was taking place.

**Figure 3.82. CO and H<sub>2</sub> over Pt/Al<sub>2</sub>O<sub>3</sub>**



Ru yielded the least amount of product, which gradually deactivated over the course of the reaction. It did not demonstrate the characteristic peak of product that was observed over Ru/La-ZrO<sub>2</sub> (figure 3.48).

**Figure 3.83. CO and H<sub>2</sub> over Ru/Al<sub>2</sub>O<sub>3</sub>**



### 3.3.7.1 Percentage CO Conversion over Rh/Al<sub>2</sub>O<sub>3</sub>

Section 3.3.3.1 described the effect that fragmentation of species in the mass spectrometer and the effect of volume change had on the actual moles of species per minute. The same treatment of results applied for the Al<sub>2</sub>O<sub>3</sub> catalysts.

There are two sections to the CO:H<sub>2</sub> reaction over Rh. Section 1 is pre-deactivation and section 2 is post-deactivation and the points of the reaction where the measurements were made are annotated on figure 3.81. For each section, a percentage conversion of CO can be calculated. The percentage CO conversion of section 1 was taken at the point where CO<sub>2</sub> reached a maximum and this is the maximum conversion of CO throughout the reaction. Table 3.78 gives the results obtained from CO and H<sub>2</sub> over Rh in section 1.

**Table 3.78. Moles/minute of each species at steady state over Rh/Al<sub>2</sub>O<sub>3</sub> (section 1)**

Species	Moles/min (from figure 3.35)	Moles/min (- splitting pattern)	Relative %
CO	$2.31 \times 10^{-2}$	$1.71 \times 10^{-2}$	25
CO <sub>2</sub>	$4.29 \times 10^{-2}$	$4.29 \times 10^{-2}$	62
CH <sub>4</sub>	$1.32 \times 10^{-2}$	$9.34 \times 10^{-3}$	13

The percentage CO conversion and the CO<sub>2</sub>:CH<sub>4</sub> product ratio were then calculated from table 3.78 and the results are given in table 3.79.

**Table 3.79. %CO conversion and CO<sub>2</sub>:CH<sub>4</sub> product ratio over Rh/Al<sub>2</sub>O<sub>3</sub> (section 1)**

Catalyst	% CO Conversion	CO <sub>2</sub> :CH <sub>4</sub> product ratio
Rh	75	5

In section 2 of the reaction, the percentage conversion was calculated after 2 hours in figure 3.81. Accounting for the time taken to flow through the by-pass, this is

approximately 1 hour and 40 minutes on stream. The results are given in table 3.80 followed by the percentage CO conversion in table 3.81.

**Table 3.80. Moles/minute of each species at steady state over Rh/Al<sub>2</sub>O<sub>3</sub> (section 2)**

Species	Moles/min (from figure 3.6)	Moles/min (- splitting pattern)	Relative %
CO	3.78x10 <sup>-2</sup>	3.40x10 <sup>-2</sup>	49
CO <sub>2</sub>	2.71x10 <sup>-2</sup>	2.71x10 <sup>-2</sup>	39
CH <sub>4</sub>	1.02x10 <sup>-2</sup>	9.54x10 <sup>-3</sup>	11

**Table 3.81. %CO conversion and CO<sub>2</sub>:CH<sub>4</sub> product ratio over Rh/Al<sub>2</sub>O<sub>3</sub> (stage 2)**

Catalyst	% CO Conversion	CO <sub>2</sub> :CH <sub>4</sub> product ratio
Rh	50	4

### 3.3.7.2 Pt and Ru/Al<sub>2</sub>O<sub>3</sub>

It was apparent from figures 3.82 and 3.83 that the % CO conversion was greater over Rh/Al<sub>2</sub>O<sub>3</sub> than Pt or Ru. For Pt, the amount of product decreased slightly with time on stream however, this loss is negligible in comparison to the loss of CO<sub>2</sub> product during the Boudouard reaction (figure 3.72). Therefore, it was likely that a relatively small amount of carbon was deposited during the reaction.

The moles/minute of each carbon-based species was taken from the Pt spectra and a relative percentage of each was calculated. The results are shown in table 3.82. From this the %CO conversion and CO<sub>2</sub>:CH<sub>4</sub> product ratio were calculated and reported in table 3.83. This was not done for Ru as the product produced was relatively very small.

**Table 3.82. Moles/minute of each species at steady state over Pt/Al<sub>2</sub>O<sub>3</sub>**

Species	Moles/min (from figure 3.6)	Moles/min (- splitting pattern)	Relative %
CO	$3.6 \times 10^{-2}$	$3.6 \times 10^{-2}$	79
CO <sub>2</sub>	$3.5 \times 10^{-3}$	$3.5 \times 10^{-3}$	8
CH <sub>4</sub>	$6.2 \times 10^{-3}$	$5.9 \times 10^{-3}$	13

**Table 3.83. %CO conversion and CO<sub>2</sub>:CH<sub>4</sub> product ratio over Pt/Al<sub>2</sub>O<sub>3</sub>**

Catalyst	% CO Conversion	CO <sub>2</sub> :CH <sub>4</sub> product ratio
Rh	21	0.6

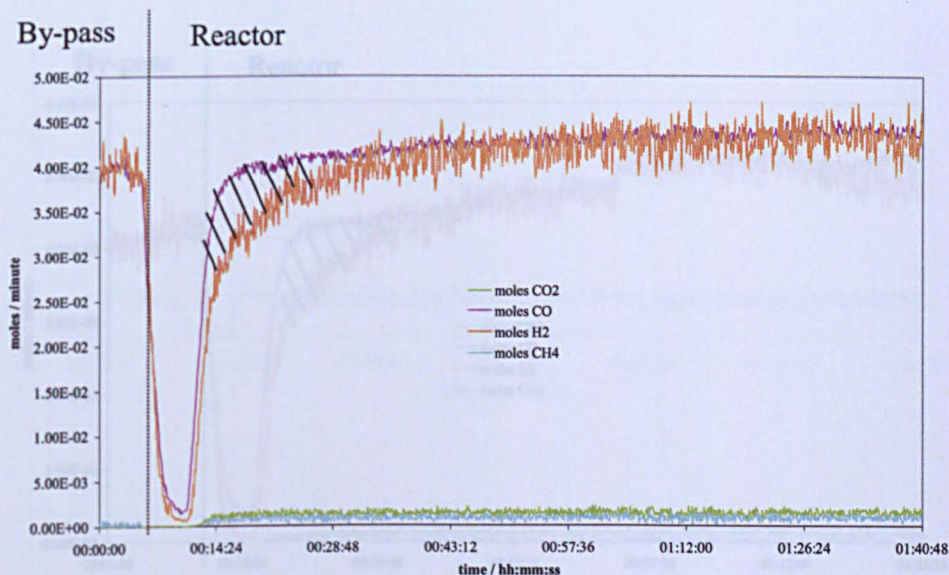
### 3.3.8 CO and CO<sub>2</sub> over Al<sub>2</sub>O<sub>3</sub> Supported Catalysts

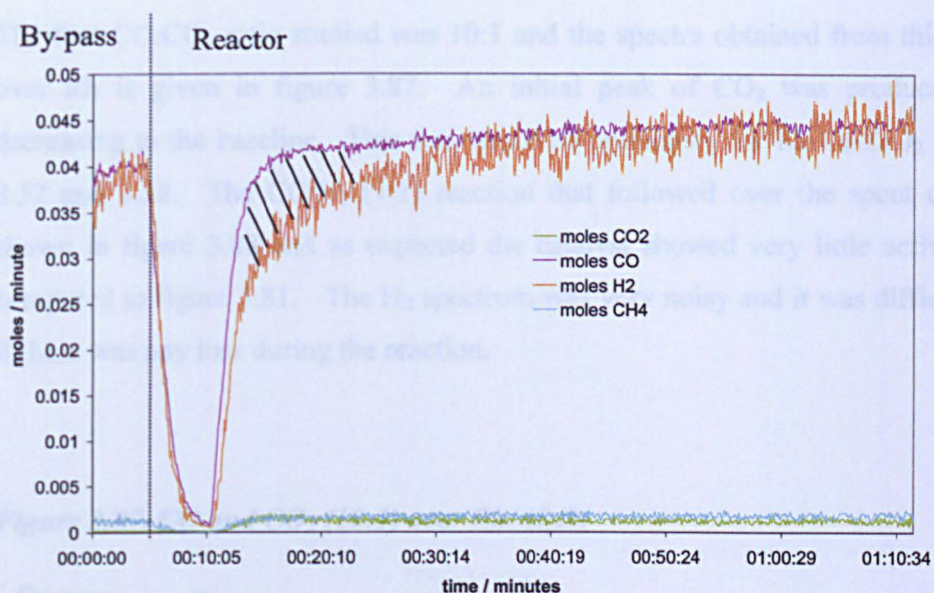
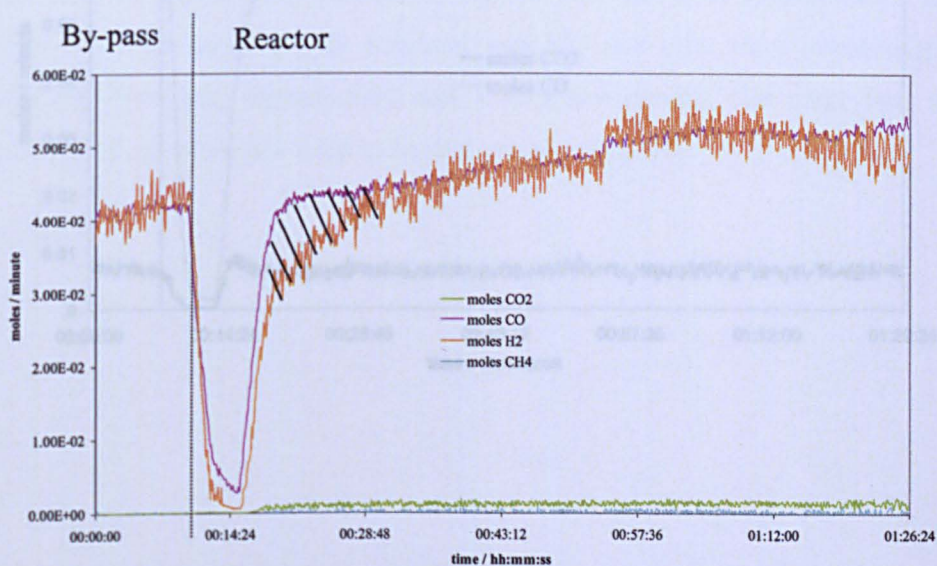
A series of CO:CO<sub>2</sub> ratios were passed over each of the Al<sub>2</sub>O<sub>3</sub> supported catalysts. In order to see how the activity of each was affected, a 1:1 ratio of CO:H<sub>2</sub> was passed over each used catalyst. Initially, CO:H<sub>2</sub> (1:1) was passed over the used Boudouard reaction catalysts from section 3.2.5 to determine if there was any residual activity.

#### 3.3.8.1 Used Boudouard Reaction Catalysts

Figures 3.84 to 3.86 show the spectra obtained for CO and H<sub>2</sub> (1:1) over used Boudouard catalysts: Rh, Pt and Ru respectively. It can be seen that there is slight residual activity from each of the catalysts and a distinct loss of H<sub>2</sub> at the start of the reaction (as indicated by hashed lines on figures).

**Figure 3.84. CO and H<sub>2</sub> (1:1) over spent Rh/Al<sub>2</sub>O<sub>3</sub> Boudouard reaction catalyst**

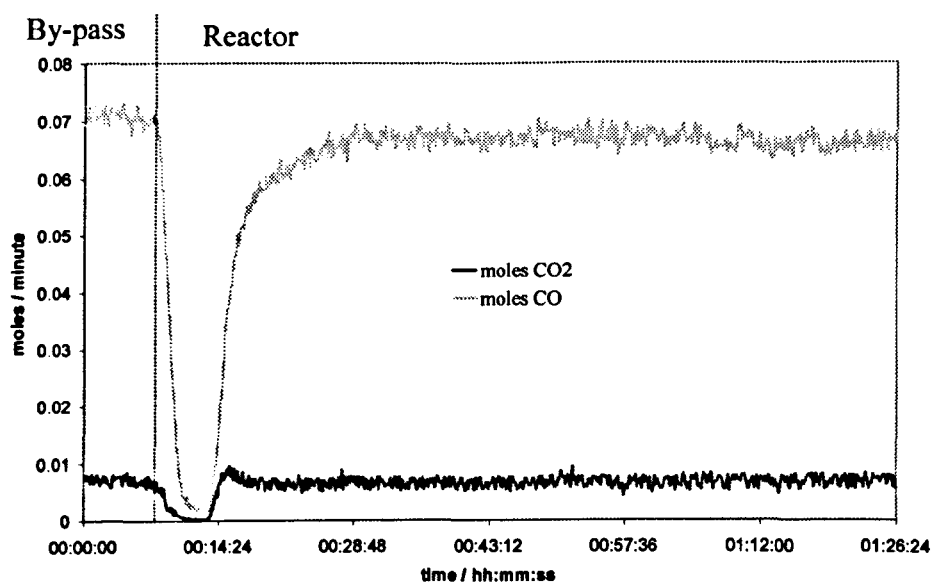


**Figure 3.85. CO and H<sub>2</sub> (1:1) over spent Pt/Al<sub>2</sub>O<sub>3</sub> Boudouard reaction catalyst****Figure 3.86. CO and H<sub>2</sub> (1:1) over spent Ru/Al<sub>2</sub>O<sub>3</sub> Boudouard reaction catalyst**

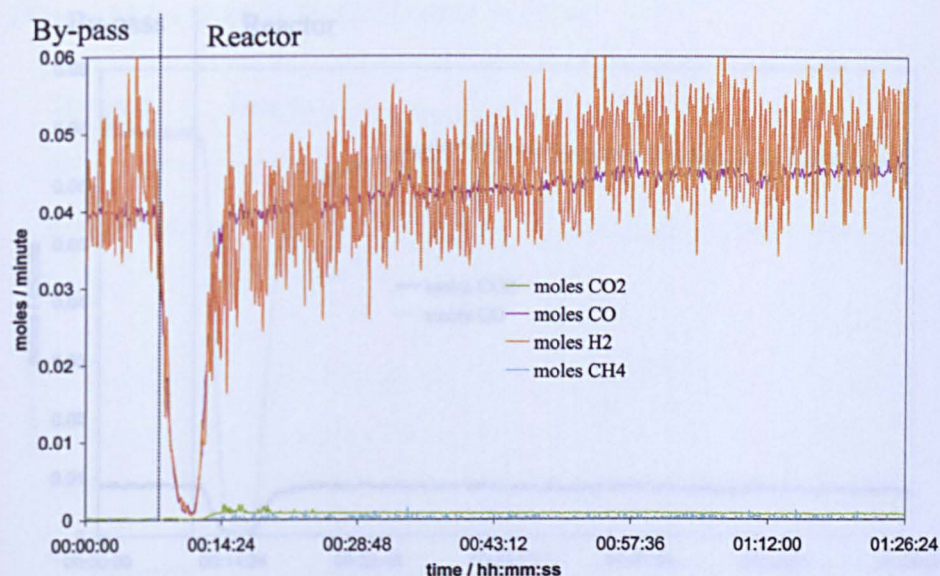
### 3.3.8.2 CO:CO<sub>2</sub> (10:1) over Al<sub>2</sub>O<sub>3</sub> Supported Catalysts

The first CO:CO<sub>2</sub> ratio studied was 10:1 and the spectra obtained from this reaction over Rh is given in figure 3.87. An initial peak of CO<sub>2</sub> was produced before decreasing to the baseline. This was observed previously for Rh/La-ZrO<sub>2</sub> in figures 3.52 and 3.58. The CO:H<sub>2</sub> (1:1) reaction that followed over the spent catalyst is shown in figure 3.88 and as expected the catalyst showed very little activity when compared to figure 3.81. The H<sub>2</sub> spectrum was very noisy and it was difficult to tell if there was any loss during the reaction.

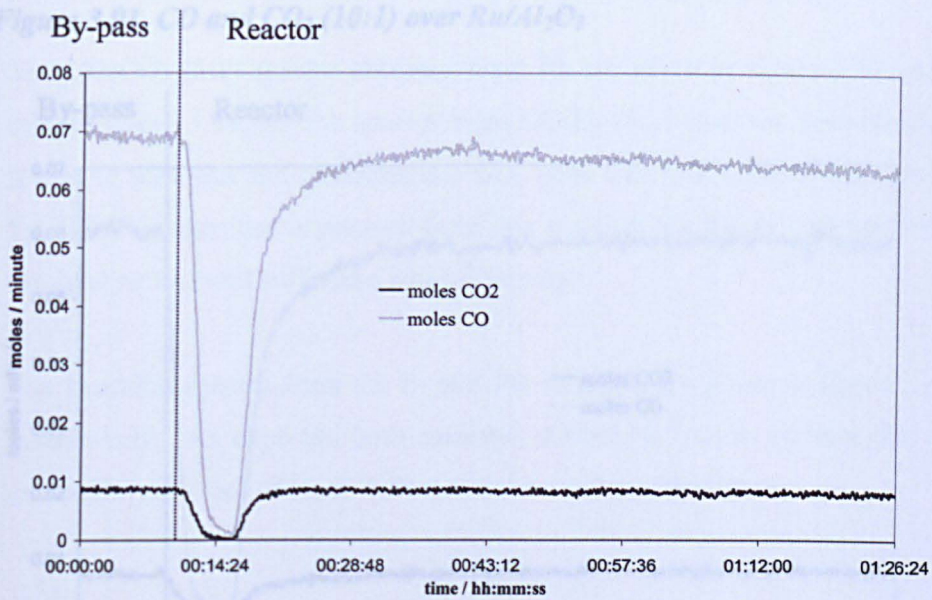
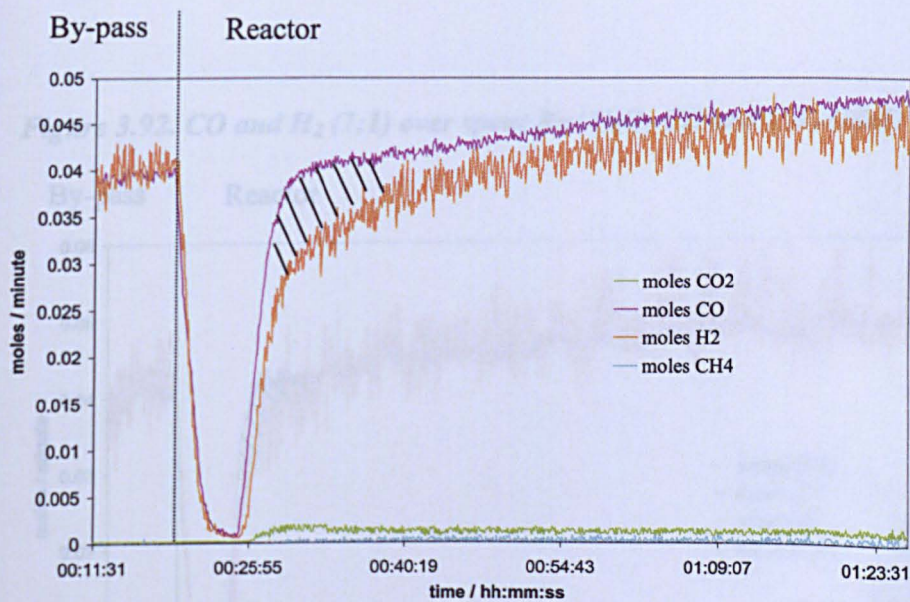
**Figure 3.87. CO and CO<sub>2</sub> (10:1) over Rh/Al<sub>2</sub>O<sub>3</sub>**

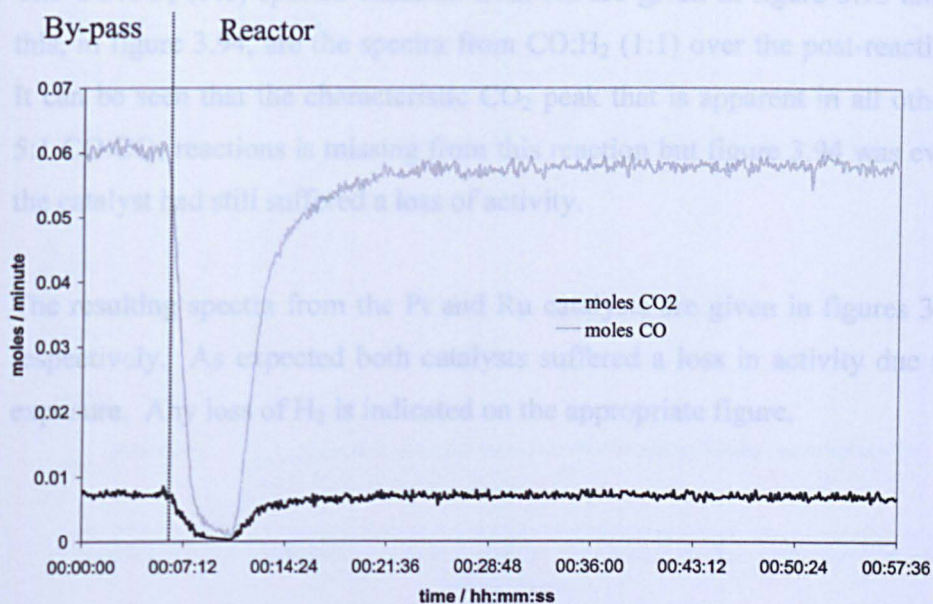
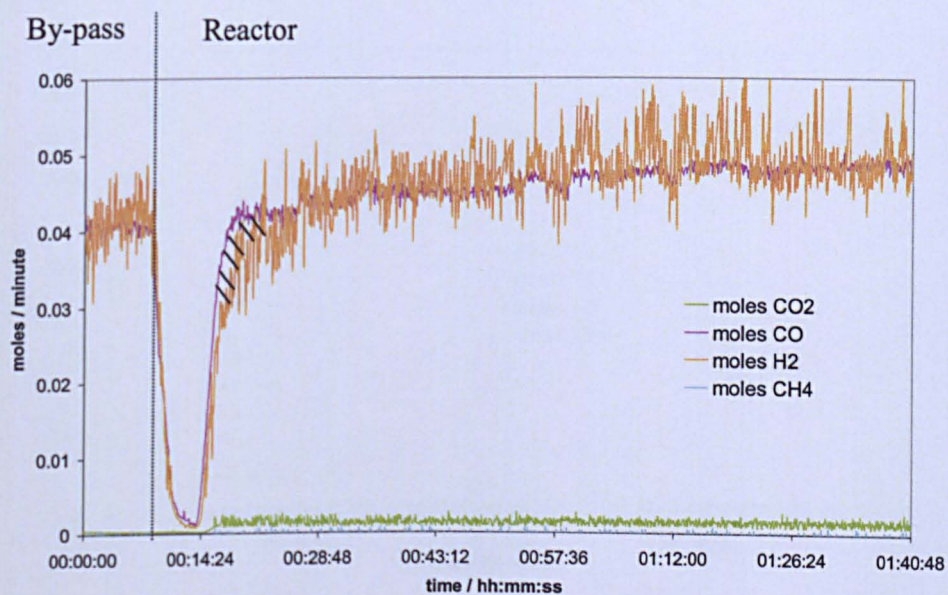


**Figure 3.88.** *CO and H<sub>2</sub> (1:1) over spent Rh/Al<sub>2</sub>O<sub>3</sub> CO and CO<sub>2</sub> (10:1)*



CO:CO<sub>2</sub> (10:1) over Pt and Ru are shown in figures 3.89 and 3.91 respectively followed by CO:H<sub>2</sub> post-reaction in figures 3.90 and 3.92 respectively. It was not clear from the mass spectra obtained how CO and CO<sub>2</sub> were interacting with the catalysts however; figures 3.90 and 3.92 show clearly, that there was a loss of activity. Loss of H<sub>2</sub> has been indicated where applicable.

**Figure 3.89. CO and CO<sub>2</sub> (10:1) over Pt/Al<sub>2</sub>O<sub>3</sub>****Figure 3.90. CO and H<sub>2</sub> (1:1) over spent Pt/Al<sub>2</sub>O<sub>3</sub> CO and CO<sub>2</sub> (10:1)**

**Figure 3.91. CO and CO<sub>2</sub> (10:1) over Ru/Al<sub>2</sub>O<sub>3</sub>****Figure 3.92. CO and H<sub>2</sub> (1:1) over spent Ru/Al<sub>2</sub>O<sub>3</sub> CO and CO<sub>2</sub> (10:1)**

### 3.3.8.3 CO:CO<sub>2</sub> (5:1) over Al<sub>2</sub>O<sub>3</sub> Supported Catalysts

The CO:CO<sub>2</sub> (5:1) spectra obtained from Rh are given in figure 3.93 and following this, in figure 3.94, are the spectra from CO:H<sub>2</sub> (1:1) over the post-reaction catalyst. It can be seen that the characteristic CO<sub>2</sub> peak that is apparent in all other 10:1 and 5:1 CO:CO<sub>2</sub> reactions is missing from this reaction but figure 3.94 was evidence that the catalyst had still suffered a loss of activity.

The resulting spectra from the Pt and Ru catalysts are given in figures 3.95 to 3.98 respectively. As expected both catalysts suffered a loss in activity due to CO/CO<sub>2</sub> exposure. Any loss of H<sub>2</sub> is indicated on the appropriate figure.

Figure 3.93. CO and CO<sub>2</sub> (5:1) over Rh/Al<sub>2</sub>O<sub>3</sub>

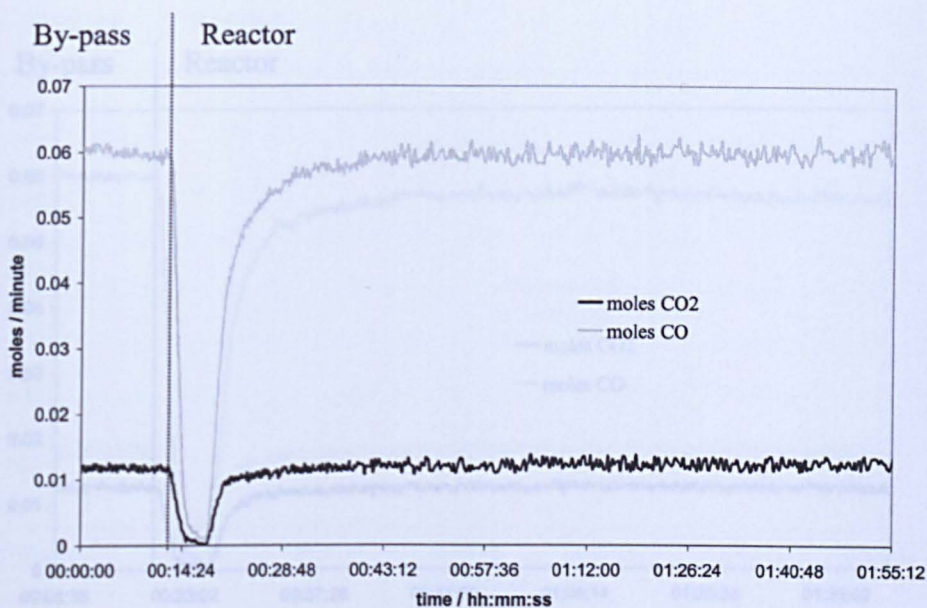


Figure 3.94. CO and H<sub>2</sub> (1:1) over spent Rh/Al<sub>2</sub>O<sub>3</sub> CO and CO<sub>2</sub> (5:1)

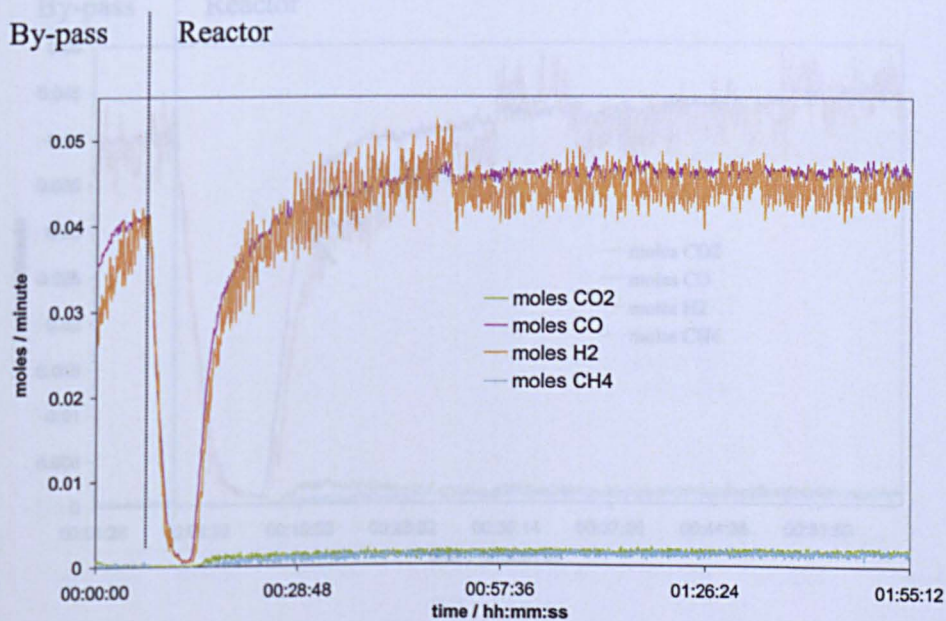


Figure 3.95. CO and CO<sub>2</sub> (5:1) over Pt/Al<sub>2</sub>O<sub>3</sub>

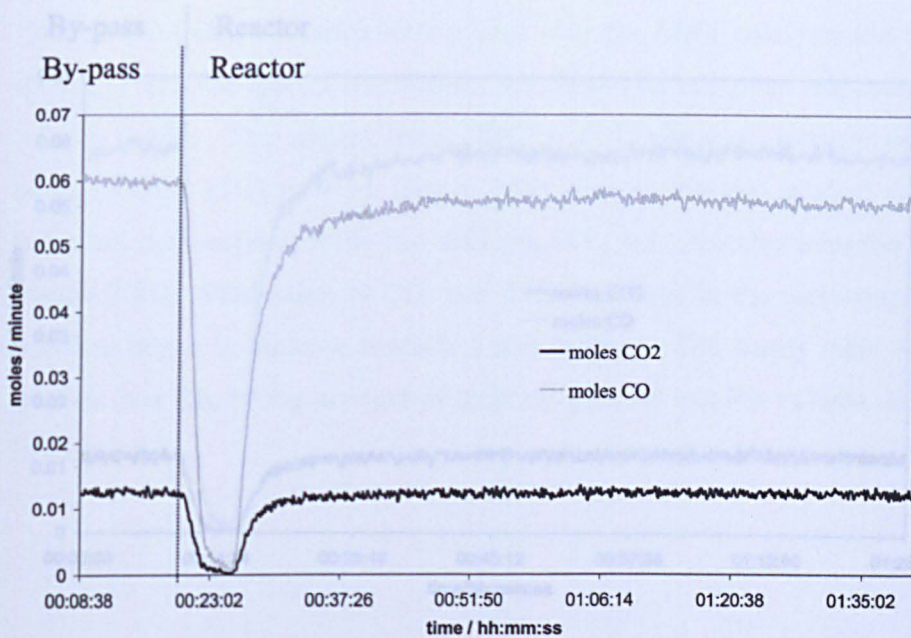


Figure 3.96. CO and H<sub>2</sub> (1:1) over spent Pt/Al<sub>2</sub>O<sub>3</sub> CO and CO<sub>2</sub> (5:1)

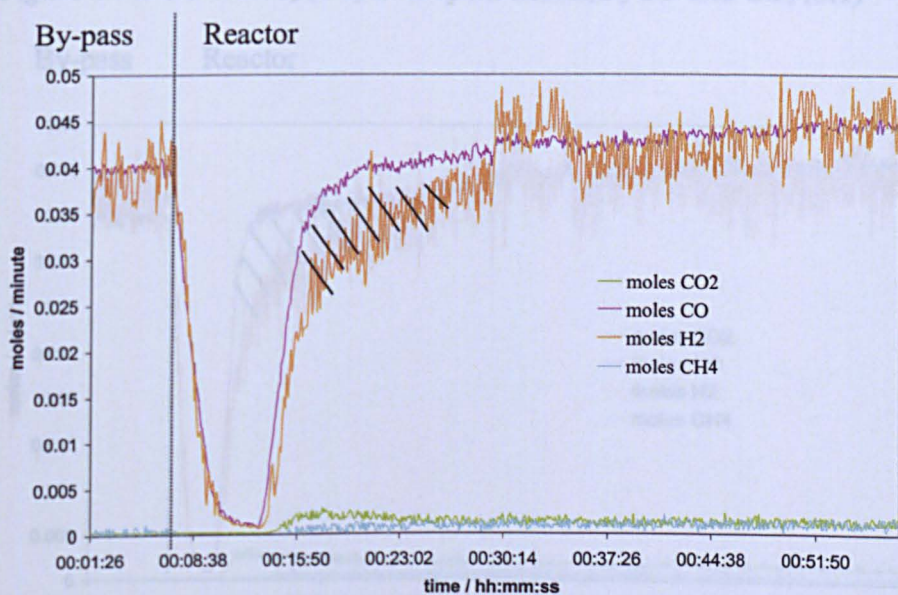


Figure 3.97. CO and CO<sub>2</sub> (5:1) over Ru/Al<sub>2</sub>O<sub>3</sub>

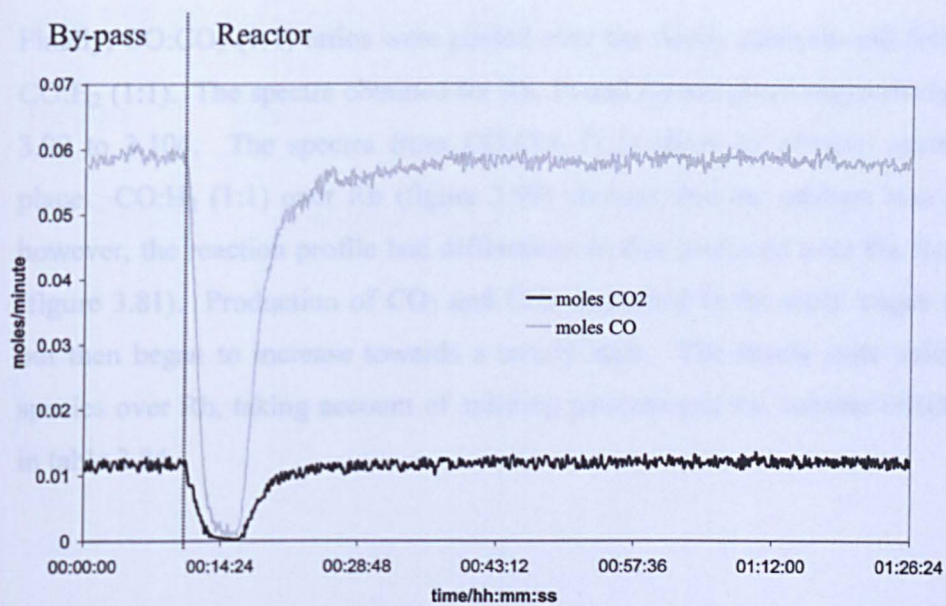
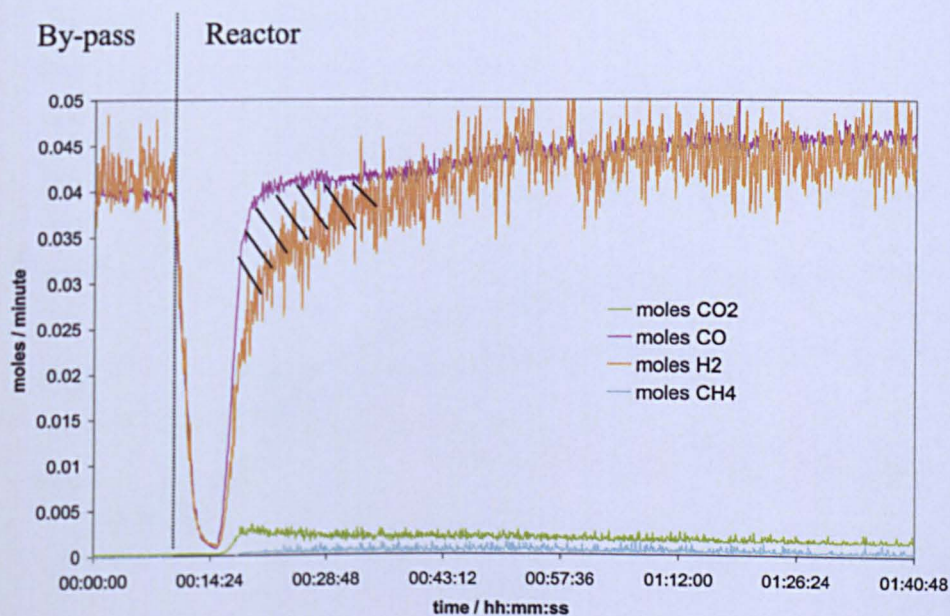


Figure 3.98. CO and H<sub>2</sub> (1:1) over spent Ru/Al<sub>2</sub>O<sub>3</sub> CO and CO<sub>2</sub> (5:1)



#### 3.3.8.4 CO:CO<sub>2</sub> (1:1) over Al<sub>2</sub>O<sub>3</sub> Supported Catalysts

Finally, CO:CO<sub>2</sub> (1:1) ratios were passed over the Al<sub>2</sub>O<sub>3</sub> catalysts and followed with CO:H<sub>2</sub> (1:1). The spectra obtained for Rh, Pt and Ru are given respectively in figures 3.99 to 3.104. The spectra from CO:CO<sub>2</sub> (1:1) show no obvious reaction taking place. CO:H<sub>2</sub> (1:1) over Rh (figure 3.99) showed that the catalyst was still active however, the reaction profile had differences to that produced over the fresh catalyst (figure 3.81). Production of CO<sub>2</sub> and CH<sub>4</sub> decreased in the early stages of reaction but then began to increase towards a steady state. The steady state values of each species over Rh, taking account of splitting patterns and the volume effect are given in table 3.84.

Figure 3.99. CO and CO<sub>2</sub> (1:1) over Rh/Al<sub>2</sub>O<sub>3</sub>

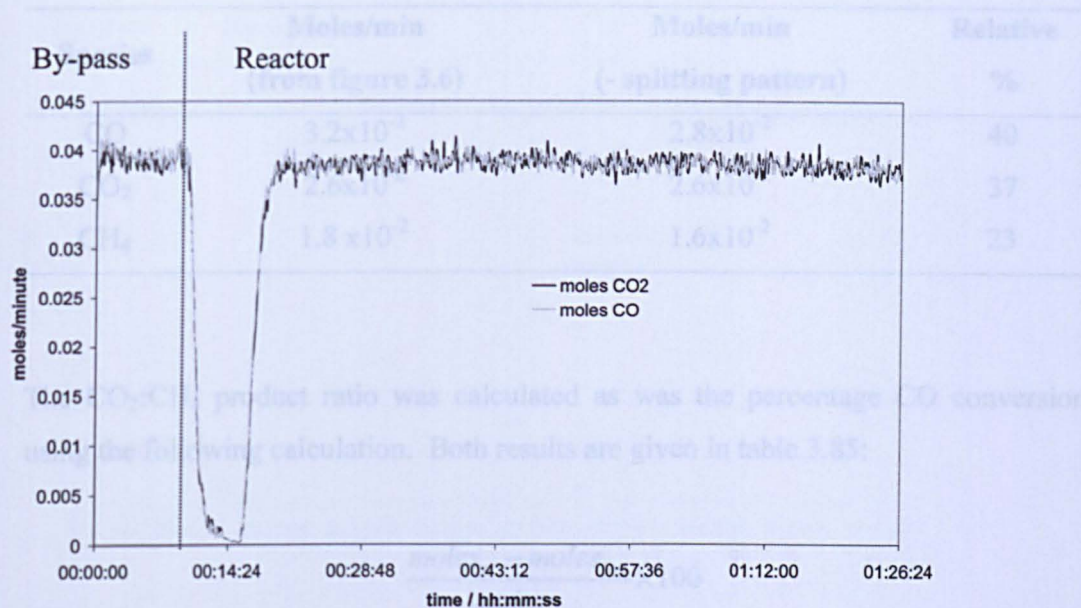
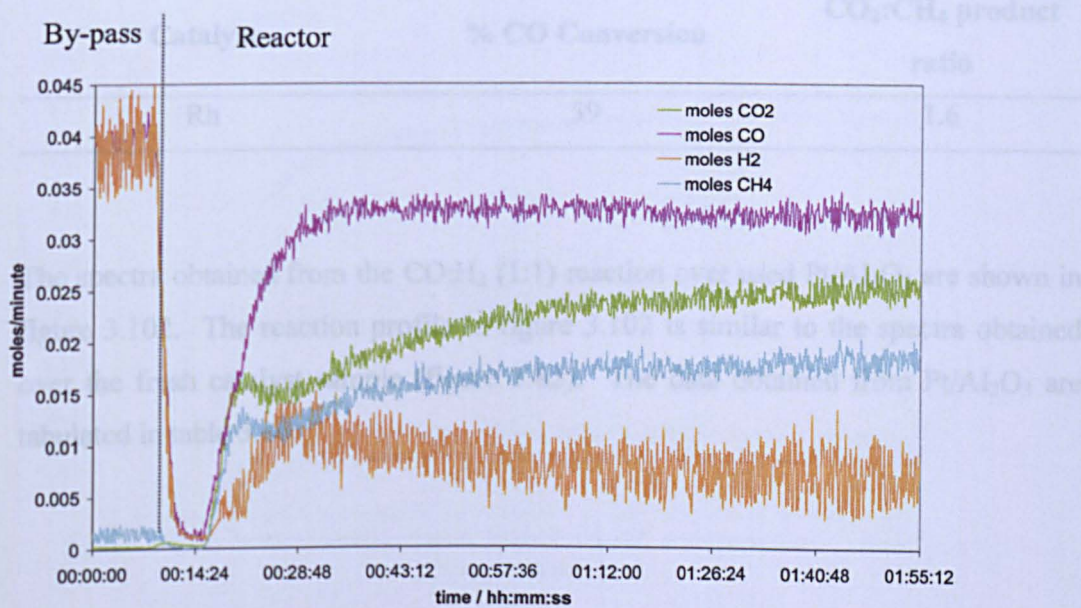


Figure 3.100. CO and H<sub>2</sub> (1:1) over spent Rh/Al<sub>2</sub>O<sub>3</sub> CO and CO<sub>2</sub> (1:1)



**Table 3.84. Moles/minute of each species at steady state over used Rh/Al<sub>2</sub>O<sub>3</sub>**

Species	Moles/min (from figure 3.6)	Moles/min (- splitting pattern)	Relative %
CO	3.2x10 <sup>-2</sup>	2.8x10 <sup>-2</sup>	40
CO <sub>2</sub>	2.6x10 <sup>-2</sup>	2.6x10 <sup>-2</sup>	37
CH <sub>4</sub>	1.8 x10 <sup>-2</sup>	1.6x10 <sup>-2</sup>	23

The CO<sub>2</sub>:CH<sub>4</sub> product ratio was calculated as was the percentage CO conversion using the following calculation. Both results are given in table 3.85:

$$\frac{\text{moles}_{in} - \text{moles}_{out}}{\text{moles}_{in}} \times 100$$

**Table 3.85. %CO conversion and CO<sub>2</sub>:CH<sub>4</sub> product ratio over Rh/Al<sub>2</sub>O<sub>3</sub>**

Catalyst	% CO Conversion	CO <sub>2</sub> :CH <sub>4</sub> product ratio
Rh	59	1.6

The spectra obtained from the CO:H<sub>2</sub> (1:1) reaction over used Pt/Al<sub>2</sub>O<sub>3</sub> are shown in figure 3.102. The reaction profile in figure 3.102 is similar to the spectra obtained over the fresh catalyst sample (figure 3.82). The data obtained from Pt/Al<sub>2</sub>O<sub>3</sub> are tabulated in table 3.86.

Figure 3.101. CO and CO<sub>2</sub> (1:1) over Pt/Al<sub>2</sub>O<sub>3</sub>

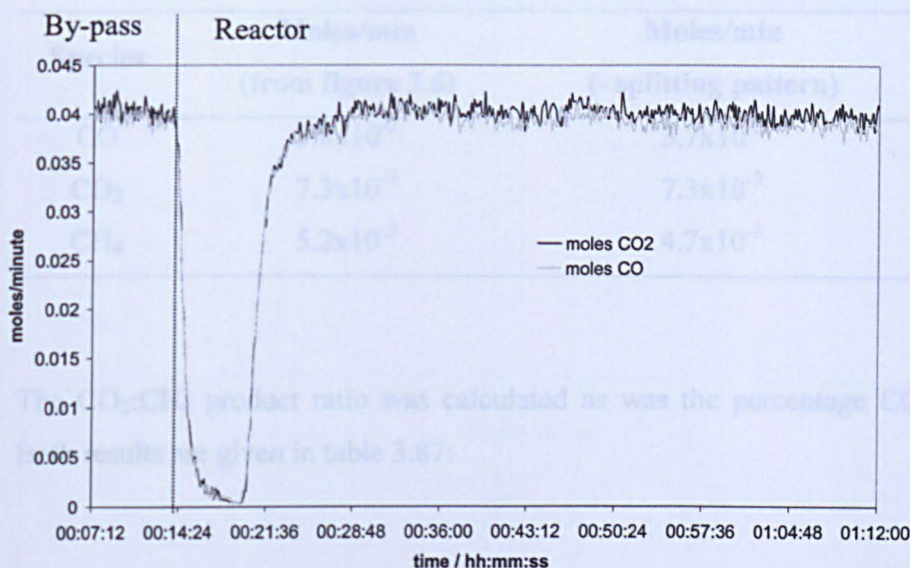
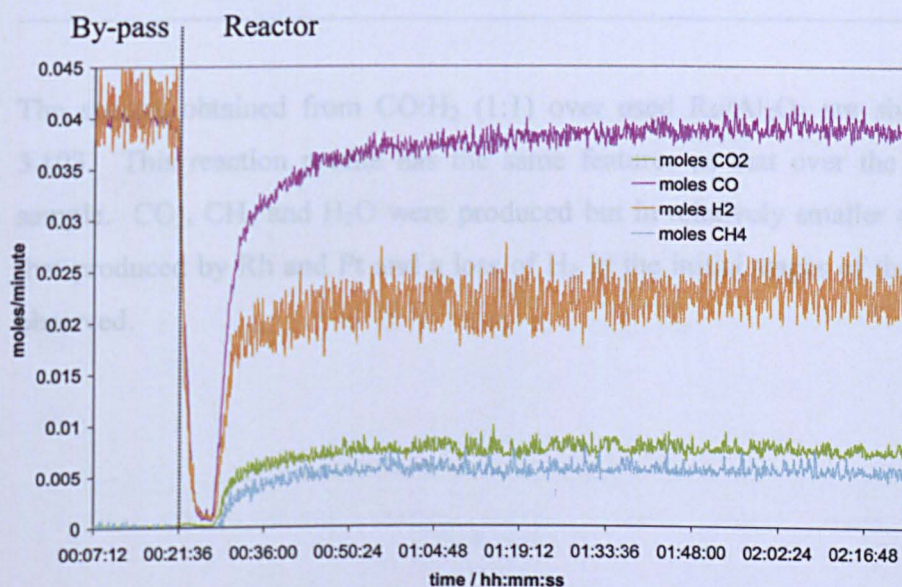


Figure 3.102. CO and H<sub>2</sub> (1:1) over spent Pt/Al<sub>2</sub>O<sub>3</sub> CO and CO<sub>2</sub> (1:1)



**Table 3.86. Moles/minute of each species at steady state over used Pt/Al<sub>2</sub>O<sub>3</sub>**

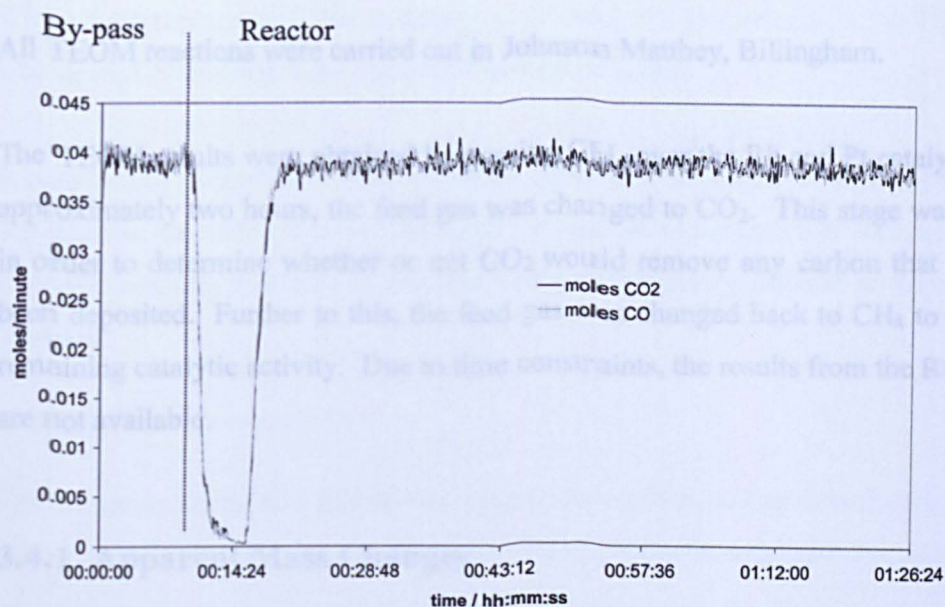
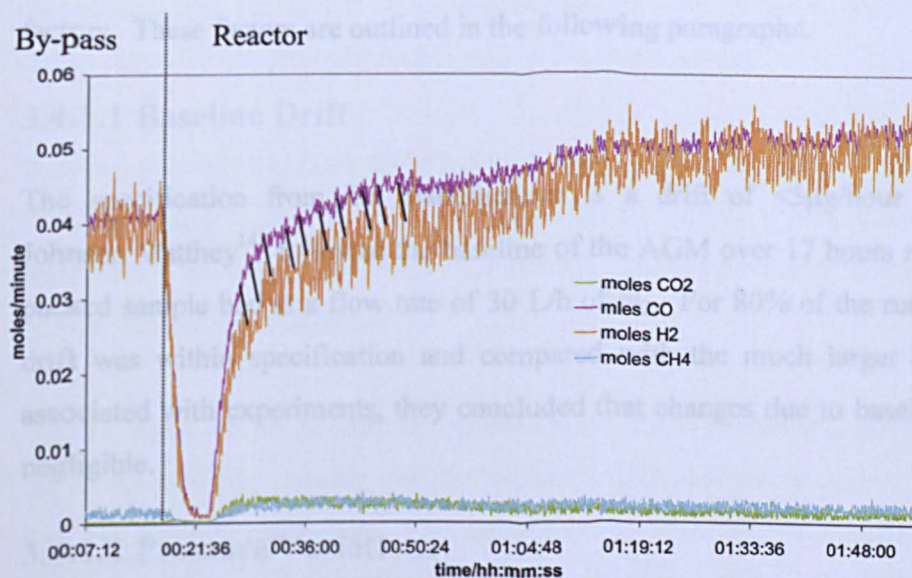
Species	Moles/min (from figure 3.6)	Moles/min (- splitting pattern)	Relative %
CO	$3.8 \times 10^{-2}$	$3.7 \times 10^{-2}$	76
CO <sub>2</sub>	$7.3 \times 10^{-3}$	$7.3 \times 10^{-3}$	15
CH <sub>4</sub>	$5.2 \times 10^{-3}$	$4.7 \times 10^{-3}$	9

The CO<sub>2</sub>:CH<sub>4</sub> product ratio was calculated as was the percentage CO conversion. Both results are given in table 3.87:

**Table 3.87. %CO conversion and CO<sub>2</sub>:CH<sub>4</sub> product ratio over Pt/Al<sub>2</sub>O<sub>3</sub>**

Catalyst	% CO Conversion	CO <sub>2</sub> :CH <sub>4</sub> product ratio
Pt/Al <sub>2</sub> O <sub>3</sub>	24	1.6

The spectra obtained from CO:H<sub>2</sub> (1:1) over used Ru/Al<sub>2</sub>O<sub>3</sub> are shown in figure 3.103. This reaction profile has the same features as that over the fresh catalyst sample. CO<sub>2</sub>, CH<sub>4</sub> and H<sub>2</sub>O were produced but in relatively smaller quantities than that produced by Rh and Pt and a loss of H<sub>2</sub> in the initial stages of the reaction was observed.

**Figure 3.103. CO and CO<sub>2</sub> (1:1) over used Ru/Al<sub>2</sub>O<sub>3</sub>****Figure 3.104. CO and H<sub>2</sub> (1:1) over spent Ru/Al<sub>2</sub>O<sub>3</sub> CO and CO<sub>2</sub> (1:1)**

### 3.4 TEOM Reactions

All TEOM reactions were carried out in Johnson Matthey, Billingham.

The TEOM results were obtained by passing CH<sub>4</sub> over the Rh and Pt catalysts. After approximately two hours, the feed gas was changed to CO<sub>2</sub>. This stage was included in order to determine whether or not CO<sub>2</sub> would remove any carbon that may have been deposited. Further to this, the feed gas was changed back to CH<sub>4</sub> to assess the remaining catalytic activity. Due to time constraints, the results from the Ru catalysts are not available.

#### 3.4.1 Apparent Mass Changes

Certain practical aspects of TEOM operation must be taken into account before an accurate analysis of the results can be carried out. Certain system perturbations can be interpreted by the TEOM as a change in mass<sup>141</sup>. The genuine mass change, which is of interest, is due to a chemical change associated with the catalyst. In this work, changes in mass were observed due to deposition of carbon on the catalyst. The apparent mass of the tapered element (TE), however can be affected by several other factors. These factors are outlined in the following paragraphs.

##### 3.4.1.1 Baseline Drift

The specification from the manufacturer is a drift of <5µg/hour below 573K. Johnson Matthey<sup>141</sup> followed the baseline of the AGM over 17 hours at 973K with a packed sample bed at a flow rate of 30 L/h of N<sub>2</sub>. For 80% of the run, the baseline drift was within specification and compared with the much larger mass changes associated with experiments, they concluded that changes due to baseline drift were negligible.

##### 3.4.1.2 Pressure Variations

As the pressure in the system is increased, so too is the density of gas within the TEOM bowl. This results in an apparent increase in the AGC.

### 3.4.1.3 Temperature Variations

When the temperature of the system is increased, the gas density in the TEOM bowl will decrease resulting in an apparent increase of mass.

A conflicting temperature affect has been reported that seems to be a more common explanation amongst other TEOM users<sup>141</sup>: As the temperature is increased, the TE expands resulting in a drop in frequency that subsequently leads to an apparent mass increase.

### 3.4.1.4 Gas Composition

For the same reason as a pressure or temperature affect, as the flow is switched from a lower to a higher density gas, the mass of the TE increases as does the AGC.

### 3.4.1.5 Changing Gas Flow Rate

A change in flow of carrier or purge gas can also affect the apparent mass and there are three possible explanations to explain the resulting affect. As the flow rate is increased, the pressure drop across the catalyst bed is increased and a change in mass equivalent to an increase in pressure is observed. Johnson Matthey, however, discovered that the affect of changing flow on the pressure drop is minimal at pressures of 20 bar so could be ignored in the present study.

It is also possible that back diffusion of purge gas into the TE bowl can affect the gas density and this affect was valid for this study. In order to combat back diffusion, the purge gas is set to the high value of 104 Lh<sup>-1</sup>. Studies have shown that a purge flow of this rate prevents diffusion<sup>141</sup>.

A third reason for an increase in apparent mass due to changing flows is the affect on the amount of heat passing into the process which can affect the AGC in a similar way to a temperature change. This affect has only been observed when varying purge flow at constant carrier gas since the purge gas is in contact with the wall where the heat is being applied. This effect can be eliminated again with a constant purge flow of 104 Lh<sup>-1</sup>.

### 3.4.1.6 Catalysis Due to Metal Cap

Figure 3.105, shows the construction of the TEOM, in particular the location of the metal cap. The cap slides on the end of the TE to hold the catalyst bed in place. It is held at reaction temperature and the exit gases flow through its perforations. Any catalysis taking place on the cap will affect the mass of the TE. Fortunately, after every reaction in this study, the cap was examined and no carbon deposits were found.

### 3.4.1.7 Noise

Although it does not have such a significant effect on the baseline as other aspects, noise can affect interpretation of the AGC. The packing of the TE is very important in noise reduction. In order to minimise catalyst movement and hence the frequency of vibration the bowl must be firmly packed with saffil and all fibres removed from around the edges of the cap. Packing which is too firm, however, leads to an increased pressure drop which may damage the TEOM.

### 3.4.1.8 Present Study

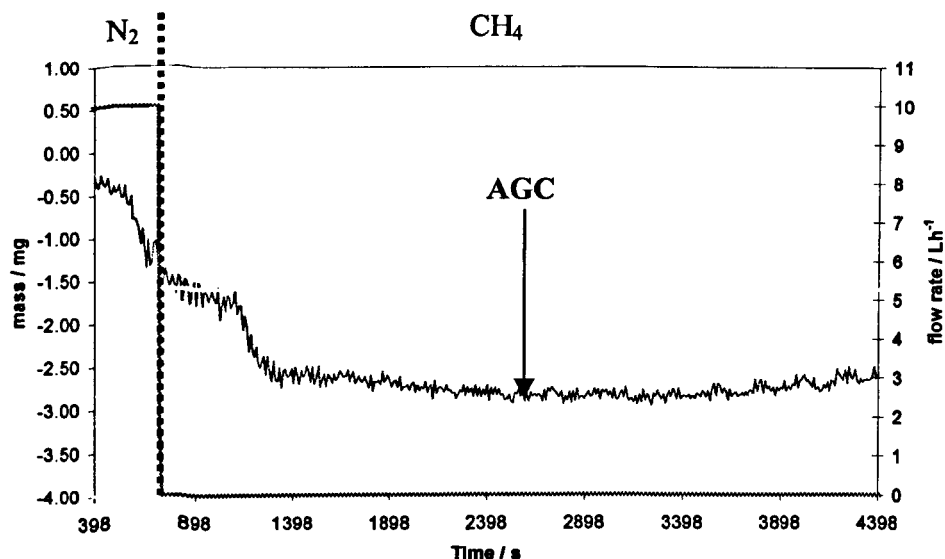
Since all reactions were carried out at constant pressure and temperature and purge flow rate, only changes in gas composition and noise were a significant factor. It was, therefore, important in this study to know the baseline value of each gas composition used. If an increase in the AGC was observed beyond this value, conclusion was that carbon was being deposited on the catalyst.

## 3.4.2 CH<sub>4</sub> Cracking Reaction over La-ZrO<sub>2</sub> Support

Figure 3.106 shows the output from the TEOM's pulse mass analyser when CH<sub>4</sub> was flowed over the La-ZrO<sub>2</sub> support material. The support was subjected to the reduction procedure (not shown in figure 3.106), and then flushed with N<sub>2</sub>. A straight dark line of flow rate 10Lh<sup>-1</sup> (right hand axis), as annotated in the figure, represents N<sub>2</sub> gas. The AGC is also labelled on the figure and its units are on the left hand axis. The gas flow was switched to CH<sub>4</sub> which is represented by a light grey line of flow rate 5.3Lh<sup>-1</sup> in the figure. On switching to CH<sub>4</sub> from N<sub>2</sub>, the AGC decreases as

expected according to section 3.4.1.4. Once the AGC reaches its baseline of approximately  $-2.5\text{mg}$ , it does not significantly increase over the course of the reaction, showing that no reaction is taking place over the support material.

**Figure 3.106.** Mass of La-ZrO<sub>2</sub> support as CH<sub>4</sub> is flushed through.



### 3.4.3 CH<sub>4</sub> Cracking Reaction over Rh/La-ZrO<sub>2</sub>

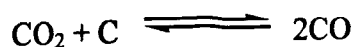
Figure 3.107 shows the TEOM data obtained from the reaction over Rh. The straight lines represent the change in gas composition during the reaction and their values are given on the right hand axis. The change in gas composition during reaction has been annotated on the figure.

The catalyst was reduced (not shown in figure), then flushed with N<sub>2</sub> before reactant CH<sub>4</sub> was passed over. While N<sub>2</sub> was flushing, AGC was constant, however, at the point of switching, the AGC can be seen to increase then decrease back to the baseline over the first few seconds. This increase was thought to occur due to an initial surge of gas as the mass flow controller was opened. The AGC then decreased by approximately 0.5mg as expected according to section 3.4.1.4 before it began to

gradually increase to a steady state over two hours. The increase, which occurred as CH<sub>4</sub> was flushing through, was due to carbon deposition on the catalyst.

Since the AGC had reached a steady state and no further carbon deposition was taking place, conclusion was made that the catalyst had deactivated. The gas feed was switched back to N<sub>2</sub> at this stage to remove any traces of CH<sub>4</sub>. As expected, on switching to N<sub>2</sub>, the AGC increased. The increase was equal to that seen on switching from N<sub>2</sub> to CH<sub>4</sub> at the start of the reaction however, note that the baseline value for N<sub>2</sub> is larger. This was because the catalyst now had extra mass due to carbon. The change in the N<sub>2</sub> baseline, from before and after addition of CH<sub>4</sub>, is equal to the mass of carbon deposited.

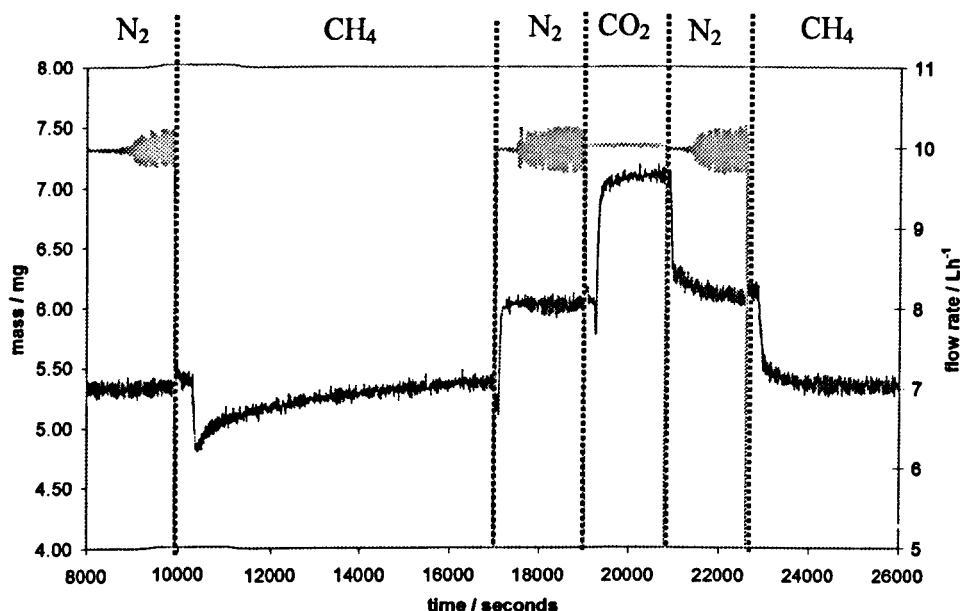
CO<sub>2</sub> was then flushed over in an attempt to re-oxidise any deposited carbon according to the reverse Boudouard reaction:



Again, since CO<sub>2</sub> is denser than N<sub>2</sub>, the AGC increased. If any matter was lost through oxidation, the AGC would have decreased while CO<sub>2</sub> was flushing however, no such decrease was seen.

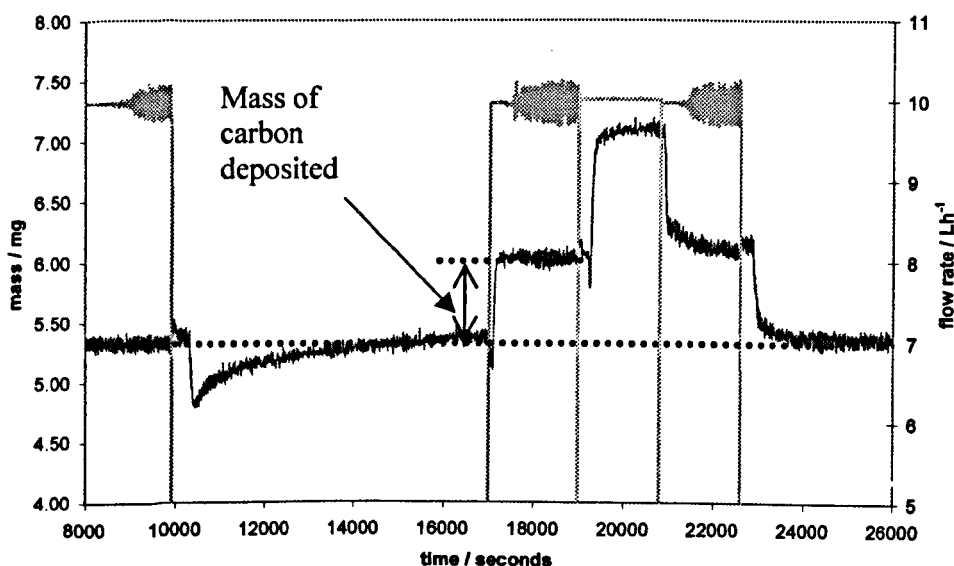
The TEOM was again flushed with N<sub>2</sub> to remove any remaining CO<sub>2</sub>. The AGC baseline at this stage appears higher than it should be compared to the previous flow of N<sub>2</sub>. This is a feature present in all CH<sub>4</sub> cracking experiments carried out on the TEOM. The catalyst was then flushed with CH<sub>4</sub> as a second check to see if the CO<sub>2</sub> had had any effect on the deactivated catalyst. As expected, the AGC reached its baseline value and did not increase showing there was no further activity from the catalyst.

**Figure 3.107. Change in mass of Rh/La-ZrO<sub>2</sub> during CH<sub>4</sub> cracking reaction.**



From the TEOM output, the mass of carbon deposited on the catalyst can be calculated. Measuring the change in the AGC baseline before and after subsection to CH<sub>4</sub> as illustrated in figure 3.108 was how this mass was determined.

**Figure 3.108. Calculating mass change by measuring baseline change.**



The mass of carbon deposited after an arbitrary time of one hour and the steady state mass of carbon were calculated and the results are given in table 3.88.

**Table 3.88. Mass of carbon deposited during CH<sub>4</sub> cracking over Rh/La-ZrO<sub>2</sub>**

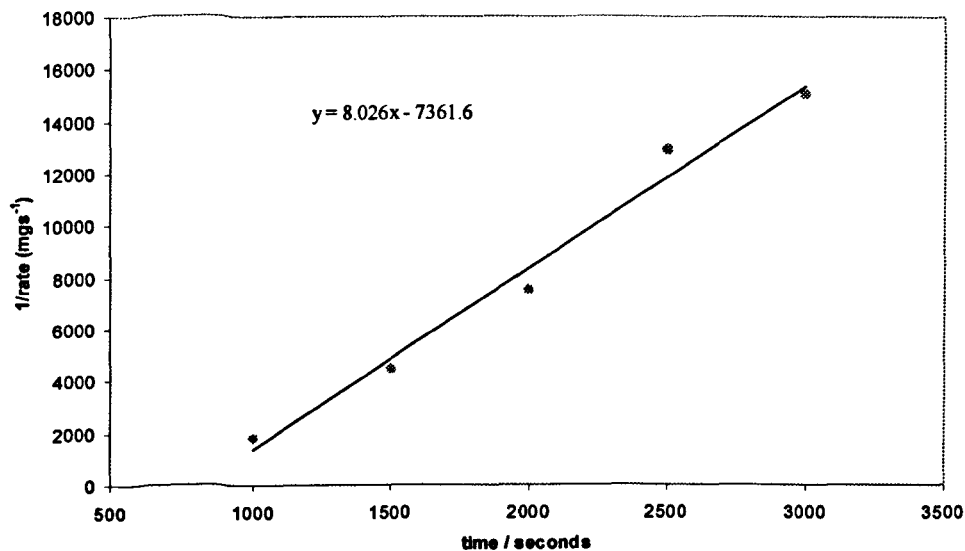
Catalyst	Mass of deposited C after 1 hour / mg	Steady State Mass of deposited C / mg
Rh/La-ZrO <sub>2</sub>	0.62	0.69

### 3.4.3.1 Rh/La-ZrO<sub>2</sub> Catalyst Deactivation

Figure 3.107 showed how there was no further activity from catalyst when CH<sub>4</sub> was passed over for the second time and conclusion was that the catalyst had deactivated. The results were plotted using the first order equation, however, the lines were very definite curves therefore, the given second order equation was applied:

$$\frac{1}{R_t} = \frac{1}{R_i} + \alpha t$$

Where  $R_t$  is the rate at time  $t$ ,  $R_i$  is the initial rate of reaction and  $\alpha$  is a deactivation parameter. A plot of  $1/R_t$  against  $t$  should give a straight line of gradient  $\alpha$ . Figure 3.109 shows the straight line and the equation of the line obtained by application of the deactivation equation for the first 3000 seconds of the CH<sub>4</sub> cracking reaction. After this time, the rate of carbon deposition was constant and when plotted, the above equation resulted in a gradient of zero. The resulting rate parameter has been tabulated below.

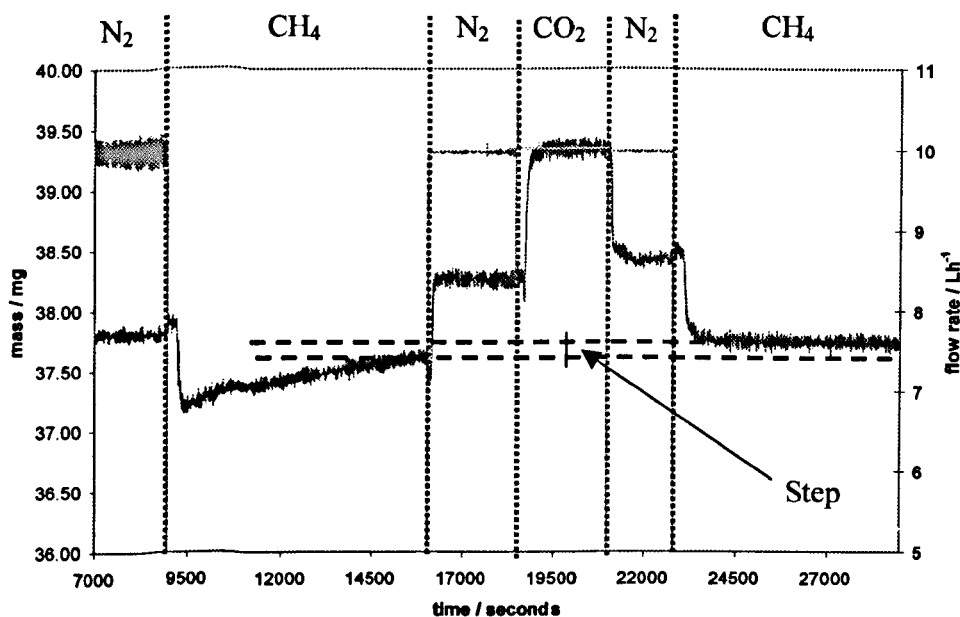
**Figure 3.109. Plot of  $1/Rt$  vs. time for Rh/La-ZrO<sub>2</sub>**

Catalyst	$\alpha$
Rh/La-ZrO <sub>2</sub>	8.03

### 3.4.4 CH<sub>4</sub> Cracking Reaction over Pt/La-ZrO<sub>2</sub>

The resultant AGC changes observed over Pt/La-ZrO<sub>2</sub> are shown in figure 3.110. As was observed during the Rh reaction, the AGC responded to different gas densities. When the gas flow was switched to CH<sub>4</sub> to N<sub>2</sub>, the AGC was seen to increase beyond the baseline level signifying the deposition of carbon on the catalyst. CH<sub>4</sub> flowed for approximately two hours over Pt however the AGC never reached steady state within this time. Again when CO<sub>2</sub> was passed over the catalyst, the AGC was constant to show there was no loss in mass, hence, deposited carbon was not being oxidised. N<sub>2</sub> was flushed to remove any remaining CO<sub>2</sub>. The AGC baseline at this stage appears to have increased immediately following the CO<sub>2</sub> flush as was observed with Rh in section 3.4.3. Finally, CH<sub>4</sub> was passed over the catalyst for a second time and no further increase in the AGC was observed hence, the catalyst had fully deactivated.

**Figure 3.110.** Change in mass of Pt/La-ZrO<sub>2</sub> during CH<sub>4</sub> cracking reaction.



It can be seen in figure 3.110, that there is a step between the two CH<sub>4</sub> AGC baselines. However, there was no AGC increase during the second purge of CH<sub>4</sub>. This suggests that steady state was reached at the point where the gas was switched and measurement was not possible. This is illustrated in figure 3.111. The mass of carbon produced was obtained from the TEOM data as also shown in figure 3.111. The results have been tabulated in table 3.89.

**Figure 3.111. Calculating mass of carbon deposited over Pt/La-ZrO<sub>2</sub>.**

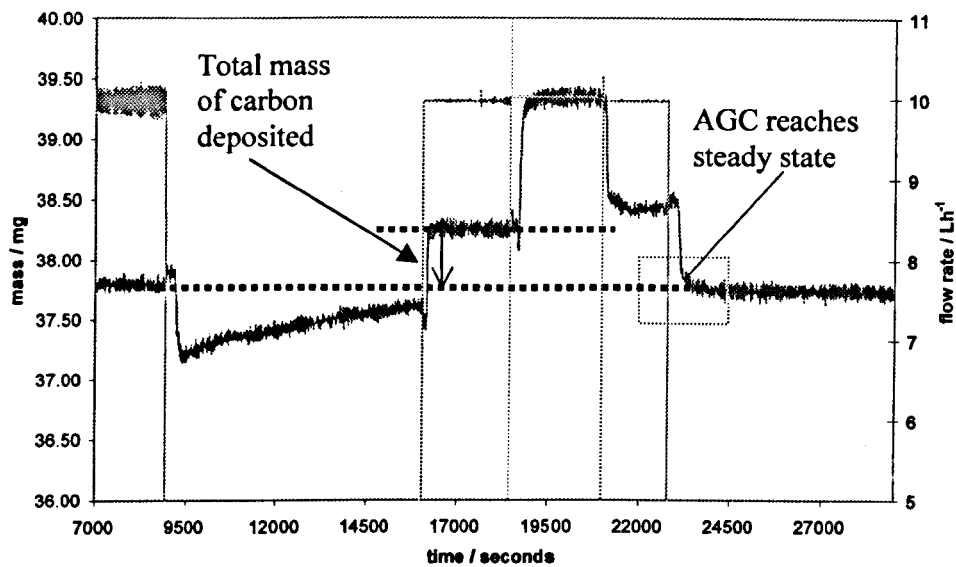


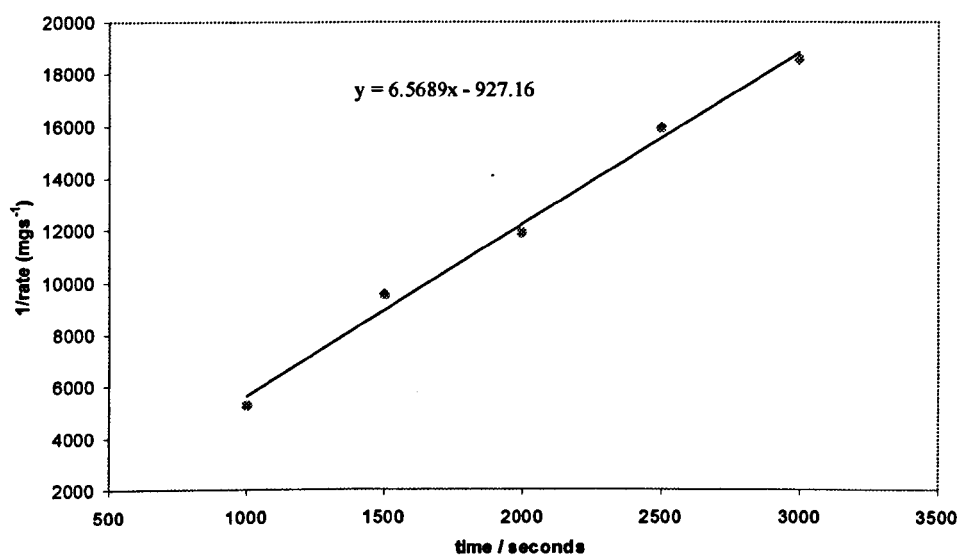
**Table 3.89. Mass of carbon deposited during CH<sub>4</sub> cracking over Pt/La-ZrO<sub>2</sub>**

Catalyst	Mass of deposited C after 1 hour / mg	Steady State Mass of deposited C / mg
Pt / La-ZrO <sub>2</sub>	0.29	0.58

### 3.4.4.1 Pt Catalyst Deactivation

By application of the second order deactivation equation, a value for the deactivation parameter,  $\alpha$ , was obtained for the first 5000 seconds of the CH<sub>4</sub> cracking reaction over Pt/La-ZrO<sub>2</sub>. The straight-line graph obtained is given in figure 3.112. After 5000 seconds the rate of carbon deposition was constant hence no points were plotted thereafter.

**Figure 3.112.** Plot of  $1/Rt$  vs. time for Pt/La-ZrO<sub>2</sub>

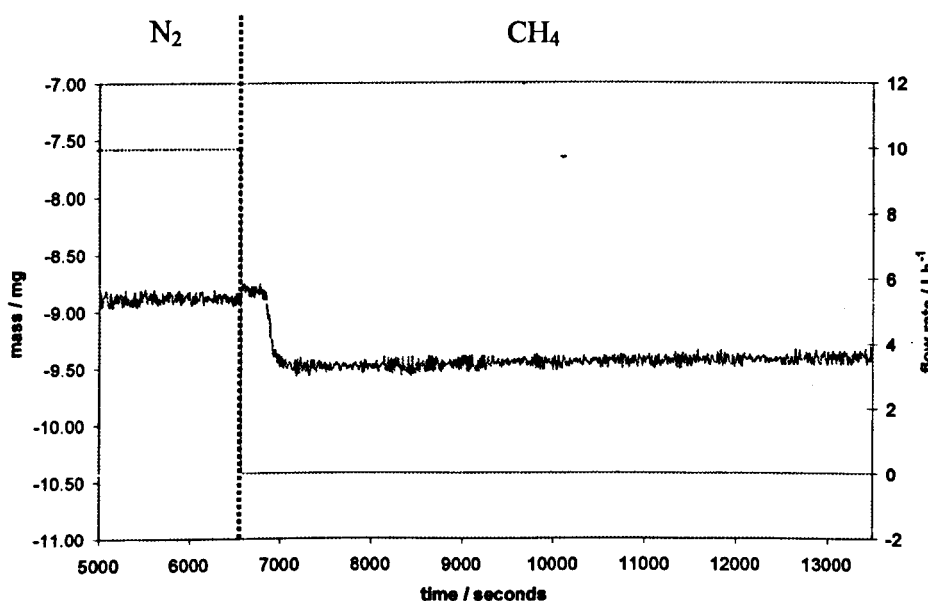


Catalyst	$\alpha$
Pt/La-ZrO <sub>2</sub>	6.57

### 3.4.5 CH<sub>4</sub> Cracking Reaction over Al<sub>2</sub>O<sub>3</sub> Support

CH<sub>4</sub> was flushed over the Al<sub>2</sub>O<sub>3</sub> support material to determine if any catalysis was taking place. The data obtained is given in figure 3.113. The support material underwent the reduction procedure (not shown in figure) and was then flushed with N<sub>2</sub> as labelled in figure. The figure shows the steady baseline until N<sub>2</sub> is switched to CH<sub>4</sub>. At this stage, the AGC decreases as expected according to section 3.4.1.4. The AGC remains constant throughout the duration of the reaction (110 minutes) showing that no catalysis is occurring due to the support.

*Figure 3.113. Change in mass of Al<sub>2</sub>O<sub>3</sub> support during CH<sub>4</sub> cracking reaction.*



### 3.4.6 CH<sub>4</sub> Cracking Reaction over Rh/Al<sub>2</sub>O<sub>3</sub>

The change in mass of the AGC for the reaction over Rh is given in figure 3.114. The catalyst was reduced (not shown in figure) then N<sub>2</sub> was flushed through. When the gas flow was switched to CH<sub>4</sub>, immediately, a peak appeared in the AGC as a result of gas switching. The AGC then decreased, as expected to the CH<sub>4</sub> baseline but immediately increased as carbon was deposited on the catalyst. CH<sub>4</sub> was passed over for one hour and within this time the AGC flattened out to show that a steady state had been reached. N<sub>2</sub> was then flushed through so at this stage the AGC

increased. When the flow was switched to  $\text{CO}_2$ , the AGC increased due to gas density increase but maintained a steady state. This shows that no carbon oxidation had taken place. Further  $\text{N}_2$  was flushed through to remove  $\text{CO}_2$  before more  $\text{CH}_4$  was introduced. When  $\text{CH}_4$  was flushing the AGC baseline did not increase therefore no more catalysis was occurring. The mass of carbon deposited during the reaction was extracted from the TEOM output by the method shown in figure 3.111. The carbon deposition results have been tabulated in table 3.90.

**Figure 3.114. Change in mass of  $\text{Rh}/\text{Al}_2\text{O}_3$  during  $\text{CH}_4$  cracking reaction.**

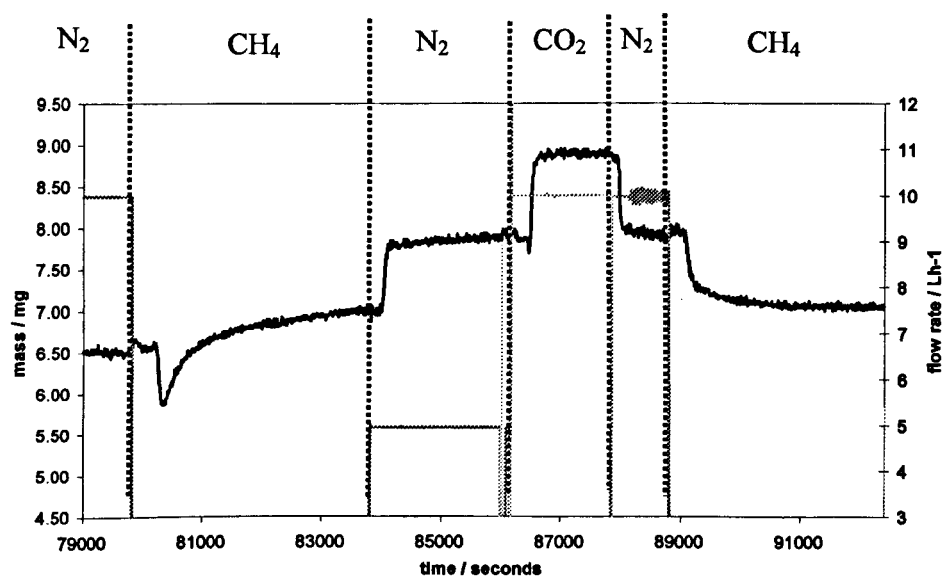


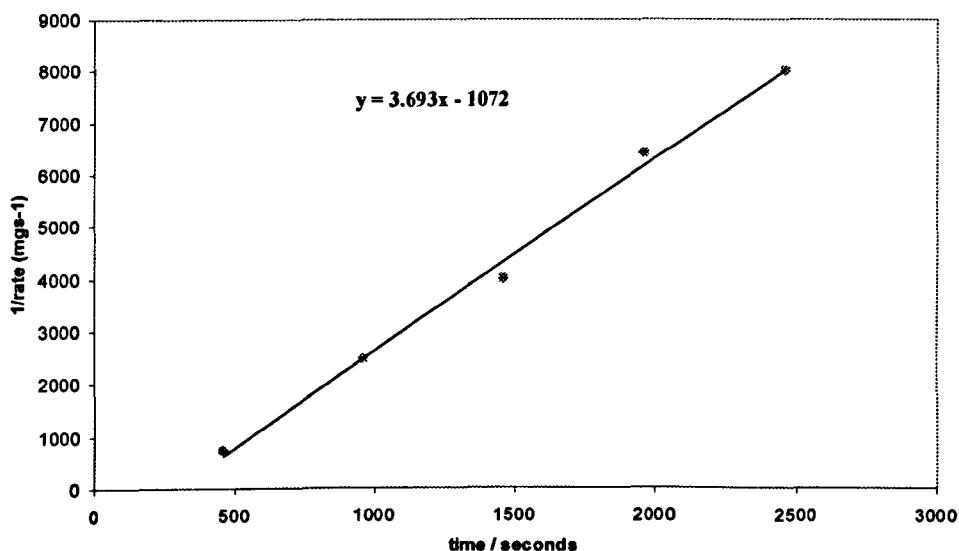
**Table 3.90. Mass of carbon deposited during  $\text{CH}_4$  cracking over  $\text{Rh}/\text{Al}_2\text{O}_3$**

Catalyst	Mass of deposited C after 1 hour / mg	Steady State Mass of deposited C / mg
$\text{Rh}/\text{Al}_2\text{O}_3$	1.21	1.21

### 3.4.6.1 Rh/Al<sub>2</sub>O<sub>3</sub> Catalyst Deactivation

By application of the second order deactivation equation, a straight line graph for the deactivation of Pt/Al<sub>2</sub>O<sub>3</sub> during the first 2500 seconds of the CH<sub>4</sub> cracking reaction is given in figure 3.115. After this time, the rate of carbon deposition was constant and the equation could not be applied.

**Figure 3.115. Plot of 1/rate vs. time for Rh/Al<sub>2</sub>O<sub>3</sub>**



Catalyst	$\alpha$
Rh/Al <sub>2</sub> O <sub>3</sub>	3.69

### 3.4.7 CH<sub>4</sub> Cracking over Pt/Al<sub>2</sub>O<sub>3</sub>

The results obtained from the CH<sub>4</sub> cracking reaction over Pt/Al<sub>2</sub>O<sub>3</sub> are given in figure 3.116. The catalyst was reduced (not shown in figure) and flushed with N<sub>2</sub>. When the baseline was steady, the flow was switched to CH<sub>4</sub>. The AGC decreased due to gas density change but immediately increased as carbon was deposited on the catalyst. After approximately two hours on stream, the AGC appeared to reach steady state. N<sub>2</sub> was flushed over the catalyst before the feed was switched to CO<sub>2</sub>. As was seen with the other catalysts, there is no loss of mass when CO<sub>2</sub> is passed

over. Unlike the other three catalysts, when  $\text{CH}_4$  was passed over for a second time, the AGC increased as further carbon was deposited. Carbon formation results were calculated from the TEOM data and are given in table 3.91.

**Figure 3.116.** Change in mass of  $\text{Pt}/\text{Al}_2\text{O}_3$  during  $\text{CH}_4$  cracking reaction.

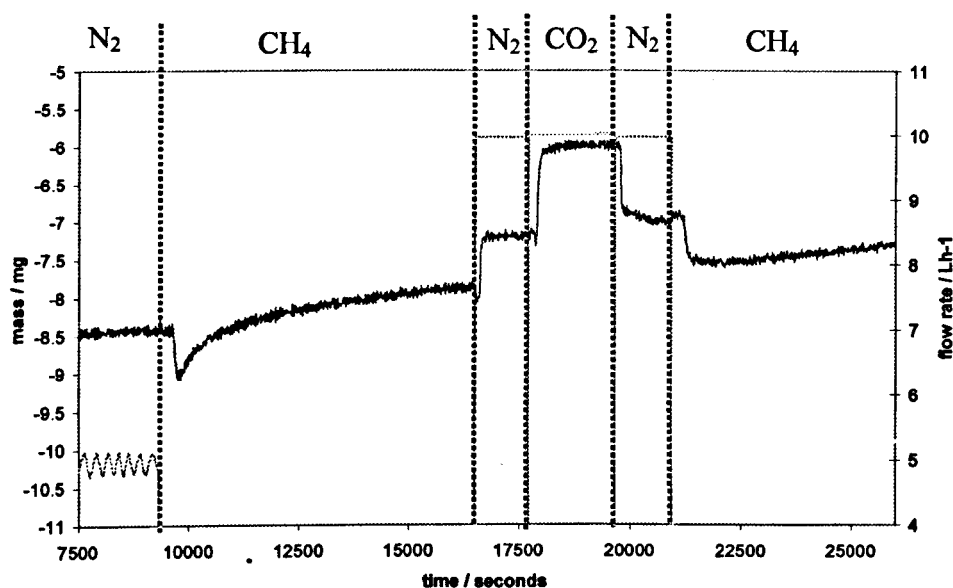


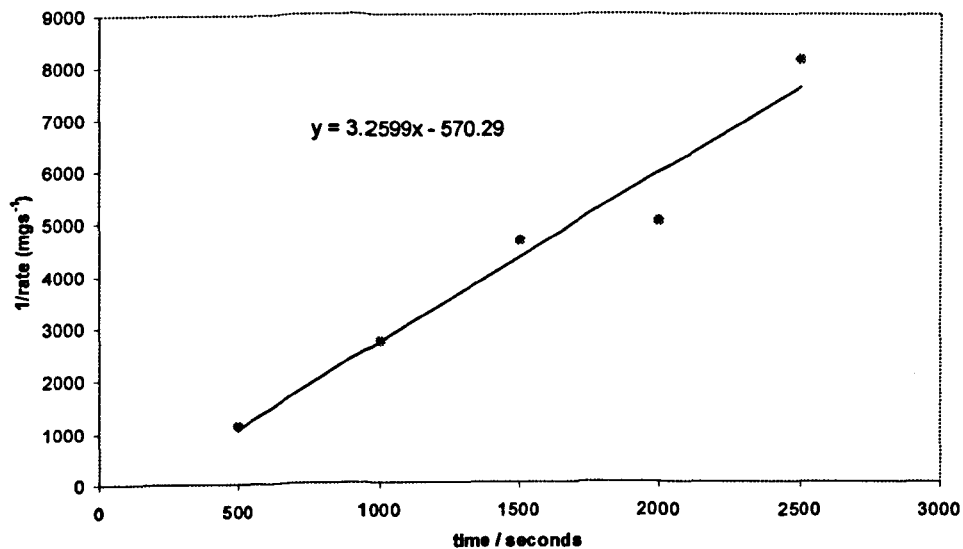
**Table 3.91.** Mass of carbon deposited during  $\text{CH}_4$  cracking over  $\text{Pt}/\text{Al}_2\text{O}_3$

Catalyst	Mass of deposited C after 1 hour / mg	Steady State Mass of deposited C / mg
$\text{Pt}/\text{Al}_2\text{O}_3$	0.97	-

### 3.4.7.1 Pt/Al<sub>2</sub>O<sub>3</sub> Catalyst Deactivation

The straight line obtained from the deactivation over the first 50 minutes of CH<sub>4</sub> cracking reaction over Pt/Al<sub>2</sub>O<sub>3</sub> is given in figure 3.117.

**Figure 3.117. Plot of 1/rate vs. time for Pt/Al<sub>2</sub>O<sub>3</sub>**



Catalyst	$\alpha$
Pt/Al <sub>2</sub> O <sub>3</sub>	3.26

### 3.4.8 Comparison of Results

Table 3.92 is a comparison of the mass of carbon formed on each catalyst after 50 minutes of CH<sub>4</sub> cracking reaction and also the steady state mass of carbon where applicable. The final column shows the deactivation parameters calculated from the gradient of the deactivation plot.

*Table 3.92. Mass of deposited carbon and deactivation rate parameter,  $\alpha$*

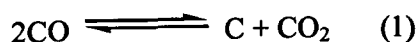
Catalyst	Mass After 1 Hour / mg	Steady State Mass / mg	$\alpha$
Rh/La-ZrO <sub>2</sub>	0.62	0.69	8.03
Pt/La-ZrO <sub>2</sub>	0.29	0.58	6.57
Rh/Al <sub>2</sub> O <sub>3</sub>	1.21	1.21	3.69
Pt/Al <sub>2</sub> O <sub>3</sub>	0.97	-	3.26

## 4 Discussion

### 4.1 Al<sub>2</sub>O<sub>3</sub> Catalysts

#### 4.1.1 CO Pulses

When CO was pulsed over the Al<sub>2</sub>O<sub>3</sub> support material only, there were small peaks of CO<sub>2</sub> produced, as expected from the Boudouard reaction:



Therefore, the support material was active. Five CO pulses were then passed over each of the catalysts (Rh, Pt, Ru and Ni supported on Al<sub>2</sub>O<sub>3</sub>). Tables 3.23-3.27 show, respectively, the number of moles of CO<sub>2</sub> produced per pulse over the support and the four catalysts. The total number of moles produced over five pulses can be calculated and compared for each substrate. Table 4.1 shows this comparison.

**Table 4.1. Total moles of CO<sub>2</sub> produced over Al<sub>2</sub>O<sub>3</sub> support and catalysts.**

Substrate	Total $\mu\text{mol}$ of CO <sub>2</sub>
Al <sub>2</sub> O <sub>3</sub>	120
Rh/Al <sub>2</sub> O <sub>3</sub>	200
Pt/Al <sub>2</sub> O <sub>3</sub>	220
Ru/Al <sub>2</sub> O <sub>3</sub>	310
Ni/Al <sub>2</sub> O <sub>3</sub>	520

Each catalyst produced more CO<sub>2</sub> than the Al<sub>2</sub>O<sub>3</sub> support material alone; therefore, not all activity was due to the support but was clearly influenced by the presence of the metal. As expected from the literature<sup>15, 25, 26</sup>, Ni was the most active catalyst on exposure to CO and as a result produced the greatest amount of CO<sub>2</sub>.

Tables 3.24-3.27 give the value of CO<sub>(moles consumed)</sub>/CO<sub>2(moles out)</sub> for each of the catalysts. According to the Boudouard reaction stoichiometry, this value is expected

to be equal to 2 after each pulse; however, the experimentally determined value from pulse 1 was approximately equal to 1 for each catalyst. Therefore, it was assumed that the support material was involved in the reaction. It has been previously reported in the literature<sup>75, 84, 87</sup> that  $\text{Al}_2\text{O}_3$  has a reservoir of OH/ $\text{H}_2\text{O}$  groups on its surface which can spillover onto the active metal phase. It is generally agreed that these groups can oxidise the carbided metal as was observed during  $\text{CO}_2$  reforming of  $\text{CH}_4$ <sup>84</sup>. Since the experimentally determined ratio was 1 rather than 2, there was either more  $\text{CO}_2$  being produced or more CO being consumed than expected. Schuurmaan et al.<sup>87</sup> noted that  $\text{Al}_2\text{O}_3$  catalysts had enhanced activity. They proposed the following equilibrium which probably took place on the acid/base groups of their  $\text{Al}_2\text{O}_3$ :

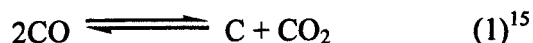


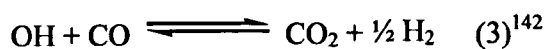
It is possible that reaction (2) took place over the  $\text{Al}_2\text{O}_3$  catalysts in the present study to give  $\text{CO}_{(\text{moles consumed})} / \text{CO}_{2(\text{moles out})}$  equal to 1.

Jackson et al.<sup>142</sup> pulsed CO over a Pt/ $\text{Al}_2\text{O}_3$  catalyst at 573 K. They found, on adsorption of CO, that  $\text{H}_2$  desorbed coincidentally with  $\text{CO}_2$ . To achieve coincident desorption, they reported that  $\text{H}_2$  must have been involved in the process at the surface. The desorbed  $\text{H}_2$  was proposed to come from a reaction of the type:



Again,  $\text{H}_2$  was not one of the masses followed on the mass spectrometer in the present study however, it was followed during the isotope pulses. Figures 3.29-3.33 clearly show the production of  $\text{H}_2$  after a CO/ $\text{CO}_2$  pulse over the  $\text{Al}_2\text{O}_3$  support material and catalysts. Therefore, there were a series of possible equilibria taking place over the  $\text{Al}_2\text{O}_3$  supported catalysts, specifically from the metal, the support and from OH groups:

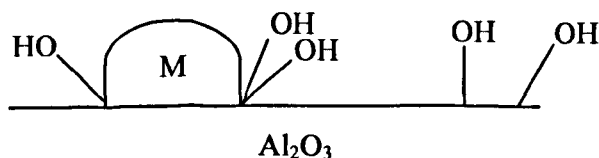




It can be seen from tables 3.24-3.27 that the percentage CO conversion gradually decreased with pulse number over all of the catalysts except for Pt. Schuurman et al.<sup>87</sup> stated that consumed hydroxyl groups are replenished with water formed via the water gas shift reaction during dry reforming or from steam during steam reforming. In the present study, there is no steam or if any is formed during side reactions it is small in comparison to that formed during reforming therefore, the hydroxyls are not being replenished which, besides coverage of the active metal with carbon, could have been responsible for a decrease in percentage CO conversion. Jackson et al.<sup>142</sup> reported that the supply of OH was finite as their CO pulse results showed a decrease in H<sub>2</sub> desorption with increasing pulse number.

It may not be expected that the OH groups could be used up in the time frame of the reaction, however a 'halo-effect' is proposed whereby, the OH groups immediately adjacent to the metal are used up and are not replenished in time. In agreement with the idea of a halo-effect, Seshan et al.<sup>109</sup> claimed that the metal catalysed CO<sub>2</sub> reforming of CH<sub>4</sub> took place on the metal support perimeter. Figure 4.1 illustrates a halo-effect.

**Figure 4.1. Halo-effect occurring on Al<sub>2</sub>O<sub>3</sub> supported catalysts**



Since the percentage CO conversion decreased with pulse number, it was no surprise that the amount of CO<sub>2</sub> detected also decreased with pulse number for each catalyst (stayed constant for the support material only). Again, a decrease in CO<sub>2</sub> production meant either OH groups were being consumed or the active metal was being fouled with carbon. It is proposed that both of these effects were taking place. As can be

seen from tables 3.24 to 3.27, the Pt and Ni catalysts consumed more CO than Rh and Ru, therefore, it was likely that accessible OH groups on the Pt and Ni catalysts were used up relatively fast in comparison to those on the Rh and Ru catalysts. A clue to this proposal was obtained from the  $\text{CO}_{(\text{moles consumed})}/\text{CO}_{2(\text{moles out})}$  ratio. Table 3.25 and 3.27 show, for Pt and Ni respectively, that the ratio had a value approximately equal to 1 after pulse 1 proving that the moles of CO consumed equalled the moles of  $\text{CO}_2$  produced. With increasing pulse number, the ratio approached a value of 2 showing that two moles of CO were consumed for every mole of  $\text{CO}_2$  produced. Therefore, OH groups were being used up quickly and residual activity took place via the Boudouard reaction to give a ratio of 2. Pt had a greater percentage metal dispersion than Rh and Ru and the greatest consumption of CO which did not appear to decrease within five pulses in support of the theory by Iglesia et al.<sup>59, 60, 61</sup>. Ni, however, had a much higher consumption of CO than Pt. This excess over Pt is not a dispersion effect but can be explained with reference to the literature: Ni favourably consumes carbon-forming CO due to Ni's affinity for whisker carbon formation. Ni can consume more CO relative to the noble metals as it will not deactivate as quickly since the carbon formed diffuses through the bulk Ni leaving the surface free to adsorb  $\text{CO}$ <sup>15, 25, 26</sup>. Out of the four catalysts, Rh and Ru had the lowest % CO conversions which decreased with pulse number. It is proposed, for both of these catalysts, that as a lesser amount of CO was consumed, not all of the OH groups were used up in the time frame of the reaction unlike those on Ni and Pt. Ru consumed so little CO that the change in pulses 3-5 could not be detected by the mass spectrometer. This theory is also supported by the  $\text{CO}_{(\text{moles consumed})}/\text{CO}_{2(\text{moles out})}$  ratios. Table 3.4 and 3.6 show for Rh and Ru respectively that the ratio was less than or approximately equal to 1 after each pulse of CO and did not tend towards 2 with increasing pulse number suggesting that the OH groups had not been consumed and were still contributing to the reactivity.

The only result which seemed to be out of place at this stage was the fact that Ru seemed to desorb more  $\text{CO}_2$  than Pt despite consuming less CO as seen in table 4.1. However, since relatively little activity was due to OH groups on Pt, more CO was used up in the Boudouard reaction (1). This reaction produces half a mole of  $\text{CO}_2$  for every mole of CO used. The reactivity of Ru, on the other hand, relied more on the

presence of OH groups than Pt did and hence, reaction (3) was prominent. This reaction produces one mole of CO<sub>2</sub> for every mole of CO used. This may also be an indication that there were more OH groups available on Ru compared to Pt.

In summary, it was shown that the Al<sub>2</sub>O<sub>3</sub> support material was involved in the high temperature, low pressure reaction of CO over Rh, Pt, Ru and Ni catalysts and this involvement was attributed to OH-groups on the support-metal perimeter. A series of reactions including CO and OH were proposed. Since Pt consumed more CO but produced less CO<sub>2</sub> than Ru, it was suggested that OH groups were not as accessible for reaction on Pt and those available were consequently consumed quicker leaving the latter CO pulses to react via the Boudouard reaction only. There was evidence for the Rh and Ru catalysts, however, that OH-groups were involved in all five pulses. Pt consumed the greatest amount of CO during five pulses which coincided with the order of increasing metal dispersion for the noble metals (Pt greatest) and backed the theory by Iglesia et al.<sup>59, 60, 61</sup> that activity increased with increasing metal dispersion. The vast CO consumption by Ni could not be compared due to its affinity for whisker carbon formation.

#### 4.1.2 High Pressure CO

In an attempt to replicate the true conditions of steam reforming, a continuous flow of CO at 873K and 20bar pressure was passed over the Al<sub>2</sub>O<sub>3</sub> support material. It can be seen from figure 3.35 that a significant but small peak of CO<sub>2</sub> was obtained which gradually decreased towards the baseline with time on stream, hence the support material had slight activity. The mass of carbon produced on the support was calculated. Figures 3.36 to 3.38 show the mass spectra obtained from CO over each of the catalysts and as was observed from the CO pulses, the reaction was enhanced by the presence of the metal. The amount of carbon produced from each catalyst was also calculated after a standard comparison time of 30 minutes and tabulated in table 3.76 (very little activity after this time). It can be observed from the figures and the table that Rh and Pt produced similar masses of carbon after 30 minutes on stream. The pulses showed that percentage metal dispersion affected initial catalyst activity but, the high pressure study shows that total mass of carbon produced does not

coincide with dispersion. The catalysts' activity was unlikely to have been an effect of OH groups at such a high pressure of CO. Seshan et al.<sup>109</sup> however, showed that carbon is deposited on the metal and on the support (activated by the metal) therefore, since the surface area of the support is large in the present study and given that the metal loading is 0.2% w/w it is not unusual that both catalysts yielded similar amounts CO<sub>2</sub> over the course of the reaction. According to the first order deactivation plot, the order of deactivation is:

Pt > Rh

Therefore, Pt initially, had a higher activity than Rh (from pulses), but had a faster rate of deactivation than Rh (from high pressure study).

Ru on the other hand produced much less CO<sub>2</sub> over the course of the reaction than Pt and Rh. Seshan et al.<sup>109</sup> reported that carbon deposition on the support alone is small but enhanced by the presence of the metal as the products are able to recombine and desorb from the metal but not the support. In the present study, it was possible that the reaction over Ru/Al<sub>2</sub>O<sub>3</sub> was limited due to recombination and desorption of CO<sub>2</sub>. Although, they are in the same group of the periodic table and may be expected to show the same behaviour, many authors have reported a range of activities regarding the reforming of CH<sub>4</sub> and carbon formation over noble metals<sup>13, 55, 56, 57, 64, 66</sup>.

Armor et al.<sup>43</sup> studied the effect of pressure on dry reforming of CH<sub>4</sub> over a Ni/Al<sub>2</sub>O<sub>3</sub> catalyst and found that under pressure, the catalyst was far more efficient at carbon formation. Specifically, they found that five times the amount of carbon produced at atmospheric pressure was produced at high pressure. For this reason, no comparison to Ni was possible under such extreme conditions in the absence of steam. This reaction was tried but resulted in the instant blockage of and long-term damage to the reactor tube.

Although Seshan et al.<sup>109</sup> report that carbon is formed on the metal and the support, they claim that deactivation is associated with the metal. Two deactivation equations were applied to the present system to determine the order of reaction and the

deactivation rate constant. The first order plots for Rh and Ru were straight lines suggesting they were in fact first order reactions however, the plot for Pt was quite ambiguous. To confirm the first order behaviour of Rh and Ru and to help determine that of Pt, a second order equation was applied to the system. It can be seen from figures 3.77 to 3.79 that the lines obtained were most definitely curves confirming that Rh and Ru are not second order. For Pt, it is proposed that the CO reaction is also first order. Discrepancies in the determination exist due to a significant level of noise on the raw data from which the rates of reaction were calculated.

It can be concluded from the reaction of CO over the  $\text{Al}_2\text{O}_3$  supported noble metals at high pressure and temperature, that only the initial activity is affected by the metal dispersion, the total amount of  $\text{CO}_2$  desorbed and hence, of carbon deposited was related to the surface area of the catalyst. Ru was the exception and desorbed a lesser amount of  $\text{CO}_2$  in comparison to the other catalysts which was attributed to a prevention of the recombination and desorption of  $\text{CO}_2$  from the surface of Ru. It was seen from the pulse study that Pt had a greater initial activity but observed in the high pressure study that it had a larger rate of deactivation than Rh. The deactivation of the three noble metals appeared to follow first order kinetics although further work will be required.

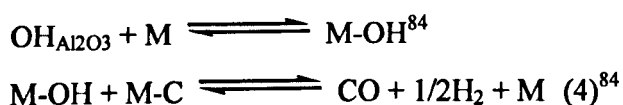
### 4.1.3 $\text{CH}_4$ Pulses

Five pulses of  $\text{CH}_4$  were passed over the  $\text{Al}_2\text{O}_3$  support material and the spectra obtained (figure 3.17) show that no  $\text{H}_2$  was produced. The percentage  $\text{CH}_4$  conversions were also calculated and were found to be less than 1% for each pulse confirming that no reaction had taken place. Therefore, any reaction that did take place over the catalysts was influenced by the active metal phase. Figures 3.18 to 3.21 show the spectra obtained from the five  $\text{CH}_4$  pulses over Rh, Pt, Ru and Ni respectively.

The percentage  $\text{CH}_4$  conversions for Rh and Pt were very similar and both decreased gradually with pulse number however, Pt yielded much more  $\text{H}_2$  than Rh. Ru showed the same trend but had lower percentage  $\text{CH}_4$  conversion. Although the percentage

CH<sub>4</sub> conversion after pulse 1 was greater over Rh than Ru, more H<sub>2</sub> was desorbed from the Ru catalyst. Percentage CH<sub>4</sub> conversions did not correlate to percentage metal dispersions as was observed for the CO pulses. Ni had almost 100% CH<sub>4</sub> conversion and showed no sign of deactivating even after the fifth pulse. It is well established that carbon forming side reactions take place readily over Ni and that carbon produced is favourably dissolved into the bulk Ni to form whisker carbon without deactivation of the catalyst<sup>15, 25, 26, 27</sup>. Only when the whiskers hit the catalyst pore walls, does carbon dissolution cease resulting in deactivation of the catalyst<sup>25</sup>. This deactivation of Ni clearly did not take place within the timeframe of the pulse reaction.

Table 3.32 compares H<sub>2</sub>(moles out)/CH<sub>4</sub>(moles consumed) ratios for each catalyst. From the stoichiometry of the CH<sub>4</sub> cracking reaction, it is expected that the ratio after each pulse should be equal to 2. It can be seen from table 3.32 that Rh produced a ratio of 2 in accordance with the CH<sub>4</sub> cracking stoichiometry and maintained it for the five pulses. After pulse 1, Pt, Ru and Ni all had a ratio approximately equal to 3, suggesting that an excess of H<sub>2</sub> was being produced. This can be explained with the occurrence of surface hydroxyls on Al<sub>2</sub>O<sub>3</sub> as has been discussed for the CO pulsed reaction. The hydroxyls can spillover from support to metal and react fast with the carbided metal to produce H<sub>2</sub> in the following equilibria:



CO was not followed on the mass spectrometer to confirm the occurrence of these reactions however, evidence for the presence of H<sub>2</sub> was observed in the isotope pulse study. Their well-known interaction during reactions involving Al<sub>2</sub>O<sub>3</sub> supported catalysts has been well documented<sup>84, 85, 86, 87, 142</sup>. It appeared from the present results that OH groups from the Al<sub>2</sub>O<sub>3</sub> support material were not spilling over onto the Rh metal. Erdohelyi et al. studied CO<sub>2</sub> reforming of CH<sub>4</sub> and found that the rate of reaction on Pd<sup>143</sup> was sensitive to the nature of the support, while, over Rh<sup>70</sup> there was no significant support effect. Reaction from the support was observed when CO was pulses over Rh/Al<sub>2</sub>O<sub>3</sub> in the present work however, the support reacted with or

without the presence of the metal. When CH<sub>4</sub> was pulsed over, it was apparent that reaction of the surface OH-groups was dependent not only on the presence of the metal but also on the nature of the metal.

Rh underwent a different reaction to Pt and Ru since surface OH-groups were not involved which may explain why there was no correlation between percentage CH<sub>4</sub> conversion and percentage metal dispersion as observed for CO pulses.

A further observation was made from the H<sub>2</sub> (moles out)/CH<sub>4</sub> (moles consumed) ratios: as pulse number increased, the ratio tended towards 2 for Pt, Ru and Ni catalysts suggesting that an excess of H<sub>2</sub> was no longer being produced. A trend towards the expected stoichiometry was also observed for Ni and Pt during the CO pulsed reaction over Al<sub>2</sub>O<sub>3</sub> and was explained as due to the usage of hydroxyl groups with no replenishment from H<sub>2</sub>O. A trend towards correct stoichiometry was not observed for Rh or Ru during the CO pulses and this was explained due to low CO consumption for these catalysts hence, the OH groups were not used up within the five pulses. It was noticed from all of the pulse reactions over Al<sub>2</sub>O<sub>3</sub> catalysts that the CH<sub>4</sub> conversions were much greater than the CO conversions therefore the available OH-groups were used up within five pulses and a trend towards the expected stoichiometry was observed for Pt, Ru and Ni catalysts.

Under the conditions of low pressure and high temperature, all four catalysts were far more active during CH<sub>4</sub> pulses than CO pulses. Pt, Ru and Ni all produced an excess of H<sub>2</sub> which was attributed to the reaction between CH<sub>4</sub> and surface OH-groups. The relationship previously observed between catalyst activity and percentage metal dispersion was not apparent during CH<sub>4</sub> pulses, however, there was no reaction between CH<sub>4</sub> and surface OH-groups on Rh therefore, it was not a fair correlation. The anomalous reaction of Rh and the fact that the Al<sub>2</sub>O<sub>3</sub> support did not react in the absence of metal lead to the conclusion that the reaction of surface OH-groups was dependent on the nature of the metal.

#### 4.1.4 High Pressure CH<sub>4</sub> (TEOM)

The results from continuous flow, high-pressure and temperature CH<sub>4</sub> reactions were obtained from the TEOM. Initially, CH<sub>4</sub> flowed over the Al<sub>2</sub>O<sub>3</sub> material only and the results showed that no significant carbon was deposited. This reaction also showed that no carbon was deposited on the metal cap which is a frequent problem in TEOM reactions. It can be seen for each catalyst that the mass of carbon obtained after one hour and at steady state was significantly less than that obtained after thirty minutes of exposure to high pressure CO. This result seemed unusual since at low pressure, CH<sub>4</sub> was more reactive than CO. Shamsi et al.<sup>47</sup> questioned whether the source of carbon formation at elevated pressure was the same as that at low pressure during dry reforming of CH<sub>4</sub>. They found, from thermodynamic calculations that the equilibrium amount of carbon from the CH<sub>4</sub> cracking reaction decreased with increasing pressure while carbon from the Boudouard reaction increased. These results were consistent over a range of their own and with the present work's catalysts. Due to the far more subtle reaction of CH<sub>4</sub> at elevated pressure, this reaction could not be carried out on the high-pressure rig in Glasgow as very noisy and inaccurate mass spectrometer data were obtained. The TEOM was more sensitive and better for detecting smaller changes. Unfortunately, the TEOM could be too sensitive and when CO was flowed through at 20bar and 873K, the result was a pressure drop across the catalyst bed and the eventual costly breakage of the glass taper.

CH<sub>4</sub> was passed over Rh/Al<sub>2</sub>O<sub>3</sub> and Pt/Al<sub>2</sub>O<sub>3</sub> at 20 bar pressure and 873K as shown in figures 3.114 and 3.116 respectively. The identification of significant mass changes was discussed in section 3 and it was shown that carbon was deposited on the catalyst immediately as the gas flow was switched to CH<sub>4</sub>. By observation of the AGC plot, it was seen how the rate of deposition was initially fast but began to slow with time on stream until a steady state was reached after approximately one hour for Rh. The mass of carbon deposited on the Rh catalyst after one hour was greater than the mass of carbon on the Pt catalyst after one hour and it appeared (see later) that Pt did not reach a steady state within the timeframe of the reaction. The high-pressure CO reaction over Al<sub>2</sub>O<sub>3</sub> catalysts went to completion after approximately thirty minutes. In contrast, the high-pressure CH<sub>4</sub> reaction took one hour or more to deposit a steady

state mass of carbon. It was clear that there was a lesser amount of carbon deposited and the rate of deposition was slower at high pressure in comparison to CO.

A second order plot was made for CH<sub>4</sub> cracking over Rh and Pt and both produced straight line to confirm the second order nature of the reaction. The initial rate of deactivation was greater over Pt compared to Rh, a trend that was also observed during the Boudouard reaction.

The latter stage of the TEOM reaction involved the passage of CO<sub>2</sub> over the catalyst in an attempt to oxidise any deposited carbon and restore the activity of the catalyst. If carbon on the catalyst was oxidised, a decrease of the AGC level would have been observed while CO<sub>2</sub> was flushing. The AGC was, however, constant suggesting no carbon had been removed. CH<sub>4</sub> was then flowed over again in order to clarify that no activity had been restored. For Rh, the AGC did not increase any further to show that no more reaction was taking place. The AGC of Pt did increase but since there was no loss in mass while CO<sub>2</sub> was flushing, it is proposed that Pt had not fully deactivated in the first hour of the reaction and therefore began to lay down more carbon as CH<sub>4</sub> was flushed for the second time. Nagaoka et al.<sup>98</sup> described the mechanism of CO<sub>2</sub> reforming of CH<sub>4</sub> over a Pt/ZrO<sub>2</sub> catalyst: decomposition of CH<sub>4</sub> occurred on the Pt surface which produced H<sub>2</sub> (desorbed into gas phase) and CH<sub>x</sub> species (CH<sub>x</sub>, 0 ≤ x ≤ 3). CO<sub>2</sub>, which was chemisorbed on the support in the vicinity of the Pt particles, then oxidised the CH<sub>x</sub> species. It is clear from this mechanism that CO<sub>2</sub> must be present in the reaction simultaneously with CH<sub>4</sub> in order to oxidise deposited carbon. High pressure reactions with CO and CO<sub>2</sub> have been carried out (section 4.4) and indeed do serve to avoid carbon formation over a certain CO:CO<sub>2</sub> ratio.

Although no carbon was removed in the latter half of the TEOM study, information was obtained on the type of carbon deposited. In the literature, McCarty et al.<sup>38</sup> and Jackson et al.<sup>39</sup> described types of carbon which formed on Ni surfaces on exposure to CO and hydrocarbons as detailed in section 1.2.3.4. Jackson et al.<sup>39</sup> stated that neither amorphous carbon (type 1), encapsulating polymer carbon (type 3) nor unreactive carbon (type 4) were oxidised by CO<sub>2</sub> or steam. Therefore, it is likely that

the carbon formed in the present study with  $\text{CH}_4$  is encapsulating polymer (type 3) or it is possible that it has aged into the unreactive form (type 4).

In summary, more carbon was formed from CO at high pressure than  $\text{CH}_4$  however, more carbon was formed from  $\text{CH}_4$  at low pressure compared to CO. This observation has been observed previously and explained through thermodynamic calculations. Rh and Pt reacted immediately on exposure to  $\text{CH}_4$  however Rh reacted and reached a steady state faster than Pt. Both catalysts reacted slower than they did on exposure to CO. The reaction of  $\text{CH}_4$  followed first order kinetics over both catalysts and as expected Rh had a greater rate of deactivation in comparison to Pt. When  $\text{CO}_2$  was passed over the catalysts post-reaction, no carbon was removed. From this, information on the type and the behaviour of the deposited carbon was obtained. It was also concluded that  $\text{CO}_2$  must be present simultaneously with  $\text{CH}_4$  in order to hinder carbon formation.

## 4.2 La-ZrO<sub>2</sub> Catalysts

### 4.2.1 CO Pulses

Five pulses of CO were passed over the La-ZrO<sub>2</sub> support material in order to determine its relative activity in comparison to the catalysts. It can be seen from figure 3.1 that small peaks of  $\text{CO}_2$  were obtained; hence, the support material is active. The pulses of CO were subsequently passed over each of the catalysts as shown in figures 3.2 to 3.4. The number of moles of  $\text{CO}_2$  produced from the support and the noble metal catalysts after each pulse were calculated and found to be equal to each other. Therefore, the presence of the active metal appeared to have no effect on the reaction.

The present study shows how La-ZrO<sub>2</sub> catalysts did not produce more  $\text{CO}_2$  than the support material alone while the Al<sub>2</sub>O<sub>3</sub> catalysts did. There are many publications in support of the observation that ZrO<sub>2</sub> catalysts are more carbon resistant than the equivalent Al<sub>2</sub>O<sub>3</sub> supported metals although many different reasons have been presented. Increasing activity with increasing metal dispersion was a possible reason

<sup>59, 60, 61</sup> but can be overruled since the La-ZrO<sub>2</sub> catalysts were more highly dispersed than the Al<sub>2</sub>O<sub>3</sub> catalysts. Results presented by Souza et al.<sup>96, 101</sup>, regarding the high stability of Pt/ZrO<sub>2</sub> and Pt/CeO<sub>2</sub> catalysts, show how strong Pt-Zr<sup>n+</sup>/Pt-Ce<sup>n+</sup> interactions are present and act to modify the CO adsorption capability on Pt. The result is a decrease in the Pt-CO bond strength and hence, an inhibition of the Boudouard reaction. Souza et al.<sup>96</sup> also claim that ZrO<sub>x</sub> species cover the Pt surface and decrease the Pt ensemble size. This effect has been well documented in the literature due to the observation that reducible oxides (ZrO<sub>2</sub>, TiO<sub>2</sub>, Nb<sub>2</sub>O<sub>5</sub> and V<sub>2</sub>O<sub>3</sub>) developed strange properties after reduction at moderately high temperatures<sup>144, 145, 146</sup>. The capacity to adsorb CO or H<sub>2</sub> was greatly diminished or in some cases completely suppressed. Much research into these so called 'strong metal support interactions' (SMSI) has been carried out with regard to TiO<sub>2</sub> supported catalysts<sup>147, 148, 149</sup>. It is claimed that SMSI occur due to migration of TiO<sub>x</sub> species onto the surface of the metal during the high temperature reduction. Theoretical calculations have shown that CO decomposition requires an ensemble size of four or five metal atoms<sup>103</sup> hence, the presence of a TiO<sub>x</sub> or ZrO<sub>x</sub> species decorating the metal surface can hamper CO dissociation. The present study shows how the support, alone, is active for CO decomposition however, from these results, it seemed like there was no further activity on addition of the metal and the theory of ensemble control seemed plausible. Ni, however, was observed to react during CO pulses but it will be discussed later how the ZrO<sub>x</sub> species is thought to suppress chemisorption of gaseous species not completely prevent it. An explanation of the apparent lack of CO chemisorption of the noble metal catalysts was invoked from the isotope study (see section 4.2.2).

Ni produced more CO<sub>2</sub> per pulse than the support material alone and the noble metal catalysts. This result was expected from the literature<sup>12, 15, 25, 26</sup> as it is well known that Ni is more active towards carbon formation than the noble metals. Ni was, however favourably affected by the La-ZrO<sub>2</sub> support as can be seen from the lower percentage CO conversions for Ni/La-ZrO<sub>2</sub> in comparison to Ni/Al<sub>2</sub>O<sub>3</sub>. The difference is proposed to be a ZrO<sub>x</sub> species on the metal surface which perturbs chemisorption of CO.

H<sub>2</sub> was not one of the species followed during the CO pulses however, it was observed in the CO/CO<sub>2</sub> isotope study. H<sub>2</sub> desorption from the support and catalysts, as seen in figures 3.25 to 3.28, invoked the probability of OH groups on La-ZrO<sub>2</sub>. Surface OH groups have been previously reported for ZrO<sub>2</sub> catalysts<sup>150</sup> and Al<sub>2</sub>O<sub>3</sub> catalysts of the present study. The following reaction between CO and OH groups originating from the support was proposed to explain the behaviour of the Al<sub>2</sub>O<sub>3</sub> catalysts:



Very little or no H<sub>2</sub> was detected from La-ZrO<sub>2</sub> support material during the isotope study however, it will be seen later how the La-ZrO<sub>2</sub> support has the ability to adsorb H<sub>2</sub> in the absence of an active metal hence, all H<sub>2</sub> formed from CO pulses over the La-ZrO<sub>2</sub> support was adsorbed. H<sub>2</sub> was, however, detected from pulses of CO/CO<sub>2</sub> over each of the La-ZrO<sub>2</sub> supported catalysts. Seshan et al.<sup>98, 109</sup> studied Pt/Al<sub>2</sub>O<sub>3</sub> under CH<sub>4</sub>/CO<sub>2</sub> reforming conditions and found very little activity on the bare support. On addition of the metal, the activity was greatly increased. They claimed that the reaction could take place over the support due to Lewis acid sites but was limited by the recombination and desorption of H<sub>2</sub>. On addition of Pt to the support, recombination and desorption of H<sub>2</sub> took place on its surface. In the present work, it is proposed that the La-ZrO<sub>2</sub> support alone could not desorb much H<sub>2</sub> but was enhanced on addition of the metal.

Therefore from low pressure, high temperature pulses of CO over the La-ZrO<sub>2</sub> supported catalysts, it can be concluded that there were support effects acting to hinder chemisorption of CO onto the metal. The effect known as SMSI was either a M-Zr<sup>n+</sup>, which decreased the Pt-CO bond strength or a decoration of the surface with ZrO<sub>x</sub> species, which served to decrease CO chemisorption by affecting the metal ensemble size. The chemisorption of CO was not completely hindered as proven by Ni/La-ZrO<sub>2</sub> but the activity of the Ni/La-ZrO<sub>2</sub> was clearly less than that for Ni/Al<sub>2</sub>O<sub>3</sub> to reinforce the idea that the La-ZrO<sub>2</sub> support is having an effect. There was evidence from the CO/CO<sub>2</sub> isotope study to suggest that surface OH-groups were present and contributing to the activity of the catalysts.

#### 4.2.2 Isotope Pulses Over La-ZrO<sub>2</sub> and Al<sub>2</sub>O<sub>3</sub> Catalysts

Evidence was obtained from the <sup>13</sup>CO/C<sup>18</sup>O<sub>2</sub> pulse study suggesting that a mechanism of oxygen transfer was also taking place over the La-ZrO<sub>2</sub> and Al<sub>2</sub>O<sub>3</sub> catalysts. Mattos et al.<sup>124</sup> noted a considerable difference in stability between Pt/Al<sub>2</sub>O<sub>3</sub> and Pt/Ce-ZrO<sub>2</sub>. The outstanding stability of doped-ZrO<sub>2</sub> has been attributed to its unique oxygen storage capacity as demonstrated in table 4.2.

**Table 4.2. Oxygen uptake at 723K (reproduced from ref.<sup>124</sup>)**

Catalyst	O <sub>2</sub> Uptake (μmol/g <sub>cat</sub> )
Pt/Al <sub>2</sub> O <sub>3</sub>	0
Pt/ZrO <sub>2</sub>	8.5
Pt/Ce <sub>0.75</sub> Zr <sub>0.25</sub> O <sub>2</sub>	625.6

Several studies have shown how cerium oxide has a very strong oxygen exchange capacity<sup>151, 152</sup>. Its ability to do this is due to the storing and release of O<sub>2</sub> via the Ce<sup>4+</sup>/Ce<sup>3+</sup> redox couple. The incorporation of ZrO<sub>2</sub> into the CeO<sub>2</sub> lattice promotes the CeO<sub>2</sub> redox properties. The presence of ZrO<sub>2</sub> increases the number of O-vacancies of the support due to the high oxygen mobility of the solid solution formed. Roh et al.<sup>78</sup> examined the difference between Ni/Ce-ZrO<sub>2</sub>, Ni/Si-ZrO<sub>2</sub> and Ni/La-ZrO<sub>2</sub> catalysts. They concentrated mainly on the Ni/Ce-ZrO<sub>2</sub> as it gave a percentage CH<sub>4</sub> conversion of 97% during steam reforming while the others gave 65 and 75% respectively. Catalyst stability was not the main interest of the paper however their results clearly show that Ni/La-ZrO<sub>2</sub> was as stable as Ni/Ce-ZrO<sub>2</sub> for the duration of the steam reforming and partial oxidation study suggesting that the same effects are taking place over both. Mattos et al.<sup>124</sup> described a mechanism of CH<sub>4</sub> reforming over Pt/Al<sub>2</sub>O<sub>3</sub> and compared it to the mechanism over Pt/Ce-ZrO<sub>2</sub> involving the storage and transfer of O-species from the support (see section 1.4.4.5).

The difference between doped-ZrO<sub>2</sub> and Al<sub>2</sub>O<sub>3</sub> has been discussed in the literature as the stability<sup>124</sup> and the reducibility<sup>116</sup>. ZrO<sub>2</sub> catalysts are described as reducible oxide supports and this means they have the ability to oxidise carbon deposited on them

(themselves being reduced) while  $\text{Al}_2\text{O}_3$  catalysts are apparently irreducible. Although  $\text{ZrO}_2$  is not as reducible as  $\text{CeO}_2$ , it has shown the same stability<sup>78</sup>, therefore it is expected that addition of a dopant ( $\text{La}^{3+}$ ) will promote the  $\text{ZrO}_2$  redox properties and increase the number of O-vacancies and as described above, the catalyst stability.

It was shown in section 3.2.9 that  $^{18}\text{O}$  was lost and an excess of  $^{16}\text{O}$  was obtained after pulsing over the  $\text{La-ZrO}_2/\text{Al}_2\text{O}_3$  supports and each catalyst. Therefore, in contrast to work by Mattos et al.<sup>124</sup> (table 4.2),  $\text{Al}_2\text{O}_3$  catalysts of the present study exchanged oxygen suggesting that a mechanism of O-transfer was possible. A mechanism can be suggested to explain occurrence of certain products obtained from  $^{13}\text{CO}/\text{C}^{18}\text{O}_2$  5:1 pulses over the  $\text{La-ZrO}_2/\text{Al}_2\text{O}_3$  substrates as detailed in scheme 4.1<sup>\*\*</sup>.  $^{13}\text{CO}$  disproportionated into  $^{13}\text{CO}_2$  and  $^{13}\text{C}$  and this process likely took place over the metal in accordance with Mattos et al.<sup>124</sup>.  $^{13}\text{CO}$  also decomposed on the metal into  $^{13}\text{C}$  and O to fill O-vacancies in the support. This was effectively an O-exchange step between  $^{13}\text{CO}$  and the support (since O from the support was transferred to  $^{13}\text{C}$  on the support, near the metal surface, to oxidise it into  $^{13}\text{CO}$ ). The exchange and the disproportionation have been shown as one step in the mechanism.  $\text{C}^{18}\text{O}_2$  dissociated on the support to give  $\text{C}^{18}\text{O}$  and  $^{18}\text{O}$  which replenished the O-vacancies in the support.  $^{18}\text{O}$  was used up by replenishing O-vacancies in the support, hence it was not detected on the mass spectrometer.  $^{13}\text{C}$  was oxidised by O originating from the support hence, there was apparently too much  $^{16}\text{O}$  accounted for from the mass balance. The lack of CO detected from the two support reactions in the present study was evidence that  $\text{C}^{18}\text{O}_2$  decomposition into CO and  $^{18}\text{O}_{(\text{supp})}$  had taken place although immediately reformed  $\text{CO}_2$  as if CO was not stable on the support surface in the absence of a metal. It was therefore possible that  $^{13}\text{CO}_2$  had formed from oxidation of  $^{13}\text{CO}$  with or without the metal. Evidence has also been given in previous sections for the occurrence of OH groups which are involved in the reaction, therefore, it was also possible that  $^{13}\text{CO}_2$  formed from a reaction of OH and CO.

---

<sup>\*\*</sup> Another explanation for the stability of  $\text{La-ZrO}_2$  catalysts compared to  $\text{Al}_2\text{O}_3$  catalysts is a La-complex formation 129-130 (section 1.4.4.6). Formation of the complex relies on the addition of  $\text{CO}_2$ . This complex may affect the reaction once  $\text{CO}_2$  is made but it does not explain the increased carbon evasion of the  $\text{La-ZrO}_2$  catalysts in comparison to the  $\text{Al}_2\text{O}_3$  catalysts during  $\text{CH}_4$  cracking on the TEOM which will be discussed later.



catalyst therefore, due to the mechanism of O-transfer, it appeared that there was no percentage CO conversion from the metal. The amount of CO<sub>2</sub> that was observed from reaction over the catalysts was equivalent to that obtained over the support, hence this CO<sub>2</sub> likely came from reaction of CO with surface OH-groups. Due to its affinity for whisker carbon formation, the rate of CO disproportionation over Ni/La-ZrO<sub>2</sub>, was probably faster than the rate of carbon oxidation by O-transfer and as a result more CO<sub>2</sub> was produced.

Besides the proposal that SMSI effects exist in the La-ZrO<sub>2</sub> catalysts, the literature also suggests that there is enhanced stability of the La-ZrO<sub>2</sub> catalysts over Al<sub>2</sub>O<sub>3</sub> catalysts due to a mechanism of O-transfer. It has been shown in the present pulse study, however, that the O-transfer mechanism occurred over the Al<sub>2</sub>O<sub>3</sub> catalysts as well as the La-ZrO<sub>2</sub> catalysts suggesting that the present Al<sub>2</sub>O<sub>3</sub> catalysts do have reducible properties. Rh is the only Al<sub>2</sub>O<sub>3</sub> supported catalyst which showed evidence of slowing of the rate of O-transfer in this particular study. A scheme was proposed which incorporates the Boudouard reaction, O-transfer, reaction of OH-groups and O-exchange. This proposal was used to explain the mechanism of the CO pulses over the La-ZrO<sub>2</sub> catalysts and why it appeared that no reaction had taken place on addition of the metal.

### 4.2.3 High Pressure CO

The CO pulses, discussed in the previous section, were carried out at 873K and atmospheric pressure. The catalysts were then subjected to more realistic reforming conditions ie continuous CO flow at a pressure of 20bar and temperature of 873K. The mass spectra obtained for the reaction over each noble metal catalyst are shown in figures 3.1 to 3.4. When CO was passed over the support only, a relatively small amount of CO<sub>2</sub> was detected which gradually decreased towards zero over a time scale of approximately 100 minutes as the catalyst deactivated. In contrast to the pulse study, a greater amount of CO<sub>2</sub> was produced from the catalysts in comparison to the support only. Due to such a large pressure of CO, the excess CO<sub>2</sub> obtained from the catalysts, but not the support, was probably from the Boudouard reaction rather than OH-groups.

In the present study, the areas under the CO<sub>2</sub> peaks were calculated and converted to a mass of carbon produced per gram of substrate. As expected after complete deactivation, the mass of carbon produced over the support material was the lowest, relative to all substrates and each of the catalysts produced equal amounts of carbon relative to one another. Therefore, the addition of the metal to the support enhanced carbon formation. Seshan et al.<sup>98, 109</sup> stated that carbon was produced on the support and on the active metal but deactivation was the result of carbon fouling of the metal and was associated with the overgrowth of the catalytically active perimeter between the support and the metal. Any differences between the La-ZrO<sub>2</sub> catalysts would be expected from the deactivation study. It may have been expected that the La-ZrO<sub>2</sub> catalysts would show better stability given the mechanism of O-transfer described in the previous section, however, Noronha et al.<sup>125</sup> found that an increase in total pressure resulted in deactivation of the catalyst as the rate of CO disproportionation became greater than the rate of O-transfer.

Each catalyst produced an equivalent amount of carbon within the first thirty minutes of reaction (relatively small amounts of carbon produced after this time) therefore, the activity was not dependent on percentage metal dispersion of the catalyst. As was proposed for the Al<sub>2</sub>O<sub>3</sub> catalysts, the total amount of carbon deposited on each is related to the total surface area. Since the catalysts were only 0.2% w/w loading and hence, most of the surface area of the catalyst was support, they were all be expected to be similar also it was expected that the La-ZrO<sub>2</sub> catalysts would deposit a smaller total amount of carbon than Al<sub>2</sub>O<sub>3</sub> as they had a smaller surface area.

The determination of a deactivation rate constant was attempted from the changing rate of CO<sub>2</sub> loss. A first order and a second order equation were applied to the system. Since a straight line was obtained from the first order equation and a curve from the second order equation, it seemed plausible to conclude that the mechanism of CO disproportion over Pt was first order. In the case of Rh and Ru, determination of a reaction order will require further attention. The first order equations did not yield a straight line. The second order equation was still slightly ambiguous for both Rh and Ru. The identity of the reaction order could have been masked by the level of noise detected on the raw mass spectra or it is possible that the reaction was neither

first nor second order. An idea of a possible mechanism, which could be taking place over Rh and Ru, was inspired by the work of Jackson et al.<sup>142</sup> who invoked strong and weak CO adsorption sites on their Pt/Al<sub>2</sub>O<sub>3</sub> and Pt/SiO<sub>2</sub> catalysts. In the present work it is possible that the strong sites are being fouled with carbon prior to the low energy sites. This idea would mean that the 'curves' observed in figures 3.39 and 3.41 were actually two straight lines. If this idea were valid, it would be expected that the rate of deactivation of the stronger sites (former part of the deactivation or 'stage 1') would be faster than that of the weaker sites (stage 2). The 'curves' from Rh and Ru were separated into two straight lines and the deactivation rate constants were calculated as shown in table 4.3. It was found for Rh and Ru that stage 1 deactivated faster than stage 2 hence, the idea of strong and weak adsorption sites on the catalysts cannot be overruled. To fully confirm the kinetics of deactivation will require further work. A deactivation study is necessary to fully appreciate the increased stability of the La-ZrO<sub>2</sub> catalysts over the equivalent Al<sub>2</sub>O<sub>3</sub> catalysts however, by comparison of the mass spectra obtained for Rh/Al<sub>2</sub>O<sub>3</sub> and Rh/La-ZrO<sub>2</sub> (figure 3.71 and 3.36 respectively), it can be seen that Rh/La-ZrO<sub>2</sub> takes approximately 80 minutes to fully deactivate while Rh/Al<sub>2</sub>O<sub>3</sub> takes approximately 30 minutes. Therefore, the increased stability probably due to a faster rate of O-transfer and a decrease in CO chemisorption due to ZrO<sub>x</sub> species is apparent for the Rh/La-ZrO<sub>2</sub> catalyst.

**Table 4.3. Deactivation rate constants of Boudouard reaction over La-ZrO<sub>2</sub> supported catalysts**

Catalyst	Deactivation Rate Constant	
	Stage 1	Stage 2
Pt/La-ZrO <sub>2</sub>		1.0
Rh/La-ZrO <sub>2</sub>	0.7	0.3
Ru/La-ZrO <sub>2</sub>	0.8	0.2

To review the information obtained from the high pressure, high temperature continuous flow CO reaction over La-ZrO<sub>2</sub> supported noble metals: the support showed small but significant reaction but was enhanced on addition of the metal. Each catalyst produced an amount of CO<sub>2</sub> determined by the surface area of the catalyst but each deactivated with time. The O-transfer mechanism probably helped

to enhance the stability compared to the  $\text{Al}_2\text{O}_3$  catalysts however at such a high pressure of CO, the rate of the Boudouard reaction would certainly swamp the rate of O-transfer resulting in deactivation. The order of the deactivation is still unclear and requires further work.

#### 4.2.4 $\text{CH}_4$ Pulses

Figure 3.6 shows that no  $\text{H}_2$  was produced over the La-ZrO<sub>2</sub> support material during pulses of  $\text{CH}_4$ , therefore, it was assumed that no reaction was taking place. Hoang et al.<sup>153, 154</sup> however, have previously shown that ZrO<sub>2</sub> is capable of  $\text{H}_2$  adsorption on its surface or  $\text{H}_2$  consumption for partial reduction in the absence of an active metal. This lead to the question of whether the La-ZrO<sub>2</sub> support, in the absence of the metal, was in fact reacting on exposure to  $\text{CH}_4$  but adsorbing all  $\text{H}_2$  product. The percentage  $\text{CH}_4$  conversion from the support after each pulse was calculated and it was found that indeed it was reacting. The percentage  $\text{CH}_4$  conversions are shown in table 4.4.

*Table 4.4. %  $\text{CH}_4$  conversion from five pulses of  $\text{CH}_4$  over La-ZrO<sub>2</sub>*

Pulse	% $\text{CH}_4$ Conversion
1	10.11
2	12.67
3	9.67
4	11.98
5	15.92

Two reactions were possibly taking place on the support:  $\text{CH}_4$  cracking,

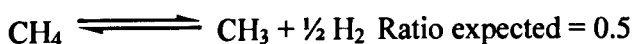
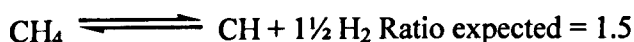


Or,  $\text{CH}_4$  reforming with surface OH groups:



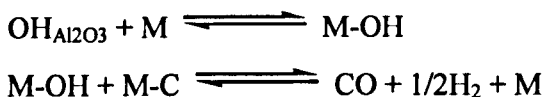
Both proposed reactions produce H<sub>2</sub> and as expected from the literature, the H<sub>2</sub> formed remained adsorbed on the support. Five pulses of CH<sub>4</sub> were subsequently passed over each of the four catalysts and production of H<sub>2</sub> was observed as shown in figures 3.7 to 3.10. The presence of active metal clearly facilitated the reaction with CH<sub>4</sub>. As expected, Ni was significantly more active on exposure to CH<sub>4</sub> than the other catalysts as was observed from percentage CH<sub>4</sub> conversions. It was noticed that the percentage CH<sub>4</sub> conversions were higher over the Al<sub>2</sub>O<sub>3</sub> catalysts in comparison to the La-ZrO<sub>2</sub> catalysts. This can be attributed to a hindering of CH<sub>4</sub> chemisorption due to SMSI effects on the La-ZrO<sub>2</sub> catalysts.

Table 3.22 compares H<sub>2</sub>(moles out)/CH<sub>4</sub>(moles consumed) between each catalyst. The stoichiometry of the CH<sub>4</sub> cracking reaction states that this value should be equal to 2 however, the value of the ratio from Rh and Pt was closer to 1 and did not change as pulse number was increased. A possible explanation is that a different mechanism took place on these catalysts involving formation of a CH<sub>x</sub> species rather than C. Solymosi et al.<sup>155</sup> have previously reported formation of a CH<sub>3</sub> species during CH<sub>4</sub> decomposition over an Ir/MgO catalyst. Therefore, possible reactions schemes for the present work are:

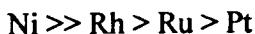


Although this idea fitted well with Rh and Pt catalyst, the value for Ru was found to be approximately 0.2 and not very easy to explain with a new mechanism. Since it has already been shown that the La-ZrO<sub>2</sub> support could adsorb H<sub>2</sub>, it was invoked that H<sub>2</sub> was being formed on the active metal and spilt over on to the La-ZrO<sub>2</sub> support where it was adsorbed. There is much literature which supports the theory of H-spillover from noble metals onto a ZrO<sub>2</sub> support<sup>153, 154</sup> and from noble metals onto other supports (zeolites, Al<sub>2</sub>O<sub>3</sub> and SiO<sub>2</sub>)<sup>156</sup>. Hoang et al.<sup>154</sup> found that active metal mediated H-spillover took place on their Pt/ZrO<sub>2</sub> catalyst and that the adsorption sites for spillover were probably formed by partial reduction of the support.

During CO pulses over La-ZrO<sub>2</sub> supported catalysts, evidence was provided for the presence of surface OH groups which were actively involved in the reaction. Therefore, an equilibria involving OH spillover from support to metal is proposed to have taken place:



H<sub>2</sub> was produced from OH groups and from CH<sub>4</sub> cracking but since the total amount of H<sub>2</sub> produced from a combination of these two reactions was unknown, an amount of H<sub>2</sub> adsorbed by each substrate could not be confirmed. The amount of H<sub>2</sub> desorbed could not be used to determine the difference in activity of the catalysts however, from the percentage CH<sub>4</sub> conversions an order of activity is proposed:

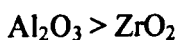


Since Rh and Pt had similar metal dispersions, it was unlikely that this defined the activity in contrast to the theory by Iglesia et al.<sup>59, 60, 61</sup> and the Al<sub>2</sub>O<sub>3</sub> catalysts of the present study.

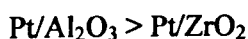
Knowing that the noble metals had facilitated reaction with CH<sub>4</sub> provides further evidence that a ZrOx species did not fully perturb the chemisorption of the reactant species, as previously discussed for the CO pulse reaction. Hoang et al.<sup>153</sup> report a total loss of H<sub>2</sub> chemisorption capacity from Pt in Pt/ZrO<sub>2</sub> after H<sub>2</sub> treatments at 823K and explain the effect as due to SMSI ie. either decoration of the Pt surface due to ZrOx species or due to Pt-Zr alloy formation. The same H<sub>2</sub> chemisorption effect was observed prior to this over Rh/ZrO<sub>2</sub> and again, explained using SMSI theory<sup>157</sup>. A partial loss of chemisorption capacity has, however, been reported but after lower temperature treatments of 773K<sup>158</sup>. The reduction and reaction in the present study were carried out at 873K. According to the literature, a total loss of CH<sub>4</sub> chemisorption would be expected at this temperature in the presence of SMSI however, the present results show that this was not the case. Hoang et al.<sup>153, 154</sup> however, studied two types of ZrO<sub>2</sub> and found that the monoclinic form did not

adsorb any H<sub>2</sub> in the absence of metal while the tetragonal sample did. This gives evidence for a change in properties of ZrO<sub>2</sub> depending on its structure. They state that this is probably a result of the stabilizing action of SiO<sub>2</sub> addition to the latter sample. It is possible in the present work that the La-dopant in ZrO<sub>2</sub> affected the properties of the catalyst and increased the temperature at which CH<sub>4</sub> chemisorption was completely hindered.

Seshan et al.<sup>98, 109</sup> found during CH<sub>4</sub>/CO<sub>2</sub> reforming that Pt/ZrO<sub>2</sub> was more carbon resistant than Pt/Al<sub>2</sub>O<sub>3</sub> and explain their findings due to Lewis acidity of the support material. They showed that carbon can be formed on the metal and the support but deactivation is caused by carbon formed on the metal and is associated with overgrowth of the catalytically active perimeter between the support and the metal. Initially, they exposed each support (Al<sub>2</sub>O<sub>3</sub> and ZrO<sub>2</sub>) to dry reforming conditions. The order of carbon formation was:



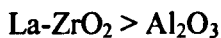
They then exposed the supported catalysts to the same reforming conditions and as expected, the order of carbon formation was:



However, they noted that the amount of carbon formed on Pt/ZrO<sub>2</sub> was less than that on ZrO<sub>2</sub> in the absence of the metal. This seemingly anomalous result was used to explain the greater carbon resistivity of ZrO<sub>2</sub> catalysts in comparison to Al<sub>2</sub>O<sub>3</sub> catalysts: they state how Pt selectively blocks Lewis acid sites on ZrO<sub>2</sub> while for Al<sub>2</sub>O<sub>3</sub>, a fraction remain after Pt deposition. In the absence of Pt on Al<sub>2</sub>O<sub>3</sub>, CH<sub>4</sub> cracking was limited by desorption of hydrogen formed but, on addition of Pt, hydrogen desorption was enhanced via proton-hydride recombination on Pt. In the present study, the idea of carbon formation due to Lewis acid sites on the Al<sub>2</sub>O<sub>3</sub> support is likely.

There was a greater % CH<sub>4</sub> conversion over M/La-ZrO<sub>2</sub> (where M = Rh, Pt, Ru or Ni) than La-ZrO<sub>2</sub> in the absence of M which disagrees with the theory by Seshan et al.<sup>109</sup>

that M selectively blocks Lewis acid sites. In the present study, the order of carbon formation due to CH<sub>4</sub> exposure increases in the order:



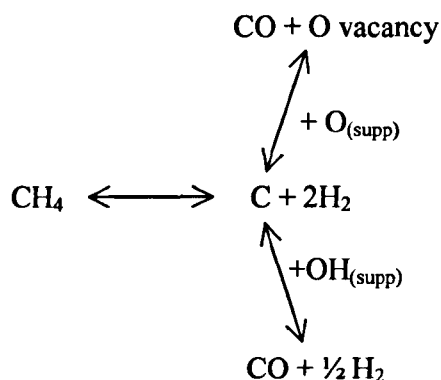
Therefore, La-ZrO<sub>2</sub> probably has a greater number of Lewis acid sites than Al<sub>2</sub>O<sub>3</sub>. Cheng et al.<sup>90</sup> suggested that spillover of H<sub>2</sub> from metal to support depended on support acidity, therefore, this could be an explanation of why H<sub>2</sub> spillover was not observed on the present Al<sub>2</sub>O<sub>3</sub> catalysts but was on La-ZrO<sub>2</sub> catalysts. On deposition of the metal onto the support, the order of carbon formation due to CH<sub>4</sub> exposure increases in the order:



In the case for La-ZrO<sub>2</sub> and Al<sub>2</sub>O<sub>3</sub>, it has been seen that the % CH<sub>4</sub> conversion is facilitated on deposition of metal therefore, the metal in the La-ZrO<sub>2</sub> catalysts must have been affected in some way by the support. In order to avoid proton-hydride recombination. It is proposed that the surface of the metal in the La-ZrO<sub>2</sub> catalysts was decorated with ZrO<sub>x</sub> species which reduced proton-hydride recombination and hence hindered the rate of CH<sub>4</sub> cracking on the catalyst.

An explanation of CH<sub>4</sub> chemisorption perturbation and carbon resistivity of La-ZrO<sub>2</sub> catalysts in comparison to Al<sub>2</sub>O<sub>3</sub> in the present study has been discussed. Using the principle of O-transfer, a mechanism for the CH<sub>4</sub> reaction has been invoked and given in scheme 4.2.

**Scheme 4.2. Proposed mechanism of CH<sub>4</sub> over La-ZrO<sub>2</sub> and Al<sub>2</sub>O<sub>3</sub> substrates**



It has been suggested in scheme 4.2 that CO was produced and it would be expected that it would disproportionate into C and CO<sub>2</sub>. However, from the study of CO over the La-ZrO<sub>2</sub> catalysts (section 4.2.1 and 4.2.2), it is known that there was effectively no reaction but an exchange of species. All noble metal catalysts, on exposure to CH<sub>4</sub>, visibly began to deactivate within five pulses. It is likely that the initial rate of carbon removal by O<sub>(supp)</sub> and OH<sub>(supp)</sub> was fast however deactivation may have resulted from a slow O-vacancy replenishment in the presence of CH<sub>4</sub>.

The results obtained from the Ni/La-ZrO<sub>2</sub> catalyst were rather different to the noble metals in terms of hydrogen spillover. As has been established previously in the present work and throughout the literature, Ni does not deactivate quickly on exposure to carbon forming reactants due to its ability for dissolution of carbon to form whiskers. As a result of this, it was no surprise that Ni had the greatest % CH<sub>4</sub> conversion and did not deactivate after five pulses of reactant. Table 3.8 shows that the % CH<sub>4</sub> conversion over Ni was significantly greater than that over the noble metal catalysts.

Table 3.22 compares H<sub>2(moles out)</sub>/CH<sub>4(moles consumed)</sub> between each catalyst and as has been discussed for the noble metals: a ratio less than two invokes the phenomena of H-adsorption/reduction from the La-ZrO<sub>2</sub> support mediated by H-spillover from the active metal. As can be seen for Ni, the ratio was greater than three. This result

provides further evidence for the occurrence of OH groups on the La-ZrO<sub>2</sub> support as previously seen for the CO reaction. Excess H<sub>2</sub> is probably produced from the following equilibria as shown in scheme 4.2:



There was no information available in the literature to suggest that Ni would not spillover hydrogen from its surface onto the support. A study by Sen et al.<sup>159, 160</sup> on CO hydrogenation over Ni/Al<sub>2</sub>O<sub>3</sub> and Ni/TiO<sub>2</sub> showed that CO adsorbs on Ni where it can be hydrogenated but also spills over onto the support where it becomes CH<sub>3</sub>O (methoxy) species. This was true for both catalysts. They found that the rate of CO hydrogenation and CO spillover were comparable for the Ni/Al<sub>2</sub>O<sub>3</sub> catalyst but for Ni/TiO<sub>2</sub>, the rate of CO hydrogenation was much greater than the rate of CO spillover. In the present study, the percentage CH<sub>4</sub> conversion over Ni/La-ZrO<sub>2</sub> was so large in comparison to that over noble metals. It is possible, therefore, that a similar effect took place to that seen by Sen et al. whereby the rate of CH<sub>4</sub> cracking was much greater than the rate of H-spillover and as a result it appeared from the pulse mass spectra that no hydrogen was spilt over and adsorbed.

It was seen in section 4.2.1 that CO disproportionates over Ni/La-ZrO<sub>2</sub> to produce CO<sub>2</sub> and C. It is likely that a balance existed between Boudouard carbon and carbon derived from CH<sub>4</sub>. The catalyst was not observed to deactivate within the timeframe of the reaction, therefore both types of carbon must result in whisker formation.

A lot of information was obtained from the CH<sub>4</sub> pulses at low pressure and high temperature over La-ZrO<sub>2</sub> supported catalysts. The catalyst activity, established from the percentage CH<sub>4</sub> conversions was not related to metal dispersion of the catalyst in contrast to previous results. The percentage CH<sub>4</sub> conversions over La-ZrO<sub>2</sub> catalysts were also found to be less than the equivalent results over Al<sub>2</sub>O<sub>3</sub> catalyst which was attributed to the ZrO<sub>x</sub> species hindering chemisorption of CH<sub>4</sub>. No H<sub>2</sub> desorption was observed from the La-ZrO<sub>2</sub> support material and it was suggested that the support had adsorbed it. H-spillover and adsorption was observed for all of the noble metal

catalysts. Ni was an exception as there was no evidence for H-spillover and adsorption. It was suggested however that spillover had taken place but the rate of CH<sub>4</sub> cracking was so large that it went unnoticed. It was established that La-ZrO<sub>2</sub> had a greater Lewis acidity than Al<sub>2</sub>O<sub>3</sub> which was used to explain the lack of H-spillover on Al<sub>2</sub>O<sub>3</sub> catalysts. A mechanism of CH<sub>4</sub> reacting over all catalysts has been proposed and the apparent deactivation of the La-ZrO<sub>2</sub> catalysts has been attributed to a slow replenishment of O-vacancies.

#### 4.2.5 High Pressure CH<sub>4</sub> (TEOM)

The TEOM measured changes in mass of the catalyst bed and so could not be used to identify reaction products such as H<sub>2</sub> or CO. Figure 3.106 shows the AGC plot obtained while CH<sub>4</sub> passed over the La-ZrO<sub>2</sub> support only. An insignificant change in mass was observed over the fifty minutes of the experiment. This reaction did not only show that no carbon was deposited on the catalyst support under the conditions of reaction but also that the metal cap was not contributing to the catalytic activity of the process which is often a problem with TEOM experiments. The difference between the support only and the presence of Rh/La-ZrO<sub>2</sub> and Pt/La-ZrO<sub>2</sub> can be seen from figures 3.107 and 3.110 respectively. The most significant AGC changes, the result of changing gas species, were separated from the changes due to carbon deposition as described in sections 3.4.1. Carbon was deposited on the catalyst immediately as CH<sub>4</sub> was passed over the catalyst. The deposition was relatively fast during the initial reaction but began to slow gradually with time on stream as the catalysts deactivated. Given the mechanism of O-transfer described in the previous section, it was expected that the catalysts would not deactivate however, during the CH<sub>4</sub> reaction, the O-vacancies were not being readily replaced which likely resulted in a slowed O-transfer.

The mass of carbon deposited was measured after one hour of reaction and it was found that almost twice as much carbon was deposited on Rh in comparison to Pt. Rh reached a steady state faster than Pt and the mass of deposited carbon at this point was equal for the two catalysts. The CH<sub>4</sub> pulse reaction gave a similar result: initially Rh had a greater percentage CH<sub>4</sub> conversion than Pt before both began to deactivate

however, steady state was not established during the pulses. In agreement with these observations, deactivation studies from the TEOM show how Pt deactivated faster than Rh in the first hour of the reaction. Since the decay of carbon deposition fitted a straight line, it was concluded that the CH<sub>4</sub> cracking reaction over Rh and Pt was second order.

The TEOM study from the Al<sub>2</sub>O<sub>3</sub> catalysts also showed second order behaviour and again, Pt deactivated faster than Rh. The initial rate of deactivation over Rh/Al<sub>2</sub>O<sub>3</sub> was greater than that over Rh/La-ZrO<sub>2</sub> and the trend was the same for Pt. This provides evidence of the greater stability of the La-ZrO<sub>2</sub> catalysts compared to Al<sub>2</sub>O<sub>3</sub> which is likely due to O-transfer and a ZrO<sub>x</sub> species. It can also be seen that similar amounts of carbon were deposited on the La-ZrO<sub>2</sub> catalysts at steady state but this was less than the steady state mass of carbon on Al<sub>2</sub>O<sub>3</sub>. This has been previously attributed to the greater surface area of Al<sub>2</sub>O<sub>3</sub> compared to La-ZrO<sub>2</sub>.

The difference between the Boudouard and the CH<sub>4</sub> cracking reaction at high pressure can be clearly understood. After thirty minutes on stream of the high pressure CO reaction, all three catalysts had equal amounts of carbon deposited on their surfaces. For the CH<sub>4</sub> cracking reaction, it took over one hour for a lesser amount of carbon to be deposited. Therefore, the Boudouard reaction was faster and deposited more carbon than CH<sub>4</sub> cracking under the same high temperature and pressure conditions. From the pulse studies, the opposite effect was observed ie there was a greater CH<sub>4</sub> conversion than CO conversion. Shamsi et al.<sup>47</sup> showed from thermodynamic calculations that as the pressure increased, the equilibrium amount of carbon from the CH<sub>4</sub> cracking reaction decreased while that from the Boudouard reaction increased.

The second stage of the TEOM reaction was an attempt to regenerate the used catalyst by CO<sub>2</sub> oxidation of the deposited carbon. After a steady state carbon deposition had been established with CH<sub>4</sub>, the catalyst was flushed with N<sub>2</sub> for approximately thirty minutes before CO<sub>2</sub> was passed over. It is well established in the literature that carbon deposition is avoided by the presence of CO<sub>2</sub> or H<sub>2</sub>O during reforming<sup>12, 15, 25</sup>. For both, Rh and Pt in the present work, there was no loss of CO<sub>2</sub> detected by the TEOM and when CH<sub>4</sub> flowed over the catalyst for a second time, the

base line of the AGC had not shifted to reinforce the fact that no carbon had been oxidised. Finally, no more carbon deposition was observed for the remaining hour of the reaction to confirm that the catalyst was fully deactivated and had not been regenerated. Nagaoka et al.<sup>98</sup> proposed a mechanism for CO<sub>2</sub> reforming of CH<sub>4</sub> and demonstrated the carbon removal ability of CO<sub>2</sub>. CO<sub>2</sub> was however, present simultaneously with CH<sub>4</sub>. This mechanism did however give suggestion about the types of carbon formed in the present study which were discussed for the Al<sub>2</sub>O<sub>3</sub> catalysts.

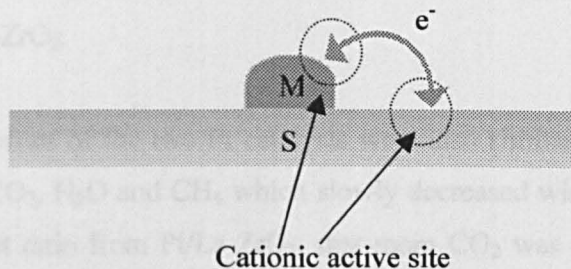
The high pressure and temperature TEOM reaction showed how no carbon was deposited on the support or the cap while CH<sub>4</sub> was flushing over. Over the Pt and Rh/La-ZrO<sub>2</sub> catalysts, carbon was deposited immediately as CH<sub>4</sub> began flushing however, the deposition rate decreased with time on stream to reach a steady state to show that the catalysts deactivated. Both reactions fitted the second order deactivation model and the rate of deactivation was greater over Pt compared to Rh which was observed over the Al<sub>2</sub>O<sub>3</sub> catalysts. It was unexpected that the catalysts deactivated at all given the proposed mechanism of O-transfer however, there was no source of O to replace the O-vacancies in the reaction and as the pressure of CH<sub>4</sub> was so high, the rate of CH<sub>4</sub> decomposition was faster than the rate of carbon removal via O-transfer. After one hour, Rh had more carbon on its surface and reached a steady state faster than Pt, a trend that was also observed with the Al<sub>2</sub>O<sub>3</sub> catalysts. At steady state, both La-ZrO<sub>2</sub> catalysts had the same mass of carbon on their surface which was related to surface area. This final mass was less than that on the Al<sub>2</sub>O<sub>3</sub> catalysts since Al<sub>2</sub>O<sub>3</sub> had a greater surface area than La-ZrO<sub>2</sub>. The CH<sub>4</sub> cracking reaction was less active than the Boudouard reaction at high pressure. The opposite trend was observed with the pulse study. Information about the type of carbon deposited was obtained from the TEOM study.

### 4.3 High Pressure CO and H<sub>2</sub> over La-ZrO<sub>2</sub> and Al<sub>2</sub>O<sub>3</sub> Catalysts

There are many reports in the literature on the reaction between CO and H<sub>2</sub><sup>161, 162, 163, 164</sup> and there seem to be a great many differences in the product distributions and CO conversions. Within this literature however, it is commonly agreed that differences exist due to the nature of the support however there are a few differing theories on exactly how the support is interacting. The results of Perez-Zurita<sup>164</sup> show that support reducibility is responsible for determination of the product selectivity i.e. with non-easily reducible supports (Al<sub>2</sub>O<sub>3</sub>, ZrO<sub>2</sub> and TiO<sub>2</sub>), alcohol production was very low while higher selectivity for alcohols was obtained over the more reducible supports (WO<sub>3</sub> and MoO<sub>3</sub>). The same author reported high conversion rates which were attributed to fast H-spillover between metal and support. Burch et al.<sup>162</sup> observed an SMSI effect over their Ni/TiO<sub>2</sub> and Pt/TiO<sub>2</sub> catalysts and an enhanced activity during reaction of CO and H<sub>2</sub> in comparison to Ni/SiO<sub>2</sub>. They noted however, that the activity was high on the TiO<sub>2</sub> catalysts with or without the presence of SMSI and therefore concluded that SMSI was not the cause of the enhanced activity. They attributed the increased activity to the creation of new active sites at the interface of the metal and the reduced support. They called them interfacial metal-support interactions (IMSI) and suggested that the support acted directly in the process by adsorbing or assisting in the adsorption of CO. The active site was assumed to be an exposed Ti<sup>3+</sup> ion adjacent to a metal particle. They noted, however, that this enhanced activity had been seen elsewhere on less reducible supports (Al<sub>2</sub>O<sub>3</sub>, La<sub>2</sub>O<sub>3</sub>, Nd<sub>2</sub>O<sub>3</sub>, ZrO<sub>2</sub>). The work of Poels et al.<sup>165</sup> differs from Burch in the suggestion that ions from the metal are involved rather than from the support, indicating that type of metal affects the catalytic activity. Similarly, Shen et al.<sup>163</sup> reported how support acidity (reducibility) influenced the product distribution but CO conversion was increased by the occurrence of a cationic species originating from the metal moreover, they related the formation of the cationic species to the strong interaction between metal and support (ZrO<sub>2</sub> and CeO<sub>2</sub>) resulting in electron transfer from metal. Finally, even for the reaction between CO<sub>2</sub> and H<sub>2</sub>, a supported TiO<sub>2</sub> catalyst was found to be more active than Al<sub>2</sub>O<sub>3</sub>, SiO<sub>2</sub> and MgO which was attributed to an electronic interaction influencing the bonding and reactivity of chemisorbed

species<sup>166</sup>. The idea of active site formation by electron transfer from support (S) or metal (M) has been illustrated in figure 4.2.

**Figure 4.2 Formation of active site by electron transfer**



By observation of the results from the present work, the reaction was clearly affected by the support and the active metal although it was not known if the active site was formed by loss of an electron from the support or from the metal. It has been previously reported that the particle size only plays a minor role in determining the catalysts behaviour in comparison to support effects<sup>164</sup>.

A 1:1 mixture of CO and H<sub>2</sub> was passed over the Al<sub>2</sub>O<sub>3</sub> and La-ZrO<sub>2</sub> support materials at 873K and 20bar pressure as shown in figures 3.80 and 3.45 respectively. No significant production of any species was observed over the supports. The 1:1 mixture of CO and H<sub>2</sub> was subsequently passed over the Al<sub>2</sub>O<sub>3</sub> and La-ZrO<sub>2</sub> noble metal catalysts. The difference between the metals in terms of CO conversion and product selectivity became very apparent from these reactions. Each catalyst produced the same three products: CH<sub>4</sub>, CO<sub>2</sub> and unquantified amounts of H<sub>2</sub>O and each had a unique reaction profile. The La-ZrO<sub>2</sub> supported catalysts were clearly more active than the equivalent Al<sub>2</sub>O<sub>3</sub> catalysts, which was possibly a result of an increased electronic interaction occurring on La-ZrO<sub>2</sub> or increased H-spillover as described in the literature<sup>164</sup>.

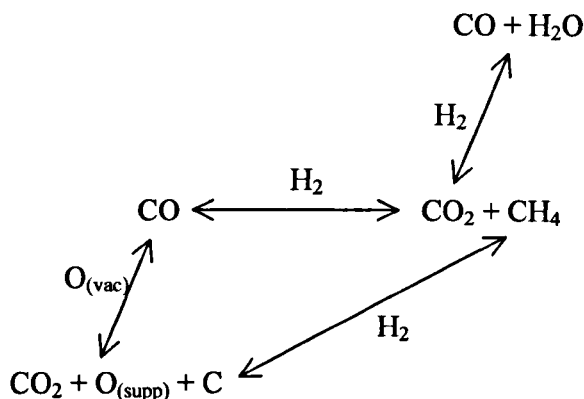
The first 40 minutes of the reaction profiles for the two Rh catalysts were almost identical in terms of moles of species produced, their relative percentages, the % CO conversion and the CO<sub>2</sub>:CH<sub>4</sub> product ratio. However, Rh/La-ZrO<sub>2</sub>, maintained this

conversion at a steady state for the duration of the reaction while CO conversion over Rh/Al<sub>2</sub>O<sub>3</sub> subsequently decreased as if the catalyst had partially deactivated. It is probable that the activity in the first 40 minutes was due to the Rh metal for both catalysts and that in the second stage was due to the support. The second stage of the reaction over Rh/Al<sub>2</sub>O<sub>3</sub> suffered a decrease in the product ratio, ie a change in product distribution which is probably a result of the different support reducibility of Al<sub>2</sub>O<sub>3</sub> compared to La-ZrO<sub>2</sub>.

The reaction profiles of the two Pt catalysts were also similar to one another in that both produced CO<sub>2</sub>, H<sub>2</sub>O and CH<sub>4</sub> which slowly decreased with time. It can be seen from the product ratio from Pt/La-ZrO<sub>2</sub>, that more CO<sub>2</sub> was produced compared to CH<sub>4</sub>. There was a smaller CO conversion over Pt/Al<sub>2</sub>O<sub>3</sub> and more CH<sub>4</sub> was produced compared to CO<sub>2</sub>. The Ru catalysts showed very different behaviour from each other. Ru/La-ZrO<sub>2</sub> appeared fairly active initially but after approximately 10 minutes on stream, it began to deactivate leaving only residual activity. Ru/Al<sub>2</sub>O<sub>3</sub> showed very little activity throughout the duration of the reaction.

From the information in the literature and results from the present study, a mechanism of CO and H<sub>2</sub> over all noble metal catalysts has been proposed and given in figure 4.3. It is likely that a major process taking place is the reverse dry reforming process to produce CO<sub>2</sub> and CH<sub>4</sub> since both species were major products from each reaction. From present results, it is suggested that CO exchanges with O-vacancies and disproportionates on the active metal to give C and CO<sub>2</sub>. Since H<sub>2</sub>O was detected, it is probable that this was formed through reaction of H<sub>2</sub> and CO<sub>2</sub> (reverse water-gas shift). Removal of carbon was also proposed to take place by two separate reactions: reduction with H<sub>2</sub> to produce CH<sub>4</sub> and oxidation with O originating from the support to give CO<sub>2</sub> and O-vacancies.

**Figure 4.3. Proposed mechanism of CO and H<sub>2</sub> (1:1) over all catalysts**



In the case of Rh/Al<sub>2</sub>O<sub>3</sub> and Rh/La-ZrO<sub>2</sub>, the initial activity appeared to be related to the nature of the metal (cationic species on metal support interface with active site: Rh<sup>n+</sup><sup>165</sup>). The metal became increasingly coked due to Boudouard carbon, however the action of O (from support) and H<sub>2</sub> ensured that the C was removed to maintain the activity. The activity however, decreased over Rh/Al<sub>2</sub>O<sub>3</sub> which was probably an effect of the support and related to either slow spillover of H<sup>164</sup> (H-spillover shown not to take place on Al<sub>2</sub>O<sub>3</sub> catalysts in this study) or a decrease in the rate of O-transfer<sup>124</sup> which allowed the metal to become partially coked and hence, decreased the conversion. The distribution of products was also affected after 40 minutes which has been previously attributed to the support reducibility<sup>164</sup>.

The reaction over the Pt catalysts seems to be affected by support and metal from the onset. They had a lower conversion of CO compared to both Rh catalysts which is obviously an effect of the metal however, the more highly dispersed Pt/Al<sub>2</sub>O<sub>3</sub> had a lower conversion than Pt/La-ZrO<sub>2</sub> which must be an effect of the support. The enhanced activity of the La-ZrO<sub>2</sub> catalyst has been postulated already as due to an electronic interaction. In terms of the proposed mechanism, it appears that Pt does not disproportionate CO as well as Rh. It was possible, over Pt, that most of the H<sub>2</sub> was initially used up in the conversion of CO<sub>2</sub> and CO while less was used for Boudouard carbon removal. This idea would explain why the reaction profile of H<sub>2</sub> is different to that of CO in the initial stages of the reaction. It would also explain the

fact that the catalyst slowly deactivated due to a lack of C removal by H<sub>2</sub>. For Pt, therefore, the product distribution was probably affected by the nature of the metal rather than the support. The calculated values for CO<sub>2</sub>:H<sub>2</sub> for both Pt catalysts do indeed show that the values were similar.

The activity over Ru/Al<sub>2</sub>O<sub>3</sub> was minimal. There appeared to be no deactivation suggesting that the adsorption of CO was very hindered. This was however, already observed when CO only was passed over the catalyst. Ru/La-ZrO<sub>2</sub> has shown previously that it is capable of CO adsorption and as has been observed from the CO/H<sub>2</sub> reaction, the activity was initially quite high which was probably due to an electronic interaction of the support. After a short time on stream the catalyst almost fully deactivated which was unexpected in comparison to the other La-ZrO<sub>2</sub> catalysts. Therefore, as was observed with Pt, it is possible that the product selectivity is affected by the nature of the metal and in this case Ru appears to be more selective towards carbon formation than removal.

In summary, the literature states that the mechanism of the CO/H<sub>2</sub> reaction takes place on an active site situated on the metal-support boundary created by electron transfer from support to metal or vice versa. It also states that the catalyst activity is defined by the nature of the support and that the more reducible support should have greater activity. In the present study, the activity was influenced by the nature of the support and the metal however, in all cases the more easily reducible catalyst (La-ZrO<sub>2</sub>) was more active. The reaction profile of each was also very much affected by the type of support and metal. The literature described how the type of support affected the product distribution however, it was suggested in the present study that it was also affected by the nature of the metal. A mechanism was proposed and an explanation of each catalyst's behaviour was offered.

#### 4.4 CO and CO<sub>2</sub> over La-ZrO<sub>2</sub> and Al<sub>2</sub>O<sub>3</sub> Catalysts

It has been previously suggested in the literature that the presence of H<sub>2</sub>O and CO<sub>2</sub> in a carbon forming reaction can act to remove carbon and help maintain the stability of the catalyst. It was seen in the TEOM reactions of the present study that the addition

of CO<sub>2</sub> after catalyst deactivation by CH<sub>4</sub> did not react with the deposited carbon and hence did not revive the activity of the catalyst. In this section, different ratios of CO:CO<sub>2</sub> were passed over the noble metal catalysts and the residual activity assessed by flowing a 1:1 ratio of CO:H<sub>2</sub> over the used catalysts. The spectra obtained were compared to that from the previous section. Initially, CO:H<sub>2</sub> (1:1) was passed over each of the used Boudouard reaction catalysts which were seen in section 3.3.1 and 3.3.5 to fully deactivate. However, as can be seen from the spectra in figures 3.49 to 3.51 and 3.84 to 3.86, on addition of CO and H<sub>2</sub> in a 1:1 ratio, there is slight activity over each catalyst. Small quantities of CO<sub>2</sub> and CH<sub>4</sub> were detected from each reaction and a loss in H<sub>2</sub> was also observed. It therefore appeared that H<sub>2</sub> had the ability to react with some of the deposited Boudouard carbon on the metal surface to produce CH<sub>4</sub>, leaving the metal free to chemisorb CO. Rh/La-ZrO<sub>2</sub> most readily underwent this 'cleaning' process while the other catalysts only showed a relatively small loss of H<sub>2</sub> in the initial stages of reaction suggesting that CO disproportionation was faster than carbon methanation over these catalysts.

Each of the catalysts were then treated with a CO:CO<sub>2</sub> (10:1) continuous flow gas mixture assuming that CO<sub>2</sub> would initiate carbon removal via oxygen transfer as described in scheme 4.3. A feature that was observed only with the two Rh catalysts was a distinctive CO<sub>2</sub> peak at the start of the reaction which decreased to the baseline value. This showed that the Rh catalysts had disproportionated CO into CO<sub>2</sub> but since the peak decreased, it was clear that the catalyst deactivated and hence, at high pressure this amount of CO<sub>2</sub> was not enough to replenish all O-vacancies and avoid carbon deposition and deactivation. It was unclear from the Pt and Ru catalysts if any reaction had taken place since the by-pass and the reaction spectra appeared identical<sup>††</sup>. Following the CO/CO<sub>2</sub> 10:1 reaction, a 1:1 ratio of CO/H<sub>2</sub> was passed over the used catalysts in order to assess the residual activity of the catalyst. The spectra were very similar to that obtained from CO/H<sub>2</sub> over the used Boudouard catalysts hence, the activity had not been restored for any of catalysts by addition of this amount of CO<sub>2</sub>. Over the Rh/La-ZrO<sub>2</sub> and Ru/La-ZrO<sub>2</sub> catalysts, there seemed to be a small effect due to CO<sub>2</sub>. there was a balance between carbon removal by H<sub>2</sub> and carbon deposition by CO since the reaction species reached a steady state. Pt/La-

---

<sup>††</sup> If CO<sub>2</sub> had been produced it may have been such a small amount relative to the amount of CO<sub>2</sub> already present that the mass spectrometer may not have been sensitive enough to detect it.

ZrO<sub>2</sub> and all Al<sub>2</sub>O<sub>3</sub> catalysts on the other hand were unaffected by this addition of CO<sub>2</sub>.

Since the activity was not restored with a 10:1 ratio of CO:CO<sub>2</sub>, a 5:1 ratio was applied. Rh/La-ZrO<sub>2</sub>, again produced a characteristic peak of CO<sub>2</sub> in the initial stages of the reaction which decreased towards the baseline. This peak was not apparent with Rh/Al<sub>2</sub>O<sub>3</sub> or any other catalyst. Figures 3.59, 3.61 and 3.63 show the spectra obtained from the reaction of CO/H<sub>2</sub> in a 1:1 ratio following the catalysts treatment in CO/CO<sub>2</sub> (5:1). The spectra showed that this amount of CO<sub>2</sub> was still not enough to completely hinder carbon formation on the catalysts. CO/H<sub>2</sub> (1:1) over used Rh/La-ZrO<sub>2</sub> and Ru/La-ZrO<sub>2</sub> reached a steady state, as was seen for the 10:1 catalysts, while Pt/La-ZrO<sub>2</sub> lost only a small amount of H<sub>2</sub> in the initial stages of the reaction. Insignificant activity was apparent from the Rh/Al<sub>2</sub>O<sub>3</sub> catalyst while the other Al<sub>2</sub>O<sub>3</sub> catalysts suffered a loss of H<sub>2</sub> at the start of the reaction. Used Rh and Ru supported on La-ZrO<sub>2</sub> showed unique behaviour from the other catalysts on reaction with CO and H<sub>2</sub>. It seemed likely for these two catalysts that the rate of O-transfer (or the rate of CO disproportionation) was balanced with the rate of carbon removal by H<sub>2</sub>. For the remaining catalysts it was possible that the rate of carbon removal by H<sub>2</sub> was relatively slower than the rate of O-transfer (or CO disproportionation rate). It has been seen in previous sections that the rate of O-transfer is faster over La-ZrO<sub>2</sub> supported catalysts in comparison to Al<sub>2</sub>O<sub>3</sub> supported catalysts. Pt, in this case, is an exception however it was shown to have a greater rate of deactivation than Rh.

The results were very different when a CO/CO<sub>2</sub> mixture of ratio 1:1 was passed over the catalysts. The reaction of CO/CO<sub>2</sub> prior to CO/H<sub>2</sub> clearly affected product ratios and hence, selectivities. Figures 3.65, 3.67 and 3.69 show the spectra obtained from the CO/H<sub>2</sub> reaction for Rh, Pt and Ru/La-ZrO<sub>2</sub> respectively which were carried out after the CO/CO<sub>2</sub> mixture. At first glance, it appeared that the Rh catalyst had maintained its full activity, however, the reaction species did not reach steady state as fast as the fresh catalyst sample. After one hour, the percentage CO conversion from the used sample was found to equal the steady state percentage CO conversion of the fresh sample, therefore, at this point, the activity of the fresh and used samples were the same. The CO<sub>2</sub>:CH<sub>4</sub> product ratios were, however, different ie the ratio obtained

from used Rh was smaller than the ratio from the fresh sample suggesting that prior treatment with CO/CO<sub>2</sub> affects the product distribution. With reference to the change in the CO<sub>2</sub>:CH<sub>4</sub> product ratio it is likely that the used Rh was more selective for carbon removal via methanation while the fresh sample underwent the Boudouard reaction more readily, with carbon removal via O-transfer.

The percentage CO conversions and the CO<sub>2</sub>:CH<sub>4</sub> product ratios were very similar for the fresh and used Pt/La-ZrO<sub>2</sub>. A noticeable difference however, was reaction selectivities, in particular, the greater uptake of H<sub>2</sub> from the fresh Pt in comparison to the used Pt. It has been suggested in the present work that the large H<sub>2</sub> up-take at the start of the reaction on fresh Pt is due to the reverse water-gas-shift reaction. Since the H<sub>2</sub> up-take seems to be the only major difference between the fresh and the used Pt, it is suggested that the reverse water-gas-shift reaction is hindered over the used sample. The used Ru/La-ZrO<sub>2</sub> catalyst was not as active for the CO/H<sub>2</sub> reaction as fresh Ru however, the same general features are present with both. It is probable for Ru/La-ZrO<sub>2</sub>, that a CO:CO<sub>2</sub> ratio greater than 1:1 would be required to remove deposited carbon.

A change in product ratios was also very apparent with the Al<sub>2</sub>O<sub>3</sub> catalysts after treatment with a 1:1 ratio of CO/CO<sub>2</sub>. The used sample spectra did bear some resemblance to that of the fresh sample although it was apparent that a 1:1 ratio was not sufficient to maintain the catalysts' activity. It is likely that more CO<sub>2</sub> would be required in order to increase the rate of O-transfer over the Al<sub>2</sub>O<sub>3</sub> catalysts and hence oxidise the deposited carbon. From the spectra of the used Rh/Al<sub>2</sub>O<sub>3</sub> catalyst, there were small peaks of CO<sub>2</sub> and CH<sub>4</sub> coinciding with a loss of H<sub>2</sub> in the first few minutes of reaction over the used Rh/Al<sub>2</sub>O<sub>3</sub> catalyst. The peaks decreased slightly then began to increase again as H<sub>2</sub> decreased. The CO<sub>2</sub>:CH<sub>4</sub> product ratio at steady state of the used sample was compared to that of the second stage of the fresh Rh/Al<sub>2</sub>O<sub>3</sub> reaction and as can be seen from section 3.37, the ratio was greater over the fresh Rh. This suggests that the selectivity for CH<sub>4</sub> production was greater over the used catalyst. No steady state was achieved for the used or fresh sample within the time frame of either study.

The fresh and the used Pt/Al<sub>2</sub>O<sub>3</sub> samples gave a similar reaction profile and the percentage CO conversions were comparable. In contrast to all other catalysts, the CO<sub>2</sub>:CH<sub>4</sub> product ratio was greater over the used Pt compared to the fresh sample moreover, the uptake of H<sub>2</sub> was greater over the fresh Pt compared to the used. This suggests that the fresh Pt/Al<sub>2</sub>O<sub>3</sub> is more selective for CH<sub>4</sub> formation and probably the reverse water-gas-shift reaction compared to the used catalyst.

The used and fresh Ru/Al<sub>2</sub>O<sub>3</sub> catalysts both had very little activity. Both show an uptake of H<sub>2</sub> at the start of the reaction only, suggesting that the Boudouard reaction is depositing carbon on the catalyst to deactivate the metal faster than the rate of methanation of deposited carbon by hydrogen.

The results from this section show, for Pt catalysts, that an approximate CO/CO<sub>2</sub> ratio of 1:1 must be present in the reactor in order to maintain the catalysts activity. For ratios of 5:1 and greater there was not enough CO<sub>2</sub> available to facilitate a sufficiently fast O-transfer mechanism to counteract the deposition of carbon by CO. As a result the active sites will be gradually covered in carbon and deactivate. A ratio of approximately 1:1 was enough to maintain the activity of Rh/La-ZrO<sub>2</sub> but not Rh/Al<sub>2</sub>O<sub>3</sub>. This was probably due to a slower rate of O-transfer on Al<sub>2</sub>O<sub>3</sub> compared to La-ZrO<sub>2</sub>. More CO<sub>2</sub> would be required for Rh/Al<sub>2</sub>O<sub>3</sub> to increase the rate of O-transfer and hence the rate of carbon oxidation. More work will be required to determine the exact CO/CO<sub>2</sub> ratio required for each catalyst to maintain its activity. Pre-treatment of all catalysts with a CO/CO<sub>2</sub> mixture was shown to affect the CO<sub>2</sub>:CH<sub>4</sub> product ratios or reaction selectivities.

## 5 Summary

### 5.1 Al<sub>2</sub>O<sub>3</sub> Catalysts

It was established, by passing pulses of CO over the Al<sub>2</sub>O<sub>3</sub> catalysts, that surface OH groups on the support-metal perimeter were interacting with the reactant species. A series of equilibria that probably took place were obtained from the literature. There was no replenishment of OH groups during reaction and the results gave evidence of their decrease within five pulses of CO. Ni and Pt were found to have the greatest consumption of CO within five pulses. Ni, however, was expected to be the most active due to its affinity to form whisker carbon on exposure to CO. The activity of the noble metals appeared to increase with increasing metal dispersion. Surface OH-groups were also involved in the reaction when CH<sub>4</sub> was pulsed over all catalysts with the exception of Rh/Al<sub>2</sub>O<sub>3</sub>. Due to the differing reaction of Rh, the percentage CH<sub>4</sub> conversion did not relate to metal dispersion. The percentage CH<sub>4</sub> conversions were greater than the equivalent percentage CO conversions and so the available OH-groups on Pt, Ru and Ni were consumed within five pulses of CH<sub>4</sub>.

At high pressure, catalyst dispersion was not important. The catalysts were subjected to CO until they fully deactivated. The mass of carbon deposited was related to the total surface area of the catalyst which was the same for Rh, Pt and Ru/Al<sub>2</sub>O<sub>3</sub>. The mass of carbon deposited on Ru, however, was less than the others. The deactivation was related to the nature of the metal and was likely first order although further work will be required to fully prove this proposal. Pt had a faster rate of deactivation than Rh despite Pt showing greater initial activity during the CO pulse study. The reaction of CH<sub>4</sub> at high pressure was less active than high pressure CO and as a result CO was not used on the TEOM and CH<sub>4</sub> was not used on the high pressure rig (Glasgow). Rh deposited more carbon than Pt in the first hour and reached a steady state while Pt never. The deactivation showed second order behaviour for both and the initial rate was greatest over Pt as was observed with high pressure CO. No carbon was removed from the catalysts by flowing CO<sub>2</sub> over subsequent to CH<sub>4</sub>, however, information on the type of carbon deposited was obtained.

## 5.2 La-ZrO<sub>2</sub> Catalysts

There was a definite difference in the reactivity of the La-ZrO<sub>2</sub> catalysts in comparison to the Al<sub>2</sub>O<sub>3</sub> catalysts which was not an effect of catalyst dispersion. CO<sub>2</sub> was detected on the mass spectrometer from CO pulses over the La-ZrO<sub>2</sub> support, however no further activity was apparent on addition of the metal (except for Ni). The percentage CO conversion was less on Ni/LaZrO<sub>2</sub> compared to Ni/Al<sub>2</sub>O<sub>3</sub> and the lesser activity of La-ZrO<sub>2</sub> catalysts was attributed to SMSI effects. Two such effects have been reported in the literature: coating of the metal with ZrO<sub>x</sub> species which affects metal ensemble size and hence, CO chemisorption or a M-Zr<sup>n+</sup> species which decreases the M-CO bond strength. Evidence for the interaction of surface OH-groups was also discussed. The results from the isotope study revealed that a mechanism of O-transfer between the support and C/CO<sub>x</sub> species was taking place over the Al<sub>2</sub>O<sub>3</sub> and La-ZrO<sub>2</sub> catalysts to show that both sets of catalysts were reducible. Isotope pulses over Rh/Al<sub>2</sub>O<sub>3</sub>, however, suggested that the rate of O-transfer was faster over the La-ZrO<sub>2</sub> catalysts. The reaction mechanism was used to show that the La-ZrO<sub>2</sub> catalysts exchanged oxygen on addition of CO-only and were not inactive.

The La-ZrO<sub>2</sub> catalysts were not as active on exposure to CH<sub>4</sub> as Al<sub>2</sub>O<sub>3</sub> catalysts were and this was attributed to SMSI effects. CH<sub>4</sub> pulses over La-ZrO<sub>2</sub> revealed that the support had the ability of adsorbing H<sub>2</sub> produced during the reaction but this was not observed during reaction with Al<sub>2</sub>O<sub>3</sub>. It was proposed that OH-groups were interacting during reaction with CH<sub>4</sub> and evidence was presented to show that the La-ZrO<sub>2</sub> catalysts were spilling H<sub>2</sub> onto the support where it was adsorbed. There was no obvious spillover effects from the Al<sub>2</sub>O<sub>3</sub> catalysts and this has been attributed to a fewer number of Lewis acid sites compared to the La-ZrO<sub>2</sub> catalysts. Ni/La-ZrO<sub>2</sub> appeared not to spillover hydrogen, however this was probably due to a fast rate of CH<sub>4</sub> cracking compared to spillover. The order of activity of the La-ZrO<sub>2</sub> catalysts was not a dispersion effect. A mechanism involving O-transfer was proposed to explain the observations from the CH<sub>4</sub> pulses over all catalysts.

During the high pressure study with CO, all catalysts deposited equal amounts of C and this has been attributed to the similarity of catalyst surface area. Each La-ZrO<sub>2</sub> catalyst was observed to deactivate as did the Al<sub>2</sub>O<sub>3</sub> catalysts. Given the mechanism of O-transfer described in the text, it was expected that the catalysts would be stable however the pressure of CO was high and the rate of disproportionation was much greater than O-transfer. The behaviour of the deactivation was related to the nature of the metal and first and second order equations were applied. It was clear that further work will be required to determine the order of the deactivation, however, by observation of the high pressure CO spectra from both Rh catalysts, it can be seen that Rh/La-ZrO<sub>2</sub> was more stable. Passing CH<sub>4</sub> over the catalysts at high pressure also resulted in deactivation. After one hour on stream, more carbon had been deposited on Rh than Pt and Rh reached a steady state faster however, the initial rate of deactivation was faster over Pt – a trend that was mirrored over the Al<sub>2</sub>O<sub>3</sub> catalysts. The deactivations fitted a second order plot. The deactivation rate parameters showed that the La-ZrO<sub>2</sub> catalysts were more stable than the equivalent Al<sub>2</sub>O<sub>3</sub> catalysts. As was observed for the Al<sub>2</sub>O<sub>3</sub> catalysts, the activity was not restored by flowing CO<sub>2</sub> post CH<sub>4</sub> cracking. Conclusions, however, were made about the type of carbon deposit.

### 5.3 Reaction with CO and H<sub>2</sub>

The literature is in agreement that the support affects the catalysed reaction of CO and H<sub>2</sub>. Disagreements exist, however, on how the metal and the support affect the activity and the product distribution. It was proposed that the enhanced activity of the La-ZrO<sub>2</sub> catalysts in the present study was due to increased IMSI effects compared to Al<sub>2</sub>O<sub>3</sub>. The same products (CO<sub>2</sub>, CH<sub>4</sub> and H<sub>2</sub>O) were produced over each catalyst but it was clear how the nature of the metal and the support affected the reaction profile. A common mechanism (incorporating O-transfer) was proposed for each catalyst and an explanation offered as to why each showed unique behaviour on reaction with CO and H<sub>2</sub>.

#### 5.4 Reaction with CO and CO<sub>2</sub>

The literature shows how CO<sub>2</sub> can be used to avoid carbon deposition on the catalyst during dry reforming. It was shown in the TEOM study that, passing CO<sub>2</sub> over following exposure to CH<sub>4</sub> did not restore the catalyst activity therefore three ratios of CO:CO<sub>2</sub> were chosen to see at what point the activity of the catalyst is maintained. For Pt catalysts, an approximate CO/CO<sub>2</sub> ratio of 1:1 was necessary in order to maintain the catalysts activity. For ratios of 5:1 and greater there was not sufficient CO<sub>2</sub> present to ensure the mechanism of O-transfer was faster than deposition of carbon by CO. A ratio of approximately 1:1 was enough to maintain the activity of Rh/La-ZrO<sub>2</sub> but not Rh/Al<sub>2</sub>O<sub>3</sub> and this was attributed to a slower rate of O-transfer on Al<sub>2</sub>O<sub>3</sub> compared to La-ZrO<sub>2</sub>. Further work is necessary to determine the exact CO/CO<sub>2</sub> ratio required for each catalyst to maintain its activity. All ratios of CO/CO<sub>2</sub> were shown to affect the CO<sub>2</sub>:CH<sub>4</sub> product ratios or reaction selectivities.

## 6 References

- <sup>1</sup>F. Press, R. Siever, in *Understanding Earth*, W.H. Freeman and Co., New York, 2<sup>nd</sup> Ed (1997) 627
- <sup>2</sup>C. Song, *Catal. Today*, 77 (2002) 17
- <sup>3</sup>Statistical Abstract of the United States (SAUS) 1998, 118<sup>th</sup> ed., US Department of Commerce, 1999
- <sup>4</sup>USCB, Historical Estimates of World Population, *US Census Bureau*, 1999
- <sup>5</sup>Energy Information Administration (EIA), *Annual Energy Outlook 2002*, DOE/EIA-0383 (2002) (Washington DC, December, 2001)
- <sup>6</sup>M.A. Pena, J.P.Gomez, J.L.G. Fierro, *App.Catal. A:Gen*, 144 (1996) 7
- <sup>7</sup>J.P. Lange, P.J.A. Tijm, *Chem. Eng. Sci.*, Vol. 51, No. 10 (1996) 2379
- <sup>8</sup>J.R. Rostrup-Nielsen, *Proceedings of the 15<sup>th</sup> World Petroleum Congress*, John Wiley and Sons (1998) 767
- <sup>9</sup>Editorial, *Fuel Process. Technol.*, 83 (2003) 1
- <sup>10</sup>R.T.K. Baker, M. Barber, P. Harris, F. Feates, R. Waite, *J. Catal.* 26 (1972) 51
- <sup>11</sup>J.N. Armor, *Appl. Catal. A: Gen.*, 176 (1999) 159
- <sup>12</sup>D.E. Ridler, M.V. Twigg, in *Catalyst Handbook*, M.V. Twigg (Ed.), Manson, London, 2<sup>nd</sup> Ed. (1997) 225
- <sup>13</sup>J.R. Rostrup-Nielsen, J-H. Bak Hansen, *J. Catal.*, 144 (1993) 38
- <sup>14</sup>S.C. Tsang, J.B. Claridge, M.L.H. Green, *Catal. Today*, 23 (1995) 3
- <sup>15</sup>J.R. Rostrup-Nielsen, in *Catalysis Science and Technology* (J.R. Anderson, M. Boudart eds.), Springer-Verlag, Vol 5 (1984) 1
- <sup>16</sup>Dr. P.K. Ingram, *Private Communication* (1)
- <sup>17</sup>D.J. Smith, L.D. Marks, *Phil. Mag. A*, 44 (1981) 735
- <sup>18</sup>N.M. Bobrov, L.O. Apel'baum, M.I.Temkin, *Kinet. Catal.*, 5 (1964) 614
- <sup>19</sup>H.F. Leach, C. Mirodatos, D..A. Whan, *J. Catal.*, 63 (1980) 138
- <sup>20</sup>B.S. Chahar, J.W. Hightower, *unpublished results*, cited in ref. 15.
- <sup>21</sup>J.R.H. Ross, M.C.F. Steel, A. Zeini-Isfahani, in *Mechanisms of Hydrocarbon Reactions* (F. Marta, D. Kallo, Eds.) Budapest (1975) 200
- <sup>22</sup>J.H. Edwards, A.M. Maitra, *Fuel Process. Technol.*, 42 (1995) 269
- <sup>23</sup>D.R. Stull, E.F. Westrum, G.C. Sinke, in *The Chemical Thermodynamics of Organic Compounds*, R.E. Krieger Co., Florida (1987)
- <sup>24</sup>J.B. Claridge, M.L.H. Green, S.C. Tsang, A.P.E. York, A.T. Ashcroft, P.B. Battle, *Catal. Lett.*, 22 (1993) 299
- <sup>25</sup>J.R. Rostrup-Nielsen, J. Sehested, in *Studies in Surface Science and Catalysis* (J.J. Spivey, G.W. Roberts, B.H. Davis, Eds.), Vol. 139, Elsevier, Amsterdam (2001) 1
- <sup>26</sup>I. Alstrup, B.S. Clausen, C. Olsen, R.H.H. Smits, J.R. Rostrup-Nielsen, *Studies in Surface Science and Catalysis*, A. Parmaliana et al. (Eds.), Elsevier Science, Vol. 119 (1998) 5
- <sup>27</sup>V.I. Zaikovskii, V.V. Chesnokov, R.A. Buyanov, *Kinet. Catal.*, 42 (2001) 813
- <sup>28</sup>J.W. Snoeck, G.F. Froment, M. Fowles, *J. Catal.* 169 (1997) 240
- <sup>29</sup>R.T.K. Baker, M. Barber, P. Harris, F. Feates, R. Waite, *J. Catal.* 26 (1972) 51
- <sup>30</sup>R.T.K. Baker, P.S. Harris, in *Chemistry and Physics of Carbon*, (P.L.Walker, P.A.Thrower. Eds.) Vol. 14, , Dekker, New York, (1978) 83
- <sup>31</sup>D. Chen, R. Lodeng, K. Omdahl, A. Anundskas, O. Olsvik, A. Holmen, in *Studies in Surface Science and Catalysis* (J.J. Spivey, G.W. Roberts, B.H. Davis, Eds.), Vol. 139, Elsevier, Amsterdam (2001) 93

- <sup>32</sup> R.T.K. Baker, R.D.Sherwood, A.J.Simoens, E.G. Derouane, in *Metal-Support and Metal-Additive Effects in Catalysis* (B. Imelik, C. Naccaache, G. Coudier, H. Praliaud, P. Meriaudeau, P.Gallezot, G.A. Martin, J.C. Vedrine, Eds.), Elsevier, Amsterdam (1982) 149
- <sup>33</sup> T. Zhang, M.D. Amidiris, *Appl. Catal. A: Gen.*, 167 (1998) 161
- <sup>34</sup> J. Wei, E. Iglesia, *J. Catal.*, 224 (2004) 370
- <sup>35</sup> P. Forzatti, L. Lietti, *Catal. Today*, 52 (1999) 165
- <sup>36</sup> J.A. Moulijn, A.E. Van Diepen, F. Kapteijn, *Appl. Catal. A: Gen.*, 212 (2001) 3
- <sup>37</sup> K.M. Hardiman, M.M.Mohammed, A.A. Adesina, *Proceedings of the International Symposium on Applied Catalysis* (S.D. Jackson, J.S.J. Hargreaves, D. Lennon, Eds.), The Royal Society of Chemistry, Cambridge (2003) 16
- <sup>38</sup> J.G. McCarty, H. Wise, *J.Catal.*, 57 (1979) 406
- <sup>39</sup> S.D. Jackson, S.J. Thomson, G. Webb, *J. Catal.* 70 (1980) 249
- <sup>40</sup> Y.G. Chen, K. Tomishige, K. Fujimoto, *App. Catal.: A: Gen.* 161 (1997) L11
- <sup>41</sup> M.C.J. Bradford, M.A. Vannice, *Appl. Catal.*, 142 (1996) 97
- <sup>42</sup> K. Tomishige, Y.G. Chen, K. Fujimoto, *J. Catal.* 181 (1999) 91
- <sup>43</sup> J.N. Armor, D.J. Martenak, *Appl. Catal. A: Gen.*, 206 (2001) 231
- <sup>44</sup> K. Tomishige, Y. Himeno, O. Yamazaki, Y. Chen, T. Wakatsuki, K. Fujimoto, *Kinet. Catal.*, 40 (1999) 388
- <sup>45</sup> K. Tomishige, Y. Himeno, Y. Matsuo, Y. Yoshinaga, K. Fujimoto, *Ind. Eng. Chem. Res.*, 39 (2000) 1891
- <sup>46</sup> C. Song, S.T. Srinivas, L. Sun, J.N. Armor, *Chem. Soc., Div. Petrol. Chem. Preprints*, 45 (2000) 143
- <sup>47</sup> A. Shamsi, C.D. Johnson, *Catal. Today*, 84 (2003) 17
- <sup>48</sup> J.R. Rostrup-Nielsen, *J. Catal.* 85 (1984) 31
- <sup>49</sup> J.H. Onuferko, D.P. Woodruff, B.W. Holland, *Surface Sci.*, 87 (1979) 357
- <sup>50</sup> F. Frusteri, L. Spadaro, F. Arena, A. Chuvilin, *Carbon*, 40 (2002) 1063
- <sup>51</sup> F. Frusteri, S. Freni, V. Chiodo, L. Spadaro, G. Bonura, S. Cavallaro, J. Power, *Sources*, 132 (1-2) (2004) 139
- <sup>52</sup> T. Osaki, T. Mori, *J. Catal.* 204 (2001) 89
- <sup>53</sup> I. Alstrup, B.S. Clausen, C. Olsen, R.H.H. Smits, J.R. Rostrup-Nielsen, *Studies in Surface Science and Catalysis*, A. Parmaliana et al. (Eds.), Elsevier Science, Vol. 119 (1998) 5
- <sup>54</sup> M.G. Poirier, J. Trudel, D. Guay, *Catal. Lett.*, 21 (1993) 99
- <sup>55</sup> M.F. Mark, W.F. Maier, *J. Catal.*, 164 (1996) 122
- <sup>56</sup> D. Qin, J. Lapszewicz, X. Jiang, *J. Catal.*, 159 (1996) 140
- <sup>57</sup> D.K. Linguras, D.I. Kondarides, X.E. Verykios, *Appl. Catal. B: Environ.*, 43 (2003) 345
- <sup>58</sup> K. Nakagawa, H. Nishimoto, M. Kikuchi, S. Egashira, Y. Enoki, N. Ikenaga, T. Suzuki, M. Nishitani-Gamo, T. Kobayashi, T. Ando, *Energy and Fuels*, 17 (2003) 971
- <sup>59</sup> J. Wei, E. Iglesia, *J. Phys. Chem. B*, 108 (2004) 4094
- <sup>60</sup> J. Wei, E. Iglesia, *J. Phys. Chem. B*, 108 (2004) 7253
- <sup>61</sup> J. Wei, E. Iglesia, *J. Catal.*, 225 (2004) 116
- <sup>62</sup> Y. Schuurman, V.C.H. Kroll, P. Ferreira-Aparicio, C. Mirodatos, *Catal. Today*, 38 (1997) 129
- <sup>63</sup> J.G. McCarty, R.J. Madix, *Surf. Sci.* 102 (1976) 121
- <sup>64</sup> S.B. Ziemecki, G.A. Jones, *J. Catal.*, 95 (1985) 621

- <sup>65</sup> A.T. Ashcroft, A.K. Cheetham, J.S. Foord, M.L.H. Green, C.P. Grey, A.J. Murrell, P.D.F. Vernon, *Nature*, 344 (1990) 319
- <sup>66</sup> J.B. Claridge, M.L.H. Green, S.C. Tsang, A.P.E. York, A.T. Ashcroft, P.D. Battle, *Catal. Lett.*, 22 (1993) 299
- <sup>67</sup> V.A. Tsipouriari, A.M. Efstathiou, X. E. Verykios, *J. Catal.*, 161 (1996) 31
- <sup>68</sup> A.M. Efstathiou, A. Kladi, V.A. Tsipouriari, X.E. Verykios, *J. Catal.*, 158 (1996) 64
- <sup>69</sup> V.A. Tsipouriari, A.M. Efstathiou, A.M. Zhang, X.E. Verykios, *Catal. Today*, 21 (1994) 579
- <sup>70</sup> A. Erdöhelyi, J. Cserenyi, F. Solymosi, *J. Catal.* 141 (1993) 287
- <sup>71</sup> X.E. Verykios, *Appl. Catal. A: Gen.*, 255 (2003) 101
- <sup>72</sup> J.R. Rostrup-Nielsen, J.-H. Bak Hansen, *J. Catal.*, 144 (1993) 38
- <sup>73</sup> S.M. Stagg, E. Romeo, C. Padro, D.E. Resasco, *J. Catal.* 178 (1997) 137
- <sup>74</sup> J.T. Richardson, S.A. Paripatyadar, *Appl. Catal.* 61 (1990) 293
- <sup>75</sup> R.L. Augustine, in *Heterogeneous Catalysis for the Synthetic Chemist*, Marcel Dekker inc., New York (1996)
- <sup>76</sup> G.R. Gavalas, C. Phichitkul, G.E. Voecks, *J. Catal.*, 88 (1984) 54
- <sup>77</sup> K. Tanabe, *Mater. Chem. Phys.*, 13 (1985) 347
- <sup>78</sup> H.S. Roh, K.W. Jun, S.E. Park, *J. Ind. Eng. Chem.*, 9(3) (2003) 261
- <sup>79</sup> E.C. Subbarao, in A.H. Heuer and L.W. Hobbs (Eds.) *Science and Technology of Zirconia, Adv. Ceram.*, 3 (1981) 1
- <sup>80</sup> T.H. Etsell, S.N. Flengas, *Chem. Rev.*, 70 (1970) 339
- <sup>81</sup> M. Ozawa, M. Kimura, *Journal of the less common metals*, 171 (1991) 195
- <sup>82</sup> J.S.H.Q. Perera, J.W. Couves, G. Sankar, J.M. Thomas, *Catal. Lett.*, 11 (1991) 219
- <sup>83</sup> A.T. Ashcroft, A.K. Cheetham, M.L.H. Green, P.D.F. Vernon, *Nature*, 352 (1991) 225
- <sup>84</sup> J.A. Dalmon, C. Mirodatos, P. Turlier, G.A. Martin, In *Spillover of Adsorbed Species*, G.M. Pajonk et al. (Eds.), Elsevier, Amsterdam (1983) 169
- <sup>85</sup> D. Wang, O. Dewaele, A.M. De Groote, G.F. Froment, *J. Catal.*, 159 (1996) 418
- <sup>86</sup> D. Wang, Z. Li, C. Luo, W. Weng, H. Wan, *Chem. Eng. Sci.*, 58 (2003) 887
- <sup>87</sup> Y. Schuurman, C. Marquez-Alvarez, V.C.H. Kroll, C. Mirodatos, *Catal. Today*, 46 (1998) 185
- <sup>88</sup> Y. Amenomiya, *J. Catal.* 55 (1978) 205
- <sup>89</sup> Y. Amenomiya, G. Pleizer, *J. Catal.*, 76 (1982) 345
- <sup>90</sup> Z.X. Cheng, X.G. Zhao, J.L. Li, Q.M. Zhu, *Appl. Catal. A: General*, 205 (2001) 31
- <sup>91</sup> W.C. Conner, G.M. Pajonk, *Adv. Catal.*, 34 (1986) 1
- <sup>92</sup> W.C. Conner, J.L. falconer, *Chem. Rev.*, 95 (1995) 759
- <sup>93</sup> R. Kramer, M. Andre, *J. Catal.*, 58 (1979) 287
- <sup>94</sup> J.F. Cevallos,-Candau, J.L. Conner, *J. Catal.*, 106 (1987) 378
- <sup>95</sup> P. Chiaranussati, L.F. Gladden, R.F. Griffiths, S.D. Jackson, G. Webb, *Trans. Inst. Chem. Eng.*, 71 (1993) 267
- <sup>96</sup> M.M.V.M. Souza, D.A.G. Aranda, M. Schmal, *J. Catal.* 204 (2001) 498
- <sup>97</sup> K. Seshan, H.W. Barge, W. Hally, A.N.J. Van Keulen, J.R.H. Ross, *Stud. Surf. Sci. Catal.*, 81 (1994) 285
- <sup>98</sup> K. Nagaoka, K. Seshan, K. Aika, J.A. Lercher, *J. Catal.*, 197 (2001) 34
- <sup>99</sup> A.N.J. Van Keulen, M.E.S. Hegerty, J.R.H. Ross, P.F. Van den Oosterkamp, *Stud. Surf. Sci. Catal.*, 107 (1997) 537
- <sup>100</sup> S.M. Stagg, E. Romeo, C. Padro, D.E. Resasco, *J. Catal.* 194 (2000) 240
- <sup>101</sup> M.M.V.M. Souza, M. Schmal, *Catal. Lett.*, 91 nos 1-2 (2003)

- <sup>102</sup> S. Roberts, R.J. Gorte, *J. Phys. Chem.*, 95 (1991) 5600
- <sup>103</sup> R.A. Van Santan, M. Neurock, *Catal. Rev.-Sci. Eng.*, 37 (1995) 557
- <sup>104</sup> C. Minot, M.A. Van Hove, G.A. Somerjai, *Surf. Sci.*, 127 (1982) 441
- <sup>105</sup> T. Horiuchi, K. Sakuma, T. Fukui, Y. Kubo, T. Osaki, T. Mori, *Appl. Catal. A*, 144 (1996) 111
- <sup>106</sup> Z.L. Zhang, X.E. Verykios, *Catal. Today*, 21 (1994) 589
- <sup>107</sup> T.F. Narbeshuber, A. Brait, K. Seshan, J.A. Lercher, *Appl. Catal.*, 146 (1996) 119
- <sup>108</sup> M. Masai, H. Kado, A. Miyake, S. Nishiyama, S. Tsuruya, *Stud. Surf. Sci. Catal.*, 36 (1988) 67
- <sup>109</sup> J.H. Bitter, K. Seshan, J.A. Lercher, *J. Catal.*, 183 (1999) 336
- <sup>110</sup> E. Iglesia, J.E. Baumgartner, G.L. Price, *J. Catal.*, 134 (1992) 549
- <sup>111</sup> E. Iglesia, J.E. Baumgartner, *Catal. Lett.*, 21 (1993) 55
- <sup>112</sup> J. Barbier, *Appl. Catal.*, 23 (1986) 225
- <sup>113</sup> J.H. Bitter, K. Seshan, J.A. Lercher, *J. Catal.*, 171 (1997) 279
- <sup>114</sup> J.H. Bitter, K. Seshan, J.A. Lercher, *J. Catal.*, 176 (1998) 93
- <sup>115</sup> A. Auroux, A. Gervasini, *J. Phys. Chem.*, 97 (1990) 6371
- <sup>116</sup> H.W. Wang, E. Ruckenstein, *Appl. Catal. A: General*, 204 (2000) 143
- <sup>117</sup> E. Ruckenstein, H.W. Wang, *J. Catal.*, 187 (1999) 151
- <sup>118</sup> X. Wang, R.J. Gorte, *Catal. Lett.*, 73 (2001) 15
- <sup>119</sup> X. Wang, R.J. Gorte, *Appl. Catal. A: General*, 224 (2002) 209
- <sup>120</sup> T. Bunluesin, R.J. Gorte, G.W. Graham, *Appl. Catal. B*, 15 (1998) 107
- <sup>121</sup> R. Craciun, B. Shereck, R.J. Gorte, *Catal. Lett.*, 51 (1998) 149
- <sup>122</sup> S. Sharma, S. Hilaire, J.M. Vohs, R.J. Gorte, H.W. Jen, *J. Catal.*, 190 (2000) 199
- <sup>123</sup> P. Pantu, G.R. Gavalas, *Appl. Catal. A: General*, 223 (2002) 253
- <sup>124</sup> L.V. Mattos, E. Rodina, D.E. Resasco, F.B. Passos, F.B. Noronha, *Fuel Process. Tech.*, 83 (2003) 147
- <sup>125</sup> F.B. Noronha, A. Shamsi, C. Taylor, E.C. Fendley, S. Stagg-Williams, D.E. Resasco, *Catal. Lett.* 90 (2003) nos. 1-2
- <sup>126</sup> T. Mizuno, Y. Matsumura, T. Nakajima, S. Mishima, *Int. Journal of Hydrogen Ener.*, 28 (2003) 1393
- <sup>127</sup> T. Mizuno, T. Nakajima, *React. Kinet. Catal. Lett.* 78 (2003) 315
- <sup>128</sup> Q. Zhuang, Y. Qin, L. Chang, *Appl. Catal.*, 70 (1991) 1
- <sup>129</sup> Z.L. Zhang, X.E. Verykios, *J. Chem. Soc. Chem. Commun.*, (1995) 71
- <sup>130</sup> Z.L. Zhang, X.E. Verykios, *Appl. Catal. A: Gen.* 138 (1996) 109
- <sup>131</sup> T.H. Fleisch, R.F. Hicks, A.T. Bell, *J. Catal.*, 87 (1984) 205
- <sup>132</sup> R.F. Hicks, A.T. Bell, *J. Catal.*, 90 (1984) 205
- <sup>133</sup> R.F. Hicks, Q.-J. Yen, A.T. Bell, *J. Catal.*, 89 (1984) 498
- <sup>134</sup> V.C.H. Kroll, H.M. Swaan, S. Lacombe, C. Mirodatos, *J. Catal.*, 164 (1996) 387
- <sup>135</sup> A. Slagtern, Y. Schuurman, C. Leclercq, X. Verykios, Mirodatos, *J. Catal.* 172 (1997) 118
- <sup>136</sup> V.A. Tsipouriari, X.E. Verykios, *J. Catal.* 187 (1999) 85
- <sup>137</sup> G. Yaluris, R.B. Larson, J.M. Kobe, M.R. Gonzalez, K.B. Fogash, J.A. Dumesic, *J. Catal.*, 158 (1996) 336
- <sup>138</sup> K.B. Fogash, R.B. Larson, M.R. Gonzalez, J.M. Kobe, J.A. Dumesic, *J. Catal.*, 163 (1996) 138
- <sup>139</sup> G.F. Froment, K.B. Bischoff, *Chem. Eng. Sci.* 16(1961)189
- <sup>140</sup> S.D. Jackson, E.H. Stitt, *Current Topics in Catalysis*, 3 (2002) 245
- <sup>141</sup> Dr. P.K. Ingram, Private Communication (2)

- <sup>142</sup> S.D. Jackson, B.M. Glanville, J. Willis, G.D. McLellan, G. Webb, R.B. Moyes, S. Simpson, P.B. Wells, R. Whyman, *J. Catal.* 139 (1993) 207
- <sup>143</sup> A. Erdohelyi, J. Cserenyi, E. Papp, F. Solymosi, *Appl. Catal. A: Gen.* 108 (1994) 205
- <sup>144</sup> S.J. Tauster, S.C. Fung, R.L. Garten, *J. Amer. Chem. Soc.*, 100 (1978) 170
- <sup>145</sup> S.J. Tauster, S.C. Fung, *J. Catal.*, 55 (1978) 29
- <sup>146</sup> S.J. Tauster, S.C. Fung, R.T.K. Baker, J.A. Horsley, *Science*, 211 (1981) 1121
- <sup>147</sup> A.J. Simoens, R.T.K. Baker, D.J. Dwyer, C.R.F. Lund, R.J. Madon, *J. Catal.*, 87 (1984) 359
- <sup>148</sup> H.R. Sadeghi, V.E. Henrich, *J. Catal.*, 87 (1984) 279
- <sup>149</sup> D.N. Belton, Y.M. Sun, J.M. White, *J. Phys. Chem.*, 88 (1984) 1690
- <sup>150</sup> A. Igarashi, T. Ohtaka, T. Honnma, C. Fukuhara, *Proceedings of the 10<sup>th</sup> International Congress in Catalysis*, Gucci et al. (Eds.) Elsevier Science (1993) 2083
- <sup>151</sup> J. Kaspar, P. Fornasiero, M. Graziani, *Catal. Today*, 50 (1999) 285
- <sup>152</sup> M.H. Yao, R.J. Baird, F.W. Kunz, T.E. Hoost, *J. Catal.*, 166 (1997) 67
- <sup>153</sup> D.L. Hoang, H. Lieske, *Catal. Lett.* 27 (1994) 33
- <sup>154</sup> D.L. Hoang, H. Berndt, H. Lieske, *Catal. Lett.* 31 (1995) 165
- <sup>155</sup> F. Solymosi, J. Cserenyi, *Catal. Today*, 21 (1994) 561
- <sup>156</sup> J.T. Miller, B.L. Meyers, F.S. Modica, G.S. Lane, M. Vaarkamp, D.C. Koningsberger, *J. Catal.*, 143 (1993) 395
- <sup>157</sup> C. Dall'Agnol, A. Gervasini, F. Morazzoni, F. Pinna, G. Strukul, L. Zanderighi, *J. Catal.* 96 (1985) 106
- <sup>158</sup> H. Yoshitake, Y. Iwasawa, *J. Phys. Chem.*, 96 (1992) 1329
- <sup>159</sup> B. Sen, J.L. Falconer, *J. Catal.*, 117 (1989) 404
- <sup>160</sup> B. Sen, J.L. Falconer, *J. Catal.*, 122 (1990) 68
- <sup>161</sup> M.Y. He, J.G. Ekerdt, *J. Catal.*, 87 (1984) 238
- <sup>162</sup> J.D. Bracey, R. Burch, *J. Catal.*, 86 (1984) 384
- <sup>163</sup> W.J. Shen, M. Okumura, Y. Matsumura, M. Haruta, *Appl. Catal. A: Gen.*, 231 (2001) 225
- <sup>164</sup> J.M. Perez-Zurita, M. Dufour, Y. Halluin, A. Griboval, L. Leclerq, G. Leclerq, M. Goldwasser, L.M. Cubiero, G. Bond, *Appl. Catal. A: Gen.*, 274 (2004) 295
- <sup>165</sup> E.K. Poels, R. Koolstra, J.W. Geus, V. Ponec, in *Studies in Surface Science and Catalysis* (B. Imelik et al., Eds.), Vol. 11, p. 233, Elsevier, Amsterdam, 1982
- <sup>166</sup> A. Erdohelyi, M. Pasztor, F. Solymosi, *J. Catal.* 98 (1986) 166